Reforestation of Steep Reclaimed Slopes: Stability and Sediment Control Considerations

Eric C. Drumm
Department of Biosystems Engineering and Soil Science
and
John S. Schwartz
Department of Civil and Environmental Engineering

University of Tennessee, Knoxville

Final Report

Submitted July 2011

U.S. Office of Surface Mines, Applied Science Program

Acknowledgements

The research described in this report would not have been possible without the dedication and hard work of a number of people over the research period. The results reported here include thesis research by Patrick White, MS student Civil and Environmental Engineering, and dissertation work by Siavash Hoomehr, Ph.D. student Civil and Environmental Engineering and Isaac Jeldes, Ph.D student Civil and Environmental Engineering. Chris Dixon, MS student Civil and Environmental Engineering, provided laboratory support, and Wesley Wright, Research Associate, Biosystems Engineering and Soil Science played a major role in the system design and field installation/supervision of the field instrumentation. Nancy Roberts, Civil and Environmental Engineering, provided guidance on much of the laboratory analysis, and the field and laboratory work was supported by the following undergraduate students:
Students:

Nathan Felosi, Civil and Environmental Engineering
Mitch Groothuis, Biosystems Engineering and Soil Science
Joe Selby, Biosystems Engineering and Soil Science
Chris Drinnon, Biosystems Engineering and Soil Science
David Jacobs, Civil and Environmental Engineering
Russell Freda, Civil and Environmental Engineering
Sam Matthews, Civil and Environmental Engineering

The authors are grateful these individuals for what was a team research effort. The authors would also like to thank David E. Lane, P.E., Office of Surface Mining, Pittsburgh, for serving as the project technical contact, and for facilitating the interactions with the mining companies.

Executive Summary

Mine reclamation activities have traditionally been very successful with regard to the establishment of grass covers, especially in areas where the slopes are moderate to low. Establishment of forest cover in reclaimed areas has been less successful, primarily due to construction techniques which focus on stability of the landforms and erosion control using high levels of compaction and aggressive grass covers. Research has established that over-compaction of the reclaimed surface soils impedes the establishment of healthy fast growing forests, which has led to the development and promotion of the Forestry Reclamation Approach (FRA). One of the most critical aspects of the FRA is the use of low compaction grading techniques to assure that a zone of "loose" material remains at the surface to encourage tree survival and growth. Unfortunately, the mass stability of steep slopes is dependent on these greater compaction levels, since the strength of the reclaimed materials is highly dependent upon the level of compaction. The increased strength associated with higher levels of compaction is also needed to reduce erosion and the limit the potential for sediment to enter nearby streams. Previous research studies on low compaction grading methods have concentrated on reclamation work in relatively flat terrain (1-3 degrees), yet the reforestation of reclaimed areas with steep slopes is perhaps even more important.

To investigate the effects of low compaction grading on slope stability, erosion, and sediment yield on steep slopes (> 20 degrees), three reclaimed mine sites in Tennessee were identified, and instruments installed to measure weather/precipitation, surface runoff, and suspended sediment load. Each of the three sites was subdivided into four plots with different ground cover treatments. Ground covers and the trees were planted in March 2009 as part of a separate research project conducted by others. However, it should be noted that ground covers were never effectively established due to the number and intensity of spring/summer storms events in 2009. The runoff and sediment erosion data were used to develop hydrologic and soil erosion parameters for sediment pond design using SEDCAD and CHIA modeling efforts. The overall objectives of the research were:

1. Develop/document appropriate construction procedures for reclamation of steep slopes to satisfy the conflicting concerns of providing a loosely compacted rooting medium for tree growth yet assuring there are zones of sufficient compaction to provide structural stability;
2. Investigate the influence of low compaction surface growth zones on the stability of steep slopes, and the extent to which complex slope geometries may serve as a strategy for increasing slope stability while avoiding long planar slopes which may lead to excessive erosion; and
3. Demonstrate that these methods provide satisfactory erosion and sediment control in order that surface water quality can be maintained. Based on field measurements, provide appropriate input parameters for commonly used hydrologic and sediment models, primarily developing a CN runoff value and sediment erodibility parameter (RUSLE K factor) for low-compacted steep slopes reclaimed mine lands.

Results of this research project are communicated in the attached report. Chapter 1 provides an introduction to the project, including the relationship between the project objectives and the identified work tasks. Also included is a preliminary review of previous work by others related to the application of low compaction methods to facilitate tree growth in reclaimed mine lands, and some preliminary background on the concept of "landforming," which is the use of more complex, non planar slope shapes to provide a natural appearing slope that is more resistant to erosion and sediment production.

Chapter 2 provides information about the study locations of the three reclaimed mine sites in eastern Tennessee, describes the low compaction construction process, and provides a summary of ground cover application rates and cover implemented by others. Details of the site instrumentation are provided, which included flumes with pressure (stage) sensors to measure runoff duration, a runoff-sediment collection system, and weather stations which recorded precipitation, solar radiation, wind speed, wind direction, and temperature. All data were recorded at intervals of 5 minutes, and could be downloaded from the acquisition-storage hardware off-site by telemetry.

The characterization of the sites is described in Chapter 3, which includes survey data and the slope inclination measurements for each of the three sites. Of the three sites, one had average slope inclination slightly greater than 20 degrees (National), while the other two (Mountainside and Premium) had average inclinations of about 28 degrees. To explore the spatial variability of the unit weight, measurements were obtained with a nuclear density gauge across each site on a 3m by 3m grid. The results were depicted across the slope graphically, and a statistical analysis of the measurements was conducted. A particle size analysis and plasticity indices tests of the materials at the three sites indicated that in spite of the high percentage coarse particles present, all three sites contain significant portions of plastic fines leading to an engineering (USCS) Soil Classification of "Clayey Gravel." It was suggested that field observations of the angle of repose of the surface materials during reclamation could be taken as an estimate the shear strength of the loose soil layer of material, and observations indicated all three sites had an angle of repose of about 38 degrees. The values were compared with friction angles from mine sites reported in the literature from large scale laboratory tests, and appear to be consistent with those reported values.

Chapter 4 describes the traditional limit equilibrium method for slope stability analysis, as well as the special case referred to as the "infinite slope" method. The low compaction construction methods employed in the FRA produce a relatively thin (1.5 m) layer of loose materials on top of a stronger structural core, providing a geometry that is very close to that assumed in the infinite slope method for stability evaluation. It is suggested that application of the infinite slope method, using strength parameters obtained from observations of the angle of repose, yields a simple yet appropriate method for evaluating the mass stability of slopes constructed according to the FRA. The stability determined from the infinite slope method was verified by both the traditional limit equilibrium method and by the Finite Element method. The long-term stability of the slopes at all three sites was found to be satisfactory, producing Factors of Safety of nearly 1.5 for the steeper Premium and Mountainside sites, and slightly over 2 for the National site. This is well above the value of 1.3 specified in the general requirements for surface mining in 30 CFR 816/817.102(a)(3). The infinite slope method was extended to evaluate the seismic stability of reclaimed mine slopes, and demonstrated through an example.
The stability of more complex slope shapes such as those resulting from "landforming" was addressed in three parts, beginning in Chapter 4 and continuing in Chapters 5 and 6. In Chapter 4, the results were reported from a literature review investigating the differences between the stability determined in the traditional manner from the analysis of a 2 dimensional (2D) slice method through a slope, and the stability obtained when the full 3 dimensional effects are included. It was found that the factors of safety considering the 3 dimensional effects are nearly always greater than the more conservative results obtained from the traditional 2D slice methods. This suggests that slopes with non-planar or complex geometry in the direction perpendicular to the cross section of the slope are generally more stable than if they are planar in this direction. In Chapters 5 and 6, the effect of non planar or complex geometry in the 2D plane of the slope cross section is explored.

Constructed slopes and reclaimed land are often designed to follow planar geometries because engineering analysis techniques and typical surveying and construction practices tend to favor this shape slope profile. However, in nature, slopes are seldom planar in cross section, and more complex slope geometries are common with the cross section often tending to be concave. In Chapter 5, the geomorphological evolution of slopes toward an equilibrium shape from the generalized principle of minimum rate of energy dissipation is proposed, suggesting that for certain boundary conditions, slopes may evolve into concave shapes in the long term. Laboratory and computational studies from the literature are reviewed, which indicate that concave slope contours may reduce erosion and sediment yield, suggest that the concave slope profiles observed in nature may be very efficient with respect to limiting erosion and sediment. Based on the critical equilibrium theory developed by Sokolovski in 1960, in which the critical shape of a slope at failure is determined from plasticity theory, a relatively simple approximate solution is developed. This solution yields the shape of the concave slope contour at failure, and it is shown how the slope shape can be determined for any desired factor of safety (FS). This new method is demonstrated through an example reclaimed slope, and solutions using the traditional Limit Equilibrium method (LEM) and Finite element (FEM) analyses showed that the proposed design methodology is accurate. For general readability and to facilitate the practical application of the design method for non planar slopes, the details, mathematical derivation, and error analysis for the concave slope approach are eliminated from Chapter 5, but described in full in Chapter 6.

Chapter 7 investigates the runoff hydrology of the instrumented sites, providing new data which is vital for the design of stormwater sediment control structures on FRA-constructed reclaimed mine lands. Engineers traditionally use the runoff curve number (CN) method to predict rainfall-runoff relationships for un-gauged watersheds, a method developed by the USDA Soil Conservation Service (now the Natural Resource Conservation Service, NRCS). CN values typically assumed for reclaimed mine surfaces have not been verified, particularly when the low compaction construction methods recommended by the FRA are used on steep slopes. The three instrumented sites were monitored over time to determine the discharge volume for a range of precipitation events, and no ground cover. The NRCS rainfall-runoff relationship is dependent on hydrologic initial abstraction (Ia) and it is a function of the maximum potential retention or storage (S) on the land surface. Historically Ia was assumed to be equal to $0.2 \cdot S$, however more recent references suggest it should be closer to $0.05 \cdot S$. An attempt was made to compute the factor (λ) between Ia and S, but due to the rapid response time for runoff to begin at these sites (< 5 minutes) an accurate estimate for λ could not be obtained. In our analysis, we assumed a λ of both 0.05 and 02. Results determined that for a λ of 0.05, the average CN to be 62.2 (range 20.5 to 98.8). Results determined that for a λ of 0.2, the average CN to be 71.8 (range 30.7 to 98.8). Further, it is shown that there are no significant differences between CN values among three sites - that they are statistically the same. These CN values would be used in hydrologic modeling representing the maximum potential runoff from a site because of the lack of ground cover. This suggests that these CN values may have wide application in practice for other sites in southern Appalachia to estimate runoff from reclaimed mine sites employing the FRA methods, in order to size sediment control ponds.

Although the FRA has been demonstrated to be effective with respect to enhancing the growth and survivability of the trees, there has been limited investigation on the effect of this technique on erosion and sediment yield. In Chapter 8, data collected from the instrumented sites was used to determine an appropriate value of the soil erodibility factor, K, for mine sites reclaimed using low compaction methods. This is an important parameter used in the widely accepted Revised Universal Soil Loss Equation (RUSLE), to predict erosion. It is also used along the CN in SEDCAD, which is used by OSM engineers to design sediment control basins. Because each site had a full weather station, erosivity or the R factor in RUSLE was computed and could be compared with the K factor. The R factor is based on

total storm rainfall energy and the maximum 30-minute intensity. Because the sites were steep and lacked ground cover rills developed over the period of study. To date, a changing K factor for a soil-land character has not been reported, however our data illustrates the K factor changes with time until rills reach some geomorphic equilibrium. Results found the average K factor to be 0.30 during rapid rill growth, 0.07 during the transition period towards geomorphic equilibrium, and 0.05 when the rills were assumed to be geomorphically stable.

In addition to the RUSLE factor computations, measurements of the particle size distribution (PSD) of the eroded and transported sediment were obtained over the study period. PSD is another key input parameter used in sediment control pond design and selection of other best management practices used to control sediment. During rill development, the median particle size was approximately 2 mm, and after the rills stabilized the median was less than 0.01 mm. Measurements of the temporal variation of the particle size distribution over the study period provides insight into how the sediment size distribution may change over time with rill development, leading to a better understanding of the erosion process and the development of best management practices.

Chapter 9 describes the sediment modeling of the instrumented slopes. In practice, the design of runoff and sediment control structures often depends on the results from computer-based hydrology and sediment erosion models. SEDCAD is a comprehensive package which has been widely used in the mining industry, primarily used in the design of sediment control basins. However, most experience with SEDCAD has been on low to moderate sloped surfaces, and it has not been verified on steep slopes constructed with low compaction/FRA methods. To address this issue, SEDCAD was investigated for the estimation of erosion and sediment delivery from the instrumented sites, and the sensitivity of SEDCAD outputs was evaluated with respect to curve number value (CN) and erodibility of reclaimed material (K). The results of this study found that generally SEDCAD over-predicted the sediment yield from the three study sites when erosivity (R factor) was greater than about 25 ft·tonf. The CN and K factor estimates derived in this study can also be used in watershed-scale sediment yield models such as AnnAGNPS or SWAT. Because AnnAGNPS was developed for watershed scale applications and SEDCAD was developed for local site specific applications, performance of the two could not be compared. In general these results provide a better understanding in interpretation of SEDCAD outputs, and the suggested parameters will be highly useful in designing runoff and sediment control structures and selection of best management practices (BMPs) in the mining industry.

Chapter 10 provides a summary of the research, presents several conclusions related to the use of low compaction methods on steep sites. The appendices include supplemental data and figures not found in the chapters themselves.

Table of Contents

Chapter 1 Introduction

Background

The Appalachian Regional Reforestation Initiative (ARRI) is a cooperative effort among the Appalachian states and the Office of Surface Mining (OSM) (Angel et al. 2005). The ARRI goals are to plant more high quality hardwoods on reclaimed mine lands, increase survival rates, and expedite the establishment of forest habitat, though the encouragement and promotion of the Forestry Reclamation Approach (FRA). One of the most critical aspects of the FRA is the use of low compaction grading techniques (Figure 1-1) to assure that a zone of "loose" material remains at the surface to encourage tree survival and growth (Sweigard et al. 2007a). Sweigard et al. suggest that leaving a zone of loose surface soils improves the survival of planted trees in the following ways:

- Helps assure that trees are planted correctly with a sufficiently deep planting hole
- Improve the infiltration of rainwater to the tree roots
- Provides increased pore space around soil particles which allows the soil to hold more water and improve air exchange needed for tree roots and soil organisms
- Allows tree roots to grow more freely which improves survival and improves growth rates.

Although these low compaction grading techniques are relatively well accepted and recognized, the desire to maintain low levels of compaction is in direct conflict with traditional practice regarding the structural stability of slopes. For a given slope to be stable, the soil must have sufficient strength to resist the gravitational and seepage forces acting on the soil mass. In general, the strength of the soil will decrease as the density decreases. This is recognized in most discussions of low compaction grading techniques and Sweigard et al. emphasize that if compaction is required for stability that the underlying compacted materials should be left in a rough configuration to assure a high strength interface with the weaker uncompacted material. However, no guidelines are presented with respect to construction or design methods for these low compaction grading techniques, nor are appropriate analysis methods suggested. The focus of this research was to develop design and analysis methods that will facilitate the application of low compaction grading techniques in areas with steep slopes, such that structural stability is preserved and surface erosion and sediment production is minimized. This was investigated at three full-scale test sites, instrumented to measure erosion and sediment yield.

Previous Studies

Instrumented field sites demonstrating low compaction grading

Angel et al. (2007) and Barton et al. (2007) have described a field demonstration site employing low compaction grading principles in Pike County, KY. Tree survival and growth were examined for yellow popular, green ash, red oak, and white oak on 6 one-acre plots. Three different mine spoil soils were used for the study: a brown weathered sandstone, a gray un-weathered sandstone, and a mixture of the brown and gray sandstone and shale, Figure 1-2. They determined that the brown weathered sandstone was the best with respect to supporting tree growth. The sites were instrumented with perforated pipe drains and soil lysimeters to collect ground water for chemical analysis. They observed a flush of constituents for two years before reaching normal levels similar to local streams.

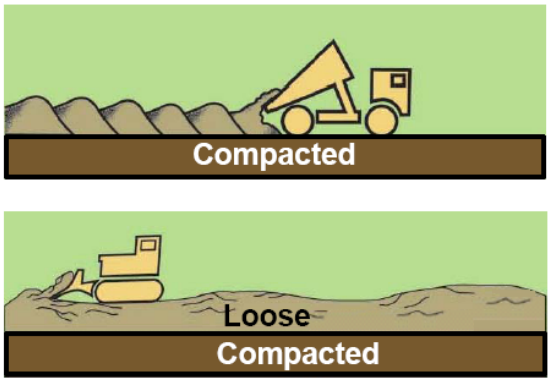

Diagram 1. End-dumping and final grading on a truck-and-haul surface mine. Subsurface materials have been placed as described in the permit and have been compacted by equipment operations. Surface materials are dumped over the compacted subsurface to a depth of 4 to 6 feet (upper) and are graded only lightly so that they remain loose and uncompacted (lower).

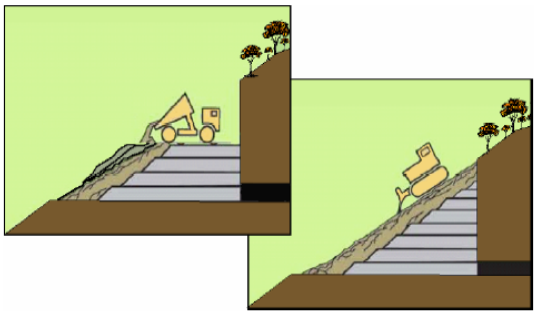

Diagram 5: Spoil can be placed and graded to achieve stability on a steep-slope contour mine where backfill compaction is specified by the permit. The backfill materials are placed and compacted using standard procedures as required for stability, and then loose materials suitable for surface placement are dumped over the compacted spoils and graded only lightly and only if necessary to shape the final surface. The surface materials can be placed over the compacted backfill as each lift is completed, or they can all be dumped from the top lift.

(a) (b)

Figure 1-1 Low compaction grading techniques to provide a loose surface zone for tree root establishment; (a) 4-6 foot thick zone of loosely compacted materials in relatively level terrain; (b) Grading of loose material on a steep slope where compaction would be required for structural stability (Sweigard et al. 2007a)

Figure 1-2 Pike County KY instrumented low compaction fill sites for examination of tree growth and monitoring of ground water chemistry (Angel et al. 2007); Barton et al. 2007).

Verification of low compaction grading conditions, density measurements

The density of the tree grow areas was measured at the Pike County, KY field demonstration (Angel et al. 2007). Bulk density in the three backfill materials varied significantly with depth. Density values of about 1.5 g/cm^3 were measured near the surface (5 cm), but the density increased to about 1.7 g/cm^3 at 15 cm depth and 1.8 g/cm^3 at a depth of 30 cm.

The density of reclaimed mine lands consisting of large rock particles can be difficult to measure, which makes it difficult to quantify and awkward to provide proper construction quality control. Sweigard et al. (2007b) provide some guidance for the loosening of compacted soil at reclaimed mine sites, and have correlated dry bulk density to shovel penetration (Table 1-1). They suggested that in rocky spoil materials, dry bulk unit weight should be less than 100 Lbf/ft^3 (1.6 g/cm^3) at a depth of 2 inches for healthy tree growth. Regardless, in view of the supporting data above, it seems that effective mine reclamation activities would include suitable measurement of compacted density to assure that the tree growth zones are not over compacted. Innovative measurement techniques for in place density of these materials are needed.

Table 1-1 Suggested relationship between spade penetration and soil density, and forest site quality (Sweigard et al. 2007b)

Table 1. The relationship among degree of compaction, spade penetration depth, forest site quality, and relative return on a forestry investment (after Burger and others 1998, 2002; and Probert 1999). Forest site quality is an indicator of the soil's ability to support growing trees.

Soil Density Condition	Very Dense	Dense	Moderately Compacted	Slightly Compacted	Loose
Spade penetration	0-1 inches	1-3 inches	3-6 inches	6-9 inches	9-12 inches
Site Quality Class	V (poor)	IV (fair)	III (medium)	II (good)	I (excellent)
Oak site index [a]	40	50	60	70	80
Use for wood products	None	Firewood	Railroad ties	Saw timber	Veneer
$ /1000 board ft stumpage value[b]	-	Less than $100	$200	$500	$2000
Relative return on investment	-2%	0%	2%	4%	8%

[a] Approximate height in feet of a white or red oak growing at age 50. These ratings assume that all other factors (other mine soil properties, ground cover, seedling quality, etc.) affecting productivity other than soil density are optimum.
[b] As of 2/07. J. Hayek, Timber Blog. Univ. of Illinois Extension Div. http://web.extension.uiuc.edu/forestry/blogs/eb94/

Effects of compaction on erosion potential and sediment production

Low compaction grading methods have also been said to reduce erosion and subsequent sediment production. Torbert and Burger (1994) investigated the effects of surface grading on ground cover establishment, tree growth, and erosion. They reported that erosion was greatest on the areas with the most intensively graded (high compaction, smoother surface) areas, and reported differences in the growth rates of various tress species as well. They suggested that low compaction grading facilitates water infiltration, and compaction of soil surface accelerates soil erosion. While the conclusion regarding infiltration would be generally viewed as correct, the conclusion that compaction accelerates erosion has not been well demonstrated. Most would agree that the increased cohesive strength that accompanies compaction would reduce erosion.

Grading techniques incorporating Landforming considerations

Landforming is an attempt to grade slopes in such a manner as to replicate the stable landforms observed in nature (Schor and Gray 2007). During the alteration or reshaping of the earth's surface, either for land reclamation or for development of steep slopes, the grading practices often tend to result in landforms which are planar or possess a "linear perspective" (Schor and Gray 2007). On the other hand, natural landscapes are typically characterized by complex shapes, which may be both concave and convex, but are seldom planar (Figure 1-3, 1-4 and 1-5).

These more complex landforms can have greater stability and erosion resistance than conventional planar landforms, which is why planar slopes are seldom found in nature. Man-made slopes are often designed to follow the more planar geometries because engineering analysis techniques and typical surveying and construction practices tend to favor the planar geometries. However, more complex slope geometries can be designed and constructed with a minimal increase in cost once the decision to adopt landforming practices is accepted (Schor and Gray 2007).

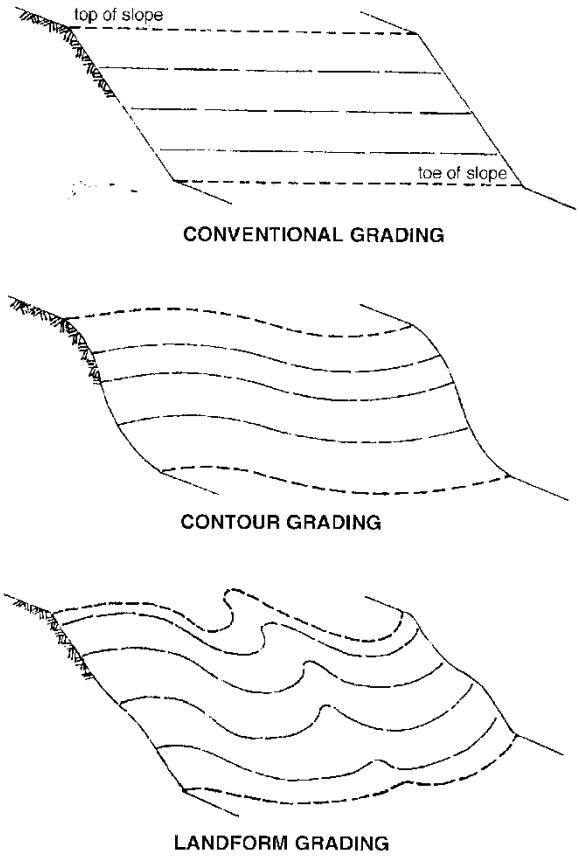

Figure 1-3 Schematic comparison of grading techniques (a) Conventional Planar, (b) Contour and (c) Landform grading (Schor and Gray 2007)

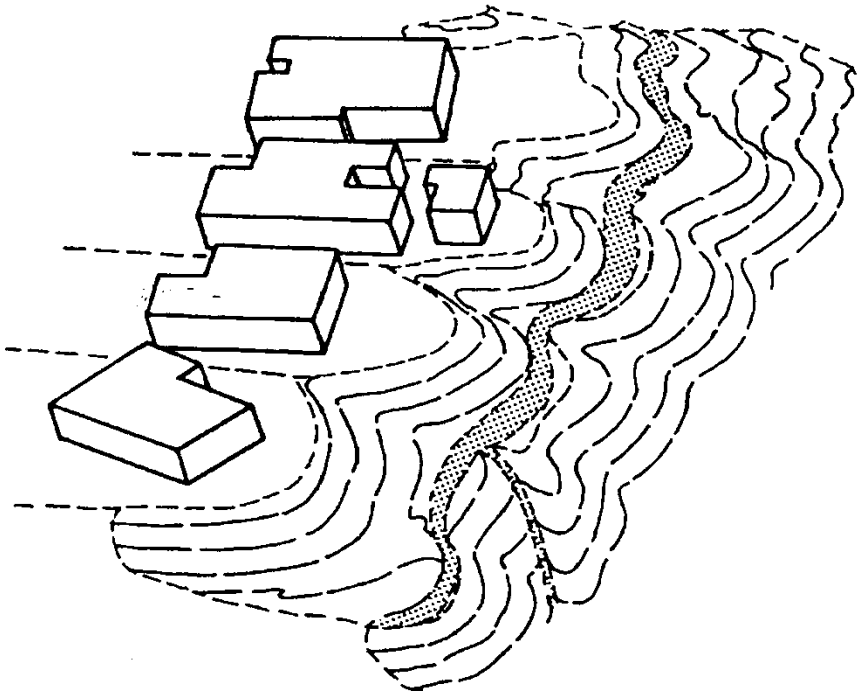

Figure 1-4 Schematic of landform grading showing constructed topography and position of drainages (Schor and Gray 2007).

Figure 1-5 Photograph of landform grading in a hillside development (Schor and Gray 2007).

The stability of a concave slope may be greater than that of a planar slope with the same soil strength and density properties, height, and overall slope. For example, the schematic in Figure 1-6 (Schor and Gray 2007) depicts a conventional planar slope subdivided into layers of equal thickness and soil properties. Because the vertical stress due to the overburden soil increases with depth, for all the soil layers to have the same level of safety with respect to stability, the lower layers will tend exist at a lower slope inclination than the upper layers. This results in a concave slope face. While this example does not consider the effects of friction on soil stability, it provides some insight into why more complex non-planar landforms may offer more than a simple esthetic advantage over planar slopes.

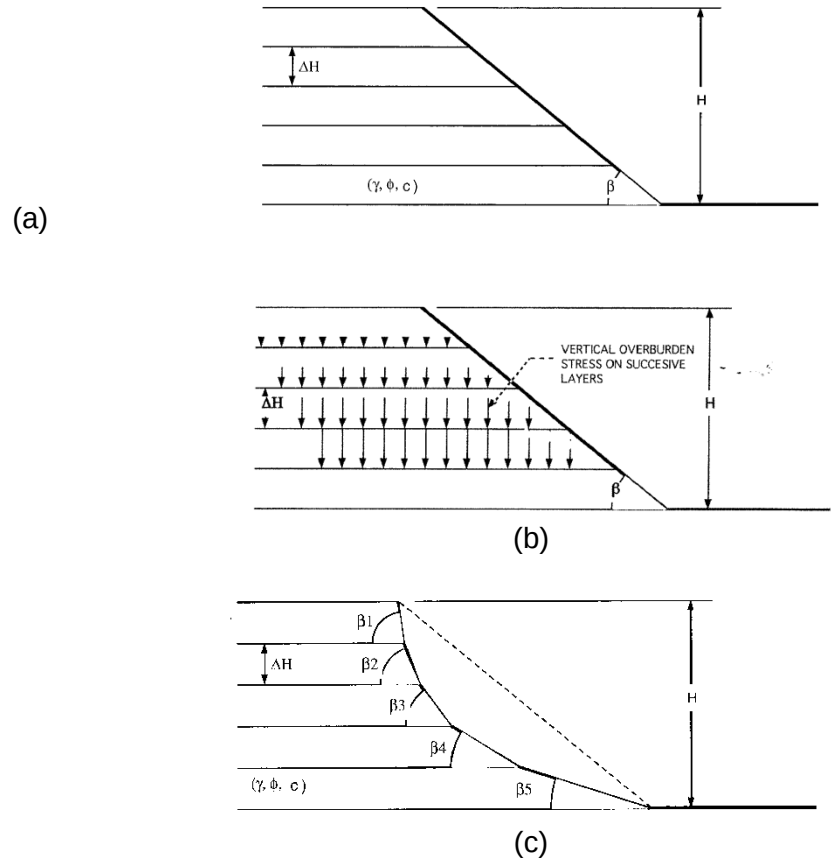

Figure 1-6 Comparison of a simple planar and a convex slope comprised of the same soil properties, illustrating the more uniform stability in the more natural convex slope: (a) Simple slope divided into equal layers, (b) Increase in vertical stress with depth, (c) Concave slope with inclination of lower layers reduced to provide the same level of stability as the upper layers with lover overburden stress (Schor and Gray 2007).

An additional explanation as to why planar slopes are not often found in nature is that concave slopes provide more resistance to surface erosion. With all factors held constant, the soil loss along a slope due to erosion increases with both the height and length of the slope. Figure 1-7 (Schor and Gray 2007) illustrates the difference between the erosion resistance of a planar slope and a concave slope. In a planar slope, the surface stress or traction induced by downslope water flow increases with increasing distance down the slope. However, in a concave slope, the surface stress is less in the lower levels of the slope because the inclination is less, leading to a more uniform loss due to erosion.

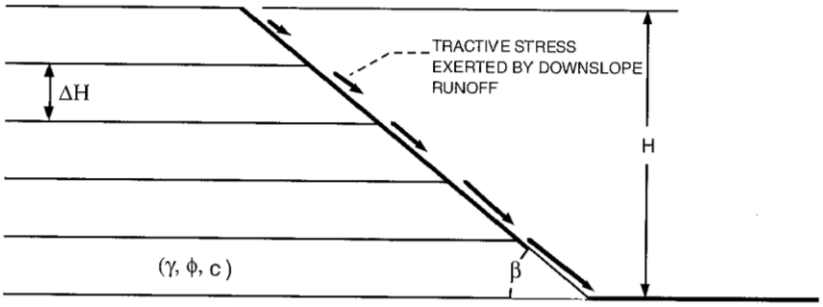

(a)

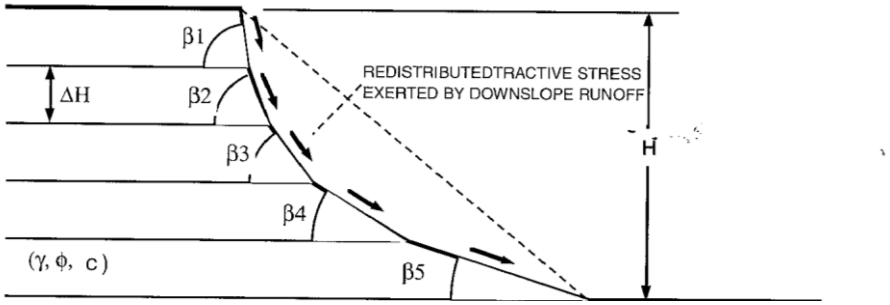

(b)

Figure 1-7 Comparison of a simple planar and a convex slope of the same height, illustrating the increased surface erosion resistance of a more natural convex slope: (a) Simple slope divided into equal layers showing the increase in surface stress due to runoff in the lower layers with increasing distance down the planar slope, (b) Concave slope with the inclination of the lower layers reduced to maintain an equal surface stress due to runoff (Schor and Gray 2007).

The low compaction grading construction techniques described above have been proven to be successful in encouraging tree growth, and demonstrate the potential for establishing healthy forests on reclaimed mine lands. However, these demonstrations have been conducted in relatively flat lying terrain. In many areas of Appalachia, the reclaimed lands include steep slopes (greater than 20 degrees), such as those from the New River watershed in Tennessee shown below (Figure 8). In the study described here, three instrumented demonstration sites in steep terrain will be developed to monitor the effects of the conflicting goals of low density and high structural stability/low erosion. Likewise, the stability resulting from the incorporation of more complex landforms in the grading plan will be investigated, to provide additional stability, greater resistance to erosion, and a more natural appearance of the reclaimed land.

Figure 1-8 Steep rocky reclaimed mine slopes in the New River, Tennessee watershed

Work Tasks in relation to Project Objectives

Objective 1: *Develop/document appropriate construction procedures for reclamation of steep slopes to satisfy the conflicting concerns of providing a loosely compacted rooting medium for tree growth yet assuring there are zones of sufficient compaction to provide structural stability*

Task 1: **Identify appropriate field sites located in steep terrain for the construction and instrumentation demonstration**

Identify, with the assistance of OSM personnel, appropriate field demonstration sites in steep terrain (slopes greater than 20 degrees) and secure the cooperation of the associated mine operators, for the construction, instrumentation, and investigation of the appropriate forestry practices.

Task 2: **Construct the field demonstration sites for stability yet incorporating low compaction grading methods Document the construction procedures, and characterize the reclaimed backfill materials.**

Monitor the construction of the field demonstration sites, and document the placement sequences for both the dense and loose fill zones. Characterize the site materials, topography, and determine the spatial variation of the density of the backfill in the compacted tree growth zones.

Task 3: **Design and install field instrumentation for surface water runoff and sediment collection.**

Design and install systems to collect surface water and sediment, as well as rainfall.

Objective 2: *Investigate the influence of low compaction surface growth zones on the stability of steep slopes, and the extent to which complex slope geometries may serve as a strategy for increasing slope stability while avoiding long planar slopes which may lead to excessive erosion*

Task 4: **Investigate with computer models the stability of slopes with low compaction surface zones, including the role of complex slope geometries to provide greater local stability and increased resistance to erosion.**

Evaluate the stability of the slopes, and conduct a parametric analysis to determine the influence of the material properties on stability. Investigate with computer models the role that increased slope complexity has on stability.

Objective 3: *Demonstrate that these methods provide satisfactory erosion and sediment control, and that surface water quality is maintained. Based on field measurements provide appropriate input for common hydrologic and sediment models, primarily developing CN runoff and sediment parameters for each site, characterizing differences in runoff, immediately following reclamation, and during intermediate re-growth stages from each reforestation scenario.*

Task 5: **Monitor the demonstration sites for slope distress and excessive erosion, and collect surface water and sediment samples. Evaluate the surface water and sediment data and draw conclusions relative to the site design.**

Following the construction of the field sites, monitor for evidence of slope stability problems, and collect basic hydrologic data (precipitation and surface water runoff flow), and sediment yield data (sediment concentration in runoff samples). If possible based on site conditions, test groundwater quality for pH, specific conductance, and turbidity. Compile and evaluate surface water runoff and sediment data, and draw conclusions relative to the site design.

Task 6: **Based on the hydrologic and sediment field measurements compute CN numbers and sediment properties for each site and reforestation design.**

Based on the field observations and measurements, provide guidance for selecting appropriate hydrologic model input parameters: CN, curve numbers and sediment yield input parameters (C factor and particle size transported per slope) for the reclaimed sites and over time with vegetation growth, These SEDCAD inputs support better site design for erosion control and stormwater BMPs.

References

Angel, P., V. Davis, J. Burger, D. Graves, and C. Zipper (2005) “The Appalachian Regional Reforestation Initiative.” U.S. Office of Surface Mining. Forest Reclamation Advisory Number 1. 2 p.

Angel, P. C. Barton, R. Warner, C. Agouridis, T. Taylor, and S. Hall (2007) “Hydrologic Characteristics, tree growth, and natural regeneration on three loose-graded surface mine spoil types in Kentucky” presentation at the Mid-Atlantic Stream Restoration Conference, Rocky Gap Lodge, Cumberland, Maryland, November 2007. http://www.canaanvi.org/canaanvi_web/events_ed.aspx?collection=cvi_workshops&id=140 accessed December 15, 2007

Barton, C., C. Agouridis, R. Warner, D. Bidelspach, P. Angel, G. Jennings, J. Marchant and R. Osborne (2007) “Recreating a Headwater Stream System on a Head-of-Hollow Fill” presentation at the Mid-Atlantic Stream Restoration Conference, Rocky Gap Lodge, Cumberland, Maryland, November 2007. http://www.canaanvi.org/canaanvi_web/events_ed.aspx?collection=cvi_workshops&id=140 accessed December 15, 2007

Maidment, D.R. 1992. Handbook of Hydrology. McGraw Hill, New York. Chapters 1-13.

Schor, H.J. and D.H. Gray (2007) *Landforming: An Environmental Approach to Hillside Development, Mine Reclamation, and Watershed Restoration*, John Wiley & Sons, Hoboken, New Jersey, 354 pp.

Sweigard, R., J. Burger, C. Zipper, J. Skousen, C. Barton, and P. Angel. (2007a) "Low Compaction Grading to Enhance Reforestation Success on Coal Surface Mines" U.S. Office of Surface Mining, Forest Reclamation Advisory No.3.

Sweigard, R., J. Burger, D. Graves, C. Zipper, C. Barton, J. Skousen, and P. Angel (2007b) "Loosening Compacted Soils on Mined Sites" U.S. Office of Surface Mining, Forest Reclamation Advisory No.4.

Torbert, J. L., J. A. Burger, and W. L. Daniels (1990) "Pine growth variation with overburden on a reclaimed surface mine in Virginia" J*. Environ. Qual.* 19:88-92.

Torbert, J. L., and J. A. Burger (1994) "Influence of grading intensity on ground cover establishment, erosion and tree establishment on steep slopes" , Proceedings 16th Int. Land Reclamation & Mine Drainage Conf., Vol. III, Reclamation and Regeneration, USDI Bureau of Mines Spec. Publ. 06C-94, USDI, Pittsburgh, PA. p. 226-231.

Warner, R.C., P.J. Schwab, and D.M. Marshall. 2001. SEDCAD™ 4: Design Manual and User's Guide. University of Kentucky, Lexington.

Chapter 2 Site Construction and Instrumentation

Site Construction and Reclamation Process

Location of field sites:
In order to investigate the potential effects on stability and erosion/sediment yield resulting from the implementation of the Forest Reclamation Approach (FRA), three mine reclamation sites in northeastern Tennessee, referred to here by the name of the initial coal operator, were chosen. Premium is located in Anderson County, National in Campbell County and Mountainside in Claiborne County (Figure 2-1).

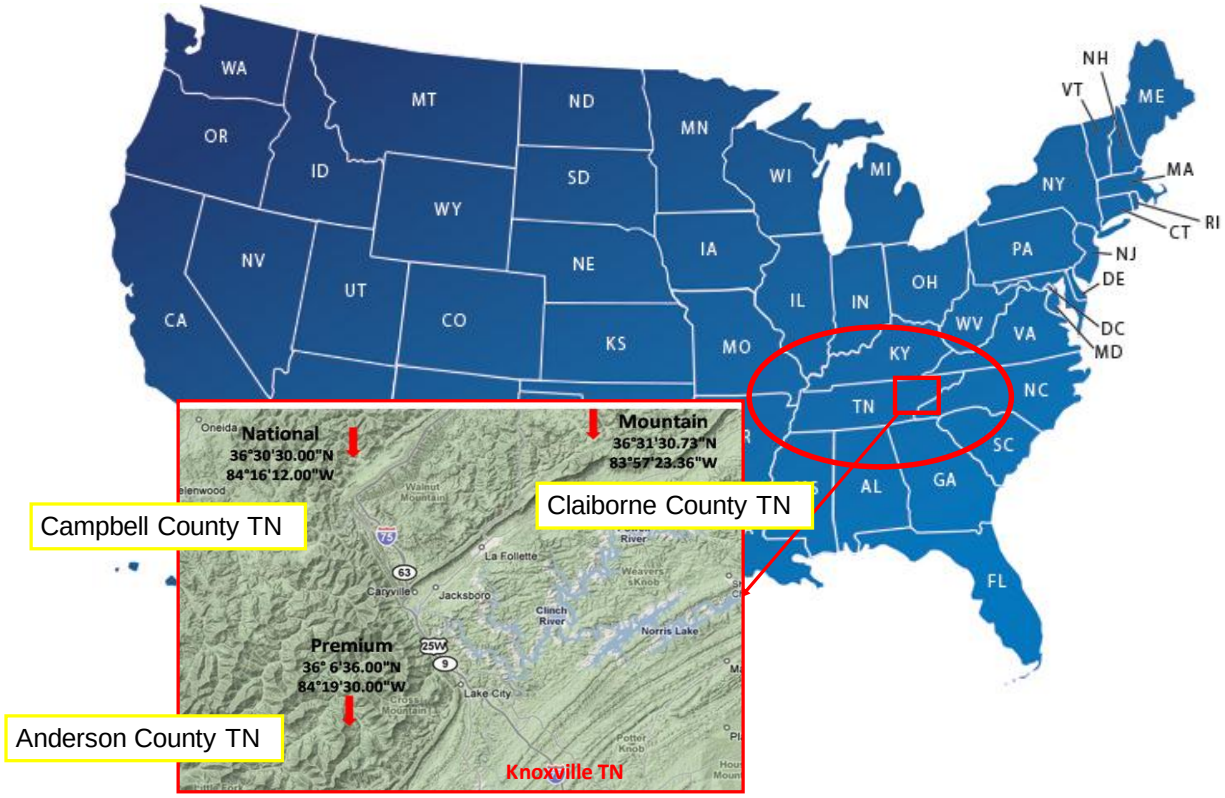

Figure 2-1 Field sites location in eastern Tennessee referred to as the Mountainside, National and Premium sites

Reclamation process
Sweigard and Kumar (2010) described several general methods of reclamation used in the Appalachian coal fields region. Although these practices were reported for highwall elimination using the FRA, at least three of them are indeed traditional techniques employed to build slopes with minimum compaction/grading of the surface. These general techniques are listed below:

- *Contour haulback*: This is the most widely used method in the Appalachian region. Here, a ramp is constructed on the contour bench and soil is hauled up the ramp and dumped over the edge of the ramp.
- *Combination of haulback and dozer push*: here, part of the highwall is eliminated by pushing material from upper benches to lower benches and the other areas are backfilled with truck and loader combination.
- *Gravity feed*: here the spoil is hauled by trucks up to the top of the highwall and damped over the edge.

At each of the three sites in this study, the construction procedure followed the *contour haulback* method. Sweigard et al. (2007) identified the four major steps of this construction process as follows:

1. Materials to construct the primary backfill are placed on the future slope area using traditional practices
2. The backfield is compacted as needed to obtain a stable backfill core.
3. Topsoil is dumped to cover the well compacted core material with 4 to 5 feet of loose material (Figure 2-2).
4. Achieve the final grade with the lightest equipment available using the fewest passes possible (Figure 2-2).

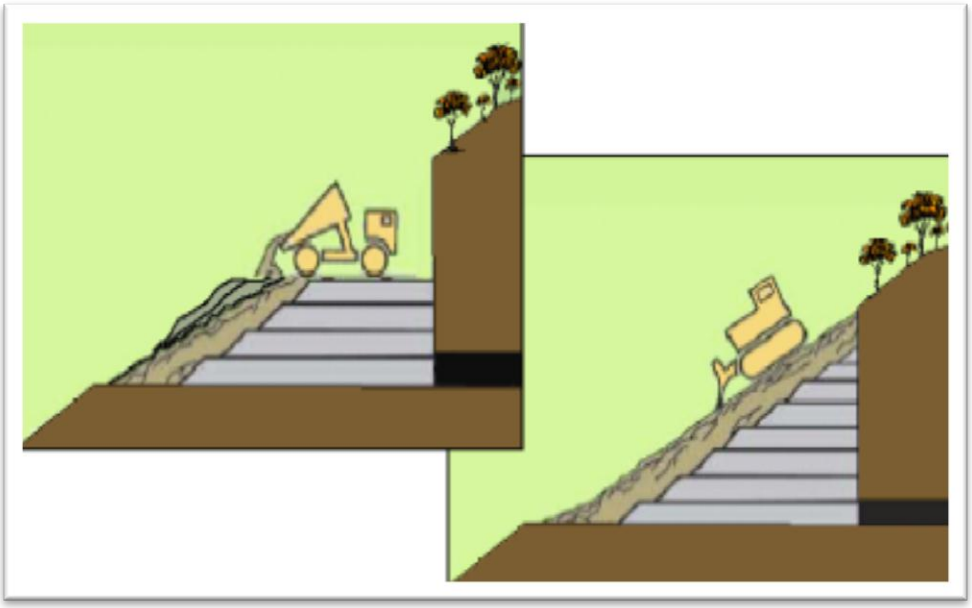

Figure 2-2 Illustration of the steps 3 and 4 of the FRA construction procedure on slopes (Sweigard et al. 2007)

The reclamation process at each of the three sites began with the construction of the denser core material, which at the same time served as a ramp for the construction equipment. Multiple passes of the hauling equipment across the ramp system produces a well compacted core contributing to the global stability of the slope (steps 1 and 2). The spoil material was usually placed in relatively small

quantities using the "end-dumping" process, where the mining trucks dumped the material into close-spaced piles along and across the area in which the slopes were going to be built. The material was then graded, typically with a dozer, and multiple passes of the hauling equipment provided compaction. In general, the design of dozers is such that not much compaction of the materials is obtained – the more significant compaction occurring under the rubber tired wheels of the mining trucks. As the ramp/core was built out to the approximate final contour, the external layer was dumped to provide a 1.2 to 1.5 m (4 to 5 ft.) thick loose layer for tree growth (step 3, Figure 2-2). As possible, the material used for the surface layer was chosen to have a higher sandstone component relative to the gray shale, to provide a better tree growth medium. At the National site, select material comprised of a higher percentage of sandstone had been stockpiled and was later used for the loose top layer.

Final grading (step 4) was accomplished by a dozer moving downslope, with the minimum possible number of passes for final slope dressing. The upslope return of the dozer was usually restricted to established roads/ramps to avoid undesirable compaction of the material. While the compaction process at the three sites was similar, the National and Mountainside sites were developed with multiple passes of the dozer, while it is understood that at Premium the dozer was more closely restricted to one or two passes. In general all of the three research sites presented a rough soil surface after the final grading, which is recommended for the FRA approach (Sweigard et al. (2007). However, because the final layer at all three sites often included boulder-sized material, significant depressions and large rocks were left on the surface of the slope which is a deviation of Sweigard's recommendations for an ideal finished slope. Figures 2-3, 2-4 and 2-5 show the three research sites shortly after they were constructed.

Figure 2-3 Mountainside site after the FRA reclamation process.

Figure 2-4 National site after the FRA reclamation process and during the construction of earthen berms. The tan sandstone surface layer can be seen in the surface materials to the right of the track hoe.

Figure 2-5 Premium site after the FRA reclamation process and during the installation of the weather station.

Experimental Design

Study sites and ground cover

Each site consisted of four different plots that were employed to study runoff and erosion sediment production under four different combinations of ground cover and trees. One of these plots was proposed to be left in bare conditions (no grass was seeded) for use as a control plot, while the other received various ground treatments as applied as part of a research project directed by others (Table 2-1). Because of the timing of the ground cover seeding, and the intensity of the 2009 spring and summer storms, ground cover was not effectively established in the study plots. The hydrology and sediment erosion study components represent bare soil, and data results were composited on the four plots per coal company study site. The hydrology and sediment erosion data generated provide valuable information for OSM engineers using SEDCAD, allowing them to use it for sediment basin design, which reflects the worst-case scenario for a coal mining site.

Each study site included a full weather station to measure climatic and hydrological (rainfall). This weather data also supported the reforestation reclamation study, which include tree planting in addition to cover seeding in March 2009.

Study experimental plots and earthen berms

Per coal mining site four plots were constructed, with earthen berms used to separate the plots. Earthen berms served as physical barriers between plots to isolate run-off and sediment. At the bottom of each plot, the earthen berms formed chevrons (Figure 2-6) to direct the flow towards an H-flume to measure runoff volume. Figures 2-6, 2-7 and 2-8 illustrate the position of the earthen berms at Mountainside, National and Premium site respectively.

Each study plot was constructed by the same FRA protocols, but basic dimensions varied slightly per coal mining site (Table 2.2). The National site plots were slightly longer and narrower than the Premium and Mountainside site plots.

Table 2-1 Summary of ground cover application rates and Percent Cover **(Klobucar et al. 2011)**

Site	Ground Cover	Seeding Rate (lbs/acre)		Average Total Ground Cover, Including Volunteer Species (%)	Average Total Ground Cover, Including Volunteer Species (%)
National		**May 20, 2009**	**June 18, 2009**	**May 3, 2010**	**July 22, 2010**
	Alfalfa	9.50	----	5.24	25.8
	Goldenrod	1.00	----	3.72	----
	Switchgrass	4.50	----	5.73	10.6
	Bare	----	----	4.77	4.8
	Rye (around trees)	----	7.00	----	----
Mountainside		**May 20, 2009**	**June 18, 2009**	**May 3, 2010**	**July 22, 2010**
	Alfalfa	9.50	----	12.20	38.0
	Goldenrod	1.00	----	5.62	----
	Switchgrass	4.50	----	22.56	5.4
	Bare	----	----	8.08	2.8
	Rye (around trees)	----	7.00	----	----
Premium		**May 20, 2009**	**June 18, 2009**	**May 3, 2010**	**July 21, 2010**
	Alfalfa	9.50	----	3.47	21.6
	Goldenrod	1.00	----	0.99	----
	Switchgrass	4.50	----	2.19	9.7
	Bare	----	----	0.26	3.3
	Rye (around trees)	----	7.00	----	----

Table 2-2 Site characteristics of study plots per coal mining site.

Site	Approx. Inclination (degrees)	Approx. Length of Slope, (m)	Approx. width (m)	Total Approx. Width , (m)
Premium	38	30	25 (top)~29 (bot.)	115 (top)~100 (bot.)
Mountain	38	36	25 (top)~22 (bot.)	90 (top)~101 (bot.)
National	37	43	21	84

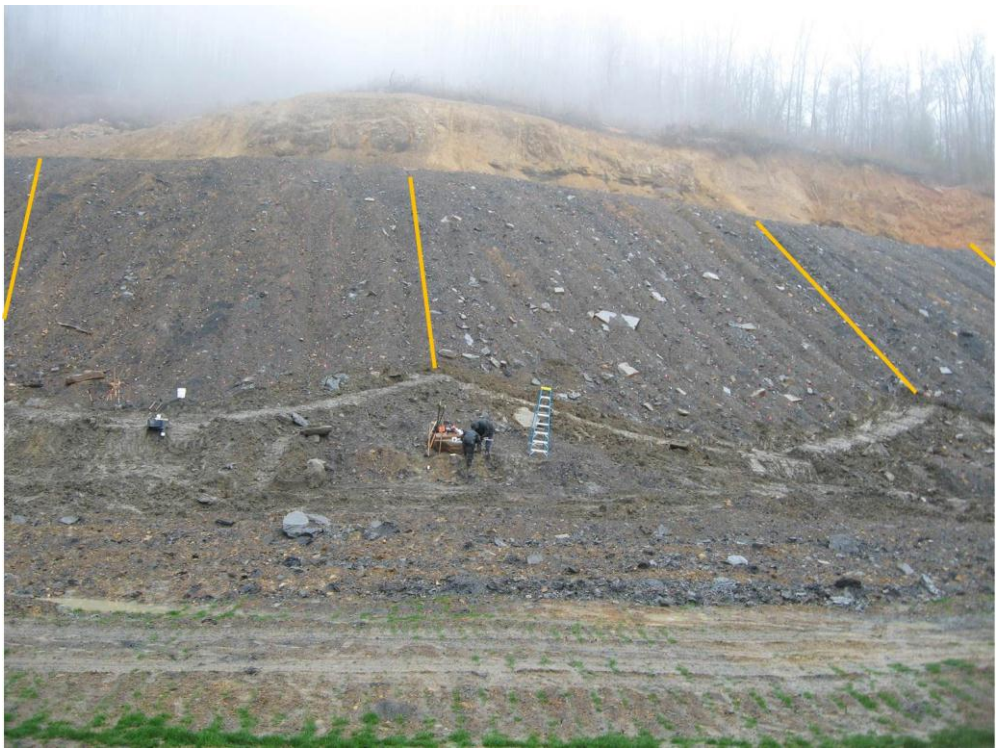

Figure 2-6 Mountainside site subdivided in plots by earthen berms (yellow lines).

Figure 2-7 National site subdivided in plots by earthen berms (yellow lines).

Figure 2-8 Premium site subdivided in plots by earthen berms (yellow lines).

Weather Stations

Each site had a weather station installed (Figure 2-9), where precipitation, solar radiation, wind speed, wind direction, and temperature were obtained in intervals of 15 minutes (Hoomehr et al. 2010). The weather sensors included: a CSI LI-200X pyranometer for solar radiation; a CSI HMP-45C temperature/relative humidity probe; a CSI R. M. Young wind set for velocity and direction; and a CSI TE525 rain gauge.

Runoff flow rates

To record the time history of runoff volume, H-Flumes with an automated Tennessee Fluid Level Indicator (TFLI) (Yoder et al. 1999) were installed at the bottom of each plot at the base of the chevron berm. The TFLI allows for the real-time measurement of the height of water (and hence the volume) flowing through the H-flume for each plot. The H-flume and TFLI provided a measurement for time of concentration (the time between the start of a storm event and runoff recorded at the H flume).

Redundancy was designed into the runoff-sediment yield collection system, where Pinson et al. (2004) collection devices were installed below the H flume and a course sediment trap and also measure runoff volumes. This runoff-sediment collection device is described in more detail next.

Runoff volumes and sediment collection

Runoff and sediment delivered from the plot was directed by the earthen berms towards the H-flume where the time history of flow was measured. The flume outflow (water and sediment) then was routed through a 100-gallon (378.54 lt.) sediment trap tank to capture coarse sediment (Figures 2-10). Large volumes of course sediment were captured in the tank during storm runoff. After which, water and fine

sediment was routed to four 5-gallon (18.93 lt.) buckets. This water-sediment collection device was developed by Pinson et al. (2004) where it divides sediment laden runoff several times yielding a smaller but representative sample that was used for further physical laboratory analysis. The first three buckets, that possessed screw-top lids, were equipped with 22.5^{o} V-notch weirs as flow dividers. The first divider had 12 notches while the 2nd, 3rd and 4th ones have 24 notches (Figures 2-11 & 2-12).

When the first bucket filled completely, the overflowing water-sediment mixture was evenly divided between the divider's notches. Flow from one of the overflowing notches was then collected by the following bucket as illustrated in Figure 2-11. In order to obtain an even division of the flow, the divider crown must be level. Therefore, triangular leveling devices were constructed. They were built of angle iron and stainless steel bolts at each of the three corners of the triangle. The divider system was designed to meet both total runoff volume and peak flow rate expectations. In general, fewer but larger notches can handle a larger peak flow rate; however, fewer notches require more divisions to store the total runoff volume (Pinson et al. 2004). Here, the combination of flow dividers to be used was selected in terms of plot sizes and their steepness, according to Pinson et al. (2004). The peak runoff rates that flow dividers can handle are summarized in Table 2-3.

Figure 2-9 Installation of the weather station at Mountainside site.

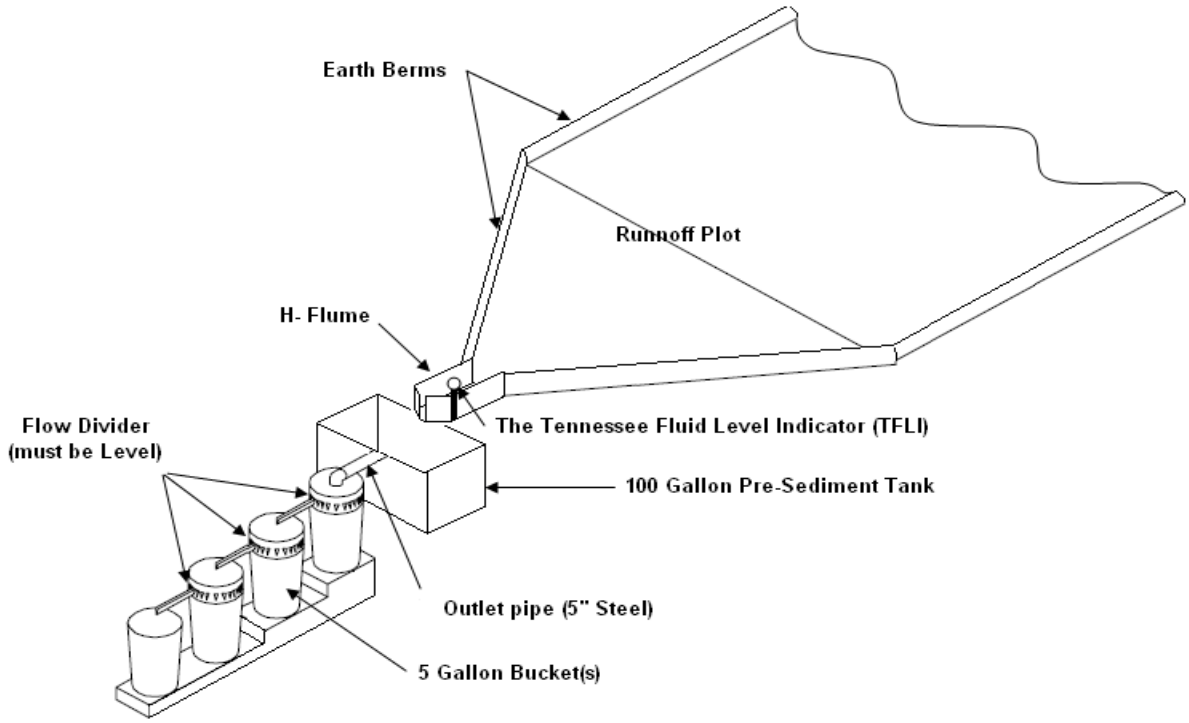

Figure 2-10 Illustration of the runoff and sediment collection system implemented at Mountainside, National and Premium sites (Hoomehr et al. 2010)

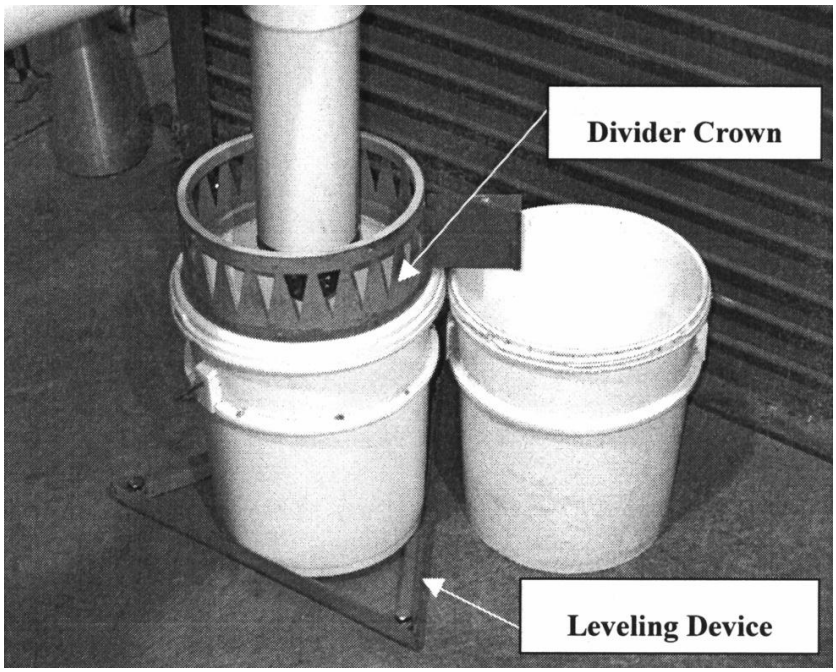

Figure 2-11 Flow divider crown and the leveling device (from Pinson, 2004).

Figure 2-12. Photo showing site arrangement of the divider crown on a bucket.

Table 2-3 Peak runoff rates that flow dividers can handle **(Hoomehr et al. 2010)**

Height of Slot (mm)	Flow Rate per Slot (L/s)	Number of Slots Fitted on the Crown	Total Flow Rate (L/s)
152	2.5	12	29.7
64	0.3	24	6.7

The overflow of the first bucket passed through a 12−notch divider and only one division was passed into a second bucket. The overflow from the second bucket was divided 24 times again, with one division passed into a third bucket. The overflow from the third bucket was divided 24 times again and one division is passed into a fourth bucket, which did not have a divider crown on it. The first divider crown limits the maximum peak runoff to about 30 L/s (1.05 cfs). The corresponding peak runoff rate for the size of our plots is 0.972 cfs. The maximum measurable runoff volume using this system was: 5 + (12×5) + (24×12×5) + (24×24×12×5) = 36065 gal (136,520 L), which corresponds to a runoff depth of 104.9 mm (4.132 in.).

The total delivered sediment mass was calculated as follows: Total calculated mass = mass in 1st bucket + (mass in 2nd bucket × 12) + (mass in 3rd bucket × 24 × 12) + (mass in 4th bucket × 24 × 24 ×12).

Data acquisition and storage

The TFLi water level sensors, employed to monitor runoff volume at each plot, were measured using a 21X Campbell Scientific Inc. (CSI) data logger on plots 1 and 2, while A CSI CR500 datalogger was used to measure the TFLi sensors on plots and 3 and 4. The weather sensors were also recorded by the 21X datalogger.

Sensors were measured every fifteen seconds, though the recording intervals were different. The average flume stage and the total rainfall were recorded every five minutes, while the other sensors were recorded hourly. Power was provided by a 20 watt solar panel and a 115 amp hour sealed lead acid battery. The data were collected via an internet protocol (IP) connection, where A MultiTech cellular modem and a GSM cellular network APN were used to establish a static IP address. Data were collected remotely via the IP connection twice per day.

References:

Hoomehr, S., Schwartz, J. S., Wright, W. C., and Drumm, E. C. (2010). "Surface erosion and sediment yields on steep-sloped coal mining reclamation sites in the Appalachian region." *World Water & Environmental Resources Congress*, ASCE/EWRI, ed.Providence, RI.

Klobucar, A. D., Franklin, J. A., and Buckley, D. S. (2011). "Seeding rates and percent cover at three OSM project sites."

Pinson, W. T., Yoder, D. C., Buchanan, J. R., Wright, W. C., and Wilkerson, J. B. (2004). "Design and evaluation of an improved flow divider for sampling runoff plots." *Applied Engineering in Agriculture*, 20(4), 433-437.

Sweigard, R., Burger, J., Zipper, C., Skousen, J., Barton, C., and Angel, P. (2007). "Low compaction grading to enhance reforestation success on coal surface mines." *Forest Reclamation Advisory No.3.*

Sweigard, R. J., and Kumar, D. (2010). "Filed investigation of best practices for steep slope mine reclamation employing the forestry reclamation approch." *2010 National Meeting of the American Society of Mining and Reclamation*, ASMR, ed., American Society of Mining and Reclamation, Pittsburgh, PA.

Yoder, D. C., Buchanan, J. R., Honea, G. S., Staley, B. F., Wilkerson, J. B., and Yoder, R. E. (1999). "The Tennessee Fluid Level Indicator." *Applied Engineering in Agriculture*, 15(1), 49-52.

Chapter 3 Characterization of Instrumented Sites

Geometry of the sites

Slope angles, profiles and spatial geometry

Preliminary information of slopes angles at each of the three sites was obtained through a Suunto Mechanical Inclinometer model PM-5/360PC during of December of 2008. Slope angles were found between 26 and 30 degrees at Premium site, between 20 and 22 degrees at National site and between 28 and 29 degrees at Mountain site (White 2009).

Validation of the preliminary information was later achieved via a Trimble™ total station topographical surveys conducted during September of 2009 at the Premium site, October-November 2009 at the National site and March 2010 at the Mountainside site. The purpose of these surveys was not only to obtain a more accurate estimation of the slope angles, but also to gather data to geo-reference the instrumented sites allowing an investigation of the spatial variation of material properties. With the acquired topographical information it was possible to generate profile maps for each plot at each site using the ArcMap software (ESRI 2010). The cross sections pass through the midpoint of each plot and they are meant to be representative section of each slope. Figures 3-1 to 3-4 illustrate the slope profile of each plot at the Premium Site fitted with a linear regression curve. Slope profiles for National and Mountainside are included in Appendix A. Absolute slope values of the linear fit range from 0.5347 to 0.5813 which correspond to slopes ranging from 28.1 to 30.2 degrees. The values of the slope based on the Topographic survey are similar to the preliminary values obtained using the Inclinometer device. Therefore, no changes occurred in the slope morphology over the study period; this information agrees with the observation of no slope failures at the sites. Table 3-1 summarizes the geometrical information of the 3 sites obtained from the topographical survey.

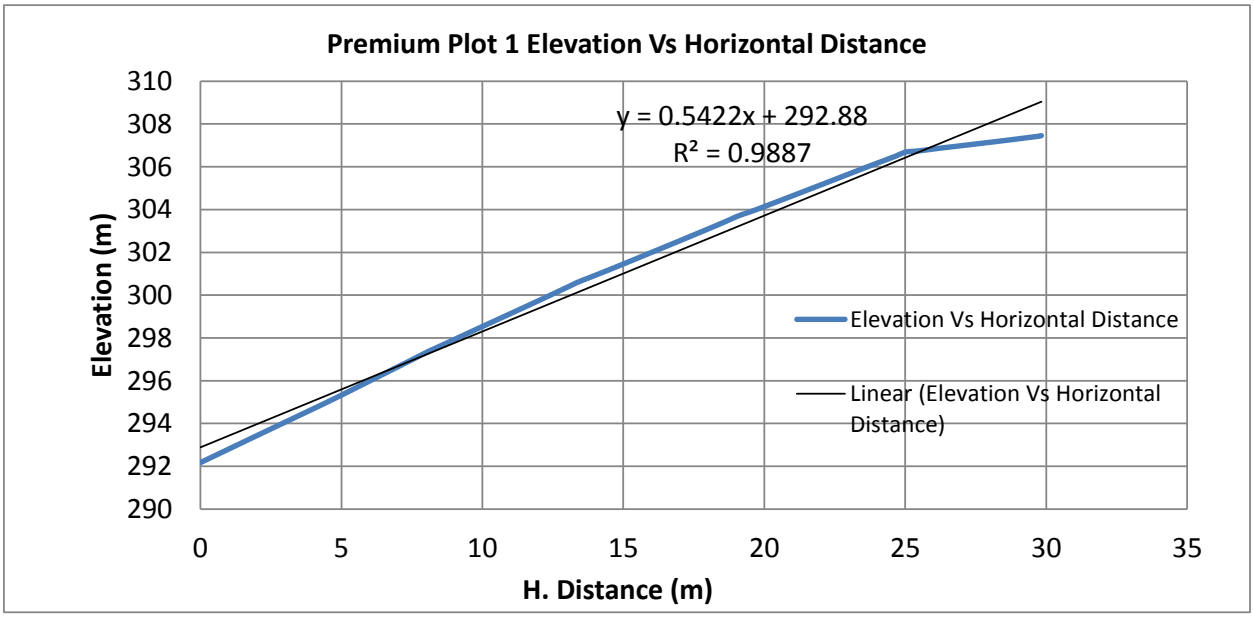

Figure 3-1 Slope profile. Plot 1 at Premium site (slope angle = arctan (0.5422) = 28.5˚)

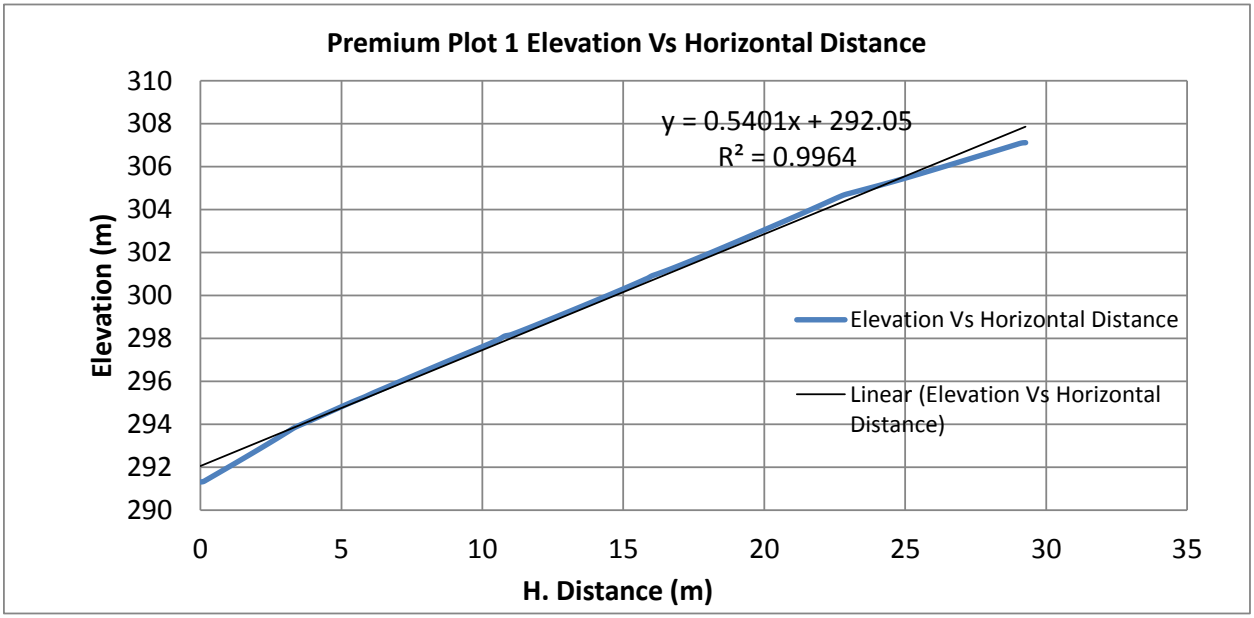

Figure 3-2 Slope profile. Plot 2 at Premium site (slope angle = arctan (0.5401) = 28.4˚)

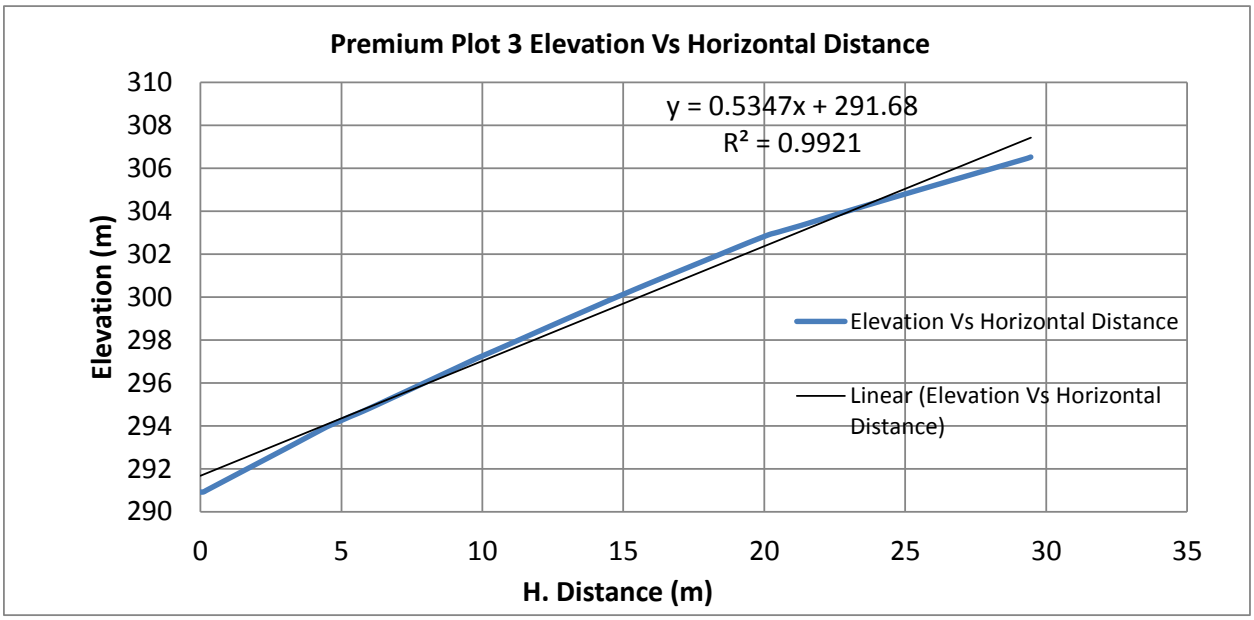

Figure 3-3 Slope profile. Plot 3 at Premium site (slope angle = arctan (0.5347) = 28.1˚)

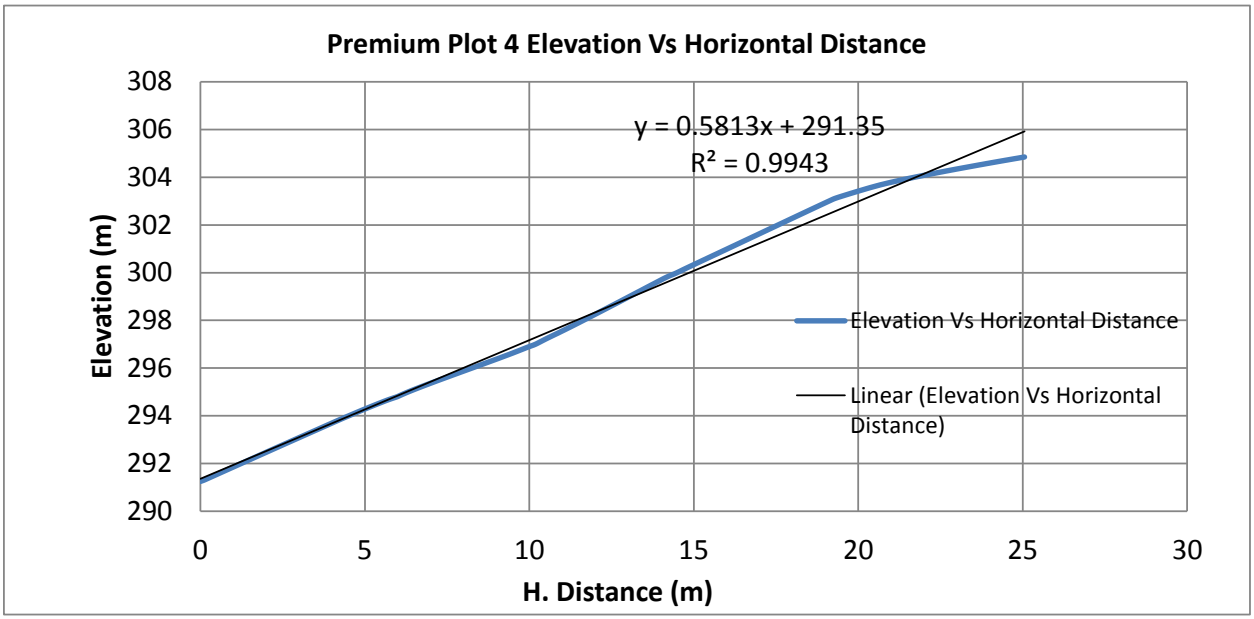

Figure 3-4 Slope profile. Plot 4 at Premium site (slope angle = arctan (0.5813) = 30.2˚)

Table 3.1 Slope length, width and inclination angle for Premium, National and Mountainside sites

Site	Plot	Angle of Slope, Degrees	Length (m)	Width (m)	
				Top	Bottom
Mountainside Site	1	27	48.8	21.5	21.5
	2	29	46.0	21.5	25.0
	3	28	44.6	25.1	22.4
	4	27	42.3	25.7	23.3
National Site	1	21	47.6	23.1	19.7
	2	20	48.4	22.1	25.3
	3	19	49.2	23.5	28.4
	4	21	48.2	20.8	28.2
Premium Site	1	28	33.5	24.8	21.7
	2	28	33.3	28.8	27.2
	3	28	33.3	27.7	25.3
	4	30	28.5	31.0	25.7

Map of spatial distribution of slope angles

Using the topographical survey data, a spatial distributional slope map of the Premium site was constructed using ArcMap software (Figure 3-5). Elevation data was interpolated and, after using a raster feature, the average slope inclination was calculated every 1 square foot. The selected interpolation method was the spline function technique, which is indeed a series of cubic functions adjusted to better fit the data. This is a regression tool that fit different functions for different intervals along the independent variable. The general idea here is to identify localized steep zones where failure may initiate. In Figure 3-5 green colors represent zones with gentle slope angles while red colors show steeper slopes.

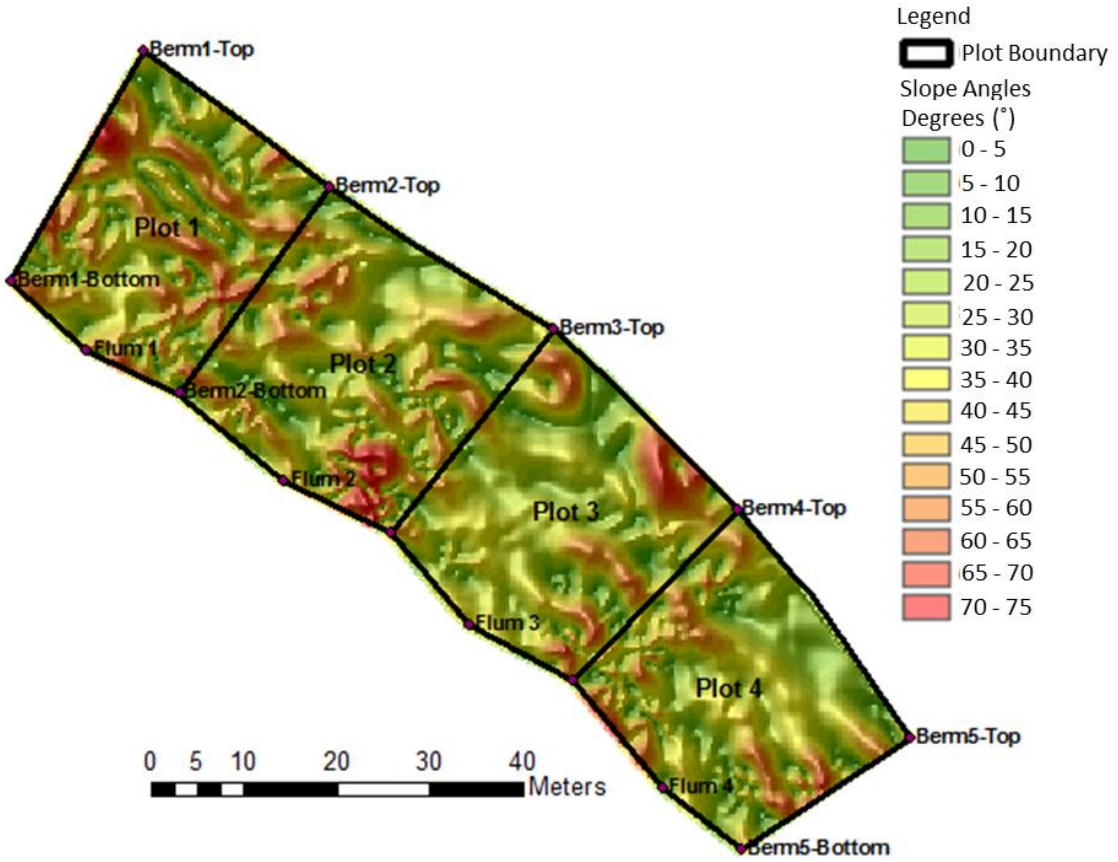

Figure 3-5 Slope angle distribution over the four plots at Premium site

Soil unit weight

Some early data on soil characterization of the three sites was reported by White (2009), where a number of unit weight measurements were made by replacement methods (water and sand cone) and Nuclear Density gauge (NDG). It was demonstrated that the NDG measurements were an effective means to measure unit weight over the slope with highly variable unit weights. However, those NDG measurements were localized in a specific area of the slope. Therefore, extensive NDG data was collected along the complete slope length at each site between June and August, 2009.

The nuclear density gauge

The Nuclear density gauge device used for the data collection is a Troxler 3411 B, which has two different nuclear sources: a) Cesium-137 which emanates gamma rays and b) Americium-241:Beryllium source which emanates alpha particles (Troxler Electronic Laboratories Inc. 1997). Figure 3-6 illustrates the NDG device.

This instrument has the ability to determine the bulk wet unit weight and moisture content independently. Wet unit weight is determined by the emission of gamma waves from the source into the soil (Randrup and Lichter 2001). Moisture content is determined as the amount of reflected neutrons hitting hydrogen in the soil moisture (Randrup and Lichter 2001). Dry unit weight is

determined indirectly from wet unit weight and moisture content measurements. The Cesium-137 source has been mounted approximately 5 cm from the end of the rod which is inserted into a vertical drill hole. The vertical drill hole was created by driving a drill rod into the soil with a hammer. Even though density measurements can be made from the surface, more accurate results are obtained when the source rod is inserted into the soil (Troxler Electronic Laboratories Inc. 1997). As soon as the source is inserted, gamma rays penetrate the soil. The beam is either absorbed by the material, redirected with a lower speed or it penetrates the material without deflection or absorption (Randrup and Lichter 2001). The amount of gamma radiation reflected is counted by the detector (placed near to the edge of the gauge base); the denser the soil, the fewer reflected rays are counted by the detector (Randrup and Lichter 2001, Troxler Electronic Laboratories Inc. 1997). Wet unit weight has to be determined after a calibration procedure employing the calibration block provided by the manufacturer; here, the nuclear count rate over this block is related to its known density and then translated to reading of wet unit weight.

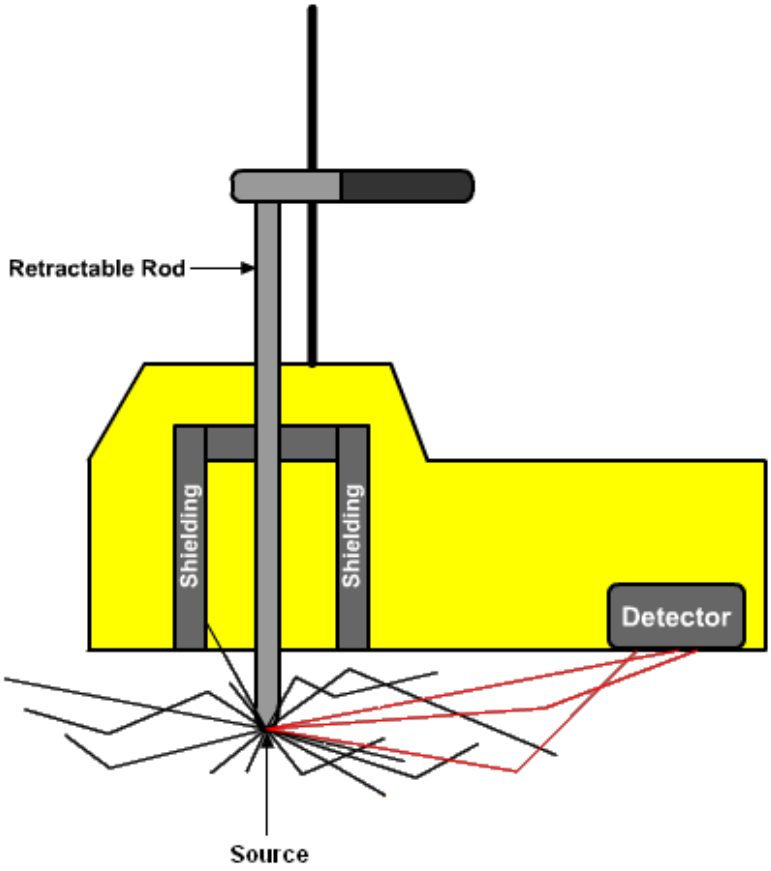

Figure 3-6 Nuclear Density Gauge Illustration (White 2009)

The moisture content is determined by detecting the hydrogen in a 2-ft sphere around the gauge (Farrag et al. 2005). The Americium-241 bombards the Beryllium producing a fast emission of neutrons that hit hydrogen atoms in the soil (Troxler Electronic Laboratories Inc. 1997). After the collision, energy dispassion occurs and therefore, a reduction in the velocity of the neutrons takes place. The velocity of these particles can be measured and related with the calibration count obtained using the calibration block.

The accuracy of the Nuclear Density Gauge in the field depends on its successful calibration and operation; a planar soil surface needs to be provided for settling the device in order to avoid air interchange between the gauge base and the soil surface. Also, periodical calibration needs to be executed, since the radioactive sources decay over time (Troxler Electronic Laboratories Inc. 2006). The use of the apparatus requires training by a licensed technician and strict regulations regarding storage and transportation must be followed.

The presence of singularities inside the soil mass (like large rock fragments and voids) may also affect the accuracy of the Nuclear Density Gauge. Density calculation is based on the velocity travel of gamma rays through the material present between the source and detector. If anomalies appear in the travel way of the beam, inaccurate measurement is yielded; large particles may suggest a higher unit weight while voids may suggest lower unit weight than actually exists.

Field procedure

For each of the three field sites, the unit weight of the loose surface layer was determined using a Troxler 3411 B Nuclear Density Gauge device. In order to avoid disturbance of the seeded plots, all unit weight measurements at each site were obtained along the bare plot. These measurements are meant to be representative of the remaining 3 plots at each site.

A randomized systematic sample technique was used for the data collection to reduce data tendency or bias in the in measurements. Figure 3-7 illustrates several types of sampling techniques (Sweigard et al. 2007). In this study, the systematic random method was used with the bare plot divided into multiple squares of 3 m side length. Bulk dry unit weight, bulk wet unit weight and moisture content were measured at random locations inside each square. It is important to mention that even though the sample location was usually randomly selected inside the square, there were occasions in which the presence of large rocks restricted the selection of the measurement location to a specific place inside the square. Figure 3-8 and 3-9 Illustrate the systematic random sample technique implemented at National Site.

Once the location inside the square was selected, the soil surface was cautiously carved to obtain a planar surface to settle the nuclear gauge device. Then, a vertical hole was driven, the source rod inserted into the hole, and the measurement was taken usually at 12 in. depth (maximum length of the source rod). Sometimes the presence of hard rock (generally Shale) forced a more shallow measurement at 8 - 10 in. depth. The obtained unit weights and moisture readings are intended to be representative of the material within the 3 m by 3 m sample square, and the overall randomized systematic measurements are intended to be representative of the unit weight distribution over the four plots.

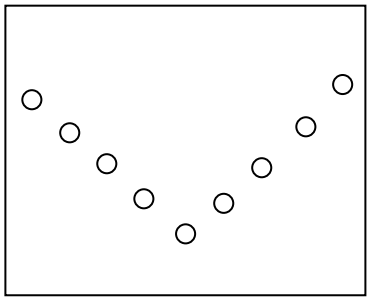

Judgmental
Sample numbers tend to be small.

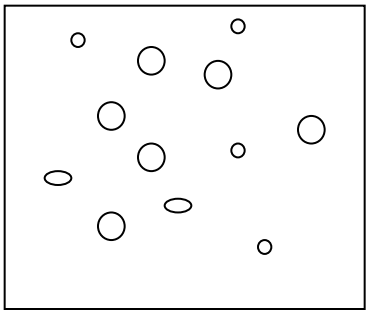

Random
Sample numbers tend to be large.

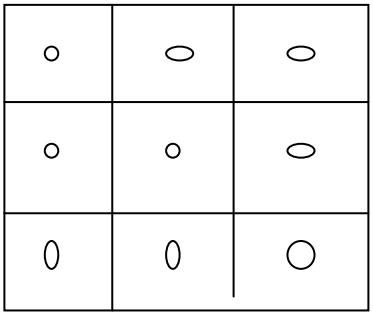

Systematic
Sample numbers tend to be less than Random.

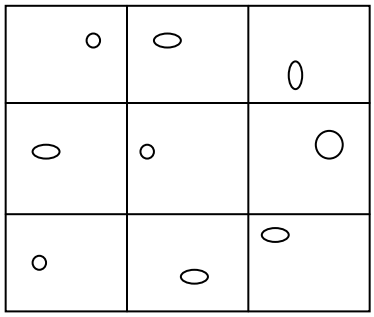

Systematic Random

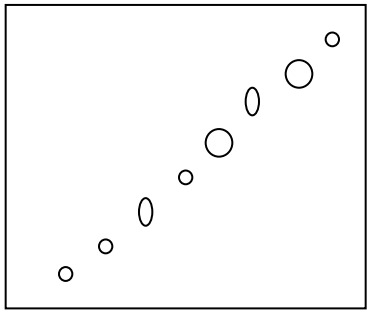

Systematic Transect
Sample numbers tend to be less than Systematic Random.

Figure 3-7 Types of sample techniques used for statistical analysis (adapted from Sweigard, Badaker and Hunt, 2007)

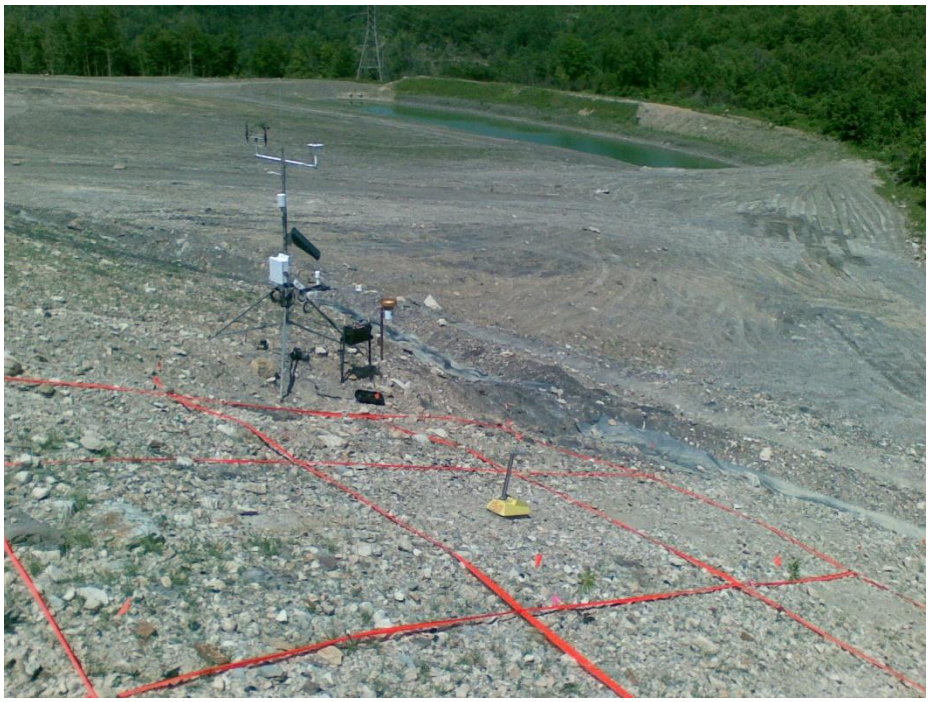

Figure 3-8 Illustration of the systematic random sample technique at National site

Figure 3-9 Nuclear Gauge settled and ready to start measuring at National site

Results

Table 3-2 shows the values of bulk dry unit weight, bulk wet unit weight and moisture content obtained at the Premium site. The results for National and Mountainside are reported in Appendix A. The tables have been organized in order to provide a visual understanding of the work done in the field; every square in the table represents a real 3 m. by 3 m. square made in the field. For example, the square in the upper right corner represents the field square at that position when facing the slope. The measured spatial distribution of the dry unit weight of the surface layer in the bare plot at Premium site is graphically illustrated by Figure 3-10. Similar interpolation maps were created for National and Mountainside sites (in Appendix A), using the spatial analysis tool inside the ArcMap software. A Kriging interpolation method was employed taking into account the information of 10 neighbors for zones around the center of the plot and at least 4 neighbors for areas located near the edges.

Table 3-2 Values of bulk dry and wet unit weights and moisture content measured within each 3 m by 3 m sampling area at the Premium site

		Top of the Plot						
	Sample Location	Column A	Column B	Column C	Column D	Column E	Column F	Column G
Depth (m)	Row 1	0.3048	0.3048	0.2286	0.3048	0.3048	0.3048	0.3048
WD (kN/m3)		20.14	19.84	19.16	16.92	17.29	17.06	17.67
DD (kN/m3)		17.10	17.28	16.71	14.42	15.03	14.24	15.33
M%		17.7	14.8	14.7	17.3	15.1	19.8	15.3
Depth (m)	Row 2	0.3048	0.3048	0.3048	0.3048	0.3048	0.3048	0.3048
WD (kN/m3)		18.16	17.69	18.10	18.14	18.99	17.87	19.23
DD (kN/m3)		15.80	15.58	16.48	15.96	16.95	15.58	15.50
M%		14.9	13.5	9.8	13.7	12.1	14.7	24.0
Depth (m)	Row 3	0.3048	0.3048	0.3048	0.3048	0.3048	0.3048	0.254
WD (kN/m3)		18.21	16.68	18.96	19.53	19.46	20.63	20.15
DD (kN/m3)		16.16	14.04	16.77	17.83	17.07	18.83	18.38
M%		12.6	18.8	13.0	9.5	14.0	9.5	9.7
Depth (m)	Row 4	0.3048	0.254	0.3048	0.3048	0.254	0.3048	0.3048
WD (kN/m3)		18.93	20.88	19.26	17.29	18.25	19.75	19.89
DD (kN/m3)		16.77	18.61	17.54	15.50	16.22	17.47	17.73
M%		12.8	12.2	9.8	11.6	12.5	13.1	12.1
Depth (m)	Row 5	0.3048	0.3048	0.3048	0.3048	0.3048	0.3048	0.3048
WD (kN/m3)		19.68	19.24	17.37	18.58	19.23	19.29	18.35
DD (kN/m3)		17.81	16.57	14.49	15.83	17.18	17.12	16.27
M%		10.5	16.1	19.8	17.4	11.9	12.7	12.8
Depth (m)	Row 6	0.3048	0.2794	0.2794	0.3048	0.2921	0.3048	0.3048
WD (kN/m3)		19.76	17.80	17.06	18.58	19.05	19.81	18.63
DD (kN/m3)		16.85	14.81	15.06	14.98	16.33	17.64	16.29
M%		17.3	20.2	13.3	24.0	16.7	12.3	14.4
Depth (m)	Row 7	0.3048	0.3048	0.3048	0.3048	0.2794	0.3048	0.2794
WD (kN/m3)		20.47	19.54	17.70	17.48	19.12	17.78	14.95
DD (kN/m3)		17.94	17.17	14.54	14.32	15.78	15.63	13.32
M%		14.1	13.8	21.7	22.1	21.1	13.8	12.3
Depth (m)	Row 8	0.3048	0.3048	0.3048	0.3048	0.2794	0.2286	0.2667
WD (kN/m3)		18.32	19.13	18.47	18.25	16.27	14.75	18.83
DD (kN/m3)		15.82	16.49	15.75	15.80	14.81	12.95	17.25
M%		15.8	16.0	17.3	15.5	9.9	13.8	9.2
Depth (m)	Row 9	0.3048	0.3048	0.3048		0.3048	0.3048	0.3048
WD (kN/m3)		19.21	20.23	16.63		17.84	16.57	17.81
DD (kN/m3)		16.71	18.06	13.79		16.66	14.68	16.13
M%		15.0	12.0	20.6		7.1	12.8	10.4
		Bottom of the Plot						

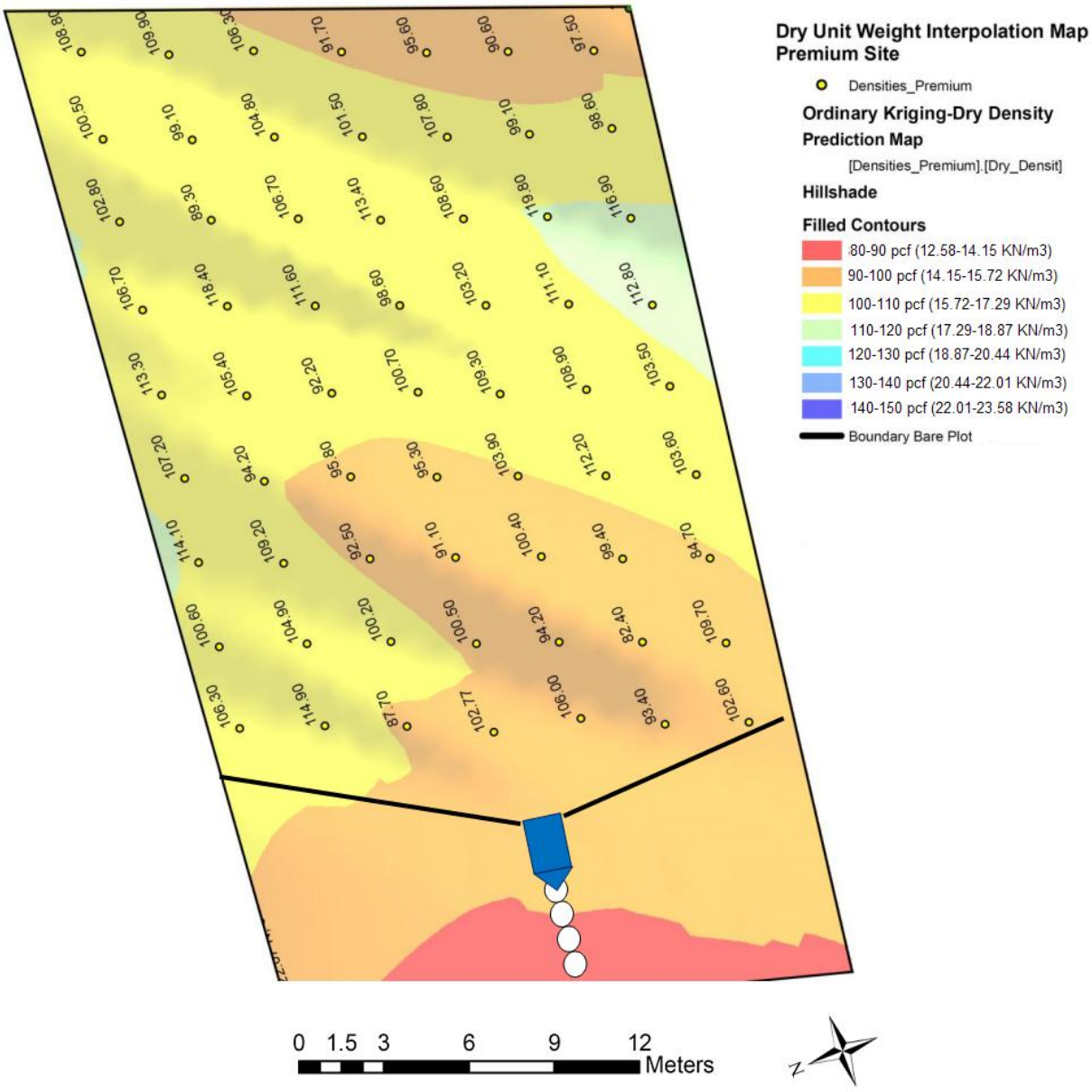

Figure 3-10 Spatial distribution of the dry unit weight of the looser layer along the bare plot in Premium site (numerical results on figure are shown in pcf)

At the Premium site, the maximum observed dry unit weight was 18.83 kN/m3 (119.86 pcf) while the minimum was 12.95 kN/m3 (82.43 pcf). Similarly, the maximum and minimum values observed for dry unit weights were 21.44 kN/m3 (136.47 pcf) and 14.56 kN/m3 (92.68 pcf) for National and 22.75 kN/m3 (144.81 pcf) and 14.94 kN/m3 (95.10 pcf) for Mountainside. Figure 3-10 suggests that unit weights at the Premium site tend to decrease toward the bottom of the slope. A similar trend was observed at National site, while at Mountainside site the unit weights were higher at the bottom of the slope. This agrees with the observation of substantial number of large (> 1 meter diameter) boulders in the bottom third of the slope with a thinner layer of surface cover at Mountainside. The unit weights of Shale and Sandstone

usually range from 23 to 27 kN/m3 (150 to 170 pcf), which are close to the measured unit weight values in the bottom third of the slope at Mountainside.

Certainly, the presence of large pieces of rock affects the measurement of the unit weight. As it was discussed before, NDG reports the unit weight of the material only present between the source and the detector. The presence of large rock fragments on the travel path of the beam may yield inaccurate higher unit weight values. Therefore, while the use of a nuclear device may be appropriate for determining overall unit weights for stability purposes (assuming that systematic random procedure minimizes the appearance of anomalies during measurements), it may not be accurate for the calculation of soil void ratio, at least if no bound or error is estimated and reported.

Statistical analysis of the data

Using the Jump 8.0 software (SAS Institute Inc. 2008), a 95% confidence interval for the true mean wet and dry unit weights was computed for each of the three sites. This analysis gives some degree of confidence about the true estimate of the mean and also gives a range of possible mean estimates considering the error bound.

The selection of the statistical tool to be used in the analysis was based on the actual distribution of the data. Figures 3-12, 3-13 and 3-14 show histograms and normal quantile plots of the wet unit weights for Premium, National and Mountainside. Due to the linear nature of the relationship between wet and dry unit weight, these plots are similar to those for dry unit weight reported in Appendix A.

The normal quantile plot is a visual tool that allows the detection of non-normality in the data. If a variable is normally distributed, the normal quantile plot approximates a diagonal straight line (SAS Institute Inc. 2008). Figure 3-11 graphically explains symbols inside the outlier Box Plot that is provided in Figures 3-12 to 3-14 (SAS Institute Inc. 2008). The box itself shows the 25th, 50th and 75th percentile, which represent the values where the 25, 50 and 75% of the data is accumulated. The horizontal extremes of the diamond show the mean while the vertical extremes show the 95% confidence interval for the true average mean. The red bracket along the edge of the box corresponds to the shortest half defined as densest 50% of the observations (Rousseeuw and Leroy 1987).

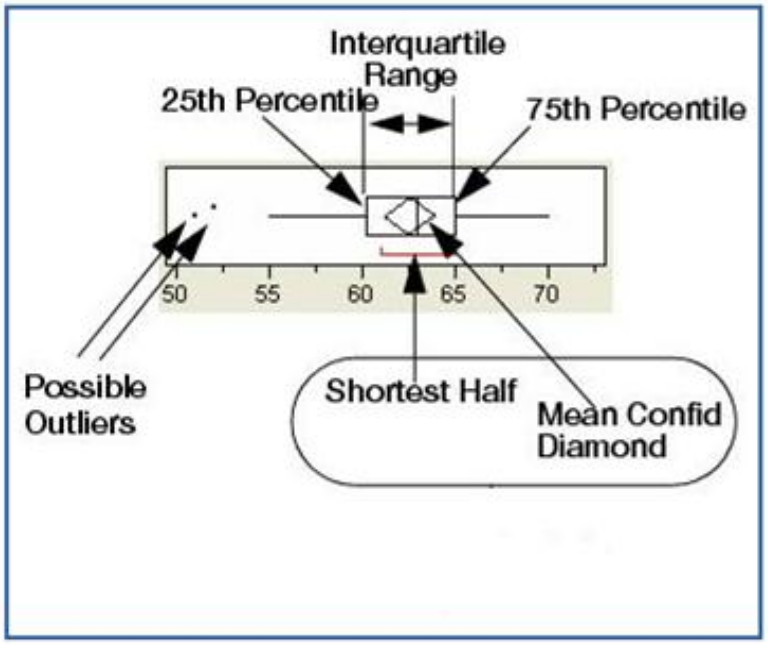

Figure 3-11 Symbols inside the outlier Box Plot (SAS Institute Inc. 2008)

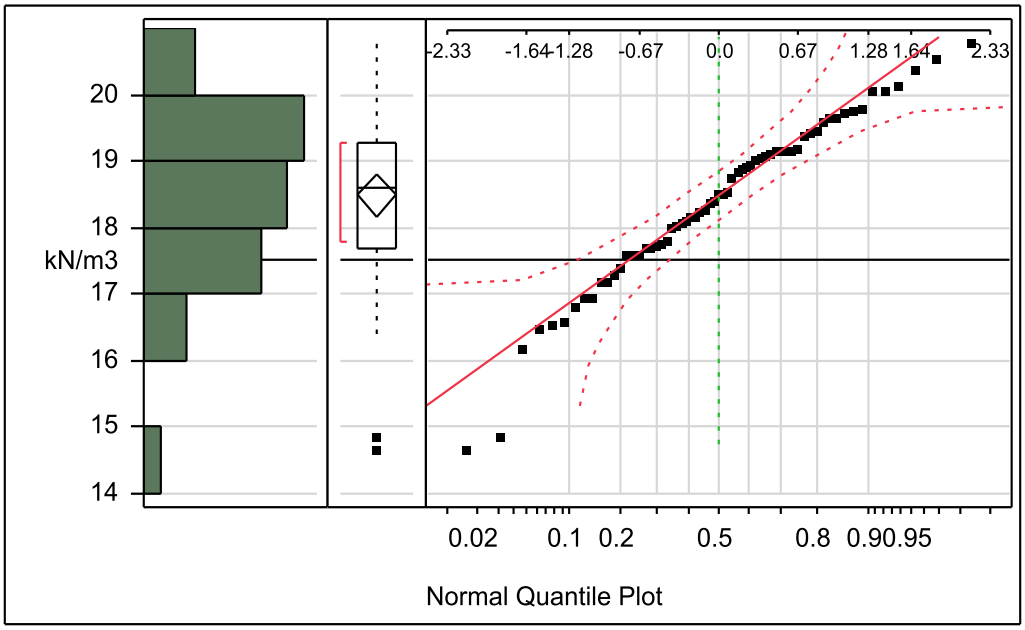

Figure 3-12 Histogram and Normal Q-Q plot of wet unit weight (kN/m3) for the Premium site

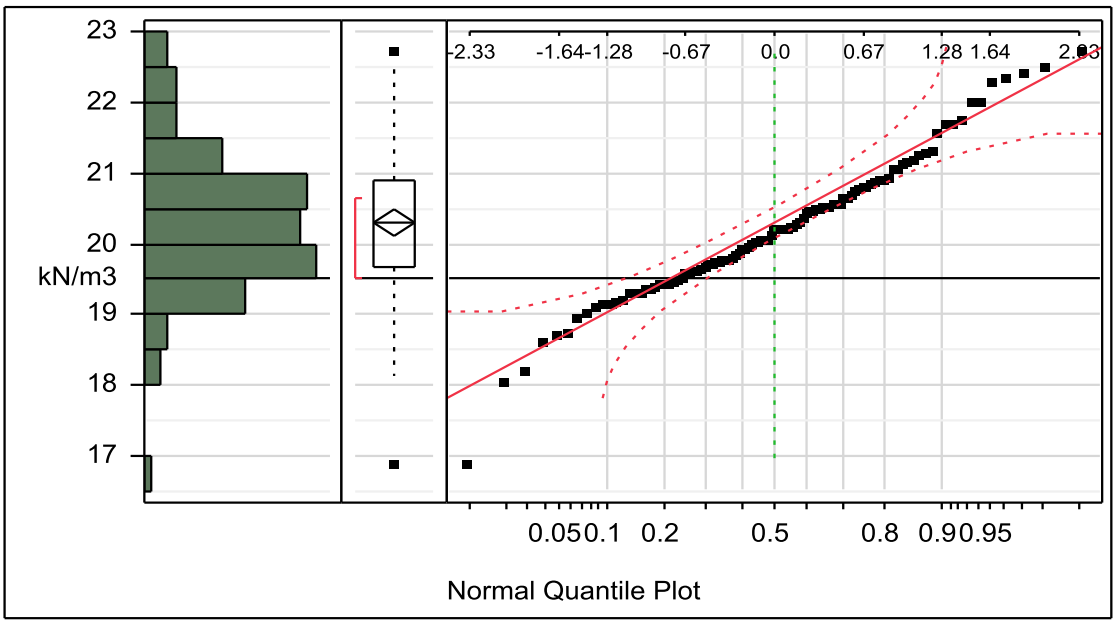

Figure 3-13 Histogram and Normal Q-Q plot of wet unit weight (kN/m3) for the National site

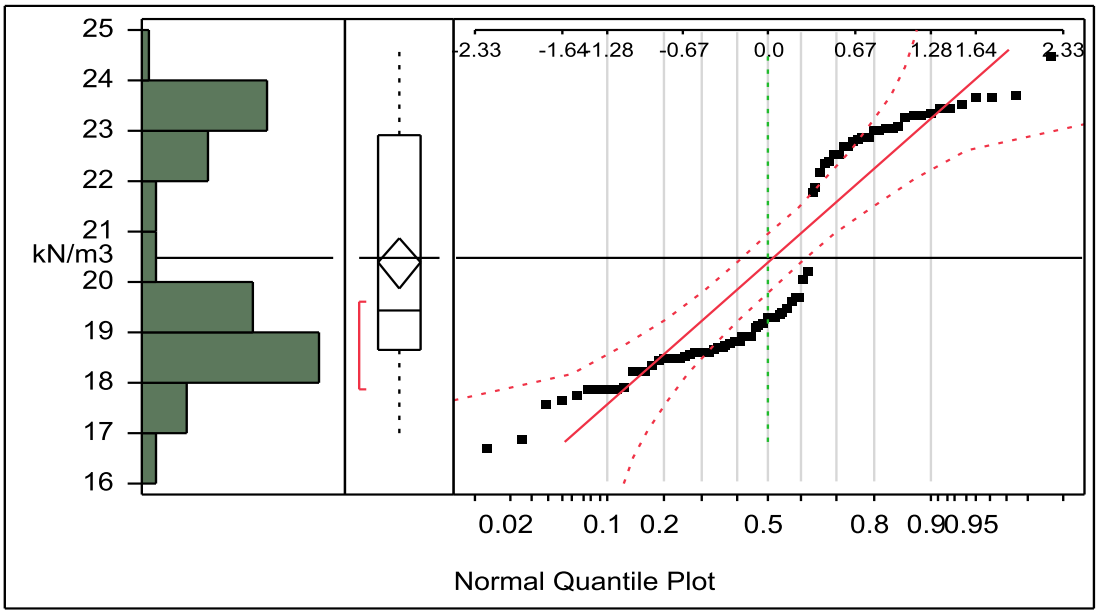

Figure 3-14 Histogram and Normal Q-Q plot of wet unit weight (kN/m3) for the Mountainside site

Plots above show that wet unit weight values measured in Premium and National sites are very close to be normally distributed. In fact, skewness values are -0.6 for Premium and 0.08 for National; The closer the skewness to zero, the closer the data to a normal distribution. Therefore, the use of a t-statistic tool for determining confidence intervals seems to be appropriate for those cases. The principal advantage of a t-statistic distribution over a normal distribution is that no assumptions of known standard deviation needs to be made; in other words t distributions account for unknowns standard deviations, which in reality the case is.

On the other hand, the normal quantile plot for Mountainside shows a distribution that does not follow a straight line and it is indication of non-normality. Nevertheless, the reported skewness is 0.4 which is a value that indicate closeness to normality. This contradiction seems to be a result of the symmetric deviation of the data from the straight line, which compensates for effects of negative and positive skewness. Then, the use of a t based tool is reasonable in this case too and non-parametric tools are not needed. Table 3-3 summarizes the means, standard deviations and 95% confidence intervals for wet and dry unit weights for the three sites. It is these mean values that were used in the stability analyses in Chapter 4.

Table 3-3 Means, standard deviations and 95% confidence intervals for Wet and Dry Unit Weights for Premium, National and Mountainside

Sites	Unit Weight	Mean kN/m^3	Mean pcf	Standard Deviation kN/m^3	Lower 95% CI for the Mean, kN/m^3	Upper 95% CI for the Mean, kN/m^3
Premium	Dry	16.16	102.86	1.31	15.83	16.49
	Wet	18.48	117.63	1.27	18.16	18.80
National	Dry	18.53	117.95	0.97	18.33	18.71
	Wet	20.30	129.22	1.00	20.10	20.49
Mountainside	Dry	18.58	118.27	2.20	18.10	19.10
	Wet	20.39	129.79	2.22	19.90	20.90

For the first row of Table 3-3 the interpretation is the following: “we are 95% confident that the true average dry unit weight for Premium site is found inside the interval from 15.83 kN/m3 to 16.49 kN/m3”. The interpretation for the remaining confidence intervals can be constructed in the same way.

One of the limitations that confidence intervals have is that the interpretation is an inference about the moment in which the data is collected and it cannot be extrapolated to future process. In cases where studies are enumerative (well defined and unchanging population), confidence intervals provide useful information, but when the interest is a certain process or the focus is on the future, confidence intervals are not satisfactory, and prediction or tolerance intervals should be employed.

For our statistical analysis of unit weight values, confidence intervals provide the essential information for further analysis of the constructed slope using low compaction grading technique. On the other hand, if the interest is to know what future range of unit weights each site will have on average, tolerance intervals computation is strongly suggested. The application of this tool allows the prediction of the average unit weight for the next reclaimed slope to be constructed using low compaction grading technique in each site. Table 3-4 summarizes 90% tolerance (80% coverage) intervals for wet and dry unit weights for the three sites.

Table 3-4 90% Tolerance (80% coverage) intervals for wet and dry unit weights for Premium, National and Mountainside

Sites	Unit Weight	Lower 90%/0.8 T.I. for the Mean, KN/m^3	Upper 95% 90%/0.8 T.I. for the Mean, KN/m^3	Lower 90%/0.8 T.I. for the Mean, pcf	Upper 95% 90%/0.8 T.I. for the Mean, pcf
Premium	Dry	14.24	18.07	90.64	115.02
	Wet	16.62	20.35	105.79	129.54
National	Dry	17.15	19.91	109.17	126.73
	Wet	18.89	21.71	120.24	138.19
Mountainside	Dry	15.48	21.70	98.54	138.13
	Wet	17.19	23.60	109.42	150.22

For the first row of Table 3-4 the interpretation is the following: “we are 90% sure that this interval (14.24 KN/m3, 18.07 KN/m3) has at least 80% of probability of containing the average dry unit weight for the next reclaimed slope to be constructed using low compaction grading technique in Premium site.” The interpretation for the remaining tolerance intervals can be constructed in the same way.

Comparison of results with previous work

In a previous characterization of these three sites made by White (2009), a series of tests were used to estimate the unit weight of the soil. Water replacement and auger replacement method were used to determine bulk unit weight at random places on the four plots at each site, while a nuclear density gauge was used for measurements in a 5 meter grid in a very specific location on the slope.

To graphically evaluate differences of unit weights between NDG measurements and both replacement methods, plots comparing mean unit weights are presented. NDG values reported by White (2009) are not included in this comparison, because they were collected in a specific zone along the slope (usually close to the bottom) and according to the distributional maps unit weights tend to vary along the slope at each site. Figures 3-15 and 3-16 show a comparison of the average dry unit weight and wet unit weight based on replacement and NDG methods for each site.

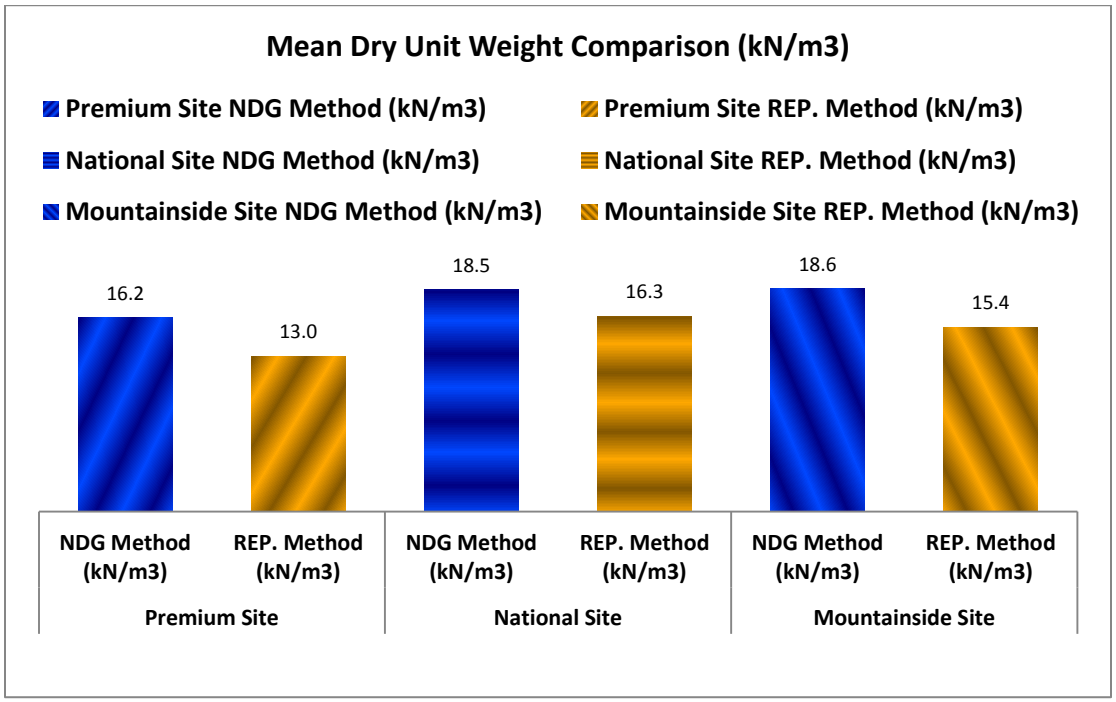

Figure 3-15 Comparison of average Dry Unit Weight at each site

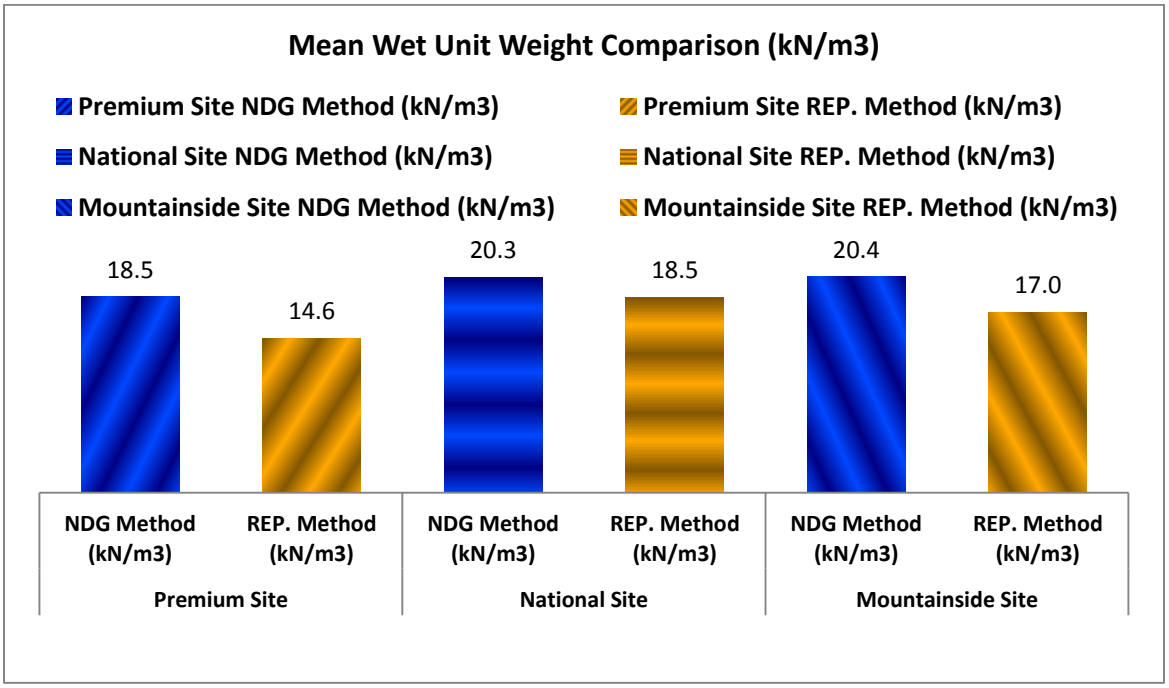

Figure 3-16 Comparison of average Wet Unit Weight at each site

From the figures above it may be concluded that NDG device gives slightly higher average unit weights than replacement methods for all three sites. In the literature, results of similar work seem to yield contradictory results. Randrup and Lichter (2001) measuring compaction in construction sites found that Nuclear Density Gauge device tend to give on average 10% higher measurements than core sampling,

but no big rock elements were present in the measured layers. On the other hand, Tesarik and McKibbin (1999) working on mine waste dumps found that NDG device gives approximately 5 pcf (0.8 kN/m3) lower unit weight measurements than water replacement method. The explanation for this phenomenon may be found in the fact that both replacement methods do not take into account the effects of large rock elements that are randomly incrusted in the looser soil layer when the mine spoil material is dumped. The previous discussion concluded that those large elements affect nuclear gauge readings if they are found in the beam path between the source and the receiver. Even though replacement methods seem to be a more precise way to measure soil unit weights, they may ignore the presence of large rock particles that are inherent in mine spoil material; therefore it is suggested that the NDG is a reliable method for determining soil unit weight in waste mine material, for any type of stability analysis. Nevertheless, this technique, as any type of sampling method, requires a sufficient number of measurements to truly represent the in situ soil behavior.

On the other hand, measurements of dry unit weight obtained through replacement methods may be preferable for calculation of void ratio and soil porosity due to better representation of the soil matrix. Figure 3-17 shows a linear regression model of average dry unit weights obtained using Nuclear Density Gauge and Replacement Methods for each site. Regression represents the average Y as a function of X; in other words every curve fit by a regression analysis is done by averaging Y, which is different than averaging X. Therefore, the selection of the horizontal axis needs to be made in terms of accuracy of the available data or in terms of variables that we have control on. For this analysis measurements obtained through replacement methods were placed on the X axis due to their precision, and measurements obtained using NDG were placed on the Y axis.

The linear regression model in Figure 3-17 reported a R^2 coefficient equal to 0.8286, which means that almost 83% of the variation is explained by the model, and it supports the decision of using a simple linear regression model. The yielded linear relationship between mean dry unit weight by NDG and mean dry unit weight by replacement methods is:

$$NGD\ Method\ =\ 0.84 * REP.\ Methods \tag{3-1}$$

Solving for replacement method the equation becomes:

$$REP.\ Methods\ =\ 1.19\ *\ NGD\ Method \tag{3-2}$$

This equation may be useful for calibrating any NDG measurement in terms of replacement methods when porosity and soil void ratio need to be calculated indirectly from dry unit weight measurements. This equation should be used carefully and the engineering criteria should prevail over any result obtained from it.

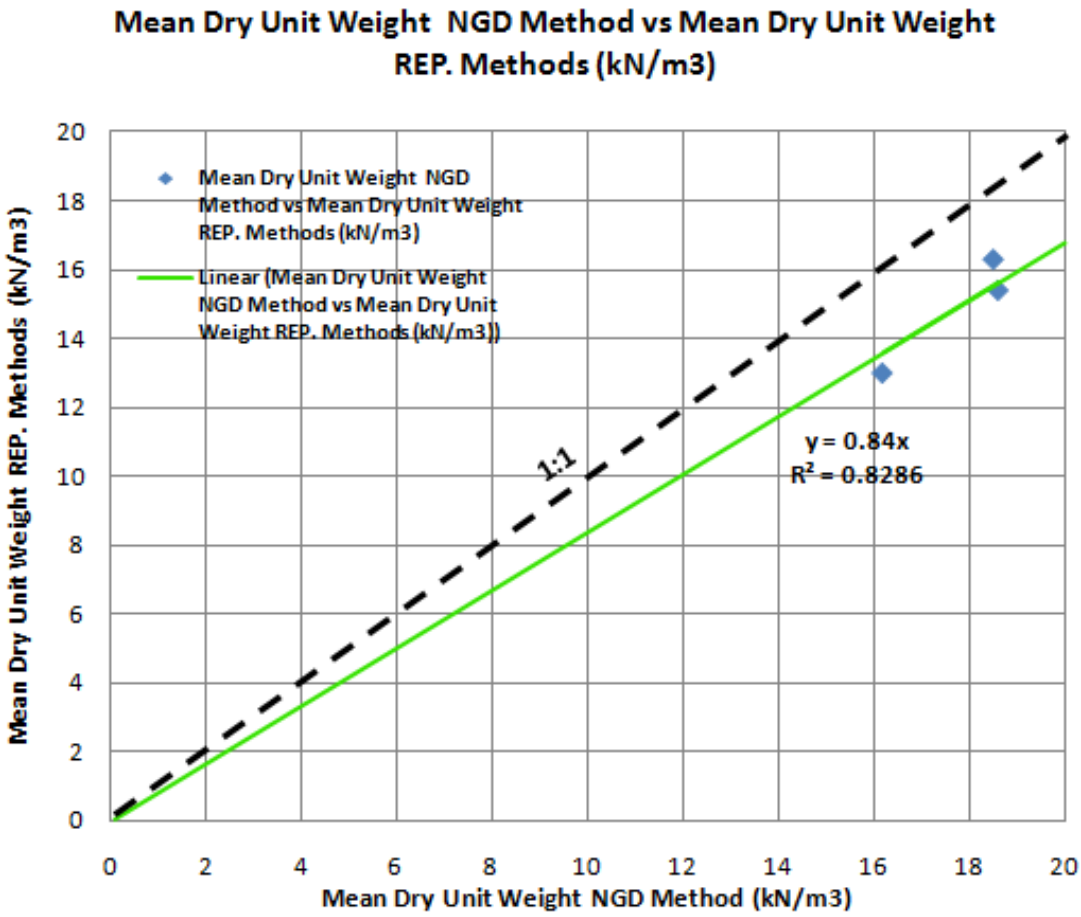

Figure 3-17 Linear regression model of average dry unit weights obtained using NDG and replacement methods for each site

Particle size analysis, index tests, and classification

Representative samples of the soil in every plot at each site were obtained. All samples were taken from a depth of at least 300 mm to avoid the effects of loss of fines from erosion or changes due to weathering of the shale materials. Particle size analysis (grain size distribution and hydrometer) and Atterberg limits tests were conducted according to ASTM D422-07 and ASTM D4318–10, respectively, and the results use to classify the materials according to the Unified Classification System, ASTM D2487-10.

Visual inspection of the samples indicated that material from Mountainside contained a large amount of degraded shale (more than at Premium and National) that adhered to the larger aggregates. This observation cast doubt on the accuracy of a traditional dry particle size analysis for the Mountainside materials. Therefore, for all the tests on the Mountainside samples, a wet preparation of soil samples was conducted according to ASTM D2217-04 to better account for these fine particles. For all samples, reduction of the sample size was made by quartering, according to ASTM C702-98. Atterberg limits were determined from a subsample of the soil below a #40 sieve after the material was sieved, this being a slight deviation of the ASTM D2217-04 standard for determination of soil constants. Table 3-5

summarizes percentage of soil passing #200 sieves, the Atterberg limits, and the soil classification at each site. Figure 3-18 shows resultant particle analysis in terms of mean grain size distribution for the Premium site. Mean grain size distribution charts for Mountainside and National sites are reported in Appendix A. Here, oversize particles (greater than 2 inches (50 mm)) were not included in the particle analysis.

Table 3-5 Percentage of soil passing #4 and #200 sieve, Liquid Limit, Plastic Limit, Plastic Index and Soil Classification (USCS)

Site	Plot	% passing # 4 sieve	% passing # 200 sieve	Liquid Limit	Plastic Limit	Plastic Index (%)	Soil Classification (USCS)
Premium	1	48.14	23.14	34	21	13	GC
	2	27.71	9.21	29	14	15	GP-GC
	3	43.33	14.96	26	16	9	GC
	4	46.04	16.49	27	13	15	GC
National	1	51.32	24.06	28	15	13	GC
	2	45.70	22.27	24	12	13	GC
	3	56.89	28.98	29	14	16	GC
	4	38.61	18.05	26	12	14	GC
Mountainside	1	64.98	45.29	34	16	17	GC
	2	67.12	46.67	31	18	13	GC
	3	61.84	42.46	31	14	17	GC
	4	59.50	38.23	32	18	14	GC

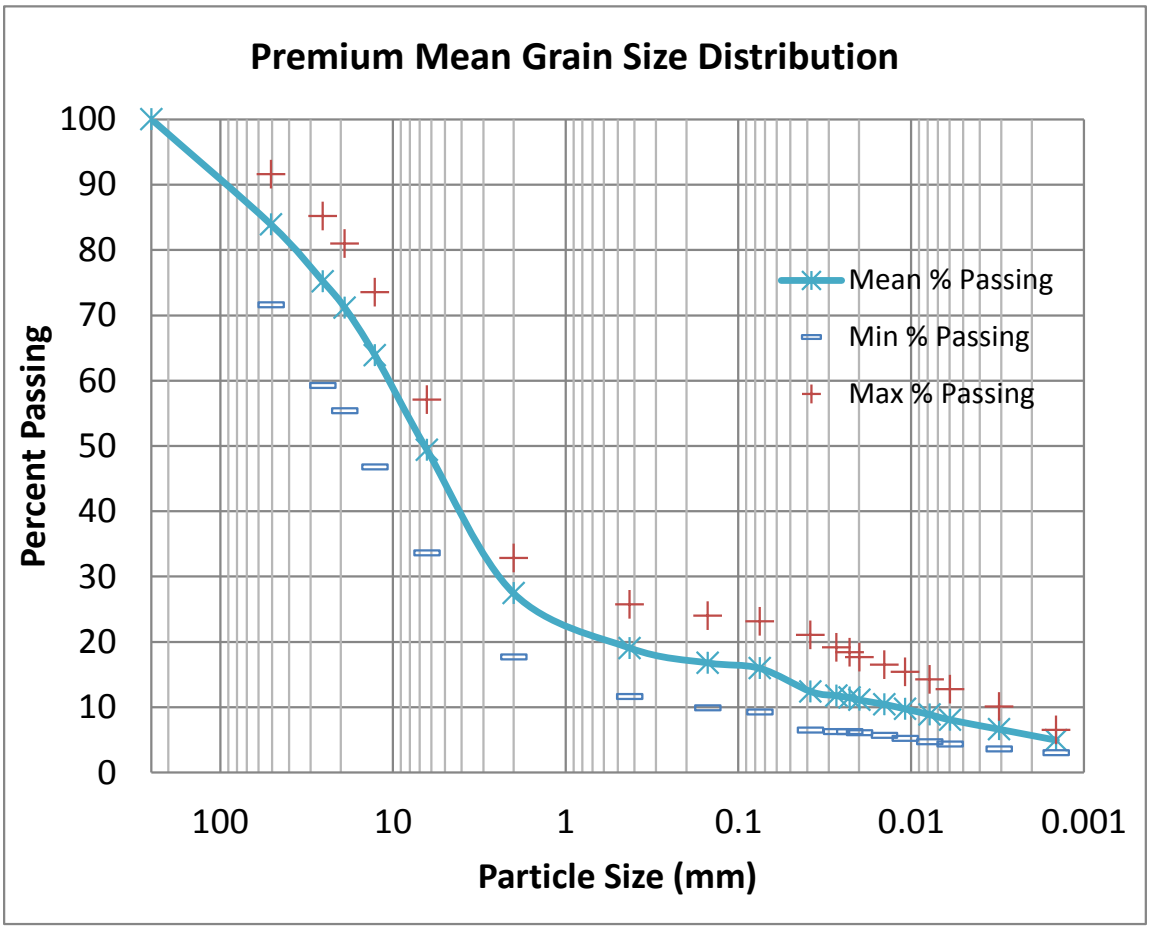

Figure 3-18 Mean grain size distribution from the Premium site.

The particle size analysis results reported here differ slightly from the preliminary results reported by White et al. (2009). In all cases the results presented here suggest a greater amount of fine material passing the # 200 sieve (0,075 mm) than that reported by White et al. (2009), which results in a slightly different Unified Classification. The difference may be explained by the fact that the samples for the preliminary tests were collected near the surface, where there was some loss of fines due to erosion. The results presented here were taken below the surface, and can be assumed to be more representative of the reclaimed material.

The particle size and Atterberg Limits analysis from all three sites suggest s that the material can be classified as a GC or GP-GC (Gravel), with significant amount of plastic or clay fines (C). The fine material represents about 15% of the total at Premium, about 23% at National and about 43% at Mountainside. In spite of the predominance of the coarse gravel particles, the classification would suggest that the large amount of fine materials present will have a significant effect on the material behavior. Further, the large amount of fine materials would suggest that the material strength would probably include a small amount of cohesion. The strength properties are discussed below.

Shear strength parameters

Shear strength parameters for long term stability analysis

Long term stability analysis assumes that all water pressures have been dissipated, and thus, requires the estimation of the drained or effective shear strength parameters. The shear strength of soil is typically described as:

$$\tau_n = c + \sigma_n \tan \phi \qquad (3\text{-}3)$$

where σ_n and τ_n are the normal and shear stresses acting on any plane within the soil body, and ϕ and c are the internal friction angle and cohesion. This expression is called the Mohr-Coulomb yielding or failure criterion.

The shear strength material properties ϕ and c are often measured in laboratory tests. However, due to the large particles present in mine spoils, traditional laboratory tests are very difficult to conduct and require very large sample sizes to accommodate the larger particles. When testing is performed, the larger materials may be removed to allow the use of reasonable sample sizes. Unfortunately this results in questions about the role of large or oversize particles on the resulting strength, with some researchers suggesting that oversize particles may increase the overall shear strength. However, the literature seems not to provide consensus on this issue.

Simoni and Houlsby (2006) conducted a series of direct shear tests on granular soils and observed an increase in peak and residual friction angles as the amount of gravel (or larger particles) was increased in the soil sample. Using a large shear box (30 x 30 cm), Rathee (1981) observed that for samples composed of a mixture of sand and gravels, the internal friction angle increased with an increase in the maximum particle size, while for gravels of uniform size no difference was observed when the particle size was increased. Hannes (1952) using a smaller direct shear test device (15 x 30 cm) on granular material, concluded that the internal friction angle increases with increasing the particle size. Contrary conclusions have been reported by Kirkpatrick (1965), who conducted triaxial tests on sands, finding a decrease in the internal friction angle as the particle size increases (for a constant value of soil porosity). Becker et al. (1972), simulating the plane strain conditions of an earth embankment by biaxial tests, concluded that the internal friction angle decreases with increasing particle size for low confining stresses, but smaller difference is observed for high confining pressures. Working with large triaxial tests on gravels with constant coefficient of uniformity, Leslie (1963) showed that in reality the intermediate particles (instead of the large particles) are those which have a greater influence on the strength.

For the case when the soil mass possesses oversize particles in a “floating” matrix of finer materials (no contact between oversize particles), Siddiqi (1984) proposed that the strength of the soil mass may be determined by the strength of the matrix of the far field only (soil matrix away from the oversize particles). Su (1989), from triaxial tests results on cohesionless soil with particles in a floating state, concluded that the overall strength is mainly controlled by the soil matrix instead of the oversize particles. These results validated the innovative modeling criteria developed by Siddiqi. Holtz and Gibbs (1956) analyzing the results from triaxial tests on sands and gravels observed a small increase in the strength when large particles were introduced to the soil mass. However, as the authors recognized, this small increase was because only a few large particles (perhaps in a floating state) existed in the tested soil. Different conclusions were obtained by Fakhimi and Hosseinpour (2011).They conducted a series of

direct shear tests in the laboratory (6 x 6 cm) and numerical simulations of both the laboratory shear tests and an in situ shear box (60 x 60 cm). The numerical modeling used the finite element method (FEM) to model the shear box and discrete element method (DEM) to model the interaction of the oversize particles and the surrounding soil. Results from the small laboratory test and its numerical simulation show an increasing internal friction angle as the size of the oversize particle increases. However, the simulation of the larger shear box showed that strength parameters are not affected by the oversize elements. This issue may be explained by the fact that the internal friction angle seems to decrease as the size of the box increases (Cerato and Lutenegger 2006). Actually, Nieble et al. (1974), suggested that the maximum particle size should be less than 5% of the shear box width in order to avoid size effects in the strength results.

Field estimation of the shear strength of the reclaimed materials

White et al. (2009) reported drained friction angles for each of the three sites based on the observed angle of repose of the material. The angle of repose is the "steepest stable slope for loose packed granular material and represents the angle of internal friction at its loosest state" (Holtz and Kovacs 1981). This approach assumes that the drained internal friction angle of the surface layer is well represented by the angle of repose when the low compaction grading technique is used. White (2009), reported values of angle of repose between 36 and 38 degrees for National site and between 37 and 39 degrees for Premium and Mountainside (Figure 3-19 and Table 3-6). Regarding the drained cohesion parameters, a cohesion value equal to zero is typically used for granular materials (Holtz and Kovacs 1981, Lambe and Whitman 1969, Salgado 2008)and would be appropriate for reclaimed mine spoil, especially the materials near the surface receiving minimum compaction effort. Thus, for the traditional stability analysis here, a value of zero cohesion would be assumed for simplicity, and the angle of repose would be taken as the friction angle.

Table 3-6 Internal friction angle reported for each site (adapted from White, 2009)

Site	Sample Number	Angle of Repose (internal friction angle), Degrees	Average Angle of repose (internal friction angle), Degrees
National	1	36	36.8
National	2	38	
National	3	37	
National	4	36	
Premium	1	38	37.6
Premium	2	38	
Premium	3	37	
Premium	4	39	
Mountainside	1	38	38
Mountainside	2	39	
Mountainside	3	37	
Mountainside	4	38	

Figure 3-19. Illustration of field determination of the angle of repose at National Site (White 2009)

Similar values of internal friction angle and cohesion for reclaimed slopes can be found in the literature. Ulusay et al. (1995), working on failed reclaimed slopes in Turkey conducted a series of in situ SPT test, Consolidated Drained Triaxial (CD) and Direct Shear laboratory tests. The N values obtained from SPT test generally correlated to friction angles between 31 and 38 degrees, while peak internal friction angles ranging from 23.9 to 39.8 degrees were obtained from direct shear tests. A linear regression analysis using the data from shear tests yielded a friction angle equal to 34.3 degrees, while consolidated drained triaxial test yielded on average an internal friction angle of 27.8 degrees (removing a reported value of 16 degrees, which is the only reported value under 23 degrees and it is considered an outlier). The cohesion value obtained from shear tests was 12 kN/m2 (250.63 psf), while the reported cohesion from triaxial test ranges from 0 to 10 kN/m2 (0 to 208.86 psf).Both tests showed negligible cohesion values from a strength perspective.

Stormont and Farfan (2005), conducting a study on mine waste slopes in Colorado, executed direct shear tests using conventional (small) laboratory shear box, a large shear box test in situ, and a large laboratory shear box test. The authors' conclusion was that large laboratory shear box test is the most reliable method for determining strength parameters. The regression analysis for the large laboratory box test showed an average internal friction angle of 37 degrees and soil cohesion equal to 4.8 kN/m2 (100.25 psf), which is also a negligible value from a strength point of view.

Gutierrez et al. (2008), performing soil characterization of Goat Hill North Rock Pile at Questa Molybdenum Mine in New Mexico, conducted a series of direct shear tests of the soil material. The

reported friction angle ranges from 42 to 47 degrees, while the cohesion was considered equal to zero. The authors suggest that these high friction angles seem to be a result of high angularity of the grain shape.

Kasmer and Ulusay (2006) working also on spoil piles instabilities in Turkey, conducted shear test analysis of the spoil and natural material. The result show a peak friction angle of 30.5 degrees for the mine spoil material and peak cohesion of 17.5 kN/m2 (365.50 psf)

Table 3-7 summarizes the internal friction angle and test characteristics from the discussion above. Figure 3-20 graphically shows the agreement between reported friction angles for different studies on reclaimed slopes, and suggests that the friction angle measurements for the instrumented sites in Tennessee are similar to those obtained from a range of test methods at other sites. Since the angle of repose is the internal friction angle at the loosest state of the material, it may be assumed that this represents a minimum value for the existing materials at Premium, National and Mountainside. More importantly, it is suggested here that careful visual observations of the angle of repose may be taken as an appropriate estimate of the shear strength of reclaimed mine materials placed in accordance with the FRA. In practice, laboratory testing is seldom performed on these materials, and uncertainties associated with the role of the oversize particles in laboratory tests seem to justify the observational approach using the angle of repose.

Table 3-7 Summary of internal friction angle and test characteristic for similar reclamation studies

Author	Origin of Material Tested	Type of Test	Dimensions, mm	Internal friction angle, Degrees	Cohesion, kN/m2	Cohesion, psf
Ulusay et al. (1995)	Limestone, Claystone and Marl	In situ SPT Test	----	31 to 38	----	----
Ulusay et al. (1995).	Limestone, Claystone and Marl	Direct Shear Test	Not Mentioned	34.3	12	250.63
Ulusay et al. (1995)	Limestone, Claystone and Marl	Triaxial (CD) Test	Diameter= 191 Height = 382	23 - 35	0 - 10	0 -208.86
Stormont and Farfan (2005)	Not mentioned	Direct Shear Test (Large Laboratory Box)	Length = 762 Width = 762 Height = 457	37	4.8	100.25
Gutierrez et al. (2008)	Not Mentioned	Direct Shear Test	Length = 51 Width = 51 Height = not mentioned	42 - 47	0	0
Kasmer and Ulusay (2006)	Limestone and marl	Direct Shear Test	Not Mentioned	30.5	17.5	365.50

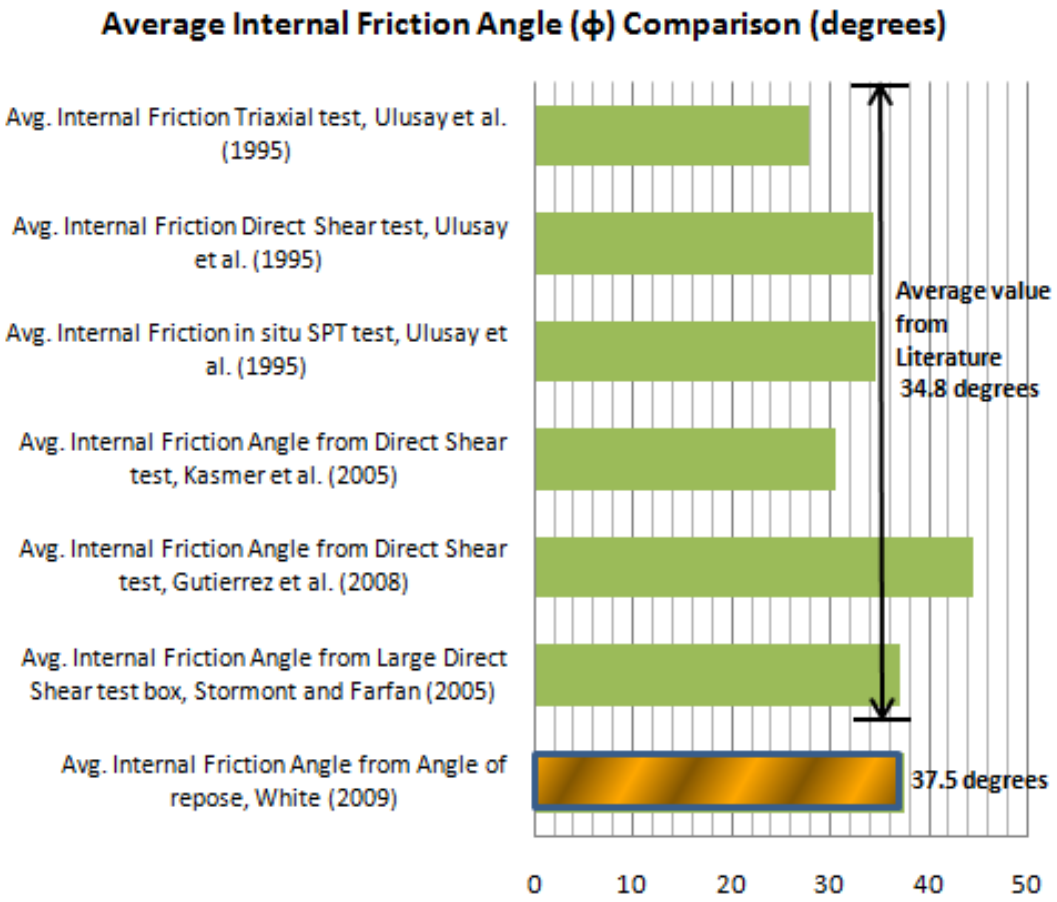

Figure 3-20. Reported friction angles for different studies on reclaimed slopes

Shear strength parameters for short term stability analysis

Stability analyses of slopes under undrained conditions are often conducted to characterize the behavior of the soil in the short term or immediately after construction, where it is assumed that loading occurs much faster than the rate of drainage of the soil. However, it is assumed that the coarse, low density material resulting from the FRA compaction methods would drain appropriately, and the probability of significant excess of pore pressure development at the end of the construction period or during an earthquake event is very low (Duncan and Wright 2005). Consequently, it is assumed that the drained and undrained strength parameters are the same for both the static stability investigated here and the dynamic slope stability analysis in the subsequent chapters. Furthermore, short term stability is not considered to be important in the reclamation of mine slopes, since any short term failure would have minimum consequences and would be repaired during construction or routine maintenance.

Conclusions

The dimensions and inclination of the four plots at each of the three instruments was documented. A comprehensive series of unit weight measurements was conducted, leading to statistical analysis and an indication of the spatial variability of unit weight at each of the three sites. Samples were collected, and particle size analyses and index testing conducted to allow the classification of the materials leading to a general estimation of the engineering properties. Due to the significant number of large particles

present in these reclaimed mine materials, laboratory measures of strength are neither routinely performed nor practical. A literature review of the effects of oversize materials on shear strength was provided, along with a summary of reported shear strength parameters from the literature on similar mine slope materials. Lastly, it was suggested that the use of careful observations of the angle of repose, taken from stored materials on site, may be an effective and logical method to estimate the strength of these materials. The resulting strength parameters agree well with the values from the literature, and the prevailing failure mode in a storage pile of loose materials is typically failure of materials near the surface of the pile or slope. In subsequent chapters, it will be shown that these shallow failures are the most critical failure mode in slopes constructed according to the Forest Reclamation approach. Thus, the proposed visual observation of shear strength is consistent with the type of failure that should be evaluated in slope constructed according to FRA principles.

References:

Becker, E., Chan, C. K., Seed, H. B., and California. Dept. of Water Resources. (1972). "Strength and deformation characteristics of rockfill materials in plane strain and triaxial compression tests." *University of California Geotechnical Engineering Report no TE-72-3*, Dept. of Civil Engineering, University of California, Berkeley, CA, xii, 121 l.

Cerato, A. B., and Lutenegger, A. J. (2006). "Specimen Size and Scale Effects of Direct Shear Box Tests of Sand." *Geotechnical Testing Journal*, 29(6), 1-10.

Duncan, J. M., and Wright, S. G. (2005). *Soil strength and slope stability*, John Wiley & Sons, Hoboken, N.J.

ESRI (2010). "ArcMap 9.3."

Fakhimi, A., and Hosseinpour, H. G. (2011). "Experimental and Numerical Study of the Effect of an Oversize Particle on the Shear Strength of Mined-Rock Pile Material." 34(2), 8.

Farrag, K., Vetter, D., Hill, B., and Esposito, R. (2005). "Evaluation of soil compaction measuring devices." G. T. Institute, ed.Des Plaines, Illinois.

Gutierrez, L. A. F., Viterbo, V. C., McLemore, V. T., and Aimone-Martin, C. T. (2008). "Geotechnical and geomechanical characterization of the Goathill North Rock Pile at the Questa Molybdenum Mine, New Mexico, USA." *First International Seminar on the Management of Rock Dumps, Stockpiles and Heap Leach Pads*The Australian Centre for Geomechanics, University of Western Australia.

Hannes, R. G. (1952). "The strength of gravel in direct shear." *ASTM special technical publication*, ASTM, ed., 51-60.

Holtz, R. D., and Kovacs, W. D. (1981). *An introduction to geotechnical engineering*, Prentice-Hall, Englewood Cliffs, N.J.

Holtz, W. G., and Gibbs, H. J. (1956). "Triaxial shear tests on pervious gravelly soils." *American Society of Civil Engineers -- Proceedings -- Journal of the Soil Mechanics and Foundations Division*, 82(SMI), 22.

Kasmer, O., and Ulusay, R. (2006). "Stability of spoil piles at two coal mines in Turkey: Geotechnical characterization and design considerations." *Environmental & Engineering Geoscience*, 12(4), 337-352.

Kirkpatrick, W. M. (1965). "Effects of grain size and grading on the shearing behaviour of granular materials." *Proc., Sixth International Conference on Soil Mechanics and Foundation Engineering*, Montreal, Canada.

Lambe, T. W., and Whitman, R. V. (1969). *Soil mechanics*, Wiley, New York.

Leslie, D. D. (1963). " Large-scale triaxial tests on gravelly soils." *Pan-American Conference on Soil Mechanics and Foundation Engineering*, 181-202.

Nieble, C. M., Silveira, J. F., and Midea, N. F. (1974). "Some Experiences on the Determination of the Shear Strength of Rock Fill Materials." *Proc., Second International Congress of the International Association of Engineering Geology*, Sao Paulo, Brazil, 1-12.

Randrup, T. B., and Lichter, J. M. (2001). "Measuring soil compaction on construction sites: a review of Surface Nuclear Gauges and Penetrometers." *Journal of Arboriculture*, 27(3), 109-117.

Rathee, R. K. (1981). "Shear strength of granular soils and its prediction by modelling techniques." *Journal of the Institution of Engineers (India): Civil Engineering Division*, 62(Compendex), 64-70.

Rousseeuw, P. J., and Leroy, A. M. (1987). *Robust regression and outlier detection*, Wiley, New York.

Salgado, R. (2008). *The engineering of foundations*, McGraw Hill, Boston.

SAS Institute Inc. (2008). "Jump." SAS Institute Inc., Cary NC, Statistical software.

SAS Institute Inc. (2008). "Jump Statistics and Graphics Guide." SAS Institute Inc., Cary, NC.

Siddiqi, F. H. (1984). "Strength evaluation of cohesionless soils with overzise particles." Ph.D. dissertation, University of California at Davis, Davis, CA.

Simoni, A., and Houlsby, G. (2006). "The Direct Shear Strength and Dilatancy of Sand–gravel Mixtures." *Geotechnical and Geological Engineering*, 24(3), 523-549.

Stormont, J. C., and Farfan, E. (2005). "Stability evaluation of a mine waste pile." *Environ Eng Geosci*, 11(1), 43-52.

Su, W. (1989). "Static strength evaluation of cohesionless soil with oversize particles." Ph.D. dissertation, Washington State University., Pullman, WA.

Sweigard, R. J., Badaker, V., and Hunt, K. (2007). "Development of a field procedure to evaluate the reforestation potential of reclaimed surface-mined land." Department of Mining Engineering, University of Kentucky, Lexington, KY, 159.

Tesarik, D. R., and McKibbin, R. W. (1999). "Material properties affecting the stability of a 50-year-old rock dump in an active mine." U.S. Dept. of Health and Human Services, Public Health Service, Centers for Disease Control and Prevention, National Institute for Occupational Safety and Health, Pittsburgh Research Laboratory, Pittsburg, PA.

Troxler Electronic Laboratories Inc. (1997). "Nuclear Gauge Safety Training Program, 8th edition." Research Triangle Park, NC.

Troxler Electronic Laboratories Inc. (2006). "Manual of Operation and Instruction: Model 3411-B Advanced Control Unit." Research Triangle Park, NC.

Ulusay, R., Arikan, F., Yoleri, M. F., and Caglan, D. (1995). "Engineering geological characterization of coal mine waste material and an evaluation in the context of back-analysis of spoil pile instabilities in a strip mine, SW Turkey." *Eng Geol*, 40(1-2), 77-101.

White, P. H. (2009). "Classification of subwatershed slopes and geotechnical characterization of steep slopes on reclaimed mine lands in east Tennessee." M.S. dissertation, The University of Tennessee, Knoxville, TN.

White, P. H., Drumm, E. C., Schwartz, J. S., and Johnson, A. M. (2009). "Geotechnical Characterization of Steep Slopes on. Reclaimed Mine Lands in East Tennessee." *2009 ASABE Annual International Meeting*, ASABE, ed., ASABE, Reno, NV.

Chapter 4 Slope Stability of the Instrumented Sites

Static long term slope stability analysis

Abstract
The stability analysis of the instrumented sites was focused on the primary failure mode that is likely to be experienced by slopes constructed using the low compaction grading technique. This failure mode is a shallow instability within the loose surface soil layer, or instability at the contact between the loose surface material and the denser, stronger core. While a deep rotational or global instability would typically be evaluated, this failure mode was determined to not be critical in slopes of this type. The failure through the loose surface layer was analyzed using various limit equilibrium approaches: the Simplified Bishop's method for circular failure surfaces, the Janbu's method for non-circular surfaces, and the Infinite Slope method. The slopes at all three study sites were observed to have Factors of Safety well above 1.3, suggesting that the FRA with low compaction surface materials does not compromise the long term stability of the slopes for the material properties encountered at the instrumented sites. It is suggest that the infinite slope stability analysis method, coupled with the estimation of the shear strength of the reclaimed materials from field observations, provides a simplified yet rational means to evaluate the stability of FRA constructed slopes.

Limit Equilibrium Basics
Limit equilibrium analysis is based on the concept of a slip surface which separates two blocks of soil that behave as rigid elements, and loss of stability comes with large relative movements of the blocks (Salgado 2008). For a potential slip surface in which the destabilizing forces have exceeded the available strength of the soil, sliding must occur to reach new equilibrium in the system. Sliding may result in large displacements reaching the ultimate limit state, or with small displacement where ultimate limit state is not yet reached (Salgado 2008). Limit equilibrium analysis gives information about the necessary conditions for equilibrium at the starting point of the sliding, but yields no information about the deformations or post failure state. Approximations of the displacements after the initiation of the sliding can be obtained by other methods (e.g. Finite Element Method), but are generally not reliable and used little in practice.

In reality, unlimited number of potential slip surfaces may be found in a single slope analysis, but one slip surface will have the lowest factor of safety (*FS*). The factor of safety is usually adopted as the ratio of resisting forces or moments divided by destabilizing/driving forces or moments.

$$FS = \frac{Resisting\ moment}{Driving\ moment} \quad (4\text{-}1)$$

The lower the *FS* value for a specific slip surface, the most likely this slip surface becomes to slide. A FS value of 1.0 implies that the driving forces just equal the resisting forces, and the system is at incipient failure. FS values under 1 mean that destabilizing forces have overcome the resisting forces and failure would occur.

In slope stability analysis, it is assumed that the resisting force is the shear strength of the soil fully and uniformly distributed along the slip surface, and the disturbing force is due to gravity or other external loads tending to make the slope fail. Then for a factor of safety equal to 1.5 for example, it is said that the shear strength along the slip surface is 50% greater than required to balance destabilizing forces (Salgado 2008). The Mohr-Coulomb expression for the shear strength is $\tau = c + \sigma tan\phi$ where *c* is the soil cohesion; σ is the normal stress and ϕ the internal friction angle of the soil.

Simplified Bishop's Method

The Simplified Bishop's method (Bishop 1955) belongs to the slice methods of limit equilibrium analysis in which a circular or rotational sliding mass is broken into several vertical slices. Though it does not satisfy all conditions of static equilibrium (only moment and vertical force equilibrium) it has been reported as accurate for almost all circumstances (Albataineh 2006, Duncan 1996, Duncan and Wright 1980). Also, the results obtained through this method have been shown to agree well with finite element procedures (Wright et al. 1973).

The immobile mass below the slip surface generates resisting shear forces that tend to stabilize the sliding. As it was discussed before, this shear force depends on the strength parameters of the soil. Also, on each slice self-weight and vertical and horizontal lateral forces act as destabilizing forces (depending on the geometry lateral forces may be resistant forces as well). Figure 4-1 illustrates the forces that are usually involved in the slice method of limit equilibrium. Y_L and Y_R are lateral vertical forces acting on the left and right side of the slice respectively, X_L and X_R are lateral horizontal forces acting on the left and right side of the slice respectively, W_i is self-weight, N_i is the component of the vertical forces reacting perpendicular to the slip surface, U_i is water force acting perpendicular to the slip surface, Δl_i is the length of the base of the slice and Δx_i is the width of the slice.

The Bishop's simplified method assumes that the slices are small enough to have almost equal values of lateral forces at either side of the slice. As shown in Figure 4-1, these forces are acting in opposite directions and therefore may be neglected. Then, Bishop's simplified method is formulated based on equilibrium of vertical forces and on equilibrium of moment (rotation).

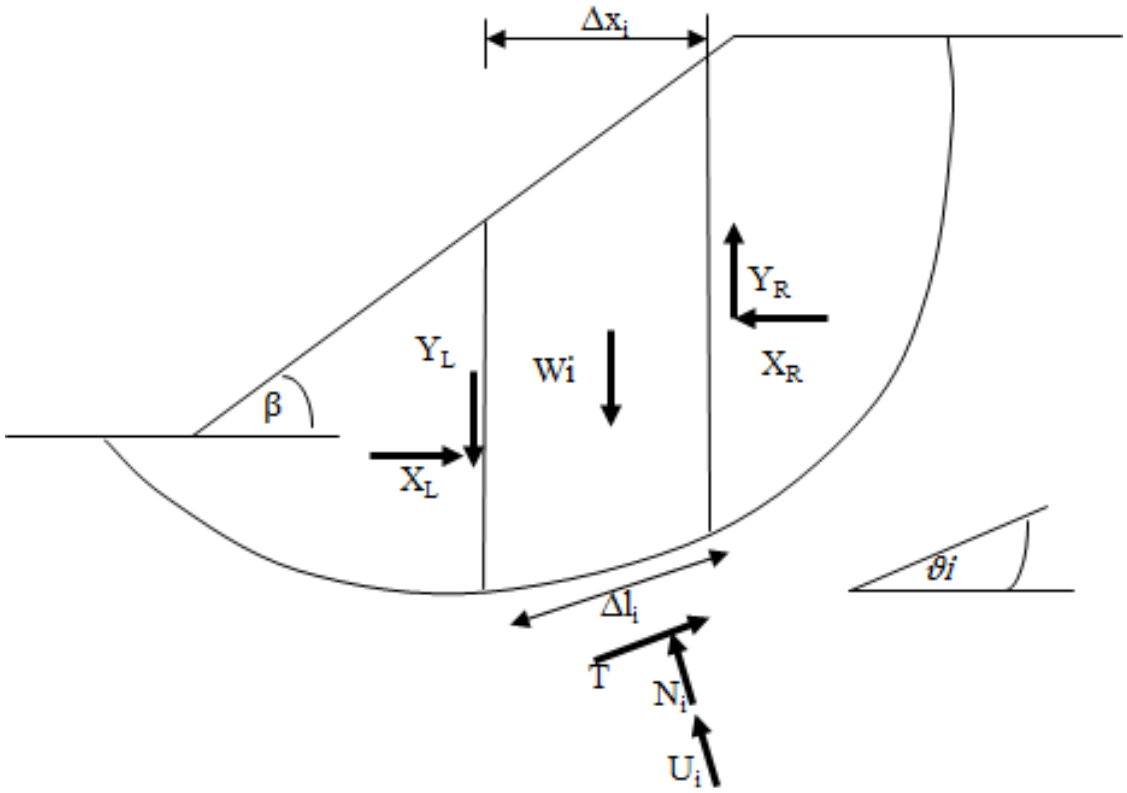

Figure 4-1 Forces considered on slice method of limit equilibrium (adapted from Lambe and Whitman, 1969; Salgado, 2008)

For any type of rotational equilibrium the FS may be written as

$$FS = \frac{Resistent\ moment}{Drining\ moment} = \frac{\sum \tau_{fi} \Delta l_i}{\sum W_i \sin \vartheta_i} \quad (4\text{-}2)$$

$$\frac{\tau_{fi}}{F_{FS}} = \frac{\bar{C}_i + \bar{\sigma}_{ni} \tan \bar{\phi}_i}{FS} \quad (4\text{-}3)$$

$$FS = \frac{\sum \bar{C}_i \Delta l_i + \overline{N_i} \tan \bar{\phi}_i}{\sum W_i \sin \vartheta_i} \quad (4\text{-}4)$$

Differences among methods of slices are found mainly in the interpretation and quantification of the effective normal stress $\overline{N}_i$. Bishop suggests that the self-weight is equal to normal and water forces acting perpendicular to the slip surface plus shear force acting tangent to the slip surface (Figure 4-2)

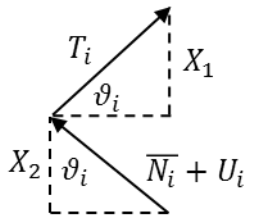

Figure 4-2 Quantification of the effective normal stress ($\overline{N}_i$) assumed by Bishop (1955)

$$sin\,\vartheta_i = \frac{X_2}{T_i} \quad \rightarrow \quad X_2 = T_i\,sin\,\vartheta_i \tag{4-5}$$

$$cos\,\vartheta_i = \frac{X_1}{\overline{N_i}+U_i} \quad \rightarrow \quad X_1 = (\overline{N}_i + U_i)\,cos\,\vartheta_i \tag{4-6}$$

$$W_i = X_1 + X_2 = (\overline{N}_i + U_i)\,cos\,\vartheta_i + T_i\,sin\,\vartheta_i \tag{4-7}$$

From the Mohr-Coulomb failure criteria, we know

$$\tau_{fi} = \frac{1}{FS}\,\overline{C}_i + \bar{\sigma}_{ni}\,tan\,\bar{\phi}_i \tag{4-8}$$

Multiplying τ_{fi} by Δl_i

$$T_i = \frac{1}{FS}\,\overline{C}_i * \Delta l_i + \overline{N}_i\,tan\,\bar{\phi}_i \tag{4-9}$$

Introducing T_i into W_i:

$$W_i = (\overline{N}_i + U_i)\,cos\,\vartheta_i + \frac{1}{FS}(\overline{C}_i \Delta l_i + \overline{N}_i\,tan\,\bar{\phi}_i)\,sin\,\vartheta_i \tag{4-10}$$

Dividing W_i by $\cos\,\vartheta_i$

$$\frac{W_i}{cos\,\vartheta_i} = \overline{N}_i + U_i + \frac{1}{FS}tan\,\vartheta_i\,\overline{C}_i\Delta l_i + \frac{1}{FS}tan\,\vartheta_i\,\overline{N}_i\,tan\,\bar{\phi}_i$$

$$\frac{W_i}{\cos\,\vartheta_i} = \overline{N}_i\left(1 + \frac{1}{FS}tan\,\vartheta_i\,tan\,\bar{\phi}_i\right) + U_i + \frac{1}{FS}tan\,\vartheta_i\,\overline{C}_i\Delta l_i$$

$$\overline{N}_i = \frac{\frac{W_i}{\cos\,\vartheta_i} - U_i\Delta l_i - \frac{1}{FS}\overline{C}_i\Delta l_i\,tan\,\vartheta_i}{1+\frac{1}{FS}tan\,\vartheta_i\,tan\,\bar{\phi}_i} \tag{4-11}$$

Multiplying $\overline{N}_i$ by $\frac{\cos\vartheta_i}{\cos\vartheta_i}$

$$\overline{N}_i = \frac{W_i - U_i \Delta l_i \cos\vartheta_i - \frac{1}{FS}\overline{C}_i \Delta l_i \, sin\,\vartheta_i}{\cos\vartheta_i \left(1 + \frac{tan\,\vartheta_i \, tan\,\overline{\phi}_i}{FS}\right)}$$

$$\Delta l_i \, cos\,\vartheta_i = \Delta x_i$$

$$\overline{N}_i = \frac{W_i - U_i \Delta x_i - \frac{1}{FS}\overline{C}_i \Delta x_i \, tan\,\vartheta_i}{\cos\vartheta_i \left(1 + \frac{tan\,\vartheta_i \, tan\,\overline{\phi}_i}{FS}\right)} \quad (4\text{-}12)$$

Finally introducing $\overline{N}_i$ into FS and nominating

$$M(\vartheta) = cos\vartheta_i \left(1 + \frac{tan\,\vartheta_i \, tan\,\overline{\phi}_i}{FS}\right) \quad (4\text{-}13)$$

the yielded value for *FS* is:

$$FS = \frac{\sum_{i=1}^{N} \left(\overline{C}_i \Delta x_i + (W_i - U_i \Delta x_i) \, tan\,\overline{\phi}_i\right) / M(\vartheta)}{\sum W_i sin\vartheta_i} \quad (4\text{-}14)$$

Because the limit equilibrium method evaluates the stability for a specific predefined failure surface, the approach is a trial and error process: a potential failure surface is identified, and the FS determined based on Eq. 4-14. Another potential failure surface is identified and its corresponding FS determined. The process is repeated until the entire range of likely surfaces have all been evaluated, and the surfaces with the lowest FS are said to govern. Computational software is typically used to evaluate a large number of surfaces quickly. The software package used here for the Simplified Bishop's Method was *Slide* (Rocscience Inc. 2011)

The Infinite Slope Method

The Infinite Slope method is a limit equilibrium analysis in which the surface is assumed to be plane roughly parallel to the ground surface (Schor and Gray 2007). The ground surface is idealized as an infinite plane with slip surfaces parallel to it (Skempton and Delory 1957). This type of analysis is appropriate when the ratio of depth to length of the sliding surface is small. Schor and Gray (2007) list slope conditions that may be satisfactory analyzed through infinite slope method:

- Loose products of weathering (residual soil) overlying and inclined bedrock contact
- Inclined planes of stratification dipping downslope that are underlain by stronger strata.

- Bedrock slopes mantled with glacial till or colluviums
- Homogenous slope of coarse-textured cohesionless soil (sand dunes, sandy embankments or fills)

The geometry of the reclaimed mine slopes constructed according to the Forestry Reclamation Approach with a loose surface layer is ideally suited for investigation by the Infinite slope method. Figure 4-3 shows a slip surface of depth z below the ground surface (adapted from Salgado 2008). The weight of the slice is $W = \gamma_T bz$, where γ_T is the total unit weight of the soil, *b* is the width if the slice and z is the depth of the slice. The width *b* may be expressed as $b = l\ cos\beta$, where *l* is the length of the corresponding slip segment.

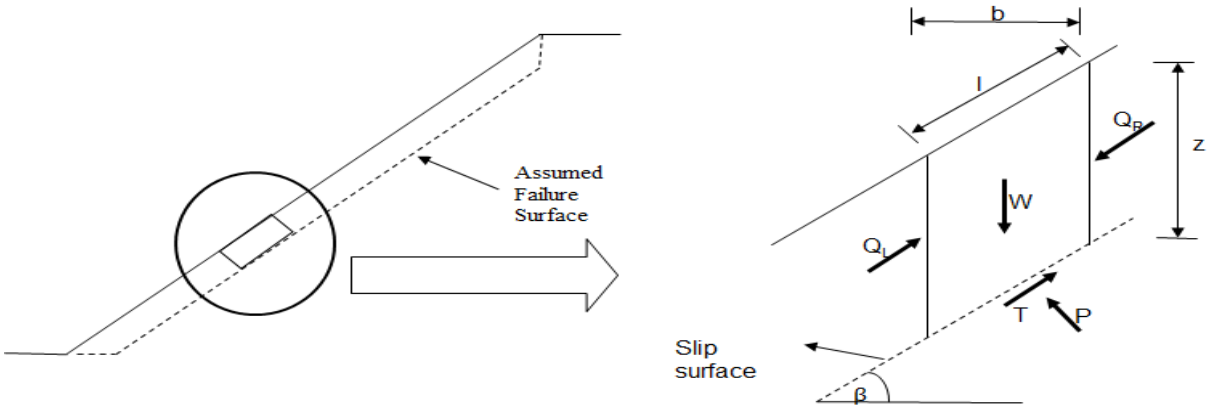

Figure 4-3 Infinite slope method (adapted from Salgado, 2008)

The normal and tangential forces may be expressed as:

$$T = \gamma_T zl\ sin\beta cos\beta \tag{4-15}$$

$$P = \gamma_T zlcos^2\beta \tag{4-16}$$

The Infinite slope assumption leads to the conclusion that Q_R and Q_L on either side of the vertical element are opposite and equal, thus those forces are neglected. At limit equilibrium, the shear force *T* needs to be a function of the strength parameter of the soil defined by the cohesion c and the internal friction angle ϕ. Consequently, the shear force may be expressed as:

$$T = \frac{cl + Ptan\phi}{FS} \tag{4-17}$$

Substituting *T* and *P* into the last equation, the factor of safety (FS) is:

$$FS = \frac{c}{\gamma_T z\ sin\beta cos\beta} + \frac{tan\phi}{tan\beta} \tag{4-18}$$

For cohesionless material (c = 0), the expression is reduced to (Lambe and Whitman 1969)

$$FS = \frac{tan\phi}{tan\beta} \tag{4-19}$$

The Eq. 4-19 suggests that for cohesionless material, any slope angle steeper than the internal friction angle will slide. Note that the unit weight does not appear in the infinite slope expression, which increases its utility when applied to materials for which the unit weight or density is difficult to determine.

The case of the infinite slope with seepage forces parallel to the surface is a condition that we find often in nature, especially in zones with considerable rainfall (Salgado 2008). Seepage parallel to the slope is often reached in the lower portions of natural slopes (Lambe and Whitman 1969). When seepage is acting in the slope, a new destabilizing force is introduced to the system. It is the total seepage force and it is expressed as:

$$F_c = bd_w\gamma_w sin\beta \tag{4-20}$$

Where *b* is the width of a submerged control volume, d_w is the water height, γ_w is the Unit Weight of water, and *sinβ* is equal to the hydraulic gradient ..

Then, the new equilibrium between resisting and destabilizing forces yields the following expression for the FS:

$$FS = \frac{cl+P'tan\phi}{T+F_c} = \frac{\frac{cb}{cos\beta}+P'tan\phi}{T+ bd_w\gamma_w sin\beta} \tag{4-21}$$

This time, normal and shear forces are functions of hydraulic gradient, buoyant γ_b and total γ_T unit weight of soil, water height, thickness of the soil layer and with of submerged control volume. The following expressions for normal and shear forces are suggested by Salgado (2008).

$$T = [\gamma_b d_w + \gamma_T(z - d_w)]bsin\beta \tag{4-22}$$

$$P' = [\gamma_b d_w + \gamma_T(z - d_w)]bcos\beta \tag{4-23}$$

Then, the general Factor of Safety expression for infinite slope whit seepage forces is:

$$FS = \frac{\frac{c}{[\gamma_b d_W+\gamma_t(z-d_W)]sin\beta cos\beta}+\frac{tan\phi}{tan\beta}}{1+\frac{\gamma_W d_W}{\gamma_b d_W+\gamma_T(z-d_W)}} \tag{4-24}$$

For the specific case of water table equal to the thickness of looser soil layer ($z = d_w$) and a cohesionless material, the expression becomes:

$$FS = \frac{\gamma_b}{\gamma_{sat}} \frac{tan\phi}{tan\beta} \quad (4\text{-}25)$$

The Eq. 4-25 suggests that since the ratio of the buoyant unit weight to the saturated unit weight is about 0.5, the factor of safety with seepage forces is about one half the factor of safety for dry conditions. Therefore, for simplicity the factor of safety when seepage forces are acting may be expressed as:

$$FS_{seepage} = 0.5\, FS_{without\ seepage} \quad (4\text{-}26)$$

Jambu's limit equilibrium method

Janbu's method (Abramson 1996) allows the investigation of specific potential failure planes of non-circular shape. As with the Bishops Simplified method above, to investigate a large number of potential planes a software package is usually used. The program Slide (Rocscience Inc. 2011) offers the possibility to investigate specific zones of interest restricting the search and was used here. The Block search generates non-circular surfaces and gives the opportunity of concentrating the surface generation within a confined zoned through search boxes that limit the upper and lower boundaries of the search (the upper block is called the active block and the lower is called the passive block). This feature was designed specifically to analyze weak layers present in soil stratum and consequently is a perfect tool to use for the investigation of shallow failure mechanisms for FRA slopes. This Block method generates the active and passive portions of the block surface using irregularly oriented segments (Sharma 2008), and provides a good check of the shallow stability and should compare favorably with the results of the infinite slope method.

Assumed material properties for the instrumented sites

Table 4-1 below summarizes the slope length, inclination and material properties (unit weight and friction angle) for the three instrumented sites. Since the geometry and material properties from all sites are reasonably similar, and those from Mountainside lead to the lowest factor of Safety, this site will be used to explore the various failure modes. As discussed in Chapter 3, it is assumed that the material has a negligible value of cohesion as would be typical for the evaluation of long term stability analysis. The specific stability results for all three sites are presented later.

Table 4-1 Summary of the geometric and material properties for the Premium, National and Mountainside sites

Sites	Slope Length (m)	Average Slope angle (Degrees)	Dry Unit Weight, γ (kN/m^3)	Wet Unit Weight, γ (kN/m^3)	Internal Friction Angle, ϕ (Degrees)
Premium	31	28	16.2	18.5	38
National	48	20	18.5	20.3	37
Mountainside	45	28	18.9	20.4	38

For the analysis of the shallow mode failure, the surface layer was assumed to run parallel to the slope, with a uniform thickness of 1.5 m. To limit failure through the core material in the computer analysis, an

arbitrarily high value of the cohesive strength parameter was assigned to the core. Additional analyses demonstrated that when the analysis is focused on the surface layer, the stability is insensitive to the assigned value of cohesion in the core material. For the circular or rotational slope stability, a homogeneous slope with the properties of the weak, loose layer was assumed, in which the shallow surface failure was found to be the most critical. The details of the various analyses are below.

Results from 2-D static long term slope stability analysis

The results from the infinite slope, infinite slope with seepage, and the Bishops Simplified Method analyses are summarized in Table 4-2. The Janbu method employing the block search, the infinite slope method (dry), and the Simplified Bishop's method all produced Factor of Safety values that were similar in spite of slight differences in the analysis assumptions. All yielded critical failure surfaces that were shallow and within the zone of the low compaction surface materials.

Table 4-2 Summary of material properties and FS obtained for long term static stability

Representation of Slope	Material Layer	Friction Angle, ϕ (Degrees)	Cohesion, c, (kN/m^2)	Unit Weight, γ (kN/m^3)	Slope Stability Analysis Results (Factor of Safety)				Critical failure mode
					Search Block Janbu Method	Infinite Slope	Infinite Slope (w/ seepage effects)	Simplified Bishop's Method (circular failure surface)	
Layered System	Surface layer	38	0	20.4	1.478	1.470	0.735	----	Shallow failure, planar failure surface
	Foundation or core material	0	1000	20.4					
Homogeneous System	Entire slope	38	0	20.4	----	----	----	1.475	Shallow failure, circular failure surface

Based on the infinite slope method, the FS for long term stability was 1.47. This means that the observed shear strength along the slip surface is 47% greater than that required to maintain equilibrium or stability in the long term. This result is valid in the absence of internal pore pressures or seepage forces, which is the likely situation due to the high drainage capability of the low compaction surface materials, and the fact that the compacted core should still have good drainage properties. However, when seepage forces were included in the analysis, the FS reduces to 0.74, indicating that the slope is not stable. Although this condition is unlikely and assumes complete saturation and downslope water flow through the complete thickness of the surface layer, it serves as a lower bound or worst case value of the FS and represents conditions that would occur if the materials could not drain and the slope was subject to large infiltration rates under high intensity storm events.

Taking advantage of the block search feature in *Slide,* the FS for long term stability was found to be 1.478, which shows very good agreement with the FS obtained from the simple infinite slope analysis. Figure 4-4 shows a schematic section of the slope (the 1.5 m thick surface layer is so small with respect to the height of the slope that it cannot be distinguished from the slope surface) and the potential trial failure surfaces investigated. The circled areas are enlargements intended to show the 10 most critical surfaces of the 10,000 analyzed failure surfaces at the top and bottom of the slope that were evaluated.

Stability analysis of a homogeneous slope having the soil properties of the weak surface layer (ϕ=38 degrees and γ=18.4 kN/m^2) was also conducted. The obtained FS for long term stability after 122,500 computed surfaces, using Simplified Bishop's method, was 1.478. It is interesting to notice that this FS is very close to the values obtained from the infinite slope equation and the Janbu approach. Also notice that the most critical failure mechanism is shallow and agrees well with the assumed failure mechanism of the infinite slope method (Figure 4-5). Because of the surface failure mode, identical results in terms of FS's and failure mechanism were found for Premium, showing that the analysis is insensitive to the unit weight of the slope material, suggesting that the Infinite Slope method is suitable for these conditions. Since the infinite slope method adequately approximated this shallow failure mode, and accurately predicted the performing FS, it can be concluded that it is a simple and reliable method to evaluate the performance of FRA slopes, and more sophisticated computer analyses are not necessary for most applications. Table 4-3 summarizes the FS determined for each instrumented site using the infinite slope equation. The higher FS found for the National site is a result of the lower inclination of the slope there.

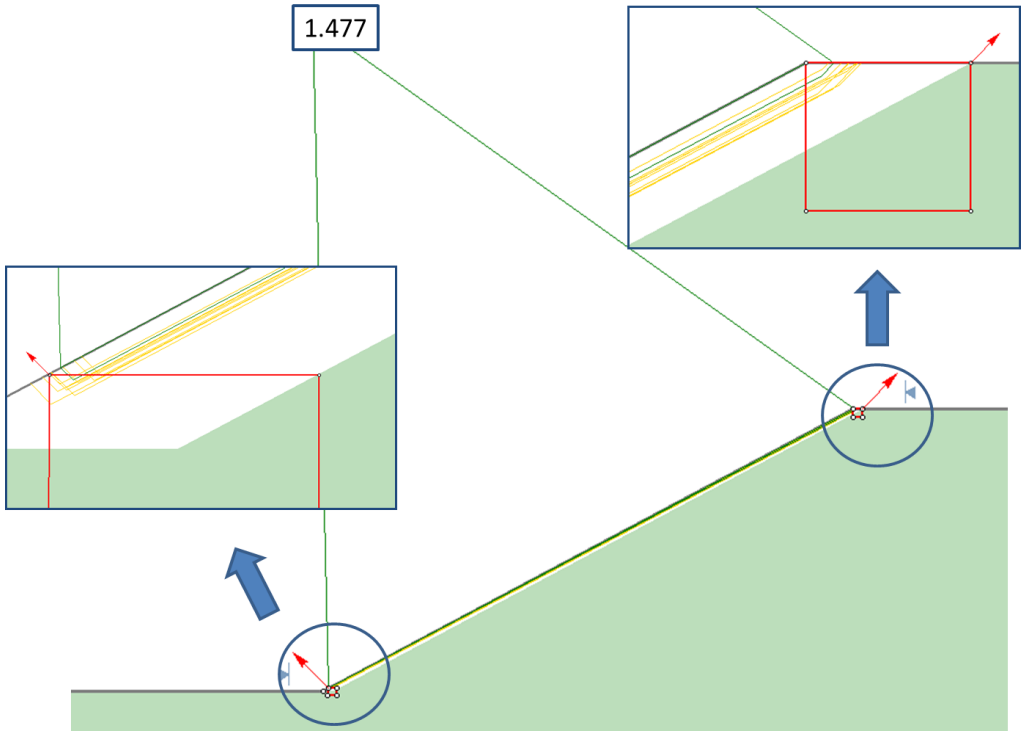

Figure 4-4 Mountainside site - 10 most critical slip surfaces analyzed with the block search feature of Slide for the long term stability analysis. Enlarged areas of the toe (left) and head (right) of the slope are illustrated. Minimum FS from Simplified Jambu method=1.477.

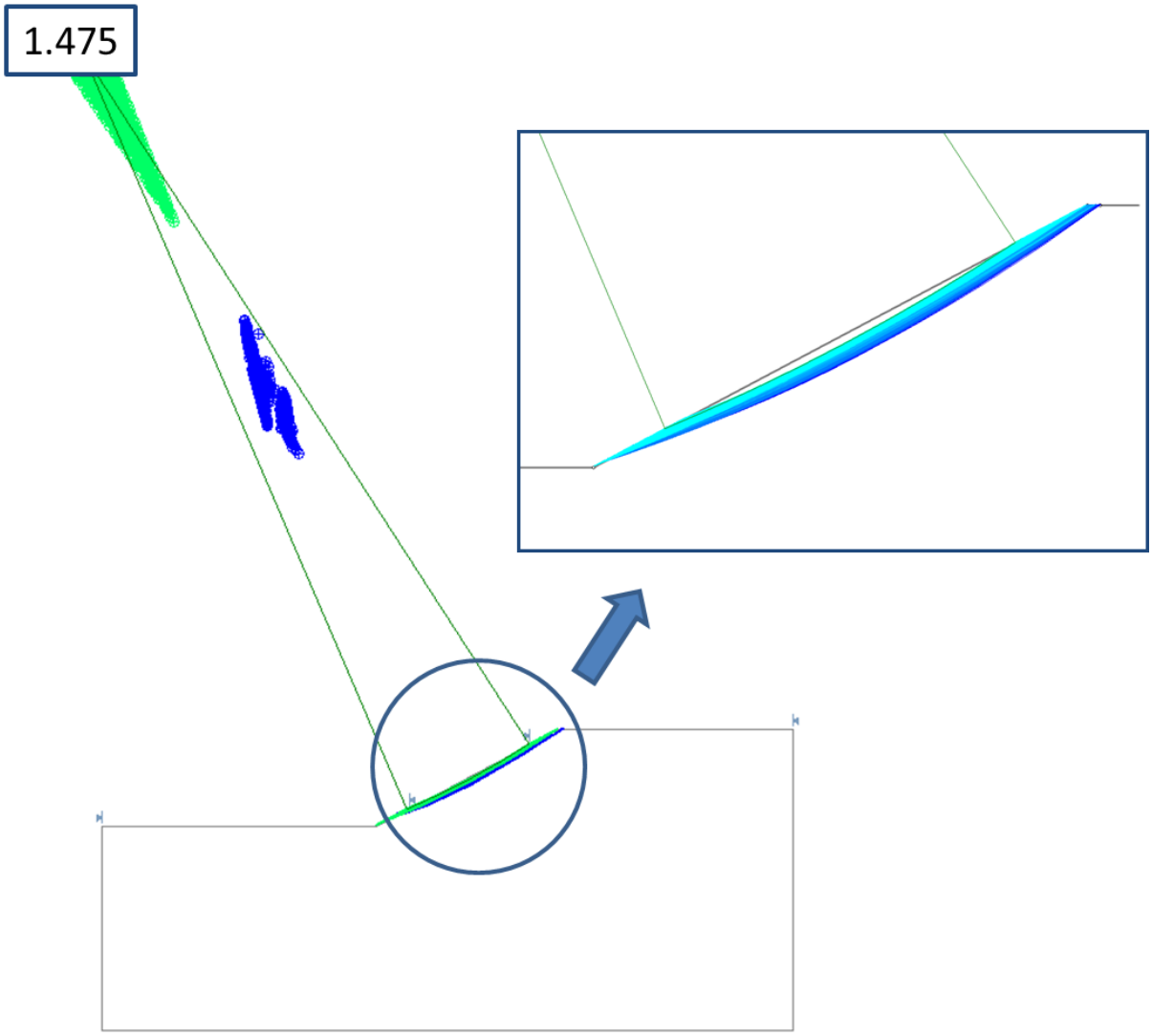

Figure 4-5 Mountainside site - Homogeneous slope analysis of long term stability by Simplified Bishop's method. Rotational failure surfaces for FS=1.4 to 1.5. Most critical FS=1.475 (Excluding trivial extreme-shallow failure surfaces).

Table 4-3 Summary of the performing long term FS of each research site (Infinite Slope Method)

Sites	Average Slope angle (Degrees)	Internal Friction Angle, ϕ (Degrees)	Factor of Safety, (FS)
Premium	28	38	1.47
National	20	37	2.07
Mountainside	28	38	1.47

Effects of the central core properties over the stability

The Forest Reclamation Approach (Sweigard et al. 2007) was developed to overcome the detrimental effects that compaction can have on tree survival, by employing low compaction in the uppermost 1-2 meters, and strong compaction below that surface. Thus, the core material is usually denser and stronger. Previous analysis showed that critical failure mechanisms of FRA slopes are shallow. Further analysis of deep failure mechanisms confirmed this finding. Even when the core material is just slightly stronger than the surface layer, deeper failure surfaces presented higher FS's. Thus, critical failure mechanisms and FS's are insensitive and independent of the strength properties of the core material, as long as it is stronger than the surface layer.

Spatial distribution of factors of safety for Premium Site

Using the software ArcGIS, the spatial distribution of factors of safety was constructed using the infinite slope equation, to graphically show distribution of Factor of Safety (Figure 4-6). In other words, this map shows the spatial variability of the slope angles with respect the assumed constant value of the internal friction angle. Orange zones represent areas where the angle of the slope is above the internal friction angle and may indicate zones with higher local failure potential (FS < 1). White zones represent areas where slope angles are similar to internal friction angle (FS between 1 and 1.3), while blue zones represent areas where slope angles are definitively lower than the internal friction angle, and therefore zones of local stability (FOS>1.3).

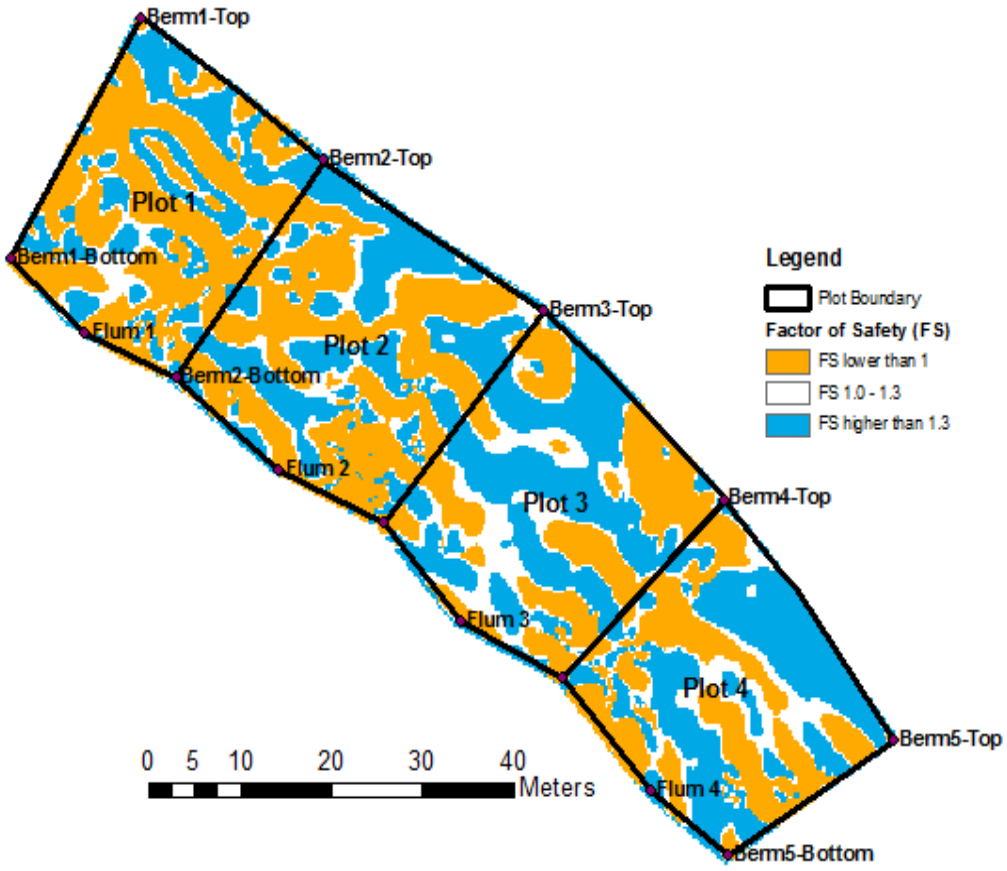

Figure 4-6 Distributional local stability map at Premium Site

3-D slope stability analysis

Introduction

Even though it is common practice to simplify slope analysis to 2-D cases, in nature, slopes are finitely wide and behave under the influence of the 3-D components. In reality, natural or real slopes will usually perform with FS's higher than those obtained from 2-D analysis, since side forces exist that will contribute to the overall equilibrium. Thus, 3-D considerations of stability analysis generally tend to provide higher Factors of Safety than 2-D considerations, and thus a 2-D approach is in general conservative producing lower values of the Factor of Safety. This observation has been found to be independent of the geometrical conditions, contour shape and soil properties of slopes. The effect of the third dimension is explored below.

3-D versus 2-D slope stability analysis

2-D slope stability analyses are based on plane-strain conditions where the width of the slope (z-direction) is assumed to be infinite; therefore the z-component of displacement vanishes everywhere and the displacements in the xy plane are functions only of x and y (Fung 1977, Malvern 1969). Since plane-strain conditions reduces the number of unknowns in a continuous medium, stabilizing forces involved in the equilibrium of a slope stability analysis, like side forces, are ignored. However, the assumption of negligible side forces used in 2-D analyses is conservative and commonly used in practice (Stark and Eid 1998).

Duncan (1996) suggested that the factor of safety obtained in a 3-D analysis is usually greater than the one from 2-D analysis, and only a few studies have shown the opposite case (Chen and Chameau 1983, Hovland 1977, Seed et al. 1990). The issue seems to arise from the fact that 3-D slope stability methods generally are extensions of 2-D procedures, where the same assumptions and simplifications are carried out to 3-D methods. In addition, the majority of the 3-D procedures have been evaluated "using parametric studies and not field case histories" (Stark and Eid 1998). As Albataineh (2006) suggested, 3-D methods are generally based on the most critical 2-D slip surface, but the real slip surface when 3-D effects are considered not necessarily matches it. Hovland (1977), proposed a method to evaluate factor of safety for 3-D slope stability analysis as an extension of Fellenius (1927) Ordinary Method of Slices, which is known for being inaccurate specially on effective stress analysis of flat slopes with high pore pressure (Duncan 1996). Chen and Chameau (1983), realizing some inaccuracies in the Hovland procedure developed an extension of the method proposed by Spencer (1967), which is recognized by its accuracy and for being one of the few 2-D procedures that satisfies all conditions of static equilibrium. However, the complexity of the extension to 3-D yielded a "misleading" procedure (Albataineh 2006) where some of the authors' assumptions where questioned by Hutchinson and Sarma (1985). Seed et al. (1990) studying the Kettleman Hills failure case, compared results for 2-D and 3-D analyses; however, as Duncan realized, the considered friction angles along the critical surface were very small (8° to 9°) being capable of produce even a 25% of discrepancy in the obtained factor of safety.

A large number of authors suggest and comment the reasonableness of a larger and then less conservative factor of safety value for 3-D slope stability analysis. Duncan (1996) concludes that "…all of the cases where F3 (3-D factor of safety) was found to be smaller than F2 (2-D factor of safety) appear to involve significant potential inaccuracies" affirming later that "studies of 3-D slope stability have progressed far enough to conclude that the factor of safety calculated using 3-D analysis will always be greater than, or equal to, the factor of safety calculated using 2-D analyses". In agreement, Cavounidis (1987) states: "methods that give F3/F2 ratios that are smaller than unity either compare inappropriate

factors or, more probably, contain simplifying assumptions that neglect important aspects of the problem". Stark and Eid (1998) studying translational failure modes concludes that if the vertical side resistance force is not considered in the analysis, the 3-D factor of safety will close to the average 2-D factor of safety for representative cross sections and concludes that "…3-D factor of safety will be greater than 2-D value for a suitable comparison." Albataineh (2006) conducted 2-D and 3-D finite element slope stability analysis using Plaxis software; the results showed higher factors of safety for 3-D finite elements analyses than for 2-D. Since the finite elements method is absent of slide forces assumptions and simplifications, it verifies the adequacy of including side forces in the 3-D analysis, and consequently, the higher factor of safety that a 3-D slope stability procedure should yield.

Duncan (1996) offers a thorough list of 3-D slope stability methods available. Table 4-4 is an adaptation of that list, where F2 and F3 are 2-D and 3-D factors of safety respectively. In nearly all cases the 3-D stability provides higher FS values than the 2-D analyses, suggesting that there should be no compromise in stability by incorporating moderate 3-D variations from the traditional planar slope.

Table 4-4 List of 3-D slope stability procedures, methods and 3-D effects (adapted from Duncan, 1996)

Authors	Method	3-D effects found
(Anagnosti 1969)	Extended Morgenstern and Price	F3 = 1.5 F2
(Baligh and Azzouz 1975)	Extended circular arc	F3 > F2
(Giger and Krizek 1975)	Upper bound theory of perfect plasticity	F3 > F2
(Giger and Krizek 1976)	Upper bound theory of perfect plasticity	F3 > F2
(Baligh et al. 1977)	Extended circular arc	F3 > F2
(Hovland 1977)	Extended ordinary method of slices	F3 < F2 for some cases
(Azzouz et al. 1981)	Extended Swedish circle	F3 = 1.07 to 1.3 F2
(Chen and chameau 1982)	Extended Spencer and Finite Element	Spencer similar to FEM
(Chen and Chameau 1983)	Extended Spencer	F3 < F2 for some cases
(Azzouz and Baligh 1983)	Extended Swedish circle	F3 > F2
(Dennhardt and Foster 1985)	Assumed slip surface	F3 > F2
(Leshchinsky et al. 1985)	Limit equilibrium and variation analysis	F3 > F2
(Ugai 1985)	Limit equilibrium and variation analysis	F3 > F2
(Leshchinsky and Baker 1986)	Limit equilibrium and variation analysis	F3 > F2 for C>0, F3=F2 for C=0
(Baker and Leshchinsky 1987)	Limit equilibrium and variation analysis	F3 > F2
(Cavounidis 1987)	Limit equilibrium	F3 must be > F2
(Hungr 1987)	Extended Bishop's modified	F3 > F2
(Gens et al. 1988)	Extended Swedish circle	F3 > F2
(Leshchinsky and Mullett 1988)	Limit equilibrium and variation analysis	F3 > F2
(Ugai 1988)	Extended ordinary method of slices, Bishop's modified, Janbu, and Spencer	F3 > F2 except for Ordinary method of Slices
(Xing 1988)	Limit equilibrium	F3 > F2
(Michalowski 1989)	Kinematic theorem of limit plasticity	F3 > F2
(Seed et al. 1990)	Ad hoc 2-D and 3-D	F3 < F2
(Leshchinsky and Huang 1992)	Limit equilibrium and variation analysis	F3 > F2

After our discussion above, the adequateness of a 3-D slope stability analysis for reclaimed slopes is at least not justified. From the inability to accurately determine mine spoil material properties, a more precise and less conservative method for slope stability analysis is probable not desired. On the other

hand, 2-D analysis offers conservatism in the procedure, helping to compensate for soil properties uncertainties, where the determined factors of safety are always situated in a safer bound.

Seismic stability analysis

Introduction

Static long term slope stability results previously reported showed that the infinite slope equation for static conditions well agrees with other limit equilibrium methods for the soil conditions present at those sites. The fundamental failure mode was observed to be shallow and concentrated inside the weak loose layer (Jeldes et al. 2010). This failure mechanism was investigated for seismic stability as well.

The natural question that emerges is how well the infinite slope equation performs for seismic conditions. In order to answer this question, a modification of the infinite slope using pseudo-static forces is proposed. This equation was tested for different pseudo static and results are summarized here. From the tested accuracy of the proposed seismic infinite slope equation, a more sophisticated procedure was developed (Jeldes and Drumm 2011). The seismic coefficient method suggested by Bray and Travasarou (2009) was unified with the proposed infinite slope equation to yield a single expression for estimating the FS of reclaimed slopes . This method allows a more realistic representation of the slope performance and hence a more accurate estimation of the FS, since spectral response analysis is included.

Seismic activity in the Appalachia

Local seismic activity in the region has been well documented. It is characterized by a cloud of events in eastern Tennessee. Although the level of seismic activity has been found to be lower than the New Madrid area (west Tennessee), the magnitude of the events have been similar. Figure 4-7 shows events of magnitude 1 to 5 recorded in the area since 1998 (http://tanasi.gg.utk.edu).

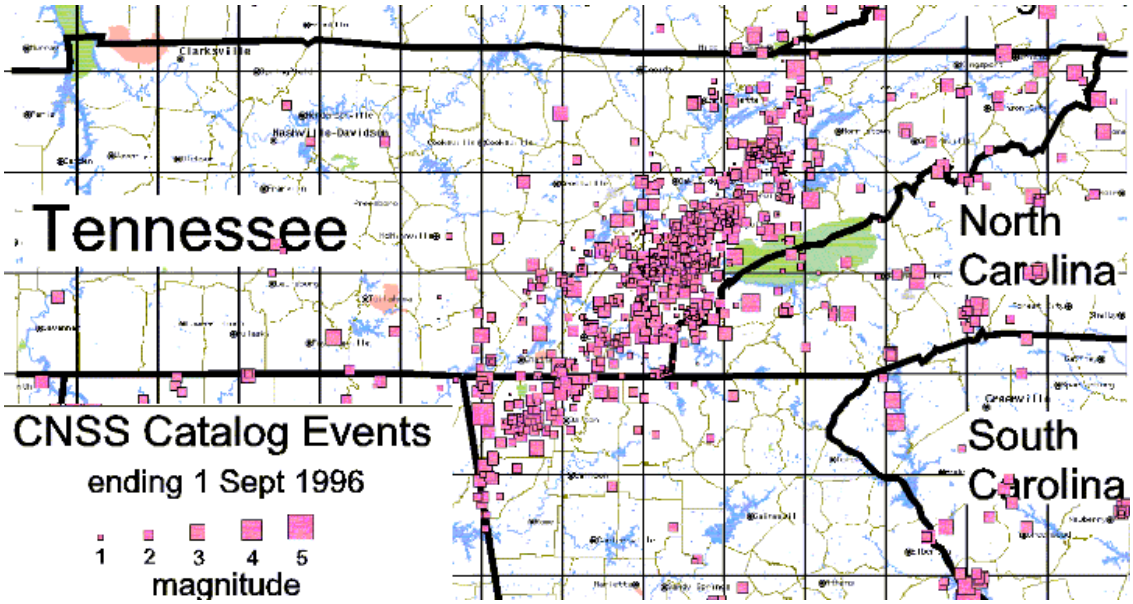

Figure 4-7 Local Seismic Activity since 1998 (University of Tennessee Geophysical Research)

Pseudo-static coefficient for seismic analysis

Pseudo-static analysis remains one of the most widely used methods for addressing seismic hazards in civil engineering practice, due to its simplicity. This method is based on d'Alembert's principle of mechanics: "A system may be set in a state of dynamic equilibrium by adding to the external forces a fictitious force commonly known as inertial force" (Paz 1997). That force is equivalent to the maximum acceleration of the structure as a fraction of the gravity of acceleration (seismic coefficient *K*) times the mass of the structure.

One of the big problems with this method is that in reality seismic forces are cyclic, going back and forward in seconds or probably tenths of the second, producing most likely a series of displacement impulses instead of failure when FS is lower than unity (Bray and Travasarou 2009, Towhata 2008). Thus, this method is recognized as being conservative. Nevertheless, a more interesting issue arises from the fact that the maximum acceleration experienced during an earthquake is not equivalent to the seismic coefficient regardless of d'Alembert's principle (Towhata 2008). Many authors have proposed expressions for horizontal seismic values as a function of the maximum or peak ground acceleration. Terzaghi (1950) proposed 0.1g for severe earthquakes, 0.25g for violent and destructive earthquakes, and 0.5g for Catastrophic earthquakes. Noda et al. (1975) developed an empirical back-calculated equation based on regression analysis of a series of acceleration records. Makdisi and Seed (1978) proposed values of 0.1g and 0.15g for earthquakes of approximate magnitude 6.5 and 8.25 respectively, accompanied by a strength reduction factor due to cyclic strength degradation. Seed (1979) listed a number of seismic coefficients accepted for design of earth dams in several countries, all ranging from 0.1g to 0.15g. Hynes-Griffin and Franklin (1984) suggested that *Kh* = 0.5PGA will not generate excessively large deformations in the slope if the factor of safety is higher than 1. Kavazanjian et al. (1997) proposed acceleration reduction equal to 0.17 if response analysis is conducted, otherwise 0.5. Bray and Rathje (1998) proposed a value of 0.75PGA along with a conservative soil strength value. Bray and Travasarou (2009) proposed a more sophisticated procedure; they assumed *Kh* is not a fraction of the PGA but a function of the 5% damped elastic spectral acceleration (*Sa*) of the site, the desired displacement (*Da*), initial fundamental period (*Ts*) and earthquake magnitude (*M*). This last approach is discussed later in this article. Table 4-5 presents a summary of the methods for estimating pseudo-static coefficients.

Table 4-5 Summary of recommended pseudo-static values and expressions, excluding coefficients for earth dams reported by Seed (1979). (Adapted from Duncan, 2005)

Method or Reference	Seismic Coefficient					
	Accel.	Accel. Reduction Factor or Expression	Strength Reduction Factor	Min. FS	Max. Allowable Displ. (m)	Other
Terzaghi (1950)	*0.10g*	-	-	> 1.00	-	-
	0.25g	-	-	> 1.00	-	-
	0.50g	-	-	> 1.00	-	-
Noda et al. (1975)	PGA_H	$\frac{PGA_H{}^{1/3}}{3}$	-	-	-	-
Makadisi and Seed (1978)	*0.20g*	0.50	0.80	1.15	≈ 1.0	For M≈6.5
	0.75g	0.50	0.80	1.15	≈ 1.0	For M≈8.25
Hynes-Griffin and Franklin (1984)	PGA_H	0.50	0.80	> 1.00	1.0	-
Kavazanjian et al. (1997) (*)	PGA_H	0.17	0.80	> 1.00	1.0	With response analysis
	PGA_H	0.50	0.80	> 1.00	1.0	Without response analysis
Bray et al. (1998)	PGA_H	0.75	-	> 1.00	0.15 – 0.30	Requires conservative strength values

(*) Acceleration reduction factor reported for soil conditions. Strength reduction factor only for saturated or sensitive clays

Regardless of the seismic coefficient developed by Noda et al. (1975), all the expressions were developed from procedures originally created to estimate displacements and in one way or the other all are based in the block principle first proposed by Newmark (1965). Performance of the slope is conditioned by allowable displacements and a minimum factor of safety; Duncan and Wright (2005) provided a good summary of displacement and factor of safeties values for an acceptable performance for many of the procedures described above.

Regarding the vertical seismic coefficient *Kv*, it has been usual practice either to assume a vertical component equal one half of the horizontal acceleration or neglect its contribution. Examples of recorded seismically activity (e.g. Towhata, 2008) shows that the maximum vertical acceleration is lower than the horizontal and it can be assumed with little error 0.5PGA, while neglecting its effect may lead to unstable slopes with factor of safety over 1.

Other issues related to this approuch have been also identified. The assumtion of locating the inertial force in the center of gravity of the slice is an issue identified by Seed (1979), where more critical Factors of Safety were obtained when the inertial force was applied in bottom of the slice. Also, Terzaghi (1950) commented about the inaccuracy of the model. Kramer (1996) based on Terzaghi's work states that the selection of the seismic coefficient is not an easy job, and even with a FS > 1 the slope may fail.

However, experience has shown that this method combined with adequate engineering judgment may produce successful engineering designs of structural and geotechnical structures.

A proposed Modification of the Infinite Slope equation for horizontal and vertical pseudo-static forces

The infinite slope method is a limit equilibrium analysis in which the failure surface is assumed to be roughly parallel to the ground surface, at a depth that is small with respect to the length of the slope. As it was shown before, this method is a simple and quick procedure for estimating the FS of a slope for cohesionless materials, when the fundamental failure mode is a shallow failure surface. Because the low compaction surface in slopes constructed according to the FRA creates a surface layer of loose material, this failure mode seems especially appropriate under these conditions. Slope stability analysis showed that the infinite slope equation for static conditions is in good agreement with limit equilibrium methods for the soil conditions present at those sites (e.g. search box feature in Slide (Rocscience Inc. 2011) with assumed soil properties for the base core material, and with a critical slip surface search focused on the upper 1.5 m) (Jeldes et al. 2010). Additional analyses using method of slices (e.g. Simplified Bishop) simulating homogeneous slopes with properties of the weak, loose layer have also demonstrated that the fundamental failure mode is shallow and concentrated approximately in the first 1.5 m. Thus this failure mechanism was investigated for seismic stability as well.

Figure 4-8 shows a slip surface of depth z below the ground surface (adapted from Salgado 2008). The weight of the slice $W = \gamma_T bz$, where γ_T is the total initial weight of the soil, *b* is the width of the slice and *z* is the depth of the slice. The width *b* may be expressed as $b = l\ cos\beta$ (where *l* is the length of the corresponding slip segment) and the slice weight may be expressed $= \gamma_T lzcos\beta$. *KhW* and *KvW* are the corresponding horizontal and vertical pseudo-static seismic forces applied in the center of mass of the segment and *P* and *T* are the corresponding resultant forces at the bottom of the slice.

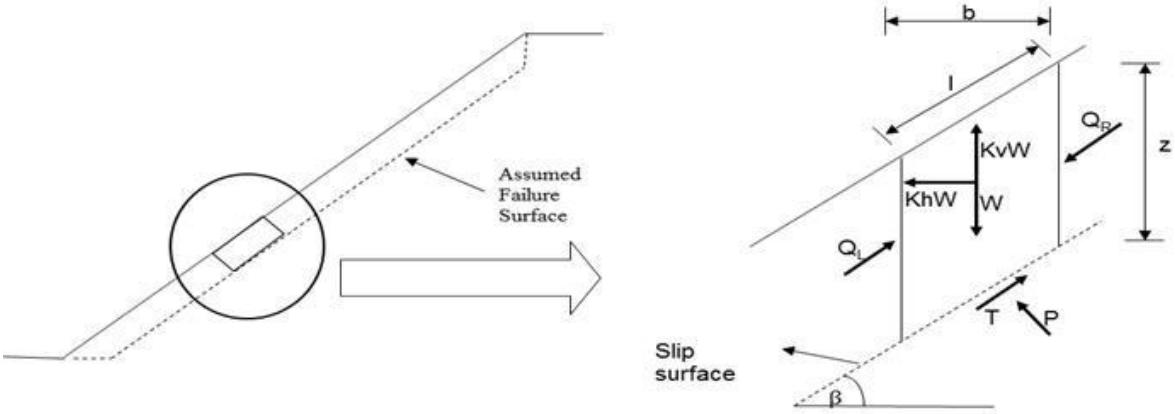

Figure 4-8 Infinite Slope Method (adapted from Salgado, 2008)

The infinite slope assumption concludes that Q_R and Q_L on either side of the vertical element are opposite and equal, and can be neglected. Analyzing all the remaining forces in a simple rotated free diagram (rotated in a *–β* angle with respect the horizontal), the corresponding resultant forces are

$$T = \gamma_T lzcos\beta[(1 - Kv)\ sin\beta + Kh\ cos\beta] \quad (4\text{-}27)$$

$$P = \gamma_T lzcos\beta[(1 - Kv\ )cos\beta - Kh\ sin\beta] \quad (4\text{-}28)$$

where $\gamma_T lzcos\beta = W$. On the other hand, the shear strength of the soil may be expressed as

$$T = \frac{Cl + Ptan\phi}{FS} \tag{4-29}$$

In term of the stresses the FS may be expressed as

$$FS = \frac{C + \frac{P}{l}tan\phi}{\frac{T}{l}} = \frac{C + \sigma tan\phi}{\tau} \tag{4-30}$$

Inserting Eq. (4-27) and (4-28) into (4-30), we obtain the following FS in terms pseudo-static forces

$$FS = \frac{C + \gamma_T zcos\beta[(1 - Kv)cos\beta - Kh\ sin\beta]tan\phi}{\gamma_T zcos\beta[(1 - Kv)\ sin\beta + Kh\ cos\beta]} \tag{4-31}$$

For cases of negligible cohesion, the equation simplifies to:

$$FS = \frac{[(1 - Kv)cos\beta - Kh\ sin\beta]tan\phi}{(1 - Kv)\ sin\beta + Kh\ cos\beta} \tag{4-32}$$

If the contribution of the vertical ground acceleration is neglected, then Eq. (4-31) simplifies to an equation equivalent to the one proposed by Duncan and Wright (2005)

$$FS = \frac{C + \gamma_T zcos\beta[cos\beta - Kh\ sin\beta]tan\phi}{\gamma_T zcos\beta[\ sin\beta + Kh\ cos\beta]} \tag{4-33}$$

Comparative Slope stability analysis

Slope stability methods and pseudo-static coefficient.

In this analysis the proposed seismic Infinite Slope equation was employed and compared with the Simplified Bishop method of slices (Interactive Software Designs INC 2008, Rocscience Inc. 2011) in terms of resulting factor of safeties. All pseudo-static coefficients based on PGA previously discussed were tested using both procedures. The suggested Bray and Travasarou (2009) approach was also employed and discussed later in this article.

Peak Ground Acceleration (PGA)

Estimation of the PGA was made based on local hazard maps developed by the U.S. Geological Survey (USGS) web site (http://earthquake.usgs.gov/earthquakes). For a 2% of probability of exceedance in 50 years, the PGA was estimated to be 0.2g and for 10% of probability of exceedance in 50 years, the estimated PGA was 0.07g. It is important to mention that the PGA varies slightly among the three sites, but the maximum PGA found among the three sites (0.2g and 0.07g) are used in the analyses.

Considered geometry and soil properties

A generic slope representative of the most probable severe condition at the 3 project sites was investigated. The slope was assumed to have a height of 14 m and an inclination of 28 degrees, with the properties given in Table 4-1 for the Premium site. For seismic analysis, typically undrained shear strength values are used since seismic excitation may be considered a short-term load condition, and excess pore water pressure may develop. However, it is assumed that the coarse, low density material resulting from the FRA compaction methods would drain appropriately, and the probability of significant excess of pore pressure development during an earthquake event is very low (Duncan and Wright 2005). Consequently, identical drained and undrained strength parameters are used for both static and dynamic slope stability analysis for these reclaimed slopes.

Makdisi and Seed (1978) reported behavior of clay soils under cyclic loads and indicated that "in most cases this value (cyclic shear strength) would appear to be 80% of the static undrained strength" suggesting later that 0.8 would be an appropriate value for stability analysis. The same reduction factor was proposed by Hynes-Griffin and Franklin (1984). Kavazanjian et al.(1997) proposed the same reduction factor only when fully saturated or sensitive clays are being analyzed. During cyclic loading, clays usually present a high non-linear shear modulus behavior that decreases with the number of cycles. Idriss et al.(1978) compared the hysteresis loop behavior of a clay soil at 1 and 10 cycles, showing that clays tend to become softer when the number of cycles increases. The reasons may be found in the excess of pore water pressure developed during the cyclic excitation that in turn decreases the effective stress, and the destruction of the electrical and chemical bounding between clay particles (Towhata 2008). On the other hand, granular material usually behaves in the opposite way; it tends to become stiffer when the number of cycles increases. After the discussion presented above, the application of the suggested strength reduction factor may be not applicable for the type of material found at these sites, and therefore no reduction was applied to the material properties.

Resulting Factor of safeties

Static slope stability analysis conducted for these sites have showed that the minimum FS is essentially the same when the slope is modeled assuming a surface layer with a uniform thickness of 1.5 m over a highly strong core-base material or when it is modeled as a homogeneous slope with the soil properties of the looser surface layer; the fundamental failure mechanism runs near the surface due to the frictional behavior of the soil present in the region. Then, a homogeneous slope model was analyzed using the software Slide (Rocscience Inc. 2011) and the Simplified Bishop method of slices. Table 4-6 summarizes the obtained FS using the proposed Infinite Slope equation and Simplified Bishop method, for a variety of pseudo-static coefficients.

Table 4-6 Summary of the horizontal and vertical pseudo-static coefficients and obtained factors of safety for a 2 and 10% of probability of exceedance in 50 yr.

Method or Reference	Seismic Coefficient			Computed Factor of Safety			
	K	For a 2% of p. of ex. in 50 yr. (PGA=0.2)	For a 10% of p. of ex. in 50 yr. (PGA=0.07)	Infinite Slope Equation	Simplified Bishop Method	Infinite Slope Equation	Simplified Bishop Method
				FS for a 2% of p. of ex. in 50 yr.		FS for a 10% of p. of ex. in 50 yr.	
Theoretical d'Alembert Principle	*Kh*	0.20	0.07	**0.91**	**0.92**	**1.24**	**1.25**
	Kv	0.10	0.04				
Makadisi and Seed (1978) (M≈6.5)	*Kh*	0.10	0.04	**1.14**	**1.15**	**1.35**	**1.34**
	Kv	0.10	0.04				
Hynes-Griffin and Franklin (1984)	*Kh*	0.10	0.04	**1.14**	**1.15**	**1.35**	**1.34**
	Kv	0.10	0.04				
Noda et al. (1975)	*Kh*	0.19	0.14	**0.92**	**0.94**	**1.07**	**1.07**
	Kv	0.10	0.04				
Bray et al. (1998)	*Kh*	0.15	0.05	**1.02**	**1.03**	**1.29**	**1.31**
	Kv	0.10	0.04				
Kavazanjian et al. (1997) (Without response analysis)	*Kh*	0.10	0.04	**1.02**	**1.03**	**1.29**	**1.31**
	Kv	0.10	0.04				

For all pseudo-static coefficients, all combination of force orientations were tested, with the most critical being when the vertical seismic force and the horizontal seismic force act simultaneously away from the slope. Notice the good agreement between the proposed infinite slope equation and the Simplified Bishop method in terms of critical factor of safety for seismic loads.

When predicted parameters for a 10% of probability of exceedance in 50 yr. are used, almost all factors of safety are well above 1. It is expected then that the shear strength along the slip surface be 25-31% greater than the required to maintain equilibrium. For a 2% of probability of exceedance, the computed factors of safety are naturally much lower. When the applied inertial force is applied directly (without acceleration reduction factors summarized in Table 1) the obtained FS=0.91 is below unity and indicates failure. Hynes-Griffin and Franklin (1984) and Makdisi and Seed (1978) approaches give a FS=1.14-1.15. Hynes-Griffin requires a minimun FS=1, while Makdisi and Seed require minimun FS=1.15. Underthese criteria, the slope should be stable. Under static conditions, the factor of safety for those sites is FS=1.47, meaning that under seismic conditions the ratio of available shear strenth to shear stress is reduced about 30%.

Notice that the equation proposed by Noda et al. (1975), for a 2% of probability of exceedance in 50 yr., gives factors of safety similar to the case when no reduction has been made to the inertial force, but for a 10% of probability of exceedance in 50 yr. Noda's procedure computes the lowest factor of safety among the authors (FS=1.07), which is even lower than the factor of safety for the maximum ground acceleration without reduction. Noda et al. (1975) developed the equation based on limit-equilibrium

analysis to structures (quay walls) that where already damaged by earthquakes, where the results and parameter selection probably have a high level of subjectivism. As Towhata (2008) states "…there are many uncertainties in this study, probably including the determination of appropriate soil strength in the limit equilibrium analysis".

Regarding seismic coefficient to be used, Hynes-Griffin and Franklin (1984), Bray and Rathje (1998) and Kavazanjian et al. (1997) seem to be the most applicable approaches for these sites. Even though the Makdisi and Seed (1978) method produces the same *K* value as Hynes-Griffin, it is based on a most general approuch. Since current hazard maps have broad coverage and easier access, a more site-based design is possible.

Slope stability charts based on spectral accelerations

Based on a new procedure proposed by Bray et al. (2009) and the proposed seismic infinite slope equation, a simple, graphical procedure is developed for a quick estimation of the factor of safety.

Bray's procedure for calculating the pseudo-static seismic coefficient

Bray and Travasarou (2007), using 688 earthquake records and a non-linear coupled stick-slip deformable sliding block model, developed a semi-empirical probabilistic equation for estimating permanent displacements due to seismic forces. Rathje and Bray (2001) in a previous work suggested that a stick-slip deformable sliding block model offer a more realistic representation than the rigid block model first proposed by Newmark (1965). Using this model, a series of displacements where calculated for different yielding seismic factors (*Ky*) and initial fundamental periods (*Ts*). Then, a relationship between induced displacement and a single value of motion intensity was found to be optimally satisfied not by PGA, but by the 5% damped elastic spectral acceleration (*Sa*) at the degraded fundamental period. They found that the spectral acceleration at the degraded period is essentially 1.5*Ts*, due to material non-linearity. Later, Bray and Travasarou (2009) offered a procedure to calculate the pseudo-static coefficient based on the Bray and Travasarou approach; now, instead of calculating displacements, the yielding seismic coefficient can be estimated as a function of allowable seismic displacement (*Da*), the 5% damped elastic spectral acceleration (*Sa*) of the site, the initial fundamental period (*Ts*), a random normal distributed variable (ε) and earthquake magnitude (*M*). The Bray and Travasarou seismic coefficient is:

$$K = e^{\frac{-a+\sqrt{b}}{0.665}} \tag{4-34}$$

$$a = 2.83 - 0.566 \ln(Sa) \tag{4-35}$$
$$b = a^2 - 1.33\,[\ln(Da) + 1.10 - 3.04 \ln(Sa) + 0.244 \ln^2(Sa) - 1.5\,Ts - 0.278\,(M - 7) - \varepsilon]$$

The assumptions behind the original model are a uniform unit weight equal to 17.6 kN/m^3, shear modulus dependent on the strain level and soil damping ratio for plasticity index of 30. However, as the authors states, adjustments to those parameters do not produce significant effect on the displacements (Bray and Travasarou 2007) and therefore do not significantly impact the calculated seismic coefficient.

Determination of the Spectral acceleration

Local spectral acceleration values as a function of the earthquake period for every site were obtained from the USGS web site (http://earthquake.usgs.gov/earthquakes) for 2 and 10% of probability of exceedance in 50 yr. Here, one or more ground acceleration records representative of the "maximum credible ground motion" are converted to response spectrum, usually for a 5% damping. After smoothing, a curve of *Sa(T)* is obtained and used for engineering purposes (National Research Council (U.S.). Committee on Safety Criteria for Dams. 1985). Figure 4-9 shows the spectral acceleration plot for the Premium site. Spectral acceleration plots for National and Mountainside are reported in the Appendix A.

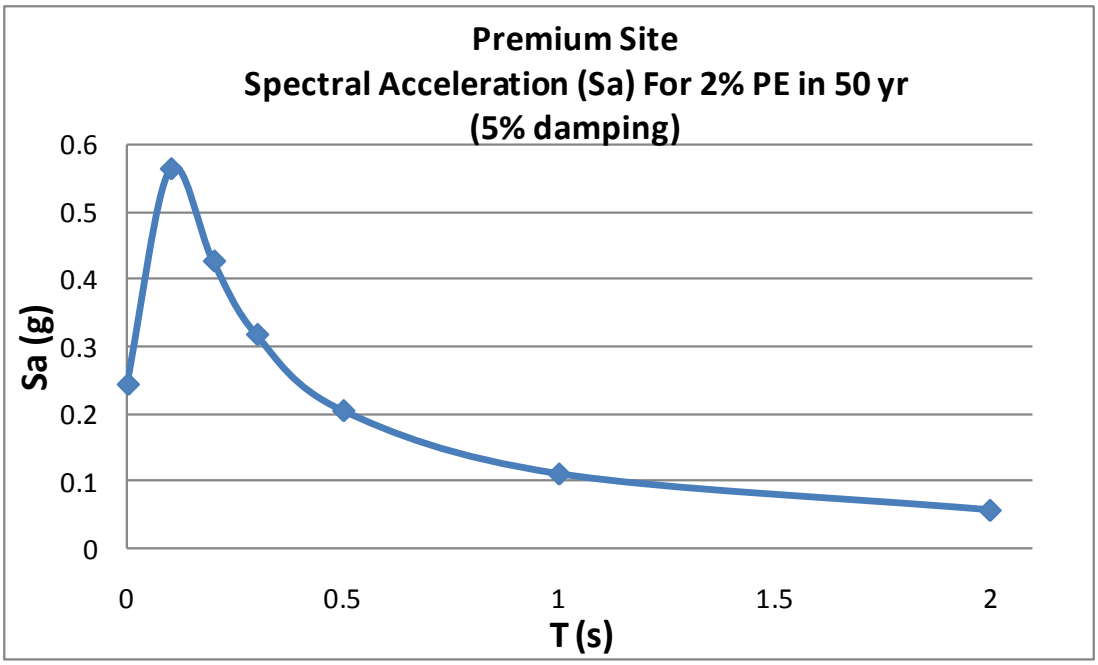

Figure 4-9 Spectral Acceleration Plot for Premium site (USGS)

Proposed equation for determining Factor of Safety

Bray's seismic coefficient was unified with the proposed infinite slope equation to yield a single expression for estimating the FS of reclaimed slopes under seismic conditions:

$$FS = \frac{C+\gamma_T z cos\beta\left[(1-0.5\exp(\frac{-a+\sqrt{b}}{0.665}))cos\beta-\exp(\frac{-a+\sqrt{b}}{0.665})\,sin\beta\right]tan\phi}{\gamma_T z cos\beta\left[(1-0.5\exp(\frac{-a+\sqrt{b}}{0.665}))\,sin\beta+\exp(\frac{-a+\sqrt{b}}{0.665})\,cos\beta\right]} \quad (4\text{-}36)$$

Where *a* and *b* are defined by the Eq. (4-35). The vertical coefficient *Kv* was assumed to be one half of the horizontal coefficient *Kh*.

Solution charts

Graphical chart solutions of Eq. (4-36) for different earthquake magnitudes, maximum allowable displacements and soil properties have been developed for each of the FRA reclaimed sites. However, the proposed solution is valid for any slope constructed with FRA and built with granular material whose fundamental failure mode shallow is (i.e. cohesionless material), and conditions similar to those at

Premium, National and Mountainside. For simplicity, the magnitude of the earthquake was assumed to be equal to 5.0, since this is about the highest earthquake magnitude usually recorded in the zone. Figure 4-10 illustrate the solution chart for the conditions at Premium site. Here the *Da* is selected to be 30 cm for a 2% of probability of exceedance in 50 years. The random variable ε was selected to be 0.66 representing a 16% of allowable displacement exceedance (Bray and Travasarou 2009). Solution charts for *Da* equal to 30, 50 and 100 cm and for 2 and 10% of probability of exceedance in 50 years are reported for each site in the Appendix A.

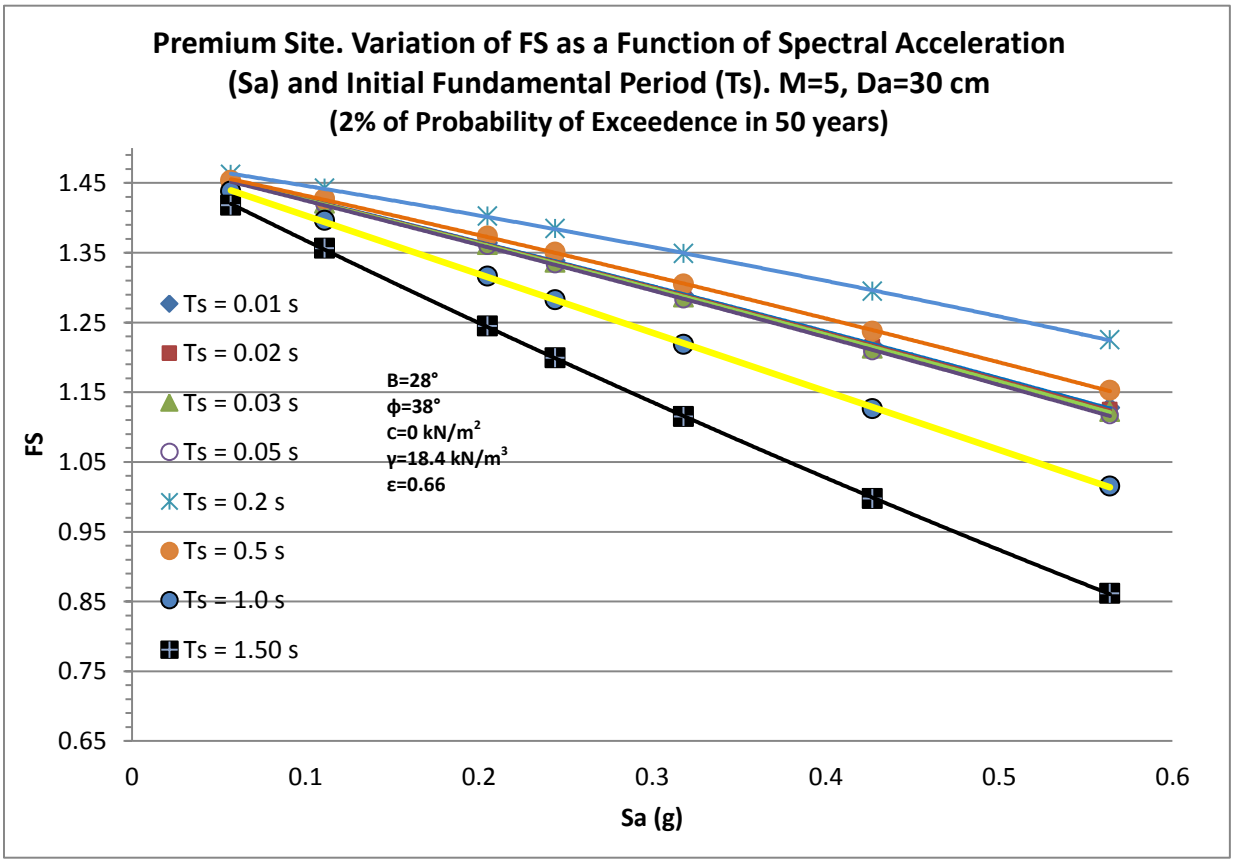

Figure 4-10 FS chart for Premium site as a function of spectral accelerations and initial fundamental period

Illustrative example

For this example, a slope with the geometric conditions and soil properties described for the Premium site is used. The designer needs to decide what magnitude M and maximum allowable displacement (Da) to use, according to the available local seismic information and importance of the project. For Premium site, M = 5.0 and Da = 30 cm (0.98 ft) may be acceptable, since those slopes are constructed in rural areas. Other magnitudes and displacements may be selected as well. The initial fundamental period of the slope may be calculated using $Ts = 4H/Vs$ where H is the slope height and Vs average shear wave velocity of the slope. Since no measurements of the shear wave velocity at the site have been made, an average Vs=200 m/s (656.17 ft/s) was assumed. For a shallow failure mode (e.g. in the upper 1.5 m) the initial fundamental period becomes Ts=0.03 and the spectral acceleration at the degraded period Sa(T=0.045) ≈ 0.45 (from Figure 4-7). Then, for Ts=0.03 s and Sa=0.45 g the computed FS is approximately 1.20.

Conclusions

Factors of safety obtained for the weak layer analysis under static conditions showed that for long term stability of the slopes with inclinations as much as 28 degrees, the observed shear strength along the slip surface is 47% greater than that required to balance the destabilizing forces and the slopes should be stable in the long term (when there is no excess pore water pressure developed in the material, or with no water movement through the upper weak layer). In the unlikely event that the entire loose zone was to become saturated with downslope seepage, the Factor of Safety is reduced by a factor of 2, suggesting that the slope would be unstable.

Results from the simple "Infinite Slope" stability calculations for long term stability are consistent with the more typical solutions based on an assumed circular failure surface, with the likely failure passing through the weak surface layer. Due to its simplicity the Infinite Slope method may be appropriate for long term stability analysis of slopes constructed using a low compaction grading techniques. In addition, it is compatible with the recommended method for the visual estimation of material shear strength based on the angle of repose, especially consideration of the typical absence of strength measurements of any type.

To address the stability of more complex slope shapes which would accompany the adoption of "landforming" construction techniques, a literature review investigating the differences between the stability determined using traditional 2-D methods, and that obtained when the full 3-D effects were included. It was shown that the factors of safety considering the 3 dimensional effects are nearly always greater than the more conservative results obtained from the traditional 2 -D slice methods. This suggests that slopes with non-planar or complex geometry in the direction perpendicular to the cross section of the slope are generally more stable than if they are planar in this direction, and suggests that reclamation activities which encourage "landforming" or more natural looking slopes should not decrease the stability.

Under seismic loading conditions, the proposed infinite slope equation showed good agreement with the simplified Bishop method of the slices. The selection of the pseudo-static coefficient requires an understanding of the assumptions behind the coefficient, and these considerations were discussed. For these instrumented sites, reasonable results were obtained when the horizontal seismic coefficient proposed by Hynes-Griffin and Franklin (1984), Bray and Rathje (1998) and Kavazanjian et al. (1997) where employed. While these methods based on a fraction of the Probable Ground Acceleration are most common, they do not consider the effects of frequency and duration (Bray 2007). A procedure based on spectral response may provide a better tool for evaluating slope stabilities, and a combination of the Bray and Travasarou (2009) approach with the proposed modification of infinite slope equation was suggested. This yields a simple procedure for estimating the factor of safety as a function of more objective parameters that are a function of the importance of the project, available seismic data, and accuracy of the site characterization. It is suggested that the use of spectral values for a 2% of probability of exceedance in 50 yr. or higher are sufficient, except when the designer has reasons for using lower local values.

The slopes at all three study sites were observed to have static Factors of Safety for long term stability that are well above 1.3, suggesting that the FRA with low compaction surface materials does not compromise the long term stability of the slopes for the material properties encountered at the

instrumented sites. It is suggest that the infinite slope stability analysis method, coupled with the estimation of the shear strength of the reclaimed materials from field observations, provides a simplified yet rational means to evaluate the stability of FRA constructed slopes.

References:

Abramson, L. W. (1996). *Slope stability and stabilization methods*, Wiley, New York.

Albataineh, N. (2006). "Slope Stability Analysis Using 2D and 3D Methods." M.S. dissertation, University of Akron, Akron, OH.

Anagnosti, P. (1969). "Three-dimensional stability of fill dams." *Proc., 7th International Conference on Soil Mechanics and Foundation Engineering*, Mexico, 275-280.

Azzouz, A. S., and Baligh, M. M. (1983). "Loaded Areas on Cohesive Slopes." *Journal of Geotechnical Engineering-Asce*, 109(5), 724-729.

Azzouz, A. S., Baligh, M. M., and Ladd, C. C. (1981). "Three dimensional stability analysis of four embankment failures." *Proc., 10th International Conference on Soil Mechanics and Foundations Engineering*, Rotterdam, The Netherlands, 343-346.

Baker, R., and Leshchinsky, D. (1987). "Stability analysis of conical heaps." *Soils and Foundations*, 27(4), 99-110.

Baligh, M. M., and Azzouz, A. S. (1975). "End effects on stability of cohesive slopes." *Journal of Geotechnical Engineering-Asce*, 101(GT11), 1105-1117.

Baligh, M. M., Azzouz, A. S., and Ladd, C. C. (1977). "Line loads on cohesive slopes." *Proc., 9th International Conference on Soil Mechanics and Foundations Engineering*, Tokyo, 13-17.

Bishop, A. W. (1955). "The use of the Slip Circle in the Stability Analysis of Slopes." *Geotechnique*, 5(1), 7-17.

Bray, J. D. (2007). "Simplified seismic slope displacement procedures." *Proc., 4th International Conference on Earthquake Geotechnical Engineering-Invited Lectures*, Springer Netherlands.

Bray, J. D., and Rathje, E. M. (1998). "Earthquake-induced displacements of solid-waste landfills." *J Geotech Geoenviron*, 124(3), 242-253.

Bray, J. D., and Travasarou, T. (2007). "Simplified procedure for estimating earthquake-induced deviatoric slope displacements." *J Geotech Geoenviron*, 133(4), 381-392.

Bray, J. D., and Travasarou, T. (2009). "Pseudostatic Coefficient for Use in Simplified Seismic Slope Stability Evaluation." *J Geotech Geoenviron*, 135(9), 1336-1340.

Cavounidis, S. (1987). "On the Ratio of Factors of Safety in Slope Stability Analyses." *Geotechnique*, 37(2), 207-210.

Chen, C. M., and chameau, J. L. (1982). "Three-dimensional stability analysis." *Proc., 4th International Conference on Numerical Methods in Geomechanics*, Rotterdam, The Netherlands, 671-677.

Chen, R. H., and Chameau, J. L. (1983). "Three-Dimensional Limit Equilibrium-Analysis of Slopes." *Geotechnique*, 33(1), 31-40.

Dennhardt, M., and Foster, W. (1985). "Problems of three dimensional slope stability." *Proc., 11th International Conference on Soil Mechanics and Foundations Engineering*, Rotterdam, The Netherlands, 427-431.

Duncan, J. M. (1996). "State of the art: Limit equilibrium and finite-element analysis of slopes." *Journal of Geotechnical Engineering-Asce*, 122(7), 577-596.

Duncan, J. M., and Wright, S. G. (1980). "The Accuracy of Equilibrium Methods of Slope Stability Analysis." *Eng Geol*, 16(1-2), 5-17.

Duncan, J. M., and Wright, S. G. (2005). *Soil strength and slope stability*, John Wiley & Sons, Hoboken, N.J.

Fellenius, W. (1927). *Erdstatische Berechnungen mit Reibung und Kohasion*, Ernst und Zohn, Berlin.

Fung, Y. C. (1977). *A first course in continuum mechanics*, Prentice-Hall, Englewood Cliffs, N.J.

Gens, A., Hutchinson, J. N., and Cavounidis, S. (1988). "Three-Dimensional Analysis of Slides in Cohesive Soils." *Geotechnique*, 38(1), 1-23.

Giger, M. W., and Krizek, R. J. (1975). "Stability analysis of vertical cut with variable corner angle." *Soils and Foundations*, 15(3), 63-71.

Giger, M. W., and Krizek, R. J. (1976). "Stability of vertical corner cut with concentrated surcharge load." *Journal of Geotechnical Engineering-Asce*, 102(1), 31-40.

Hovland, H. J. (1977). "Three-Dimensional Slope Stability Analysis Method." *Journal of the Geotechnical Engineering Division-Asce*, 103(9), 971-986.

Hungr, O. (1987). "An extension of Bishop simplified method of slope stability analysis to three dimensions." *geotechnique*, 37(1), 113-117.

Hutchinson, J. N., and Sarma, S. K. (1985). "Discussion of 'Three-dimensional limit equilibrium analysis of slopes' by RH Chen and JL Chameau." *Geotechnique*, 35(2), 215-216.

Hynes-Griffin, M. E., and Franklin, A. G. (1984). "Rationalizing the seismic coefficient method." Army Engineer Waterways Experiment Station Vicksburg Ms Geotechnical Lab Vicksburg, MS.

Idriss, I. M., Singh, R. D., and Dobry, R. (1978). "Nonlinear Behavior of Soft Clays during Cyclic Loading." *Journal of the Geotechnical Engineering Division*, 104(12), 1427-1447.

Interactive Software Designs INC (2008). "XSTABL." *Interactive Software Designs INC*Moscow, ID.

Jeldes, I. A., and Drumm, E. C. (2011). "Preliminary static and seismic stability of steep slopes in reclaimed mine lands constructed with low compaction in appalachia, USA." *Proc., 5th International Conference on Earthquake Geotechnical Engineering*, Santiago, Chile.

Jeldes, I. A., Hoomehr, S., Wright, W. C., Schwartz, J. S., Lane, D. E., and Drumm, E. C. (2010). "Stability And Erosion On Steep Slopes Constructed By The Forest Reclamation Approach In The Southern Appalachian Region." *Proc., 2010 National Meeting of the American Society of Mining and Reclamation*, American Society of Mining and Reclamation, Pittsburgh, PA.

Kavazanjian, E., Matasovic, N., Hadj-Hamou, T., and Sabatini, P. J. (1997). "Design Guidance: Geotechnical Earthquake Engineering for Highways." *Design Principles, Geotechnical Engineering Circular 3*, Federal Highways Administration, Washington, DC.

Kramer, S. L. (1996). *Geotechnical earthquake engineering*, Prentice Hall, Upper Saddle River, N.J.

Lambe, T. W., and Whitman, R. V. (1969). *Soil mechanics*, Wiley, New York.

Leshchinsky, D., and Baker, R. (1986). "Three-dimensional slope stability: end effects." *soils and Foundations*, 26(4), 98-110.

Leshchinsky, D., Baker, R., and Silver, M. L. (1985). "Three dimensional analysis of slope stability." *International Journal For Numerical And Analytical Methods In Geomechanics*, 9(2), 199-223.

Leshchinsky, D., and Huang, C. C. (1992). "Generalized Three-Dimensional Slope-Stability Analysis." *Journal of Geotechnical Engineering-Asce*, 118(11), 1748-1764.

Leshchinsky, D., and Mullett, T. L. (1988). "Design Charts for Vertical Cuts." *Journal of Geotechnical Engineering-Asce*, 114(3), 337-344.

Makdisi, F. I., and Seed, H. B. (1978). "Simplified Procedure for Estimating Dam and Embankment Earthquake-Induced Deformations." *Journal of the Geotechnical Engineering Division-Asce*, 104(7), 849-867.

Malvern, L. E. (1969). *Introduction to the mechanics of a continuous medium*, Prentice-Hall, Englewood Cliffs, N.J.,.

Michalowski, R. L. (1989). "Three-dimensional Analysis of Locally Loaded Slopes." *Geotechnique*, 39(1), 27-38.

National Research Council (U.S.). Committee on Safety Criteria for Dams. (1985). *Safety of dams : flood and earthquake criteria*, National Academy Press, Washington, D.C.

Newmark, N. M. (1965). "Effects of Earthquakes on Dams and Embankments." *Geotechnique*, 15(2), 139-&.

Noda, S., Uwabe, T., and Chiba, T. (1975). "Relation between seismic coefficient and ground acceleration for gravity quay wall." *Report of the Port and Harbour Research Institute*, 67-111.

Paz, M. (1997). *Structural dynamics : theory and computation*, Chapman & Hall, New York.

Rathje, E. M., and Bray, J. D. (2001). "One- and two-dimensional seismic analysis of solid-waste landfills." *Can Geotech J*, 38(4), 850-862.

Rocscience Inc. (2011). "Slide." *Slope Stability Software*, Rocscience Inc., Toronto, Canada.

Salgado, R. (2008). *The engineering of foundations*, McGraw Hill, Boston.

Schor, H. J., and Gray, D. H. (2007). *Landforming : an environmental approach to hillside development, mine reclamation and watershed restoration*, John Wiley & Sons, Hoboken, N.J.

Seed, H. B. (1979). "19th Rankine Lecture - Considerations in the Earthquake Resistant Design of Earth and Rockfill Dams." *Geotechnique*, 29(3), 213-263.

Seed, R. B., Mitchell, J. K., and Seed, H. B. (1990). "Kettleman-Hills Waste Landfill Slope Failure .2. Stability Analyses." *Journal of Geotechnical Engineering-Asce*, 116(4), 669-690.

Sharma, S. (2008). "XSTABL reference manual." *Interactive Software Designs Inc.*Moscow, ID.

Skempton, A. W., and Delory, F. A. "Stability of natural slopes in London clay." *Proc., 4th International Conference on Soil Mechanics & Foundation Engineering*, London, 378-381.

Spencer, E. (1967). "A Method of analysis of the Stability of Embankments Assuming Parallel Inter-Slice Forces." *Geotechnique*, 17(1), 11-26.

Stark, T. D., and Eid, H. T. (1998). "Performance of three-dimensional slope stability methods in practice." *J Geotech Geoenviron*, 124(11), 1049-1060.

Sweigard, R., Burger, J., Zipper, C., Skousen, J., Barton, C., and Angel, P. (2007). "Low compaction grading to enhance reforestation success on coal surface mines." *Forest Reclamation Advisory No.3.*

Terzaghi, K. (1950). "Mechanisim of Landslides." *Eng Geol*, Berkey, 83-123.

Towhata, I. (2008). *Geotechnical earthquake engineering*, Springer, Berlin.

Ugai, K. (1985). "Three-dimensional stability analysis of vertical cohesive slopes." *Soils and Foundations*, 25(3), 41-48.

Ugai, K. (1988). "Three-dimensional slope stability analysis by slice methods." *Proc., 6th International Conference on Numerical Methods in Geomechanics*, Rotterdam, The Netherlands, 1369-1374.

Williams, R. T. "Geophysical Research." <http://tanasi.gg.utk.edu/>. (July 20, 2010).

Wright, S. G., Kulhawy, F. H., and Duncan, J. M. (1973). "Accuracy of Equilibrium Slope Stability Analysis." *Journal of the Soil Mechanics and Foundations Division*, 99(10), 783-791.

Xing, Z. (1988). "Three-dimensional Stability Analysis of Concave Slopes in Plan View." *Journal of Geotechnical Engineering-Asce*, 114(6), 658-671.

Chapter 5 Design of Non-Planar Slopes for Stability and Erosion Resistance

Abstract

Although most constructed slopes are planar in cross section, slopes observed in nature tend to be more complex in shape, and often tend towards concave profiles. Laboratory and computational studies have shown that concave slope contours may reduce erosion and sediment yield, suggesting that the concave slope profiles observed in nature may be very efficient with respect to limiting erosion and sediment. The geomorphological evolution of slopes toward an equilibrium shape from the generalized principle of minimum rate of energy dissipation is discussed, suggesting that for certain boundary conditions, slopes may evolve into concave shapes in the long term. The literature in the geomorphology area supports this finding, which may find application for designing concave slopes profiles in practice. Based on the critical equilibrium theory developed by Sokolovski (1960), a relatively simple approximate solution for the critical concave slope contour was developed. The solution can be used to determine the non planar slope profile for a given factor of safety (FS). The method is demonstrated through an example problem, and comparisons with solutions from the Limit Equilibrium method (LEM) and Finite element (FEM) analyses suggest that the proposed design methodology is accurate.

Introduction

Constructed slopes have traditionally been designed to be planar in cross section, with planar slopes encountered in most types of land development, highway cut and fill sections, constructed embankments, and reclaimed mine lands. Planar slopes are well suited to engineering analysis techniques, and typical surveying and construction practices tend to favor this shape slope profile because it is easy to depict on construction plans, and easy for construction equipment operators to build. However, in nature slopes are seldom planar in cross section, and more complex slope geometries are common with the cross section often tending to be concave. Schor and Gray (2007) suggested that slopes constructed with more complex shapes may appear more like natural slopes, and suggested that concave slopes may have superior stability and erosion resistance tendencies. With the widespread use of GPS based controls on construction equipment, the construction of slopes with complex shapes may become straightforward. This would lead to the development of slopes that appear natural in shape, are less susceptible to erosion, yield less sediment, and yet be just as mechanically stable.

Erosion is typically reduced by ensuring a quick establishment of ground cover, since vegetation absorbs raindrop impact, reduces flow energy impact by reducing runoff velocity, increases soil infiltration, and increases soil resistance (Römkens et al. 2008, Stokes et al. 2008, Yoder 2009). However, in spite of the establishment of ground cover, some erosion will occur, and structures such as porous sediment ponds, basins, and interceptor barriers must be constructed (Römkens et al. 2008, Yoder 2009). In this chapter the literature relative to slope shape and soil loss is reviewed, a brief review of the geomorphology of slopes is provided. This is followed by a presentation of the classical solution of the critical slope shape at failure, and the development and demonstration of a design method for determining the optimum shape of a non-planar slope from a stability perspective.

Slope shape and soil loss

Schaefer et al. (1979), working on reclaimed mine land, observed that concave profiles are more efficient in terms of runoff with minimal soil detachment. D'souza and Morgan (1976) conducted a series of laboratory tests on scale model slopes of equal surface area to determine how soil loss was related to slope shape and steepness. The soil employed was sand that was subjected to artificial rainfall of 53 mm/hr. intensity with duration of 30 minutes. It was found that for the studied range of slope inclinations, concave slopes experienced less soil loss (expressed in terms of grams, g) than planar and convex slopes, and the difference was most significant when slopes were steeper (Figure 5-1). Young and Mutchler (1969) constructed field plots with convex, planar and concave shapes under artificial rainfall of 63.5 mm/hr. applied in 30 minute intervals for 2 hrs. Those plots were at least 5 feet deep, were composed of 83% fine material and 17% of sand. Results showed that concave slope yielded 33% less erosion than the convex slopes and 10% less erosion than planar ones. They also reported an important reduction in average runoff velocities in the bottom half of the slopes after 30 minutes of a rainstorm. Figure 5-2 shows their results in terms of the initial and final slope shape, and indicates that after 2 hours of rainfall, deposition started about 12 feet from the bottom. Rieke-Zapp and Nearing (2005), conducted a series of laboratory analysis for a variety of slopes shapes constructed of soil that has 72% silt subjected to artificial rainfall of 60 mm/hour for a duration of 90 minutes. Results showed that concave slopes reduced the amount of sediment delivered. Table 5-1 summarizes total soil loss for the studies mentioned above, and the ratio of soil loss in concave slopes to that in planar slopes indicates that in all cases concave slopes yielded less soil loss than planar.

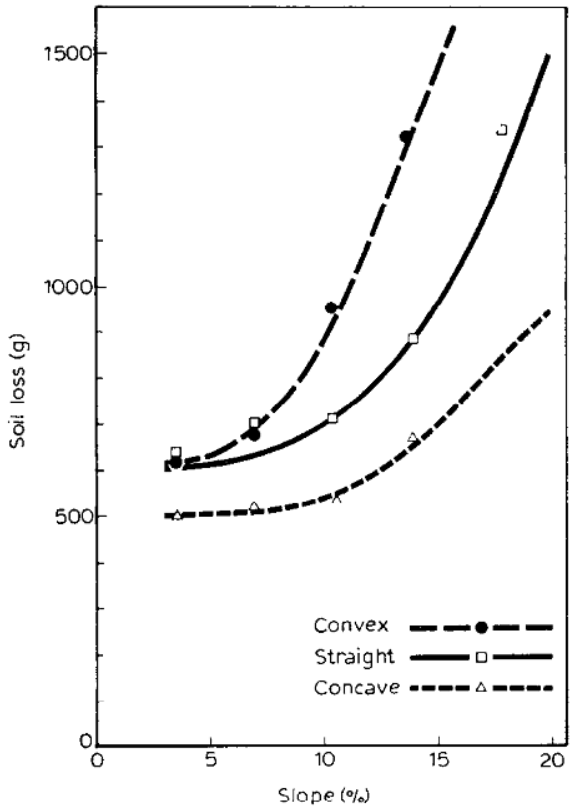

Figure 5-1 Soil loss (g) vs. slope steepness (%) for 30-min rain (Dsouza and Morgan 1976)

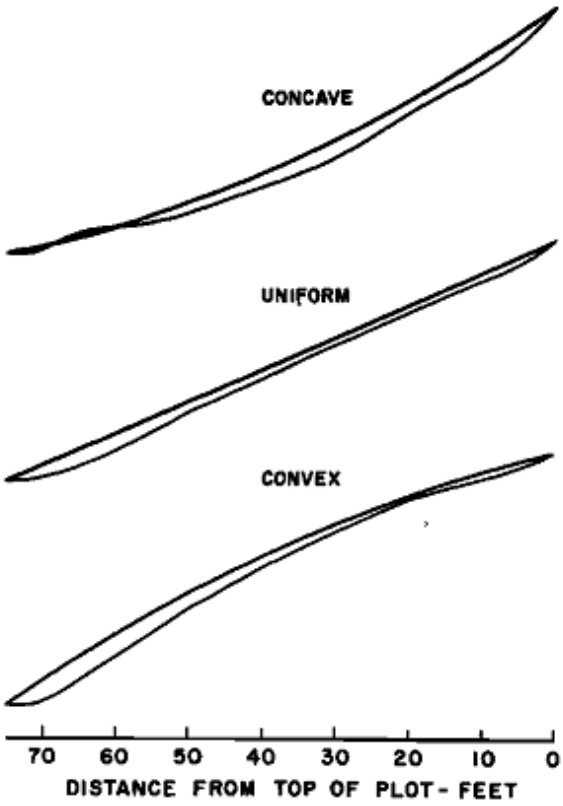

Figure 5-2 Pictorial of elevation change on slope shape plot for 2-hr rain (Young and Mutchler 1969)

Table 5-1 Summary of total soil loss for different slope shapes

Authors	Average Slope (%)	Slope Shape (soil loss in g)			Loss Concave/Loss Uniform
		Convex	Uniform	Concave	
Young and Mutchler (1969)[a]	9	890315.6	666226.8	596667.6	0.90
D'Souza and Morgan (1976)[b]	3.5	617	622	502	0.81
	7	678	683	518	0.76
	10.5	956	717	530	0.74
	14	1347	864	636	0.74
	18	----	1373	----	
Rieke-Zapp and Nearing (2005)[c]	13	51300	58500	14900	0.25

Note: Reported plot dimensions: a. 75 x 13.33 ft; b. 4 x 4 m; c. 3 x 2 m eroded only 1 m wide band down the center.

In addition to field and laboratory studies indicating that concave slopes reduce soil loss, computer models have suggested erosion reduction in concave slopes. Meyer and Kramer (1969), estimated soil loss for convex, concave, planar and complex slopes using the Universal Soil Loss Equation, dividing each slope into 10 foot increments. Soil loss for concave profiles was found to be significantly lower than

convex, planar and complex slopes (Figure 5-3), especially as slope length increased. Hancock et al. (2003) using a digital terrain model known as SIBERIA, estimated sediment delivered for planar and concave slopes. They not only found that concave slopes reduce soil loss, but also reported lower sediment delivered for higher slope concavities, for a constant slope length value. Other authors (Renard and Foster 1983, Renard et al. 1997, Toy et al. 2002) have also commented on the role of concave slopes in reducing the amount of sediment. The use of concave slopes in the reclamation of mine lands may be an effective means of reducing erosion, and may prove economical in the long term since it may reduce the size of sediment basins and lower construction and maintenance costs. An added benefit is that concave slopes may provide a more natural appearance as described subsequently.

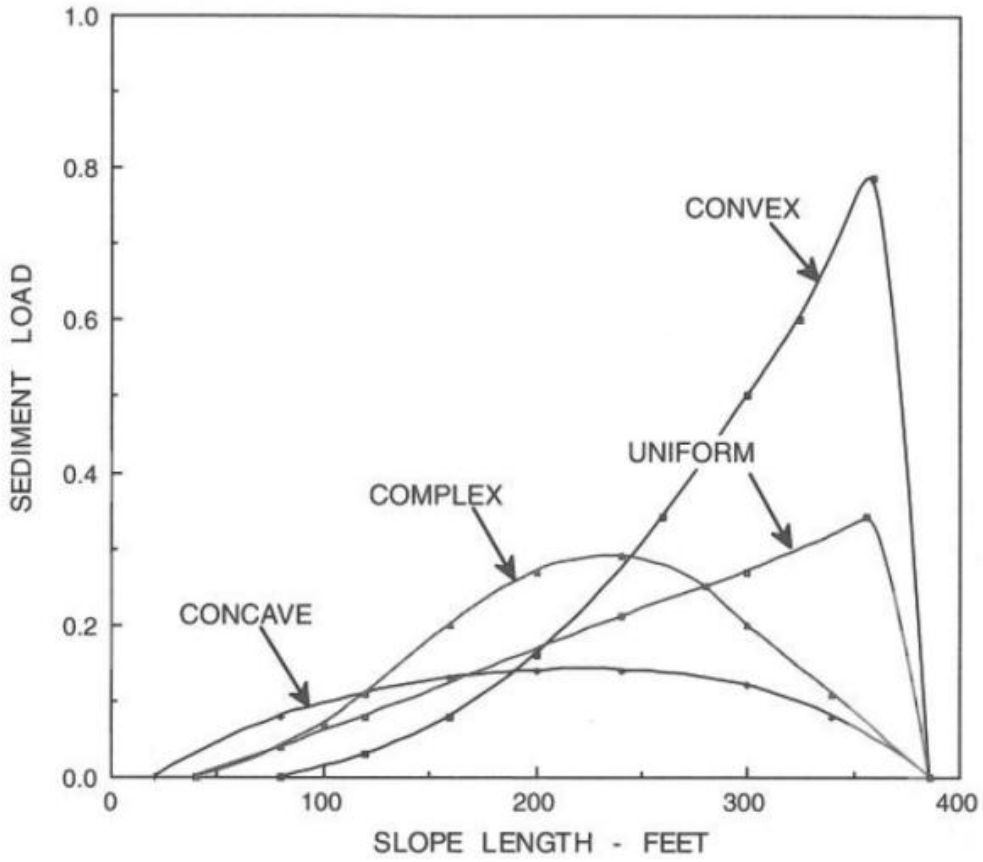

Figure 5-3 Predicted sediment load in t/ft. (Meyer and Kramer 1969)

Slope shaping processes and contours observed in nature

In nature slope profiles are rarely uniform, but usually curvilinear. Weathering and creep seem to be the principal shaping mechanisms and the principal reason for these curved profiles. The general concept of "form following function" is observed in geomorphological evolutionary processes like the evolution of streams and slopes that transport water and sediment, where concave equilibrium profiles seem to be the fundamental resulting shape of this optimization (Schor and Gray 2007). However, convex and compound (convex-concave) slopes profiles may also be observed in nature. Figures 5-4, 5-5 and 5-6 show examples of concave slope profiles found in nature.

Brunsden and Kesel (1973), following a sequence history of slopes in aluvial materials along the Mississippi river, identified zones of high, intermediate, and low base river erosion activity (Figure 5-7). For slopes formed under all except the high intensity basal erosion (region A in Figure 5-7), it is possible to see how concave shapes have been formed through the history of those bluff structures by rainfall activity (assuming that mainly rainstorm water has influenced the morphology of the slopes in the low intensity areas)

Figure 5-4 Rocky Mountains, Alberta, Canada. (Campbell 2011)

Figure 5-5 Petrohue Falls, Osorno, Chile. (Bridgepix 2011)

Figure 5-6 Cerro Chena (Chena Hill), Santiago, Chile. (Panoramio 2011)

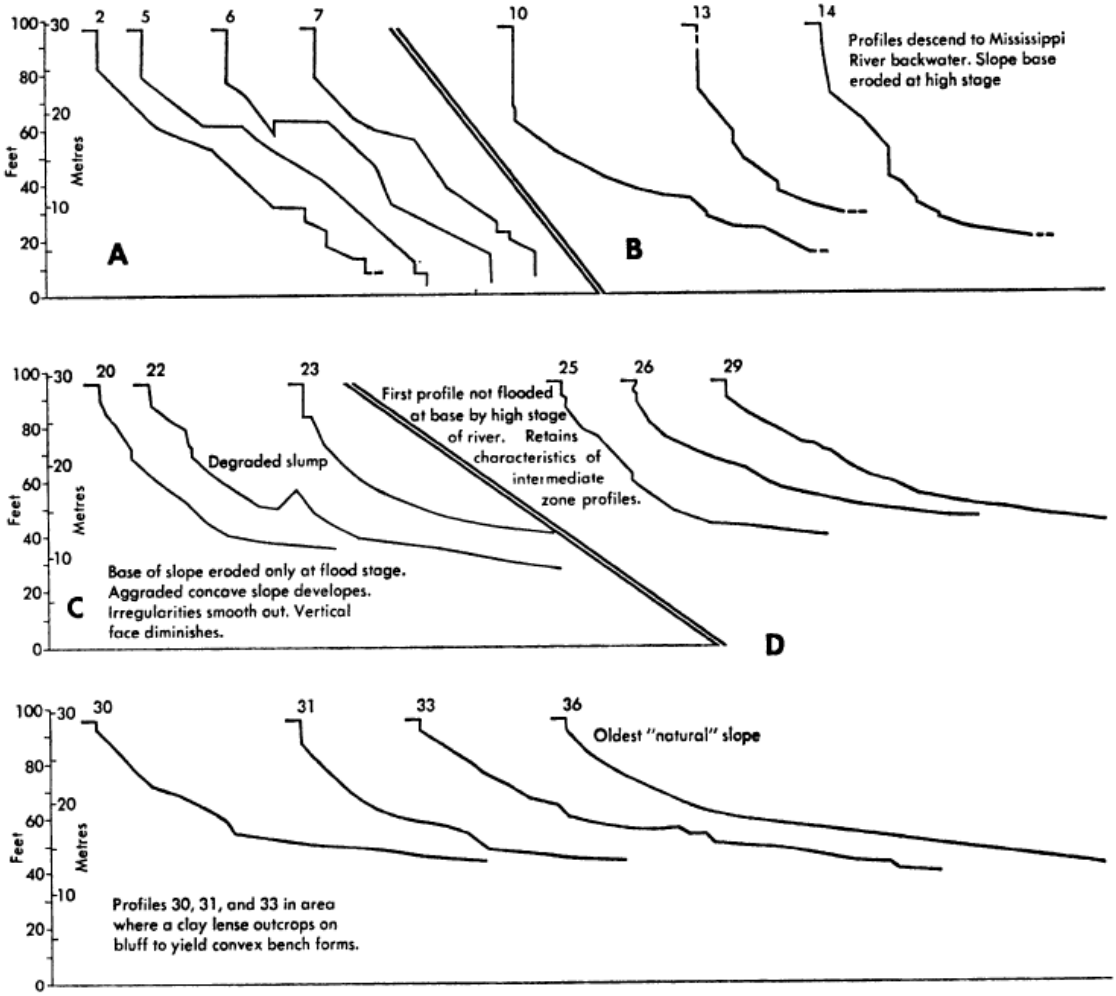

Figure 5-7 Slope profiles along Port Hudson bluff. Region A, high and intermediate base erosion intensity; region D, low intensity base zone (Brunsden and Kesel 1973)

Nash (1980) studied new and old formations of bluffs in Emmet County Michigan, with similar soil properties among them (mostly sand and gravel). Figure 5-8 shows slope profiles of those formations. It can be seen how the new bluffs are mostly planar with a slight tendency to become concave, while medium age bluffs are concave in shape, with a soft roundness in the top, which suggest effects of runoff from the outside of the slope. The oldest bluff formations show a more enhanced compound shape, however the author suggests that erosion is unlikely to be significant in old bluffs, since they become covered with vegetation. Instead, he attributed the changes in morphology to surficial creep.

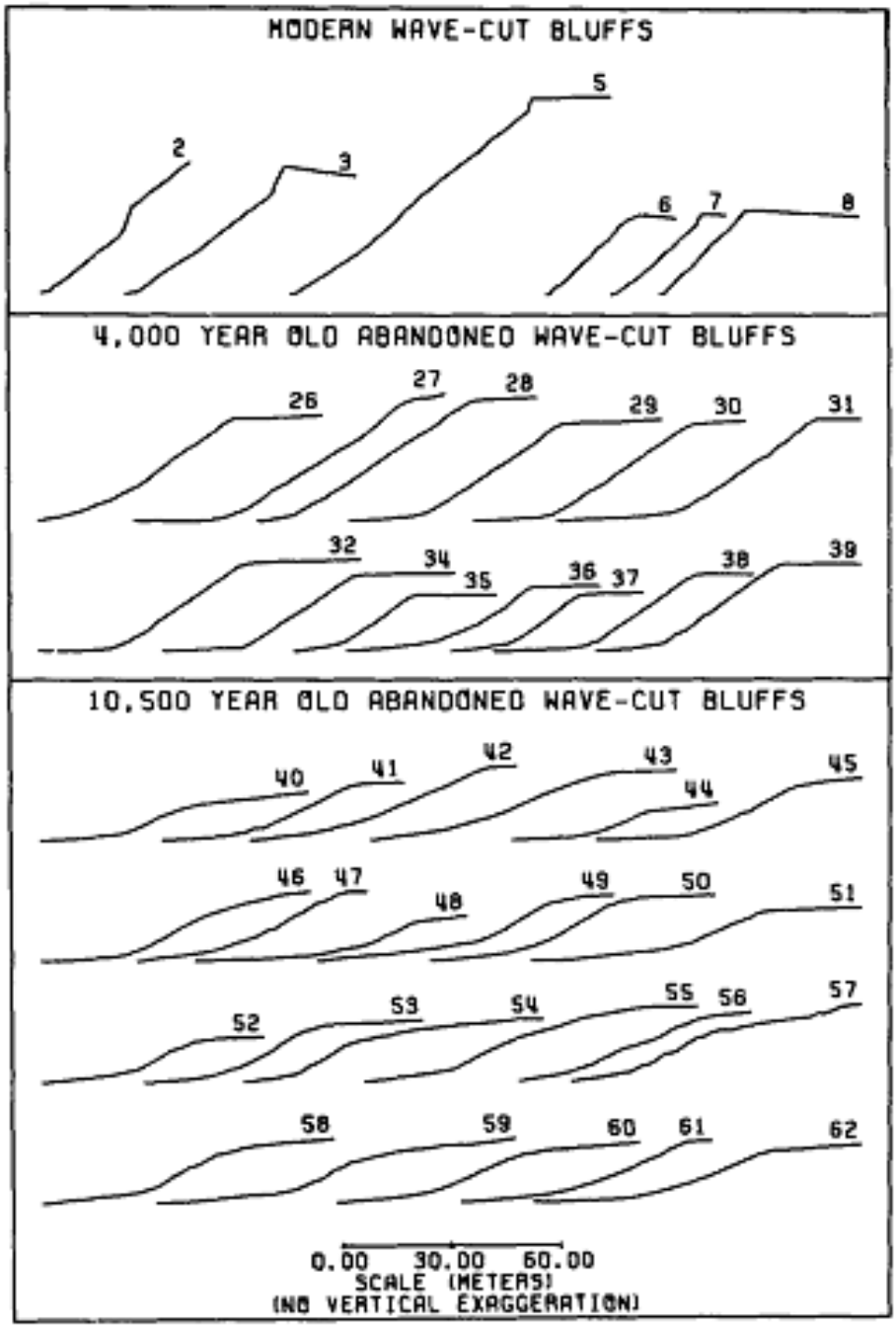

Figure 5-8 Topographic profiles of new and old bluffs in Emmet County, Michigan (Nash 1980)

It is suggested that natural slopes tend to seek a concave equilibrium shape in the long term. Compound shapes may be obtained in the long term as well, when runoff coming from the above the slope starts shaping the slope or the steep upper portion of the slope experiences creep. On the other hand, convex slopes are believed to be formed in zones where deposition at the bottom is not possible (e.g. water courses running across the toe of the slope) and an equilibrium state is not reached.

Slope profile in equilibrium: an introduction to a conceptual model

From physics we understand that a discrete mass moving on a slope will be at equilibrium state if the potential energy reaches a minimum. This concept has been widely used in a range of applications from field micro structural evolution studies to open channel flow studies. Yang and Song (1979), based on field and laboratory data, generalized the concept of minimum rate of energy dissipation to flows that transport sediment. They suggested that under this theory the rate of energy dissipation is minimum under steady equilibrium conditions, and if the conditions deviate from the equilibrium state (or minimum rate of energy dissipation), the slope inclination, roughness, channel geometry and velocity will experience continuous adjustments in order to reach the steady equilibrium state again.

The generalized principle of minimum rate of energy dissipation may be well applied to the slope erosion process (a special case of flows with sediment transport). If we assume a slope is initially in an imbalanced state, it may be expected that continuous changes in the slope geometry and flow velocities will take place in order for the system to adjust and reach equilibrium. Then, the overall erosion rate would be minimal and uniform, and constant amount of sediment loss would be observed, since the energy dissipation has reached a minimum.

What is the equilibrium or minimum energy shape?

From the concept of minimum rate of energy dissipation, a simple conceptual model that attempts to explain the evolution of slopes actively eroded by water is presented here. For erosion to occur along a slope, the transport capacity of the flow (T_c) must be greater than its sediment load (q). In other words, the difference between transport capacity and sediment load has to be greater than zero for erosion to occur.

$$T_c - q > 0 \tag{5-1}$$

Assuming a uniform planar slope shape as an initial condition, it may be observed that the transport capacity will uniformly increase downslope, since runoff velocity increases moving down slope. Thus the difference between T_c and q, will positively increase, increasing the tractive or shear forces acting on the soil surface, and a significant increase in the amount of soil detached downslope will be observed (Figure 5-9). Experimental results from Young and Mutchler (1969) support this fact (Figure 5-2). At the bottom of the planar slope, a sudden decrease of flow velocity is observed, which decreases the transport capacity and results in sediment deposition. Thus, soil starts being deposited at the bottom of the slope. This weathering process continuous over time (Figure 5-9) allowing erosion and deposition to slowly form the slope. If the contribution of the runoff coming over the top is neglected, then the final product would be a concave slope shape. This concave shape would be characterized by a natural optimization or minimization of the soil eroded. Since a concave slope reduces its steepness at each point, it would dissipate the increasing flow energy and detachment capacity downslope. This natural adjustment would finally reach an equilibrium state where the concave geometry would allow a uniform decreasing detachment rate along the slope; in other words, a decreasing positive difference between T_c and q would be found downslope. When this equilibrium state is reached, a minimum, uniform total soil loss rate would be observed over time; the slope would start eroding backwards in a parallel retreat maintaining the same concave slope geometry as it is illustrated in Figure 5-10, provided the material

properties remain unchanged. Figures 5-11, and 5-12 show real examples of what may perhaps be soil slopes in the equilibrium state.

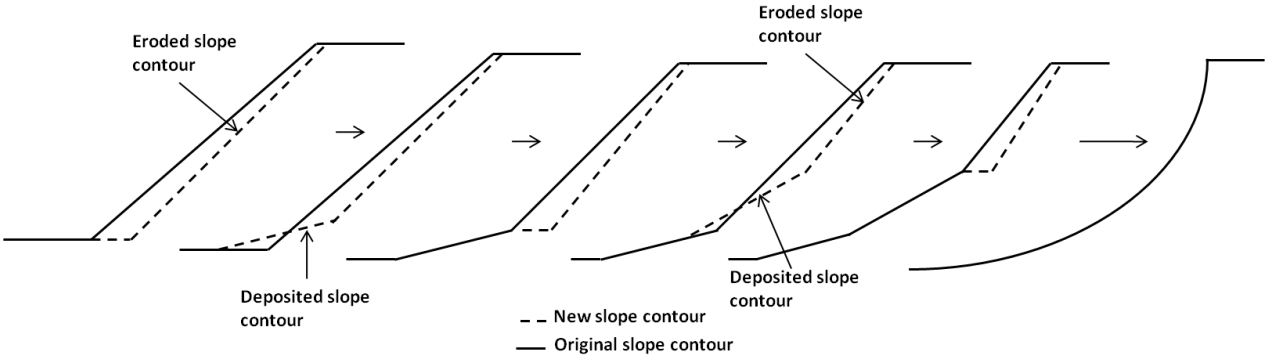

Figure 5-9 Conceptual model of slope morphology evolution by water erosion

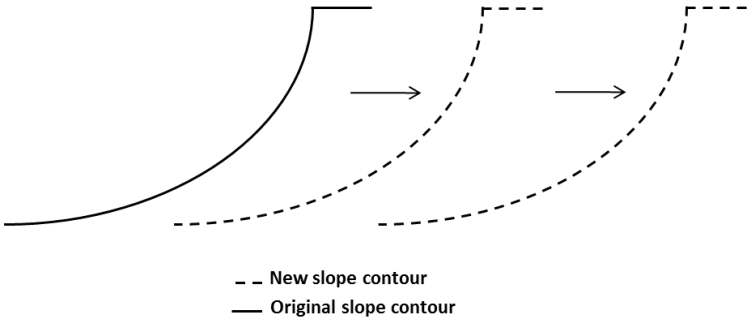

Figure 5-10 Illustration of the parallel retreat concept

Figure 5-11 Dark Hills Ollague, Chile. (Trip Down 2011)

Figure 5-12 Reclaimed surface coal mine, Appalachian Regional Reforestation Initiative. (ARRI 2011)

According to Schor and Gray (2007) there are two important schools of thought regarding geomorphic evolution. Davis (1899) suggested that morphological changes on the slope are dominated by a process called “downwearing” in which the slope will become progressively less steep until reaching “the ultimate step level of the erosion” (Angel et al. 2007). On the other hand, Penck (1953) suggested that slope morphology is governed by a process called “backwearing” in which the slope parallel retreats maintaining a relatively constant shape. The conceptual model proposed here seems to go along with Penck’s postulate, which is also consistent with the equilibrium state reached by the concave slope shape.

In this conceptual model of equilibrium slope shape, two extremes can be identified. First, let’s consider a slope comprised of loose sand; soil easily to detach but hard to transport due to the large particle size. In this case, since transportation downslope is obstructed by an earlier deposition, it may result in the formation of a gentle, low concavity slope, where the maximum steepness is perhaps conditioned by the negligible soil cohesion. On the other hand, in a slope comprised of clay, the soil is hard to detach but easy to transport, and this material may evolve toward a more concave slope, since the very small particles are easily carried away and fewer are deposited at the toe of the slope. Here, a vertical face in the top of the slope may be more evident due the cohesive component of the soil strength. These two extreme cases are illustrated in Figure 5-13.

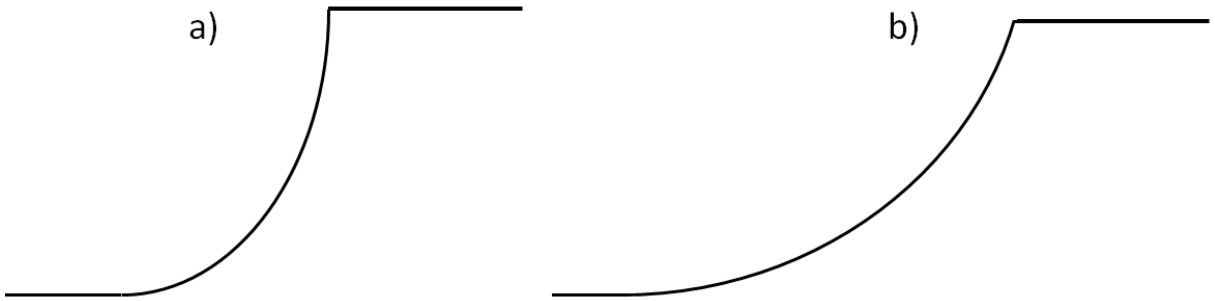

Figure 5-13 Two extreme cases in this conceptual model of slope morphology a) slope in “clayey” material; b) slope in “sandy” material.

From the discussion presented here, the construction of concave slopes may be effective in reducing the sediment yield, and may better represent the natural shape that slopes evolve to over time. While the mechanical stability of planar slopes is relatively well understood, there is less experience evaluating the stability of non-planar slopes. Further, the definition or description of the shape of a concave slope that provides the greatest stability is of interest, as well as how the stability of this concave slope may compare to that of a similar planar slope.

Slope contour in a critical mechanical state

Recognizing that the concave slope profile may reduce erosion and sediment production, it becomes important to investigate and define the optimum shape of concave shapes relative to slope stability. Sokolovski (1960), based on plasticity theory, studied the shape of slopes in the critical state or at imminent failure. Surprisingly, he found that the slope profile at critical equilibrium has a concave shape and its profile can be mathematically described as a function of the soil strength parameters and the soil

unit weight. The mathematical details of this formulation are provided in Chapter 6, but the general approach and a design procedure are provided below.

Sokolovski's formulation

The theory of the critical state in soil mechanics states that limiting equilibrium will occur when the stresses are equal to the strength. At this point, plastic deformation will take place along slip lines or planes. The shear strength of soil is traditionally assumed to be represented by the Mohr-Coulomb yielding or failure criterion $|\tau_n| \leq \sigma_n \tan\phi + c$, where σ_n and τ_n are the normal and shear stresses acting on any plane within the soil body, and ϕ and c are the internal friction angle and cohesion, defined as the strength components of the soil. Therefore, limiting equilibrium suggested by Sokolovski can be mathematically described as following:

$$max\ |\tau_n| = (\sigma_n + H)\tan\phi \tag{5-2}$$

where $H = c\cot\phi$ is the tensile strength of the soil and $\sigma_n \geq -H$

Based on this concept, Sokolovski (1960) developed the equations of the characteristics that describe slip lines where the plastic deformation occurs in the soil medium. Expressed in an x-y plane coordinate system, the equations of characteristics or slip lines are:

$$\frac{dy}{dx} = tan(\xi \mp \varepsilon) \tag{5-3}$$

$$d\sigma \mp 2\sigma \tan\phi\, d\xi = \frac{\gamma}{\cos\phi}[sin(\alpha \mp \phi)\, dx + cos(\alpha \mp \phi)\, dy] \tag{5-4}$$

Where $\xi \pm \varepsilon$ is the initial angle between the slip lines and the x-axis, σ is one half of the sum of the principal stresses plus the tensile strength, γ is the unit weight of the soil medium, and α is the angle between the horizontal plane and the x-axis.

For a weightless soil medium, Eq. 5-4 gives a constant solution for the slope contour, meaning that in the absence of gravity forces the critical slope profile is planar. On the other hand, if the medium possesses self-weight, as any natural slope would, it can be observed that the stresses are not uniform along the contour, and the critical slope condition will be satisfied by a curved slope profile. The presence of the unit weight in the Eq. 5-4 has hampered the development of an exact analytical solution. Sokolovski (1960) solved this problem numerically, and showed that the slope shape in a critical state is concave and can be obtained as a function of ϕ, c and γ. The numerical solution provided by Sokolovski was restricted to specific values of ϕ and the ratioc/γ, making practical implementation difficult in slope design, especially for larger slopes.

Proposed solution for the slope contour in critical equilibrium for a medium with weight

An approximate analytical expression was developed for the problem of the slope at the critical state for a medium with self-weight, working from the method proposed by Sokolovski. Like Sokolovski's solution, this is an approximation due to the form of Eq. 5-4, but the expression proposed here shows good agreement with Sokolovski's results in terms of the geometry, the fundamental failure

mechanisms, and the resulting factors of safety. The advantage of this expression is that it permits simple determination of the plane coordinates of concave shapes that yield factor of safety values nearly 1. Details of the development of this formulation are provided in Chapter 6, with the application of the method to practical problems described here.

By serendipity, the contour of the slope with self-weight in a critical state was found to be satisfied by the following equation:

$$x = \begin{cases} 0 & , \quad -h_{cr} \le y \le 0 \\ \int_0^y \frac{\cot\phi}{2} ln\left[\frac{\frac{c}{\gamma(1-\sin\phi)}+y+\frac{c}{\gamma}\cot\phi}{\frac{c}{\gamma}\cot\phi}\ \frac{1-\sin\phi}{1+\sin\phi}\right] dy, & y > 0 \end{cases} \tag{5-5}$$

Here, h_{cr} is the maximum height of a vertical slope that a soil medium can withstand (critical height), defined by Sokolovski (1960) as:

$$h_{cr} = \frac{2c\cos\phi}{\gamma(1-\sin\phi)} \tag{5-6}$$

Solving the integral in Eq. 5-5, the solution for contour of the slope with self-weight in a critical state can be expressed as:

$$x = \begin{cases} 0 & , -h_{cr} \le y \le 0 \\ A\left[\sigma_y\ (B-1)(cosec\,\phi - 1) + H\ B\ (cosec\,\phi + 1)\right], & y > 0 \end{cases} \tag{5-7}$$

where:

$$A = \frac{cos\,\phi}{2\gamma(1-sin\,\phi)} \tag{5-8}$$

$$B = ln\left[\frac{\sigma_y}{H}\ K_a + 1\right] \tag{5-9}$$

$$\sigma_y = \gamma y \tag{5-10}$$

$$H = c\ cot\,\phi \tag{5-11}$$

Note that σ_y is the vertical stress and H is the tensile strength defined before. Also observe that the factor B is a function of the active coefficient of earth pressure defined as (Perloff and Baron 1976, Scott 1963):

$$K_a = \frac{1-sin\,\phi}{1+sin\,\phi} \tag{5-12}$$

Sokolovski developed his theory employing a reference frame that implies a horizontal x-axis positive toward the left, and a vertical y-axis positive downward. The convention of a positive y-axis downward is common in geotechnical engineering, and is utilized in Eq. 5-7. Thus, the proposed solution describes a slope contour in critical state in the quadrant where x-axis is positive and y-axis positive (on the adopted

reference frame), starting from the origin of the system (Figure 5-14). Above the origin h_{cr} lies vertically with coordinates ranging from (0,- h_{cr}) to (0, 0). Hs is the total slope height.

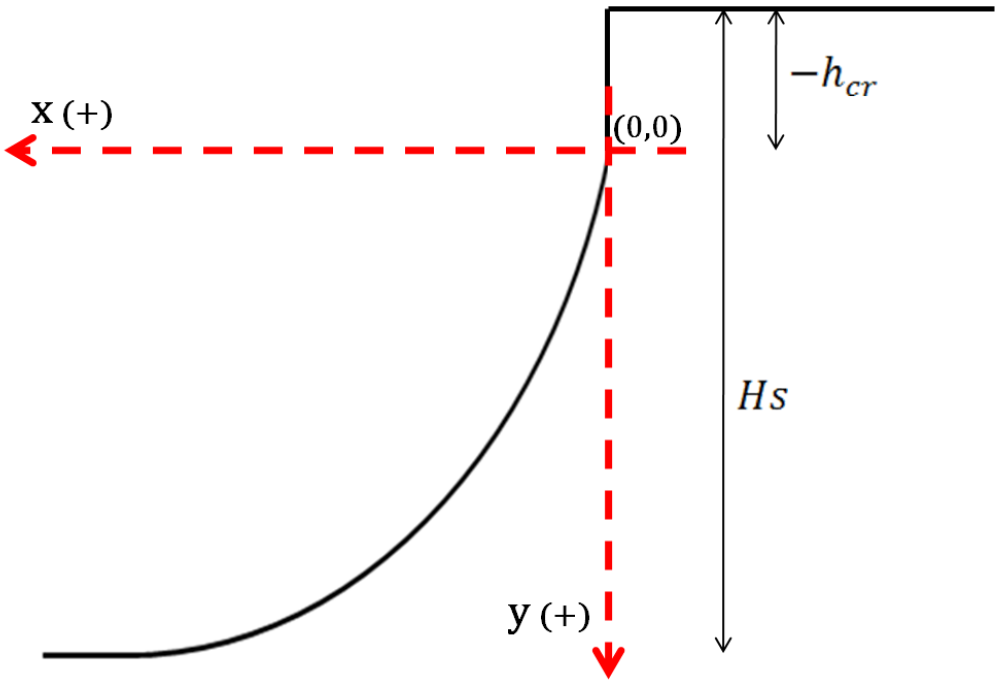

Figure 5-14 Schematic of slope profile and the adopted reference frame.

A parametric study of the proposed solution was conducted, and it was found to agree well with the Sokolovski solution in terms of geometry, failure mechanism, and obtained factors of safety, yielding FS values very close to 1. Limit equilibrium stability analyses of concave slope contours obtained with the proposed solution revealed the existence of a geometrical limiting slope height (h_L), for which the failure mechanism usually changes from a face to a toe failure. It was also observed that at slope heights less than h_L, the expression yields values of FS that are slightly higher than 1.0. An approximate relationship between h_L and c/γ was determined to be:

$$h_L = 15.8\,\frac{c}{\gamma} + 0.3 \qquad (5\text{-}13)$$

The slope contour obtained from the expression in Eq. 5-7 gives in general FS's slightly greater than 1 for slope heights smaller that h_L and $1 \pm error$ for slopes heights greater than h_L. The error is a consequence of the approximate nature of the proposed solution, and it was found to be a function of the internal friction angle ϕ only. For the typical range of ϕ found in practice, this error ranges from -1% at low values of ϕ to about 6% at high values of ϕ. Details of this error are provided in Chapter 6, but in view of the magnitude of errors associated with the determination of ϕ, this error may be considered negligible for practical design. The magnitude of this small error is determined below in the example problem.

Mechanical stability of concave slopes: a design procedure

The advantages of constructing concave slopes to reduce the amount of sediment delivered have been discussed and evidence that slopes may evolve into concave profiles over time has been presented. From the critical equilibrium theory it was observed that the shape of the slope profile at failure is concave, and an approximate analytical expression to obtain slope contours at failure for a given γ, ϕ and c were provided. However, in practice, it is usually desired to design slopes such that they have more strength than necessary for the given shape, providing a FS greater than 1. FS is indeed a measure to account for the uncertainty of all the information used in the analysis, with larger FS's used in cases where the implications due to failure would be significant, and lower FS's used in applications where failure may have limited impact, such as many reclamation designs. For example, static slope design of highways typically provides a FS in the range of 1.25 to 1.5 (Abramson 1996), whereas a value of 1.3 might be more typical in reclaimed mine slopes. The method presented here allows the designer to obtain concave slope contours that will provide the desired FS against failure.

Strength Reduction Factor (SRF) as the selected FS.

In traditional limit equilibrium methods FS is defined as the ratio of the available to the required shear strength to just maintain the equilibrium. For cases when a circular failure mechanism is assumed (e.g. Simplified Bishop's Method) this definition is equivalent to the ratio of the moments resisting rotation to the moments producing rotation. In other words, FS can be defined as the value whereby the available shear strength (or the shear strength parameters) needs to be divided such that the slope is in exact equilibrium or at incipient failure. Thus, the value of the FS becomes the Strength Reduction Factor (SRF) (Griffiths and Lane 1999).

$$c_f = \frac{c}{SRF} \tag{5-14}$$

$$\phi_f = \arctan\left(\frac{\tan\phi}{SRF}\right) \tag{5-15}$$

where c_f and ϕ_f are the soil cohesion and internal friction angle at incipient failure.

A parametric study was conducted to investigate the proposed solution for a range of SRF values. Critical concave slope contours were obtained from Eq. 5-7 and broken down into different heights. As before, limiting equilibrium stability analyses were conducted for each height and a range of SRF values. SRF values of 0.25, 0.5 and 0.75, 1.0 and 1.25 were chosen, corresponding to FS values of 4, 2, 1, 1.33 and 0.8. Figure 5-15 shows the relationship between the FS and slope height (Hs) for a critical slope profile obtained for $\phi = 20^o$ and $c/\gamma = 0.54\ m$ for the range of SRF values. Results show that SRF's do not produce any variation on the limiting height h_L and a constant FS is achieved after h_L has been reached. For SRF= 0.25, 0.5, 0.75, the obtained steady FSs were 3.982, 1.991 and 1.328 respectively. These values reflect the small error in the approximation, and are about -0.4% different from the target values of FS's in the parametric study. As mentioned above, this error depends on the design value of ϕ, and is insignificant for practical design purposes. Similar trends were observed across the selected range of soil parameters in this study and are reported in the Appendix A.

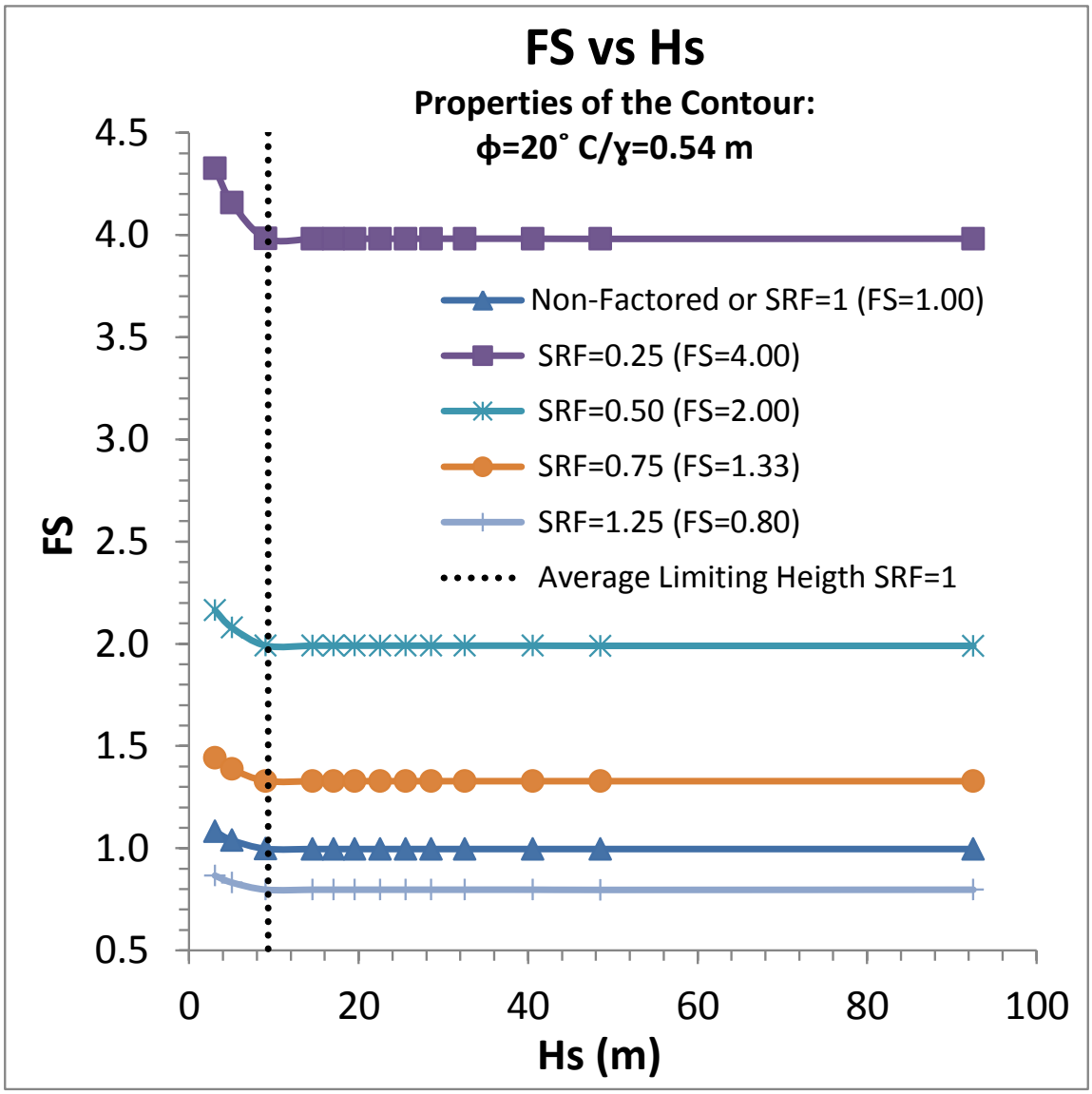

Figure 5-15 Factor of safety (FS) from Limiting Equilibrium analysis vs Slope Height (Hs) for $\phi = 20^o$, $c/\gamma = 0.54\ m$ and $SRF = 0.25, 0.5, 0.75, 1.25$.

Recommended soil properties for the research sites

Earlier, due to the granular nature of the material identified at the Mountainside, National and Premium sites, a negligible value of the cohesion was assumed for the stability analysis. However, the mathematical function described here (Eq. 5-7) for a concave slope profile requires a value of $c \neq 0$, otherwise the solution becomes immediately indeterminate. Thus, it is essential that even a small, but justified value of c be assumed even for cases when the soil medium is mostly granular.

The shear strength parameters obtained from the literature for other mine reclaimed sites (Table 3-7) suggests that the cohesion for similar materials ranges from 0 to as much as 17.5 kN/m2 (365.5 psf). In view of the large amount of fine particles (>15%) encountered in the site materials (Table 3-5), it is reasonable to assume that a small but important amount of cohesive strength would be present.

Therefore, a value of $c = 15$ kN/m2 (313.28 psf) was assumed to represent the site materials, along with the previously suggested internal friction angle $\phi = 38^o$ and the average wet (total) unit weight reported in Table 4-1 for each site.

Proposed design procedure

Below are listed the suggested steps to be followed in the design of concave slopes that will perform with a FS selected by the designer.

Step 1:

Having obtained the soil strength parameters ϕ, c and the total soil unit weight γ_T, the designer needs to decide what factor of safety (FS_o) would be appropriate for the concave slope. The decision needs to be made in terms of the reliability of the obtained soil data, performance requirements, and the consequences of failure. For many reclaimed mine sites, FS = 1.3 may be sufficient.

It may also be useful to know at this point how tall the slope would be, to see if the selected vertical height (Hs) would be greater or smaller than the limiting height h_L.

Step 2:

Reduce the original strength parameters ϕ and c by the selected FS_o to obtain ϕ^* and c^*, according to:

$$c^* = \frac{c}{FS_o} \tag{5-16}$$

$$\phi^* = \arctan\left(\frac{\tan\phi}{FS_o}\right) \tag{5-17}$$

where ϕ^* and c^* are the values of internal friction angle and soil cohesion required to provide the desired factor of safety.

Step 3:

With the new ϕ^* and c^* parameters and the original γ_T, the contour of the slope will be obtained from Eq. 5-7. The solution describes the curved profile from top to bottom, where the vertical y-axis is the independent variable and defines the domain. The y-axis increases downward and y = 0 corresponds to the point on the top of the slope just below the critical height, and h_{cr} would lie on the negative side of y-axis on the adopted reference frame.

At this point, a concave slope shape that will perform with a factor of safety approximated to the selected FS_o has been obtained.

Step 4:

Using Eq. 5-13 and c^*/γ_T, estimate the value of h_L.

Step 5:

Check the following cases:

If the design slope height $Hs \geq h_L$, the expected failure mechanism would be face failure. Here h_L may serve as rough indicator of the location of the most critical slip surface. In this case, the real performing

FS of the obtained concave profile would be slightly greater (0-6%) for high ϕ^* values and slightly lower (0-1%) for those with lower values of ϕ^*.

If the design slope height $Hs \leq h_L$, for most of cases, the expected failure mechanism would be toe failure, and the real performing FS would be always more conservative than the desired FS_o.

Step 6:
This step may only be necessary if the designer wants to know the cases for which the obtained concave slope will be more stable than a planar one.

Employing Taylor's slope stability charts (Taylor 1948) with ϕ, c, γ_T, Hs, and the design FS_o as the input parameters, estimate the angle β_p of the planar slope that would perform with an approximate value of FS_o. Planar slopes inclined at angles steeper than β_p will be less stable than the obtained concave slope for a fixed value of Hs, while gentler ones will be more stable. Taylor's chart is provided in Appendix A

Example problem

Find a concave slope profile that will perform with $FS \approx 1.5$ for the soil properties recommended for Premium [$\phi = 38^o$, $c = 15\ kN/m2\ (313.28\ psf)$, $\gamma_T = 18.5\ kN/m3\ (117.76\ pcf)$]. Report the coordinates of the contour for a maximum $Hs = 15\ m\ (49.21\ ft)$ and find the inclination of a planar slope that would perform with the same FS.

Step 2:
Employing Eq. 5-16 and 5-17 the original strength parameters ϕ and c will be reduced by $SRF = FS_o = 1.5$ to obtain ϕ^* and c^*:

$$c^* = \frac{15}{1.5} = 10\ kN/m2\ (208.86\ psf)$$

$$\phi^* = \arctan\left(\frac{\tan 38^o}{1.5}\right) = 27.51^o$$

Step 3:
Introducing ϕ^*, c^* and γ_T into Eq. 5-7, the coordinates of the concave slope contour that will perform with a $FS \approx FS_o = 1.5$ are obtained. The x values were computed for 0.2 m incremental values of y. Figure 5-16 shows the obtained contour, while Table 5-2 reports the obtained coordinates of the profile in the adopted reference frame. The Critical height $h_{cr} = 1.78\ m\ (5.84\ ft)$ was calculated from Eq. 5-6.

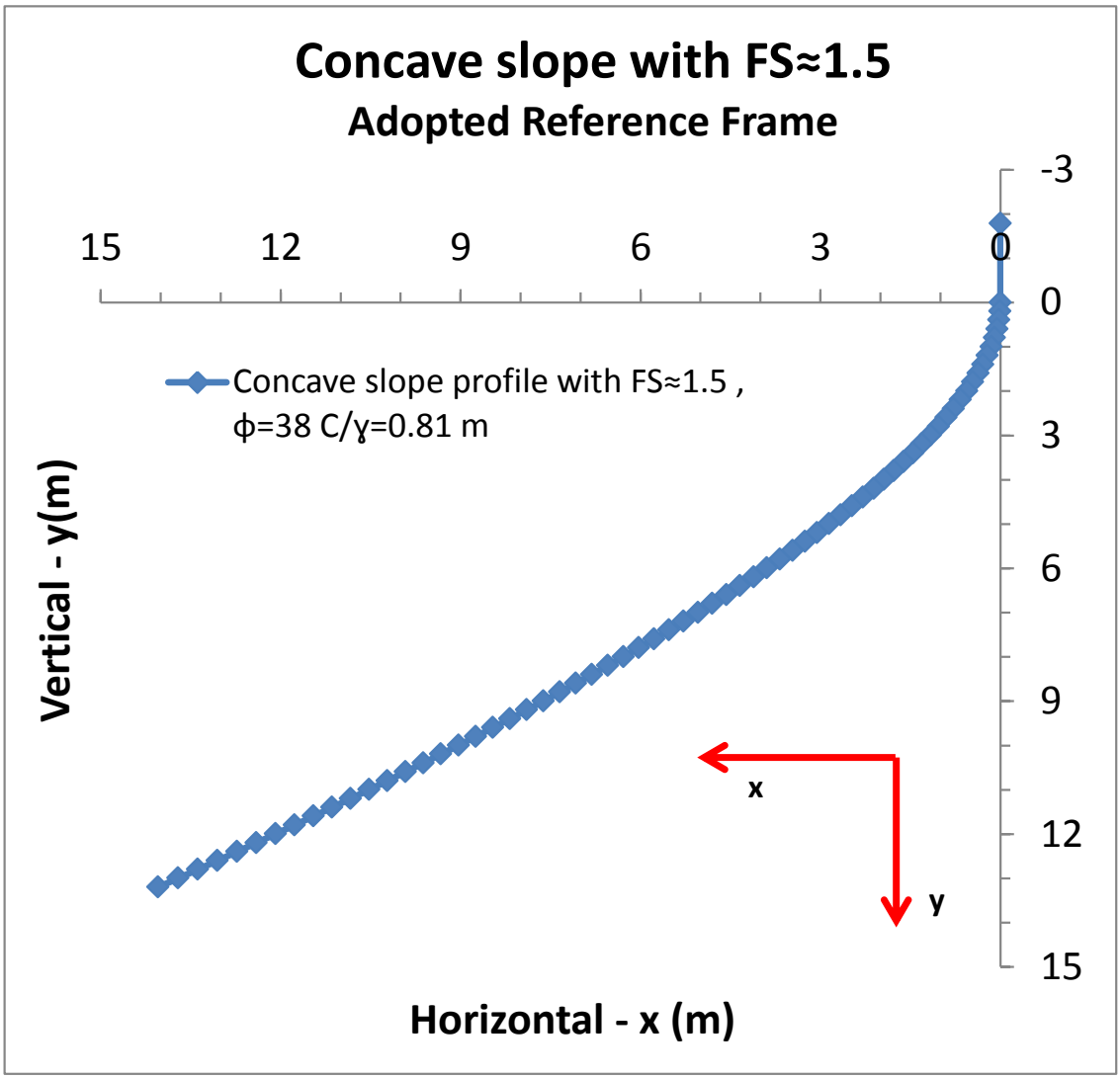

Figure 5-16 Obtained concave slope contour with a $FS \approx FS_o = 1.5$ for $\phi = 38^o$ and $c/\gamma_T = 0.81\ m$

Table 5-2 Coordinates of the concave profile for the example problem in the adopted reference frame

X (m)	Y (m)	X (m)	Y (m)	X (m)	Y (m)
0.00	1.78	4.57	6.60	14.38	13.40
0.00	0.00	4.81	6.80	14.72	13.60
0.01	0.20	5.04	7.00	15.06	13.80
0.03	0.40	5.28	7.20	15.40	14.00
0.06	0.60	5.53	7.40	15.74	14.20
0.10	0.80	5.78	7.60	16.09	14.40
0.15	1.00	6.03	7.80	16.44	14.60
0.22	1.20	6.29	8.00	16.79	14.80
0.29	1.40	6.55	8.20	17.14	15.00
0.37	1.60	6.81	8.40		
0.46	1.80	7.08	8.60		
0.56	2.00	7.35	8.80		
0.67	2.20	7.62	9.00		
0.78	2.40	7.90	9.20		
0.90	2.60	8.18	9.40		
1.03	2.80	8.46	9.60		
1.17	3.00	8.75	9.80		
1.31	3.20	9.04	10.00		
1.46	3.40	9.33	10.20		
1.61	3.60	9.63	10.40		
1.78	3.80	9.92	10.60		
1.94	4.00	10.22	10.80		
2.11	4.20	10.53	11.00		
2.29	4.40	10.83	11.20		
2.48	4.60	11.14	11.40		
2.66	4.80	11.46	11.60		
2.86	5.00	11.77	11.80		
3.06	5.20	12.09	12.00		
3.26	5.40	12.41	12.20		
3.47	5.60	12.73	12.40		
3.68	5.80	13.06	12.60		
3.90	6.00	13.38	12.80		
4.12	6.20	13.71	13.00		
4.34	6.40	14.04	13.20		

Step 4:
From Eq. 5-13 the limiting height h_L can be estimated. Here, $c^*/\gamma_T = 0.54\ m$ and therefore $h_L \approx 8.8\ m\ (28.87\ ft)$.

Step 5:
Since $Hs \geq h_L$, it would be expected that the failure mechanism would be a face failure mode, with the most critical failure surface intersecting the slope contour somewhere around y = 8.8 m (the value of h_L). Also, it would be expected that the actual performing factor of safety FS would be slightly higher than the design FS_o, due to the inherent error in the approximation for the relatively high value of $\phi^* = 27.51^o$. This error would be less than 6%.

Step 6:
For comparison with a planar slope, Taylor's stability charts (Taylor 1948). For $\phi = 38^o$, $c = 15\ kN/m2$, $\gamma_T = 18.5\ kN/m2$, $Hs = 15\ m$ and $FS = 1.50$, the obtained stability number is:

$$N = \frac{c}{H\,\gamma\,FS} = \frac{15}{15 \cdot 18.5 \cdot 1.50} = 0.036$$

Entering Taylor's stability chart, the angle of inclination for an equivalent planar slope would be $\beta_p \approx 45^o$. Figure 5-17 compares the concave and the equivalent planar contours obtained from the example problem. In terms of geometrical extension, both profiles have similar starting and ending points; however, the concave profile seems to be more efficient since less material would be involved in its construction and its sediment production rate would be lower. In the long term, the planar contour would eventually start eroding toward a concave profile. Therefore, the construction of a concave slope would abbreviate the time required for a slope to reach equilibrium and would reduce the amount of sediment produced.

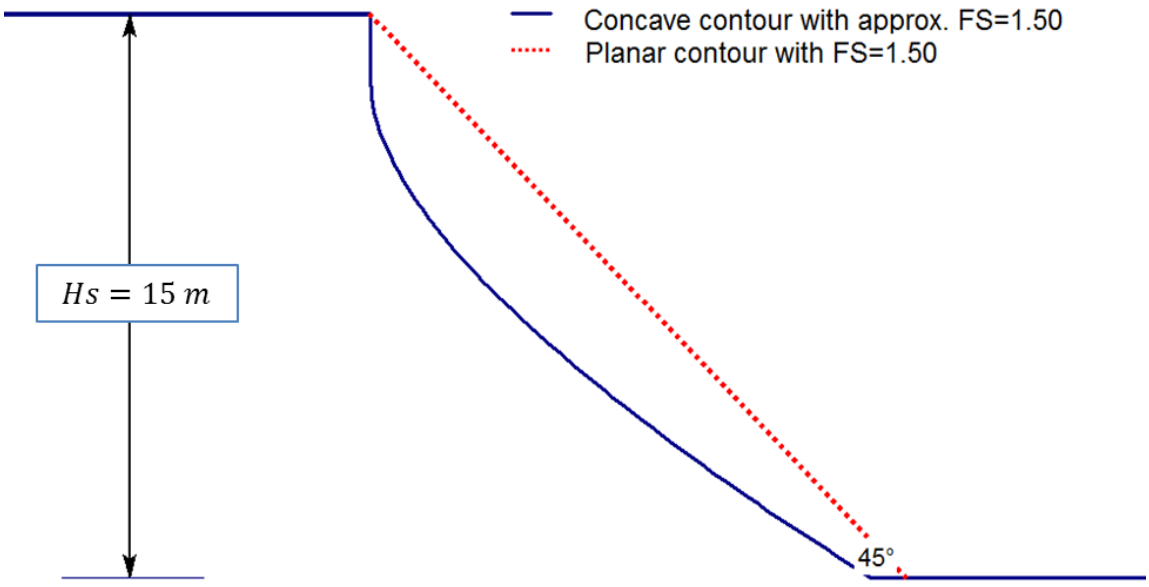

Figure 5-17 Comparison of the concave and the equivalent planar slope for the example problem, $FS = 1.50$

For additional verification of the non-planar slope solution, both Finite Element Method (FEM) and Limiting Equilibrium Method (LEM) solutions for the stability of the example problem were obtained (Figures 5-18 and 5-19). The FEM solution was obtained from the commercial code Phase2 (Rocscience Inc. 2011), and yielded a SRF = 1.54, while the LEM solution was obtained from Slide (Rocscience Inc. 2011), and yielded a FS = 1.554. These solutions yield FS's that compare well with the design FS of 1.5, differing by 3.6%. Note also that the critical failure mode in Figure 5-18 and 19 is a face failure mechanism and intersects the slope contour at $y = 9.38\ m$ from the top, being close to the estimated value of $h_L = 8.8\ m$.

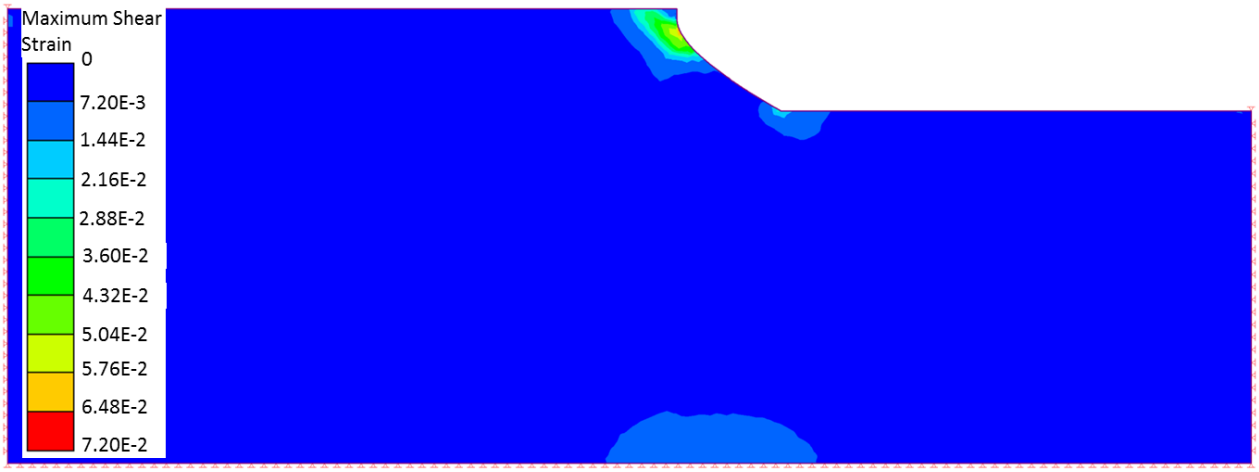

Figure 5-18 FEM results in terms of shear strains for the example problem with strength reduced SRF=1.56 (Critical SRF=1.54) to emphasize failure mode. Assumed E=20,000 kPa.

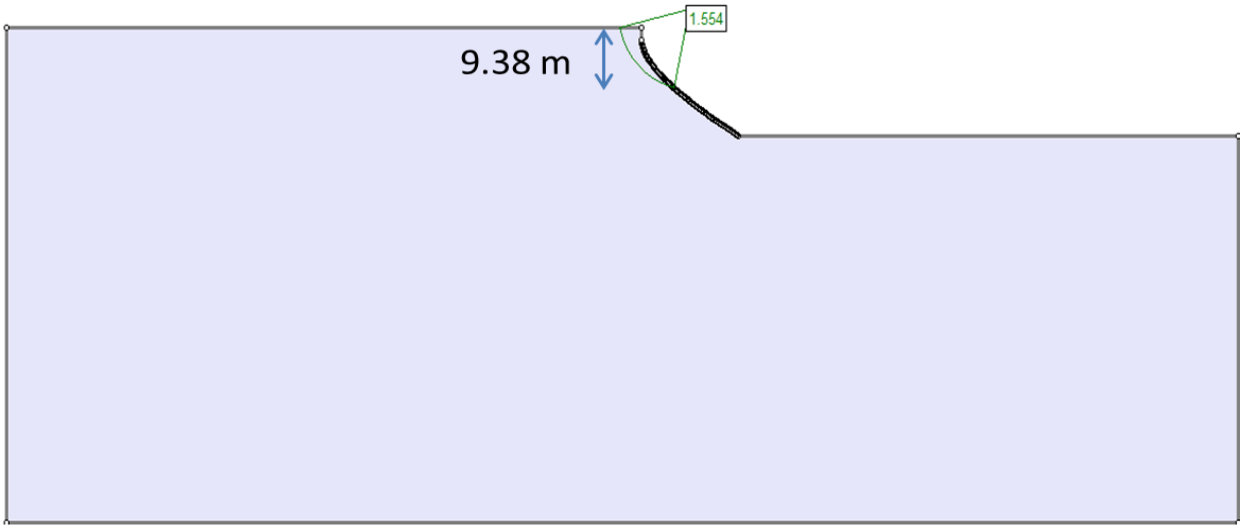

Figure 5-19 LEM stability analysis of the concave slope in the example problem. The critical failure surface corresponding to the FS=1.554 is shown, which emerges from the slopes at a height of 9.38 m.

Conclusions

Evidence that soil slopes in nature may evolve into concave shapes in the long term was presented, and the advantages of the concave slope in terms of the reduction in sediment were suggested. A conceptual model that attempts to explain this geomorphological development of a concave slope was proposed. From the theory of the critical equilibrium of a soil medium developed by Sokolovski (1960), an approximate solution was proposed yielding the coordinates of a non-planar slope at failure. An approach was demonstrated using the SRF to obtain the slope contour for a given FS, and a rational design method was presented. The method was shown to be satisfactory, and was illustrated via an example problem. The stability of non-planar slope in the example problem was also investigated by the FEM and LEM, and the results shown to provide similar FS's as the proposed approximate solution.

References:

Abramson, L. W. (1996). *Slope stability and stabilization methods*, Wiley, New York.

Angel, P. C., Barton, C., Warner, R., Agouridis, C., Taylor, T., and Hall, S. (2007). "Hydrologic characteristics, tree growth, and natural regeneration on three loose-graded surface mine spoil types in Kentucky." *Mid-Atlantic Stream Restoration Conference*Cumberland, MD.

ARRI (2011). "2011 ARRI Conference Web Site." <http://fwf.ag.utk.edu/arri/ARRI.html>. (July 21, 2011).

Bridgepix (2011). "Petrohue Falls, Osorno." *Bridgepix's photostream*, <http://www.flickr.com/photos/80651083@N00/2202959038>. (March 03, 2011).

Brunsden, D., and Kesel, R. H. (1973). "Slope Development on a Mississippi-River Bluff in Historic Time." *J Geol*, 81(5), 576-598.

Campbell, D. (2011). "Rocky Mountains." *Photos In Cancun's Blog*, <http://photosincancun.wordpress.com/>. (March 03, 2011).

Davis, W. M. (1899). "The geographical cycle." *Geography Journal*, 14, 481-504.

Dsouza, V. P. C., and Morgan, R. P. C. (1976). "Laboratory Study of Effect of Slope Steepness and Curvature on Soil Erosion." *J Agr Eng Res*, 21(1), 21-31.

Griffiths, D. V., and Lane, P. A. (1999). "Slope stability analysis by finite elements." *Geotechnique*, 49(3), 387-403.

Hancock, G. R., Loch, R. J., and Willgoose, G. R. (2003). "The design of post-mining landscapes using geomorphic principles." *Earth Surf Proc Land*, 28(10), 1097-1110.

Meyer, L. D., and Kramer, L. A. (1969). "Erosion Equations Predict Land Slope Development." *Agr Eng*, 50(9), 522-&.

Nash, D. (1980). "Forms of Bluffs Degraded for Different Lengths of Time in Emmet-County, Michigan, USA." *Earth Surf Proc Land*, 5(4), 331-345.

Panoramio (2011). "Cerro Chena, San Bernardo, Santiago." *Cerro Chena, San Bernardo, Santiago*, <http://www.panoramio.com/photo/20543995>. (March 03, 2011).

Penck, W. (1953). *Morphological analysis of land forms; a contribution to physical geology*, St. Martin's Press, New York,.

Perloff, W. H., and Baron, W. (1976). *Soil mechanics : principles and applications*, Ronald Press Co., New York.

Renard, K. G., and Foster, G. R. (1983). "Soil conservation: Principles of erosion by water." *Dryland Agriculture*, H. E. Dregne, and W. O. Willis, eds., Society of Agronomy, Crop Science Society of America, and Soil Science Society of America, Madison, WI, 155-176.

Renard, K. G., Foster, G. R., Weesies, G. A., McCool, D. K., and Yoder, D. C. (1997). *Predicting soil erosion by water: a guide to conservation planning with the Revised Universal Soil Loss Equation (RUSLE)*, United States Department of Agriculture [for sale by the U.S. Government printing Office, Washington, D.C.

Rieke-Zapp, D. H., and Nearing, M. A. (2005). "Slope shape effects on erosion: A laboratory study." *Soil Sci Soc Am J*, 69(5), 1463-1471.

Rocscience Inc. (2011). "Phase2." *Finite Elements software*, Rocscience Inc., Toronto, Canada.

Rocscience Inc. (2011). "Slide." *Slope Stability Software*, Rocscience Inc., Toronto, Canada.

Römkens, M. J., Yoder, D. C., and Lightle, D. (2008). "RUSLE2 Science Documentation." USDA-Agricultural Research Service, Washington. D. C.

Schaefer, M., Elifrits, D., and Barr, D. J. (1979). "Sculpturing reclaimed land to decrease erosion." *Proc., Symposium on surface mining hydrology, sedimentology and reclamation*, Lexington, KY, Medium: X; Size: Pages: 99-109.

Schor, H. J., and Gray, D. H. (2007). *Landforming : an environmental approach to hillside development, mine reclamation and watershed restoration*, John Wiley & Sons, Hoboken, N.J.

Scott, R. F. (1963). *Principles of soil mechanics*, Addison-Wesley Pub. Co., Reading, Mass.,.

Sokolovski, V. V. (1960). *Statics of Soil Media*, Butterworths Scientific Publications.

Stokes, A., Norris, J. E., Beek, L. P. H., Bogaard, T., Cammeraat, E., Mickovski, S. B., Jenner, A., Iorio, A., and Fourcaud, T. (2008). "How Vegetation Reinforces Soil on Slopes." *Slope Stability and Erosion Control: Ecotechnological Solutions*, J. E. Norris, A. Stokes, S. B. Mickovski, E. Cammeraat, R. Beek, B. C. Nicoll, and A. Achim, eds., Springer Netherlands, 65-118.

Taylor, D. W. (1948). *Fundamentals of soil mechanics*, J. Wiley, New York,.

Toy, T. J., Foster, G. R., and Renard, K. G. (2002). *Soil erosion : processes, predicition, measurement, and control*, John Wiley & Sons, New York.

Trip Down (2011). "Dark Hills Ollague, Chile " *Failing in the Salt Flats (Salar de Uyuni) and crossing to Ollague, Chile*, <http://tripdown.regioncoding.com/2010/05/failing-in-the-salt-flats-salar-de-uyuni-and-crossing-to-ollague-chile/>. (June 07, 2011).

Yang, C. T., and Song, C. C. (1979). "Theory of Minimum Rate of Energy Dissipation." *Journal of the Hydraulics Division*, 105(HY7), 769-784.

Yoder, D. C. (2009). "BsE/EE 525 Lecture Notes.", The University of Tennessee, Knoxville, TN.

Young, R. A., and Mutchler, C. K. (1969). "Soil movement on irregular slopes." *Water Resour. Res.*, 5(5), 1084-1089.

Chapter 6 Development of the Solution for a Concave Slope at Critical Equilibrium

Abstract

Topography and hydrology are probably the two variables that have the greatest influence on the erosion and stability of slopes of a given material. Studies have suggested that concave slope profiles reduce the amount of sediment produced. Further, natural slopes are usually curved in profile and rarely planar. The conceptual model presented in Chapter 5 indicated that slopes usually seek an equilibrium concave profile. Thus, it becomes necessary to define or describe the critical slope contour that corresponds to a Factor of Safety (FS) equal to 1. Sokolovski (1960) found that the slope contour in a critical equilibrium has a concave shape and its profile can be mathematically described as a function of the soil strength parameters and the soil unit weight. Unfortunately, due to the complexity of the fundamental equations of critical equilibrium for mediums possessing self weight, his solution is difficult to implement in practice and the available data from his results are highly limited.

In this chapter, the theory of critical equilibrium of a soil medium developed by Sokolovski (1960) will be explored and the mathematics behind his implementation will be visited in detail. Here, an approximate solution in the form of an analytical expression for the shape of the slope in the critical state is proposed. Though this expression is an approximate solution as well, it shows good agreement with Sokolovski's results in terms of geometry, fundamental failure mechanisms, and obtained factors of safety. The errors resulting from the approximation are investigated as a function of material strength properties.

Introduction

In Chapter 5, from the concept of minimum rate of energy dissipation proposed by Yang and Song (1979), a conceptual model to explain the geomorphological evolution of slopes toward concave profiles was presented and case studies were used to support this model. Concave slope profiles were suggested as the final equibrium shape that slopes would attain, and it was suggested that this shape would be maintianed due to a parallel retreat. Further, it was suggested that concave slope profiles experience lower erosion rates and produce less sediment than planar slopes. An approximate solution for the shape of the concave slope at failure for given soil strength parameters was presented, and a method to determine the shape for a desired Factor of Safety was demonstrated. While Chapter 5 was intended to provide a practical guide and an example of the application of the method, this chapter provdes the mathamatical backgorund behind the approximate solution, and evaluates the errors introduced into the solution due to the matematical approximation.

Slope contour in a critical mechanical state

To identify stable concave slope shapes, the first step would be to investigate the shape of slopes in a critical mechanical state. Sokolovski (1960), based on plasticity theory, studied the shape of slopes in the critical state or at imminent failure. He found that the slope profile at critical equilibrium has a concave

shape and its profile can be mathematically described as a function of the soil strength parameters and the soil unit weight. This formulation is explained below.

Equations of internal equilibrium and principal stresses

From the assumption that soil medium can be treated as a continuum, the complete state of stresses acting on any plane can be specified if the resultant stresses in the directions of the axes of the reference frame are known. From the equations of internal equilibrium (Malvern 1969):

$$\frac{\partial T_{i,j}}{\partial x_j} - B_j = 0 \tag{6-1}$$

Where $T_{i,j}$ represents the internal stresses and B_j are the body forces. Notice that the negative sign in this equation comes from assuming compressive stresses as positive and tensile stresses as negative (adopted convention in soil mechanics). For the plane strain condition (e.g. the profile of a 2D slope case), strains and shear stresses in the z direction (perpendicular to the paper) vanish. Therefore, Eq. (6-1) can be expressed as the following set of partial differential equations for the xy space:

$$\frac{\partial \sigma_{xx}}{\partial x} + \frac{\partial \tau_{xy}}{\partial y} = X \tag{6-2}$$

$$\frac{\partial \tau_{yx}}{\partial x} + \frac{\partial \sigma_{yy}}{\partial y} = Y \tag{6-3}$$

Here, σ_{xx} and σ_{yy} are the normal stresses acting on the x and y direction respectively, and $\tau_{xy} = \tau_{yx}$ are the shear stresses. *X* and *Y* are the body forces acting in the x and y directions respectively. For a soil medium, body forces are inevitably related to its unit weight. For a general case, when the reference frame is not aligned with the horizontal and vertical axes, the body forces can be expressed as:

$$X = \gamma \, sin\alpha \tag{6-4}$$

$$Y = \gamma \, cos\alpha \tag{6-5}$$

where α is the angle between the horizontal plane and the x-axis, and γ is the unit weight of the soil.

The complete state of stresses at a point can be mathematically expressed as a second order tensor, whose invariants are the principal stresses and directions. The importance of the principal stresses lies in the fact that they act on planes with no shear stresses and are independent of the selected reference frame. For plane strain conditions, the stress tensor can be simplified as shown in Eq. 6-6, and the major and minor principal stresses can be easily calculated from Eq. 6-7 and 6-8 respectively (Scott 1963).

$$\sigma_{ij} = \begin{bmatrix} \sigma_{xx} & \tau_{xy} & 0 \\ \tau_{yx} & \sigma_{yy} & 0 \\ 0 & 0 & \sigma_{zz} \end{bmatrix} \tag{6-6}$$

$$\sigma_1 = 0.5\left(\sigma_{xx} + \sigma_{yy}\right) + \sqrt{0.25\left(\sigma_{xx} - \sigma_{yy}\right)^2 + {\tau_{xy}}^2} \quad (6\text{-}7)$$

$$\sigma_3 = 0.5\left(\sigma_{xx} + \sigma_{yy}\right) - \sqrt{0.25\left(\sigma_{xx} - \sigma_{yy}\right)^2 + {\tau_{xy}}^2} \quad (6\text{-}8)$$

Critical equilibrium of a soil medium in plane-strain conditions

From the stress-strain behavior of solid bodies observed in laboratory tests, it is possible to identify a stress state at which plastic or non recoverable deformation starts. This stress, called the yield stress, imposes a limiting condition between elastic and plastic strains developed within the soil mass. In general, this limiting condition can be described in terms of stress and deformation. Though important for real geotechnical problems, stress and displacement boundary conditions together impose a statically indeterminate stress distribution in the soil even for elastic analysis, because compatibility equations must be satisfied by the strains obtained from the proposed solution (Scott 1963). Therefore, it has been usual practice in soil mechanics to define the limiting condition only in terms of stresses by assuming an ideal plastic behavior of the soil, either *elastic perfectly plastic* or *rigid perfectly plastic behavior*. In that way, the specification of the failure or limiting stress is independent of the strains and the compatibility conditions do not need to be satisfied, at least, as in elasticity (Scott 1963). In reality, any solid material presents more complex stress-strain behavior after the yield stress has been reached (e.g. work-hardening or work-softening). Modeling this intricate behavior is indeed difficult, and may require the implementation of numerical techniques like non-linear finite elements. Analytical-closed form solutions for only a limited number of problems have been found. Nevertheless, the assumption of an ideal plastic soil behavior has permitted the development of solutions for a wide range of geotechnical problems, since the yielding stress is assumed to be the limiting or failure stress and it is the base of the critical equilibrium theory in soil mechanics.

When a soil body is deformed until it is just on the point of flowing plastically, static equilibrium is still observed and therefore the equilibrium equations (Eq. 6-2 and 6-3) must be satisfied. If the deformation continuous, plastic deformation will take place with a constant value of principal stresses. This plastic deformation occurs by the sliding of planes on which the inclination of the stresses has reached a maximum (Scott 1963). The question that arises is the following: what is the yield stress at which soil will start deforming plastically? The implementation of a constitutive law for modeling purposes requires the selection of a yield stress criterion. For frictional materials like soils, Mohr-Coulomb is the most widely accepted yield criterion. In soil mechanics, it has been also employed as a failure condition. Sokolovski (1960) employed thi limiting condition, and suggested that plastic deformation or slip across a plane will not occur if the following equations are satisfied:

$$|\tau_n| \leq \sigma_n \tan\phi + c \quad (6\text{-}9)$$

$$\sigma_n \geq -c\cot\phi = -H \quad (6\text{-}10)$$

where σ_n and τ_n are the normal and shear stresses acting on any plane within the soil body, and ϕ and c are the internal friction angle and cohesion, respectively, defined as the strength components of the soil. Note that H is the tensile strength of the soil. In order to bring the body into a critical or limiting equilibrium state, the stresses have to be equal to the strength defined by the Mohr-Coulomb criterion. This limiting condition is mathematically expressed by Eq. 6-11.

$$max\ |\tau_n| = (\sigma_n + H)\ tan\ \phi \tag{6-11}$$

Sokolovski (1960) expressed this limiting equilibrium state as in Eq. 6-12, where it can be seen that the critical equilibrium requires two conditions to be satisfied: a) the difference between shear stress and shear strength must be zero and b) that difference needs to be maximized.

$$max\ \{|\tau_n| - (\sigma_n + H)\ tan\ \phi\} = 0 \tag{6-12}$$

If we plot the stress state of point within the soil medium in the $\tau - \sigma$ stress space, assuming that the conditions are just at the point of flowing plastically, we will find that the planes at which the obliquity of stresses is maximum are the planes formed from the pole of the Mohr Circle to the point of contact with the failure condition line: $|\tau_n| = (\sigma_n + H)\ tan\ \phi$ (Figure 6-1). Consequently, those planes are the slip planes on which soil will experience plastic deformation with no further increase in stress. In reality, for a wide range of stress boundary conditions, those planes are not straight but curved. Then, at the point of the zone of critical equilibrium there is a family of 2 isogonal curves called slip lines.

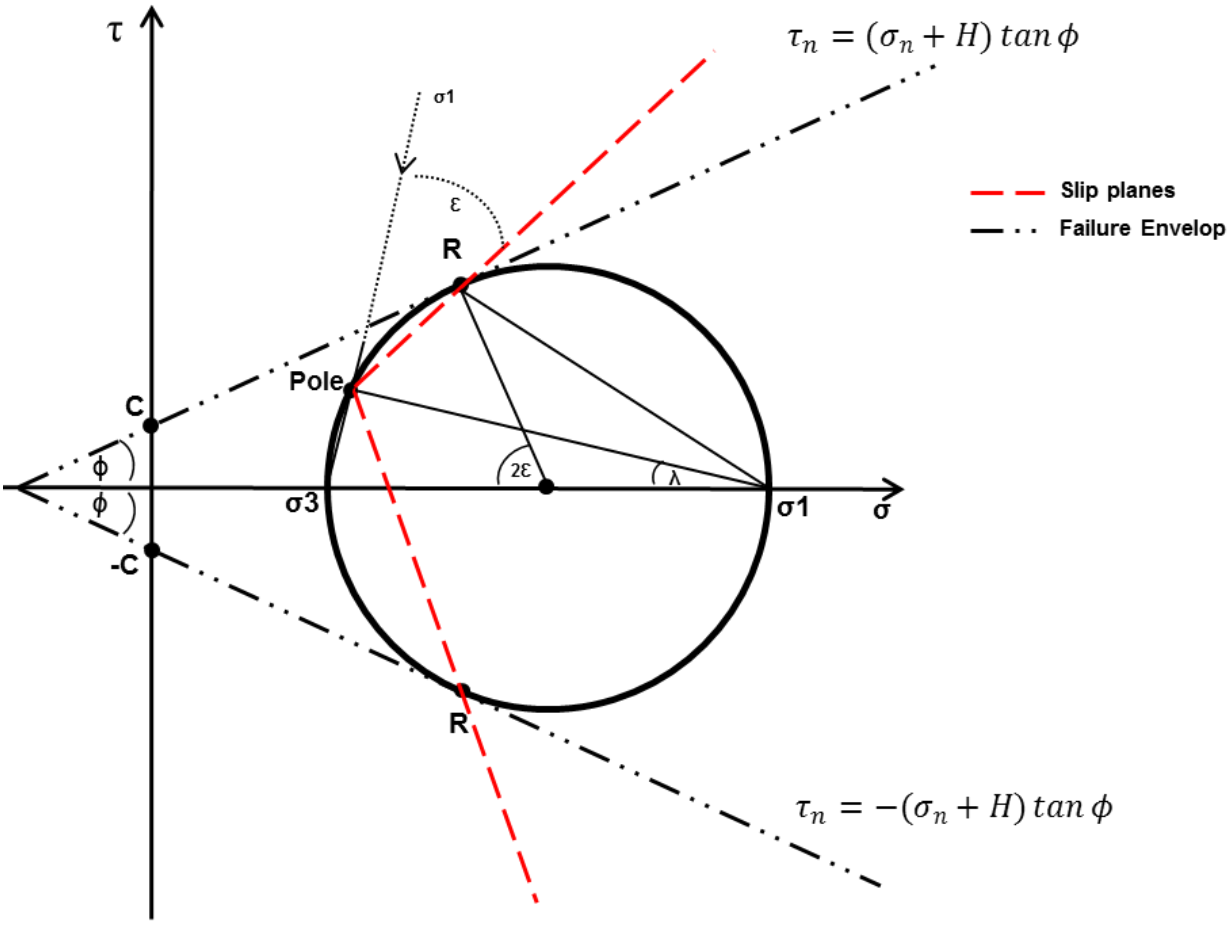

$\tau_n = (\sigma_n + H)\ tan\ \phi$

$\tau_n = -(\sigma_n + H)\ tan\ \phi$

Figure 6-1 Illustration of slip planes on Mohr-Coulomb diagram.

If we define λ as the angle between the direction of the normal stress and the direction of the major principal stress, the normal and tangential components of the stress at any plane can be expressed as a function of the principal stresses (Holtz and Kovacs 1981, Lambe and Whitman 1969):

$$\sigma_n = 0.5\ (\sigma_1 + \sigma_3) - 0.5\ (\sigma_1 - \sigma_3)\ \cos 2\lambda \tag{6-13}$$

$$\tau_n = 0.5\ (\sigma_1 - \sigma_3) \sin 2\lambda \tag{6-14}$$

Introducing Eq. 6-13 and 6-14 into 6-12, the critical state condition can be expressed in terms of the invariants of the stress tensor:

$$\max \{0.5\ \cos\phi\ [(\sigma_1 - \sigma_3) \sin(2\lambda - \phi) - \sin\phi\ (\sigma_1 + \sigma_3 + 2H)]\} = 0 \tag{6-15}$$

The condition of maximum difference requires a mathematical derivation or optimization problem. Deriving the Eq. 6-15 in terms of λ and making the expression equal to zero, it is found that the maximum condition is reached when:

$$2\lambda = \phi + \frac{\pi}{2} \tag{6-16}$$

After introducing Eq. 6-16 into Eq. 6-15, the expression for a medium in critical state $\max\ \{|\tau_n| - (\sigma_n + H) \tan\phi\} = 0$ can be written as (Sokolovski 1960):

$$0.5\ (\sigma_1 - \sigma_3) = 0.5 \sin\phi\ \ (\sigma_1 + \sigma_3 + 2H) \tag{6-17}$$

The adopted 2D reference frame by Sokolovski implies a horizontal x-axis positive toward the left, and a vertical y-axis positive downward. This convention is in reverse direction of what it is usually employed; however it is mathematically rigorous and it will be adopted here.

In Figure 6-1 it is observed that the slip plane is oriented at ε^o from the major principal stress direction. For a plane whose normal is inclined μ^o from the horizontal x-axis and whose principal major stress direction is oriented ξ^o from the same, it will be observed that the curved slip lines will be initially oriented at $(\xi \pm \varepsilon)^o$ from the x-axis (Figure 6-2)

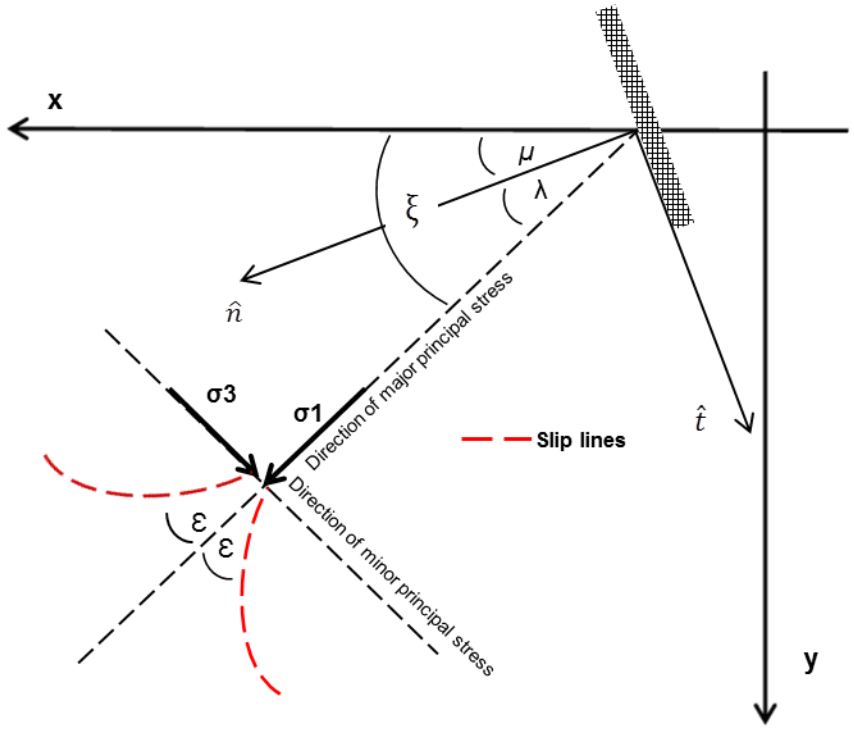

Figure 6-2 Orientation of slip lines (adapted from Sokolovskii, 1965)

Consequently, stresses in x and y directions in terms of the principal stresses can be expresses as (Sokolovski 1960):

$$\sigma_x = 0.5\ (\sigma_1 + \sigma_3) + 0.5\ (\sigma_1 - \sigma_3)\ \cos 2\xi \tag{6-18}$$

$$\sigma_y = 0.5\ (\sigma_1 + \sigma_3) - 0.5\ (\sigma_1 - \sigma_3)\ \cos 2\xi \tag{6-19}$$

$$\tau_{xy} = 0.5\ (\sigma_1 - \sigma_3) \sin 2\xi \tag{6-20}$$

Using the equation for critical equilibrium (Eq. 6-17) and Eq. 6-18, 6-19 and 6-20, it is possible now to obtain equations of critical stress (Sokolovski 1960):

$$\sigma_x = \ \sigma\ (1 + \sin\phi \cos 2\xi) - H \tag{6-21}$$

$$\sigma_y = \ \sigma\ (1 - \sin\phi \cos 2\xi) - H \tag{6-22}$$

$$\tau_{xy} = \sigma\ \sin\phi \sin 2\xi \tag{6-23}$$

where $\sigma = 0.5(\sigma_1 + \sigma_3) + H$

Similarly, equations of critical state in the n-t space (see Figure 6-2) can be written (Sokolovski 1960):

$$\sigma_n = \ \sigma\ [1 + \sin\phi \cos 2(\xi - \mu)] - H \tag{6-24}$$

$$\sigma_t = \sigma\,[1 - \sin\phi\cos 2(\xi - \mu)] - H \tag{6-25}$$

$$\tau_{nt} = \sigma\ \sin\phi\sin 2(\xi - \mu) \tag{6-26}$$

Up to this point, the equations of equilibrium (Eq. 6-2 and 6-3) and the equations of a soil medium in a critical state (Eq. 6-21, 6-22 and 6-23) have been presented. Combining these 5 equations, the fundamental equations of critical equilibrium, as proposed by Sokolovskii (1965), are obtained:

$$(1 + \sin\phi\cos 2\xi)\frac{\partial\sigma}{\partial x} + \sin\phi\sin 2\xi\frac{\partial\sigma}{\partial y} - 2\sigma\sin\phi\left(\sin 2\xi\frac{\partial\xi}{\partial x} - \cos 2\xi\frac{\partial\xi}{\partial y}\right) = \gamma\sin\alpha \tag{6-27}$$

$$\sin\phi\sin 2\xi\frac{\partial\sigma}{\partial x} + (1 - \sin\phi\cos 2\xi)\frac{\partial\sigma}{\partial y} + 2\sigma\sin\phi\left(\cos 2\xi\frac{\partial\xi}{\partial x} + \sin 2\xi\frac{\partial\xi}{\partial y}\right) = \gamma\cos\alpha \tag{6-28}$$

These two first order partial differential equations govern the variation of the stresses. Hill (1950), proposed that the best way to solve this system is by the *method of characteristics*. Then, multiplying Eq. 6-27 by $\sin(\xi \pm \varepsilon)$, Eq. 6-28 by $\cos(\xi \pm \varepsilon)$ and adding them, the following expression is obtained (Sokolovskii 1965):

$$\left[\frac{\partial\sigma}{\partial x} \mp 2\sigma\tan\phi\ \frac{\partial\xi}{\partial x} - \gamma\frac{\sin(\alpha\mp\phi)}{\cos\phi}\right]\cos(\xi \mp \varepsilon) + \left[\frac{\partial\sigma}{\partial y} \mp 2\sigma\tan\phi\ \frac{\partial\xi}{\partial y} - \gamma\frac{\cos(\alpha\mp\phi)}{\cos\phi}\right]\sin(\xi \mp \varepsilon) = 0 \tag{6-29}$$

Sokolovski suggested the use of auxiliary quantities in order to simplify the expression above. For convenience, these quantities (*M* and *N*) can be selected as in Eq. 6-30 and 6-31 to let the Eq. 6-29 be expressed as in Eq. 6-32.

$$M = \frac{\partial\sigma}{\partial x} \mp 2\sigma\tan\phi\ \frac{\partial\xi}{\partial x} - \gamma\frac{\sin(\alpha\mp\phi)}{\cos\phi} \tag{6-30}$$

$$N = \frac{\partial\sigma}{\partial y} \mp 2\sigma\tan\phi\ \frac{\partial\xi}{\partial y} - \gamma\frac{\cos(\alpha\mp\phi)}{\cos\phi} \tag{6-31}$$

$$M + N\tan(\phi \mp \varepsilon) = 0 \tag{6-32}$$

Obtaining the characteristic differential equations requires the expression of the auxiliary quantities in ordinary derivative form. Employing the transformation in Eq. 6-33 and 6-34 and introducing a new auxiliary quantity *P* (Eq. 6-35), the new quantities *M* and *N* are obtained (Eq. 6-37 and 6-38) (Sokolovskii 1965).

$$d\sigma = \frac{\partial\sigma}{\partial x}dx + \frac{\partial\sigma}{\partial y}dy \tag{6-33}$$

$$d\xi = \frac{\partial\xi}{\partial x}dx + \frac{\partial\xi}{\partial y}dy \tag{6-34}$$

$$P = \frac{d\sigma}{dx} \mp 2\sigma\tan\phi\frac{d\xi}{dx} - \frac{\gamma}{\cos\phi}\left[\sin(\alpha \mp \phi) + \cos(\alpha \mp \phi)\frac{dy}{dx}\right] \tag{6-35}$$

$$Mdx + Ndy = Pdx \tag{6-36}$$

$$M = \frac{P\,dx\,\sin(\xi \mp \varepsilon)}{\sin(\xi \mp \varepsilon)dx - \cos(\xi \mp \varepsilon)dy} \tag{6-37}$$

$$N = \frac{P\,dx\,\cos(\xi \mp \varepsilon)}{\sin(\xi \mp \varepsilon)dx - \cos(\xi \mp \varepsilon)dy} \tag{6-38}$$

Note that the characteristics will be found when the numerator and denominator of Eq. 6-37 and 6-38 are simultaneously set to zero, and therefore the equations of characteristic are (Sokolovskii 1965):

$$\frac{dy}{dx} = \tan(\xi \mp \varepsilon) \tag{6-39}$$

$$d\sigma \mp 2\sigma \tan\phi\, d\xi = \frac{\gamma}{\cos\phi}[\sin(\alpha \mp \phi)\, dx + \cos(\alpha \mp \phi)\, dy] \tag{6-40}$$

Eq. 6-39 imposes the condition that the characteristics have to be inclined at $(\xi \mp \varepsilon)^o$ from the x-axis. Therefore, they are indeed slip lines in the x-y space (Sokolovskii 1965). For cases when the body forces are aligned in the direction of vertical y-axis (such as the forces due to gravity), $\alpha = 0$ and Eq. 6-40 simplifies to:

$$d\sigma \mp 2\sigma \tan\phi\, d\xi = \gamma[dy + \tan\phi\, dx] \tag{6-41}$$

Contour of a non-planar slope: application of critical equilibrium theory

Due to the complexity of the equations of critical equilibrium presented here, Sokolovski first analyzed a slope problem for a medium without gravity forces (weightless medium), under the action of an external stress $q(x)$ (Figure 6-3). In order to explain in more detail the mechanics behind this formulation, we propose to divide the analysis of this problem into 3 major steps.

Step 1: analysis of the stress boundary conditions at the top of the slope

Along the x-axis the stresses are $\sigma_{xx} = 0$, $\sigma_{yy} = q(x)$, $\tau_{xy} = 0$. Since the only stress acting is in the direction of the vertical y-axis, principal stress directions are aligned with the selected reference frame, i.e. major principal direction parallel to y-axis and minor principal direction parallel to x-axis. Therefore, the angle between the x-axis and the major principal direction is $\xi = \frac{\pi}{2}$. From Eq. 6-22, $\sigma_{yy} = \sigma\,(1 - \sin\phi\cos 2\xi) - H = q(x)$, then $\sigma = \frac{q(x)+H}{1+\sin\phi}$ (Sokolovski 1960).

Step 2: analysis of the stress boundary conditions on the contour

Along the slope profile the tangential component of the stress is zero. Notice that $\mu = \frac{\pi}{2}$, since the plane on which the external stress is acting is horizontal. At *y=0,* $\xi = \frac{\pi}{2}$; then, using Eq. 6-25 $\sigma_{tt} = 0 = \sigma\,[1 - \sin\phi\cos 2(\xi - \mu)] - H$ we obtain $\sigma = \frac{H}{1-\sin\phi}$ (Sokolovski 1960). Also notice that ξ is indeed the angle of the slope measured from the x-axis. This observation is one of the pillars in determining the

geometry of the slope in critical equilibrium state. Eq. 6-42 and 6-43 summarizes the boundary conditions at the top and contour of the slope respectively.

$$\sigma = \frac{q(x)+H}{1+\sin\phi}, \quad \xi = \frac{\pi}{2} \tag{6-42}$$

$$\sigma = \frac{H}{1-\sin\phi}, \quad \xi = \beta \tag{6-43}$$

Step 3: Analytical solution of the equation of critical equilibrium
For the case of a weightless material the differential Eq. 6-41 can be simplified to:

$$\frac{d\sigma}{\sigma} = -2\tan\phi\, d\xi \tag{6-44}$$

Integrating the equation above,

$$\frac{\cot\phi}{2}\ln|\sigma| + c1 = -\xi \tag{6-45}$$

where *c1* is a constant left by the integration. At the slope profile, the Eq. 6-45 becomes:

$$\frac{\cot\phi}{2}\ln\left[\frac{H}{1-\sin\phi}\right] + c1 = -\beta \tag{6-46}$$

To find *c1*, let's use the stress condition at the top of the slope. Introducing Eq. 6-42 into 6-45 and solving for *c1*:

$$c1 = -\frac{\cot\phi}{2}\ln\left[\frac{q(x)+H}{1+\sin\phi}\right] - \frac{\pi}{2} \tag{6-47}$$

Finally, introducing Eq.6-47into 6-46 it is possible to find the angle of the slope when the soil medium is in a critical state. This expression is equivalent to the one reported by Sokolovski (1960), and the difference in form may be attributed to the change of reference frame.

$$\beta = \frac{\pi}{2} + \frac{\cot\phi}{2}\ln\left[\frac{q(x)+H}{H}\frac{1-\sin\phi}{1+\sin\phi}\right] \tag{6-48}$$

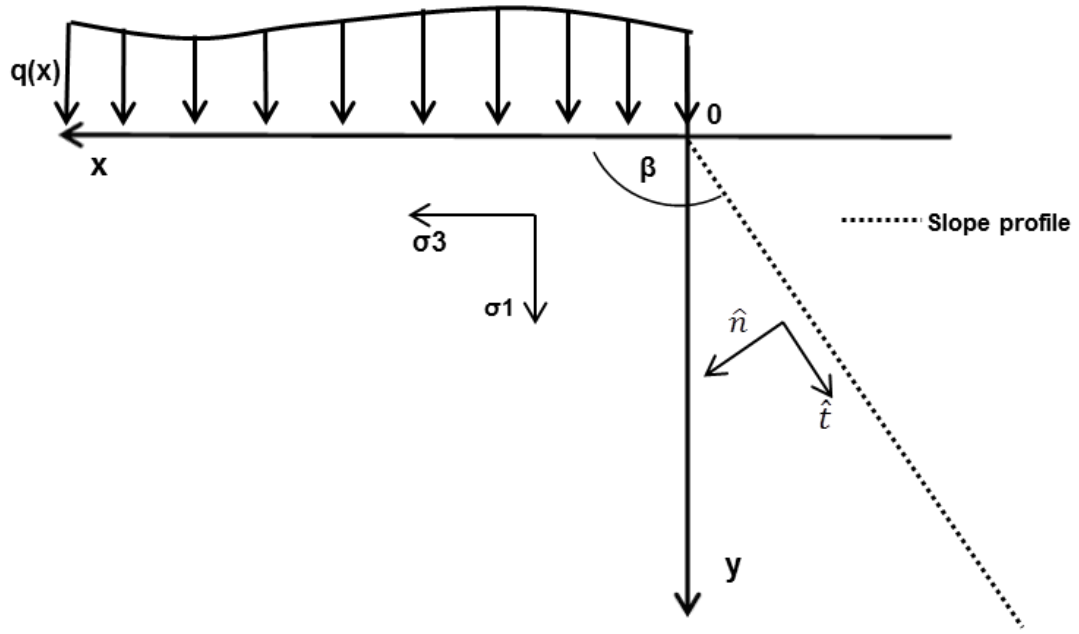

Figure 6-3 Critical slope shape for a weightless medium

From Eq. 6-48 it is possible to conclude that for a weightless medium the contour of the slope is planar, since β is constant (Figure 6-3). However, for a medium possessing weight, the stress condition changes along the y-axis and with it the principal directions along the contour of the slope. This condition implies that for a medium possessing weight, the critical slope will be curved, and the ξ may be described as a function of the space coordinates. The presence of the unit weight in the Eq. 6-41 imposes a constraint in the attempt to find an analytical solution, and numerical techniques must be used. Sokolovski (1960) solved this problem numerically via canonical transformations. His solution showed that the slope shape in a critical state is concave and can be obtained as a function of ϕ, c and γ.

Unfortunately, the available resulting data from his numerical implementation is restricted to specific values of ϕ. Geometrical constraints (e.g. slope height) for any desired analysis arise, since the coordinates of the slope contour are limited by the ratio c/γ. Furthermore, the numerical nature of his solution is not simple, making its implementation difficult in practical slope design, especially for larger slopes.

Proposed solution for the slope contour in critical equilibrium for a weighty medium

The equations of critical equilibrium with body forces preclude the finding of exact solutions, and until now, the approximate numerical implementation conducted by Sokolovski (1960) seems to be the only available solution.

In this research, a solution in the form of an analytical expression was developed for the problem of the slope shape in critical state. Though this expression is an approximate solution as well, it has shown reasonably good agreement with the Sokolovski solution.

The contour of the slope in a critical state was found to be approximately satisfied by the following equation:

$$x = -\int_0^y \frac{\cot\phi}{2} \ln\left[\frac{q(x)+Y(y)+H}{H}\frac{1-\sin\phi}{1+\sin\phi}\right] dy \quad (6\text{-}49)$$

Sokolovski (1960), showed that the maximum height of a vertical slope that a soil medium can withstand (critical height) under an elastic state was:

$$h_{cr} = \frac{2c\cos\phi}{\gamma(1-\sin\phi)} \quad (6\text{-}50)$$

The introduction of the critical height into the equation will allow a vertical slope contour at the top of the slope (Figure 6-4).

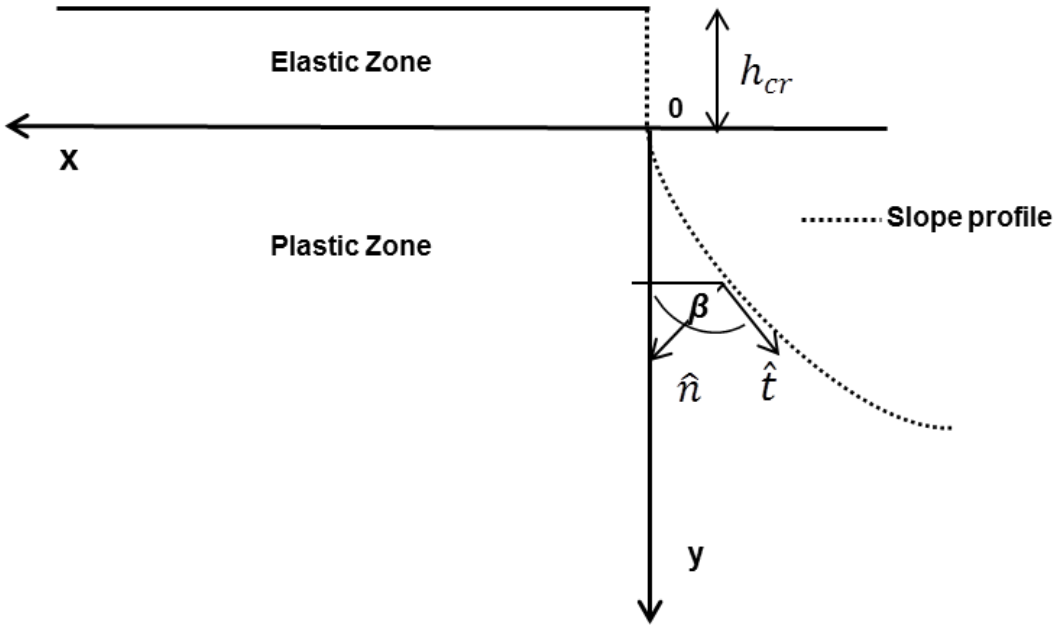

Figure 6-4 Elastic and plastic zones in a medium possessing weight (adapted from Sokolovski, 1965)

The contour of the slope below the elastic zone will be affected by the stress of the overburden above it and it is necessary to account for it. Therefore, assuming no external stresses:

$$q(x) + Y(y) = \frac{2c\cos\phi}{1-\sin\phi} + \gamma y \quad (6\text{-}51)$$

Then, Eq. 6-49 can be finally expressed as:

$$x = -\int_0^y \frac{\cot\phi}{2} \ln\left[\frac{\frac{c}{\gamma}\frac{2\cos\phi}{(1-\sin\phi)}+y+\frac{c}{\gamma}\cot\phi}{\frac{c}{\gamma}\cot\phi}\frac{1-\sin\phi}{1+\sin\phi}\right] dy \quad (6\text{-}52)$$

A more rigorous mathematical expression for the complete solution of the problem would be:

$$x = \begin{cases} 0 & , \quad -h_{cr} \le y \le 0 \\ -\int_0^y \frac{\cot\phi}{2} \ln\left[\frac{\frac{c}{\gamma}\frac{2\cos\phi}{(1-\sin\phi)}+y+\frac{c}{\gamma}\cot\phi}{\frac{c}{\gamma}\cot\phi}\ \frac{1-\sin\phi}{1+\sin\phi}\right] dy\,, & y > 0 \end{cases} \tag{6-53}$$

Solving the integral in Eq. 6-53, the solution for contour of the slope with self-weight in a critical state can finally be expressed as:

$$x = \begin{cases} 0 & , -h_{cr} \le y \le 0 \\ -A\left[\sigma_y\,(B-1)(cosec\,\phi - 1) + H\,B\,(cosec\,\phi + 1)\right], & y > 0 \end{cases} \tag{6-54}$$

where:

$$A = \frac{cos\,\phi}{2\gamma(1-sin\,\phi)} \tag{6-55}$$

$$B = ln\left[\frac{\sigma_y}{H}\,K_a + 1\right] \tag{6-56}$$

$$\sigma_y = \gamma y \tag{6-57}$$

$$H = c\,cot\,\phi \tag{6-58}$$

Notice that σ_y is the vertical stress and H is the tensile strength, as defined earlier. Also observe that the factor B is a function of the active coefficient of earth pressure defined as (Perloff and Baron 1976, Scott 1963):

$$K_a = \frac{1-sin\,\phi}{1+sin\,\phi} \tag{6-59}$$

Sokolovski developed his theory employing a reference frame that implies a horizontal x-axis positive toward the left, and a vertical y-axis positive downward. Note that the negative sign in Eq. 6-53 and 6-54 was added in order to obtain solutions in the same quadrant that Sokolovskii (1965) did. Thus, the proposed solution describes a slope contour at the critical state in the quadrant where x-axis is negative and y-axis positive (on the adopted reference frame), starting from the origin of the system (Figure 6-4). Above the origin h_{cr} lies vertically with coordinates ranging from (0,- h_{cr}) to (0, 0).

Notice that Eq. 6-54 is not a function of three soil parameters, but instead a function of only two: c/γ ratio and ϕ, which simplifies its manipulation.

Comparison of the proposed solution with that of Sokolovshi

The proposed solution (Eq. 6-54) will be compared with the data reported by Sokolovski (1960) for a limited range of soil properties and slope heights. The slope contour coordinates are found only for cases when $\phi = 10, 20, 30$ and 40^o, and the extension of the vertical height is limited by the ratio c/γ. Therefore, for a selected range of c/γ, the vertical coordinates of the Sokolovski's solution were used as the input in the Eq. 6-54. In this way, the solutions will only differ in the values of the horizontal axis and the comparison will be simplified. Figures 6-5, 6-6 and 6-7 show the slope contours obtained from the proposed and Sokolovski (1960) solutions, for $\phi = 20, 30$ and 40^o and for a $c/\gamma = 2\ m$. Similar comparative curves for $c/\gamma = 0.2,\ 1,\ 3$ and $4\ m$ are found in the Appendix A. The range of c/γ values investigated in this comparison where chosen to represent the range typically observed in soils.

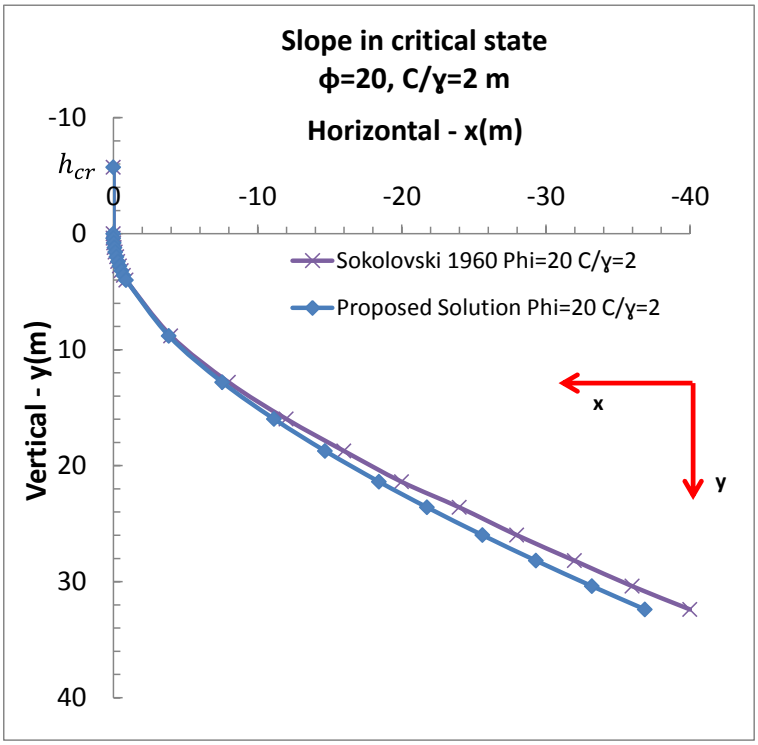

Figure 6-5 Concave slope profiles obtained from Sokolovski (1960) and the proposed solution (Eq. 6-54) for $\phi = 20^o$ and $c/\gamma = 2\ m$

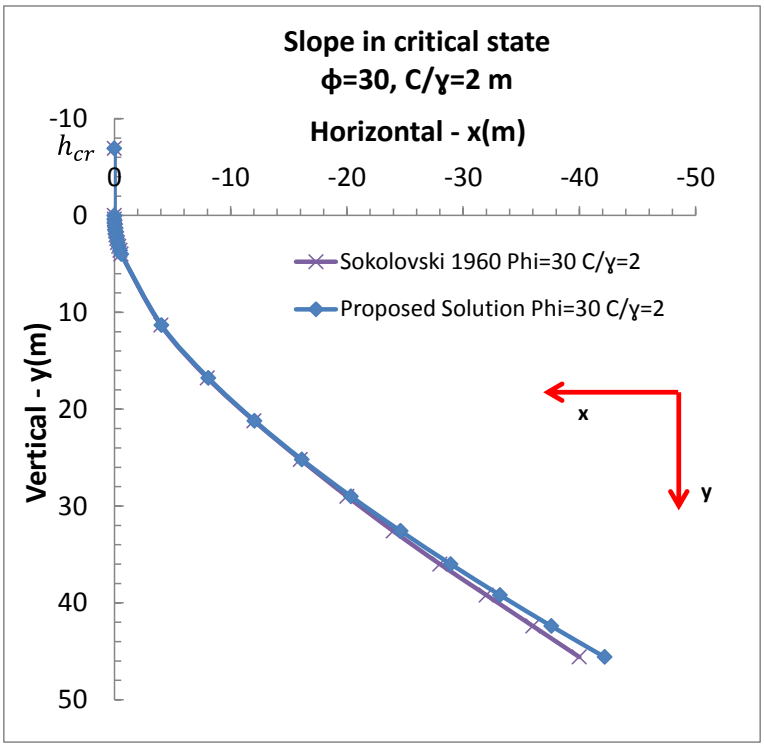

Figure 6-6 Concave slope profiles obtained from Sokolovski (1960) and the proposed solution (Eq. 6-54) for $\phi = 30^o$ and $c/\gamma = 2\ m$

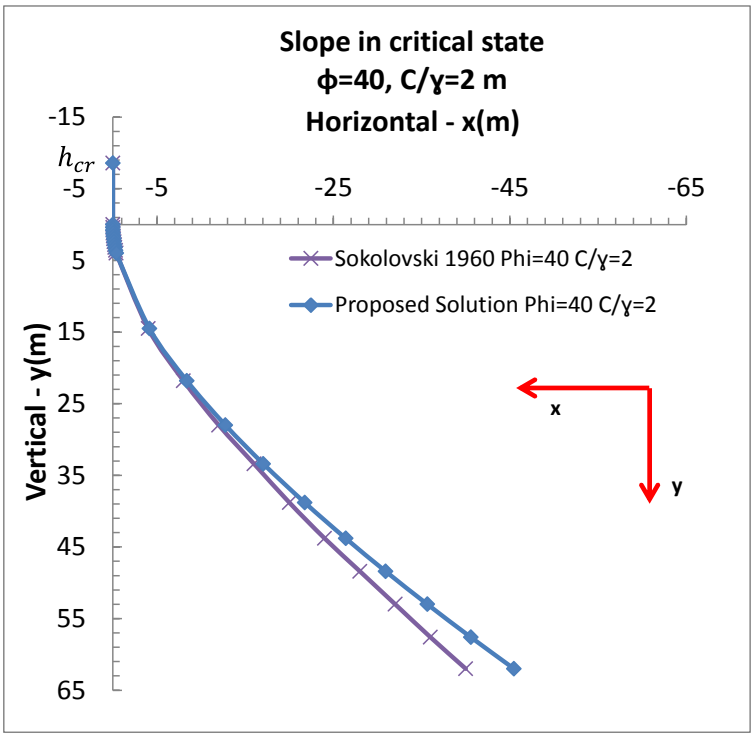

Figure 6-7 Concave slope profiles obtained from Sokolovski (1960) and the proposed solution (Eq. 6-54) for $\phi = 40^o$ and $c/\gamma = 2\ m$

In all cases there is observed to be relatively close agreement between the contours, especially at the upper portion of the curve. It is interesting to note that the agreement in the contour shape depends on the internal friction angle. To further investigate the stability of these slope contours, Finite Element (FEM) and Limit Equilibrium (LEM) analyses were conducted. These analysis were carried out using the FEM software *Phase2* (Rocscience Inc. 2011) and the LEM Software *Slide* (Rocscience Inc. 2011) employing the Simplified Bishop's Method. Table 6-1 summarizes the obtained FS for the selected range of soil properties obtained with the LEM procedure. Results from the FEM analysis agree closely with the LEM results and are reported in the Appendix A. The analysis shows very good agreement between factors of safety for both set of curved slopes. Please notice that in both cases FSs seem to be invariants of the selected value of c/γ, but they change slightly with the internal friction angle. It is also observed that the proposed solution tends to be slightly less conservative than Sokolovski's for lower internal friction angles and to some extent more conservative for higher ones, being somewhere around $\phi = 30^o$ the inflection point in this behavior. The difference between both solutions is still small, however. Numerically, FSs were observed to be only 3.8% different when $\phi = 20^o$, 0.9% when $\phi = 30^o$ and 2.8% when $\phi = 40^o$.

On the other hand, when the slope is at the critical state any loss of strength will cause the slope to fail, and therefore the FS in this critical state must be 1. Results showed that neither Sokolovski's nor the proposed solution give an exact FS of 1 for all the analyzed cases, which may be explained from the fact that both procedures are approximations to the real solution. Assuming FS=1 as the correct answer, the error produced by the proposed solution would be approximately: -0.4% when $\phi = 20^o$, 4.4% when $\phi = 30^o$ and 5.5% when $\phi = 40^o$. The negative sign in the error means that the FS of the proposed solution lies below the value of 1.These errors may be interpreted as small for the range of internal friction angles usually found in nature and perhaps insignificant in terms of practical applications in geotechnical design.

Table 6-1 Summary of FS obtained from LEM analysis for both sets of curved slopes (Simplified Bishop's method with 495000 surfaces computed)

	LEM Simplified Bishop's method (4950 interpreted surfaces)					
	ϕ = 20		ϕ = 30		ϕ = 40	
	Sokolovski Solution	Proposed Solution	Sokolovski Solution	Proposed Solution	Sokolovski Solution	Proposed Solution
c/γ = 0.2 m	Hcr = 0.57 m	H = 3.81 m	Hcr = 0.69 m	H = 5.25 m	Hcr = 0.86 m	H = 7.06 m
	1.04	**1.00**	**1.03**	**1.04**	**1.03**	**1.06**
c/γ = 1 m	Hcr = 2.86 m	H = 19.06 m	Hcr = 3.46 m	H = 26.26 m	Hcr = 4.29 m	H = 35.29 m
	1.04	**1.00**	**1.03**	**1.04**	**1.03**	**1.06**
c/γ = 2 m	Hcr = 5.71 m	H = 38.11 m	Hcr = 6.93 m	H = 52.53 m	Hcr = 8.58 m	H = 70.58 m
	1.04	**1.00**	**1.03**	**1.04**	**1.03**	**1.06**
c/γ = 3 m	Hcr = 8.57 m	H = 57.17 m	Hcr = 10.39 m	H = 78.79 m	Hcr = 12.87 m	H = 105.87 m
	1.04	**1.00**	**1.03**	**1.04**	**1.03**	**1.05**
c/γ = 4 m	Hcr = 11.43 m	H = 76.23 m	Hcr = 13.86 m	H = 105.06 m	Hcr = 17.16 m	H = 141.16 m
	1.04	**1.00**	**1.03**	**1.04**	**1.03**	**1.06**

Comparing failure mechanisms, both FEM and LEM analyses predict, with some degree of agreement, that the critical failure surface will exit the face of the slope. The maximum developed shear strain in the finite element model coincides well with the failure mechanism of the lowest factor of safety found in the limit equilibrium model. Failure mechanisms are similar for both sets of curved slopes (Figures 6-8 and 6-9). However, the face failure mechanism may not be the case for slopes with shorter heights, which will be studied in more detail in the next section.

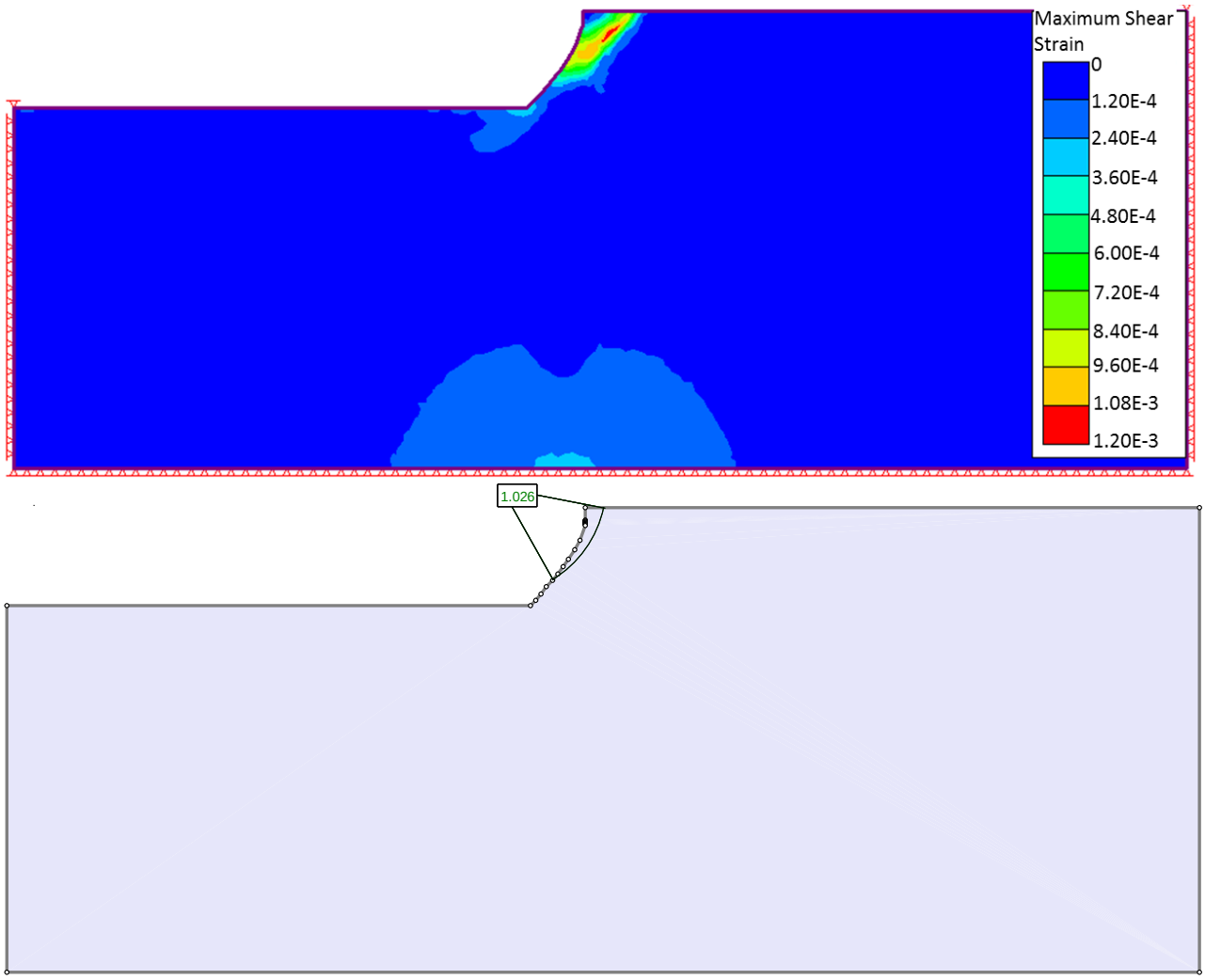

Figure 6-8 Observed failure mechanism for Sokolovski's solution of the critical slope shape. $\phi = 40^o,\ c/\gamma = 0.2\ m$. FEM (SRF=1.04) analysis above and LEM (FS=1.026) below. Assumed E=20,000 kPa

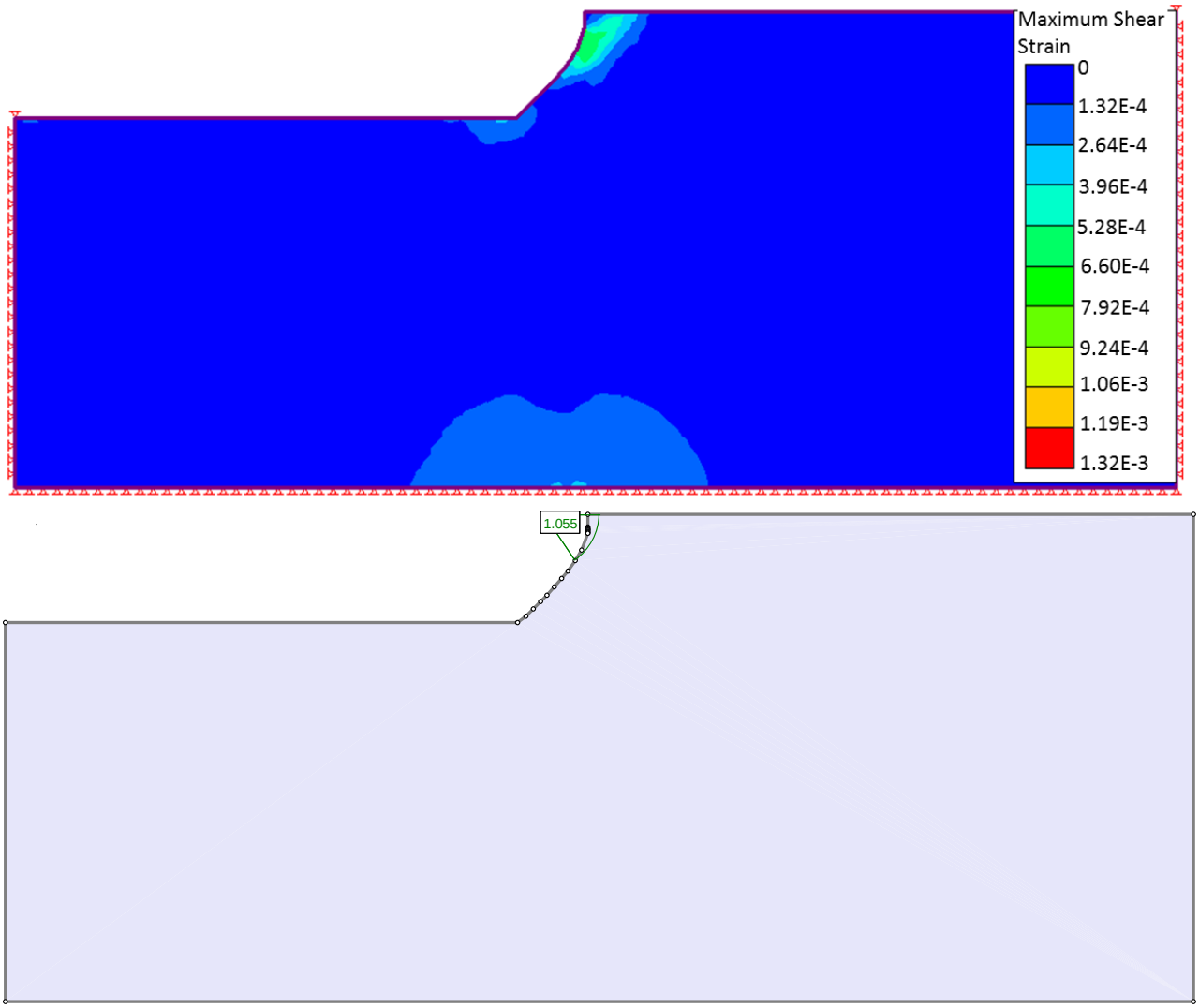

Figure 6-9 Observed failure mechanism for the proposed solution of the critical slope shape. $\phi = 40^{o},\ c/\gamma = 0.2\ m$. FEM (SRF=1.05) above and LEM (FS=1.055) below. Assumed E=20,000 kPa

Effect of the slope height on the failure mechanism and FS's

Further analyses were conducted to observe the effects of the slope height (Hs) on the type of failure mechanism. Solutions for the slope contour of slopes with heights up to 108 m were obtained from Eq. 6-54 for a selected range of soil parameters, and the slopes were investigated for a range of slope heights. LEM stability analyses were conducted at each height for each solution. Values of $\phi = 20, 30, 38$ and 45^{o} and $c/\gamma = 0.27,\ 0.54, 1.08, 2.16$ and $3.52\ m$ were employed in this investigation. Results show that at smaller heights these curved slopes usually have a critical failure surface that exits at the toe of the slope. Results also indicates the existence of a slope height at which the failure mode changes from that of a toe failure to a face failure; this point will be defined as the limiting height h_L.

On the other hand, it is noted that at smaller heights the values of FS's are somewhat greater, but with a decreasing tendency as the heights become greater. Then, a point is reached where the FS's do not

further decrease and maintain a constant value independently of how tall the slope becomes (Figure 6-10). This equilibrium point was observed to coincide with h_L, which allows one to conclude that the most critical slip surface for heights equal or greater than h_L would be the same. In theory, this steady FS value should be 1; however, as it was discussed before, the approximate nature of the proposed solution induces a small error that was observed to be independent of c/γ, but dependent on the internal friction angle ϕ. Figure 6-10 shows that the steady FS for any curved slope with $\phi = 30^o$, obtained from Eq. 6-54, would be 1.044 with an approximat error of 4.4%. Figure 6-12 shows the estimated variation of the error for the different internal friction angles investigated.

Figure 6-11 displays each of the cases in Figure 6-10 with its corresponding value of h_L. Here, it is observed how the mean value of h_L coincides relatively well with the starting point of the steady FS behavior. Also it is noted that h_L becomes larger as c/γ increases. Similar charts for $\phi = 20, 38$ and 45^o are found in the Appendix A.

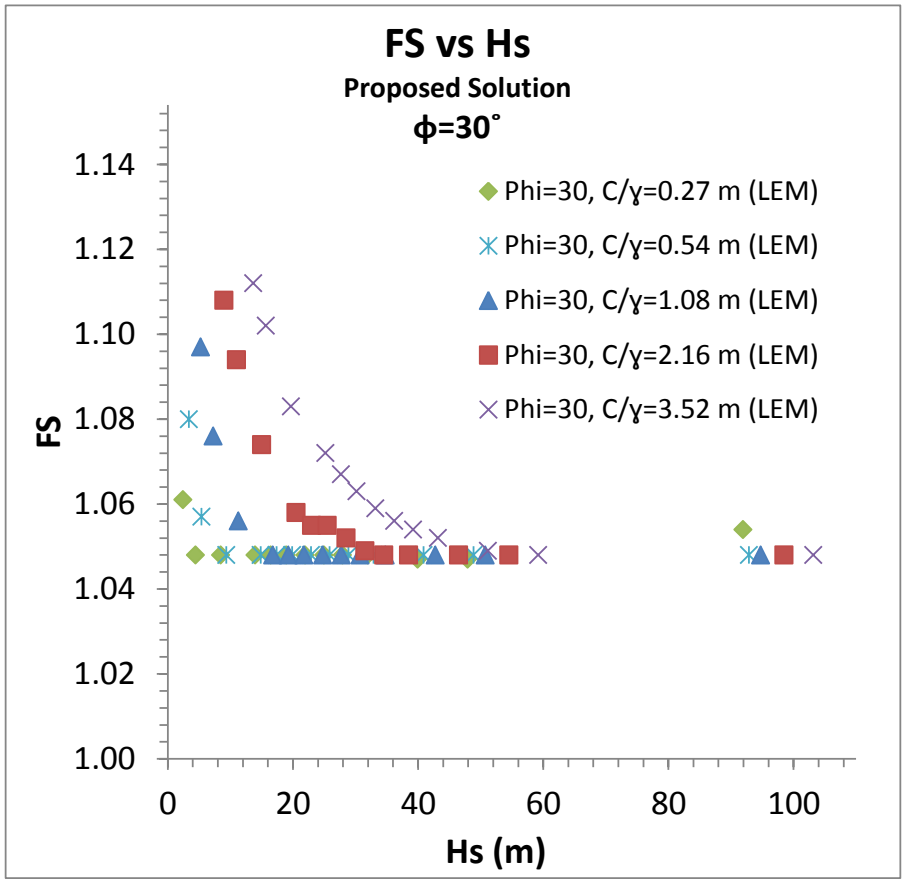

Figure 6-10 Factor of safety (FS) vs Slope Height (Hs) for $\phi = 30^o$, $c/\gamma = 0.27, 0.54, 1.08, 2.16, 3.52$ m. LEM analysis.

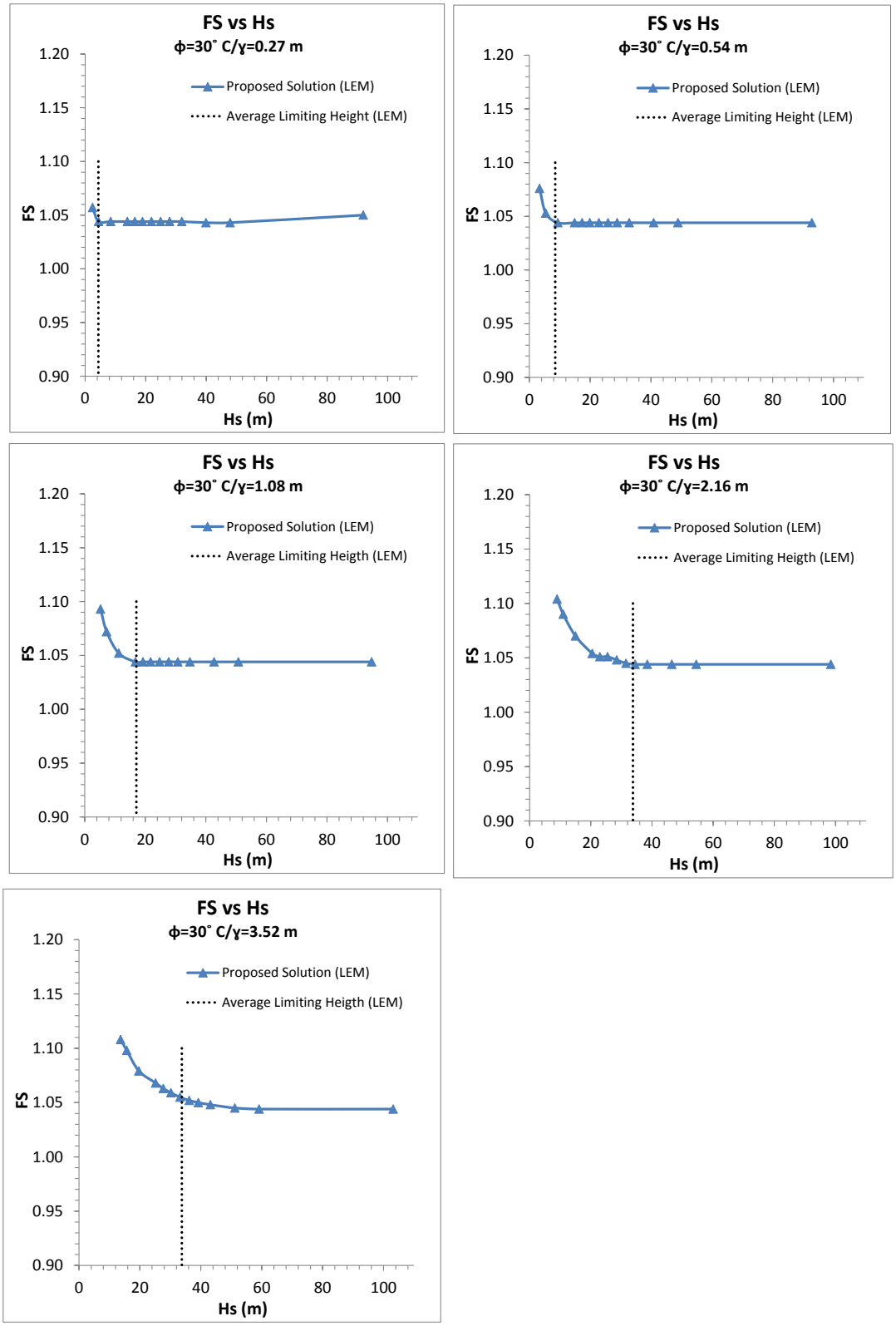

Figure 6-11 Factor of safety (FS) vs Slope Height (Hs) and Limiting Height (h_L) for $\phi = 30^o$, $c/\gamma = 0.27, 0.54,\ 1.08, 2.16, 3.52\ m$. LEM analysis.

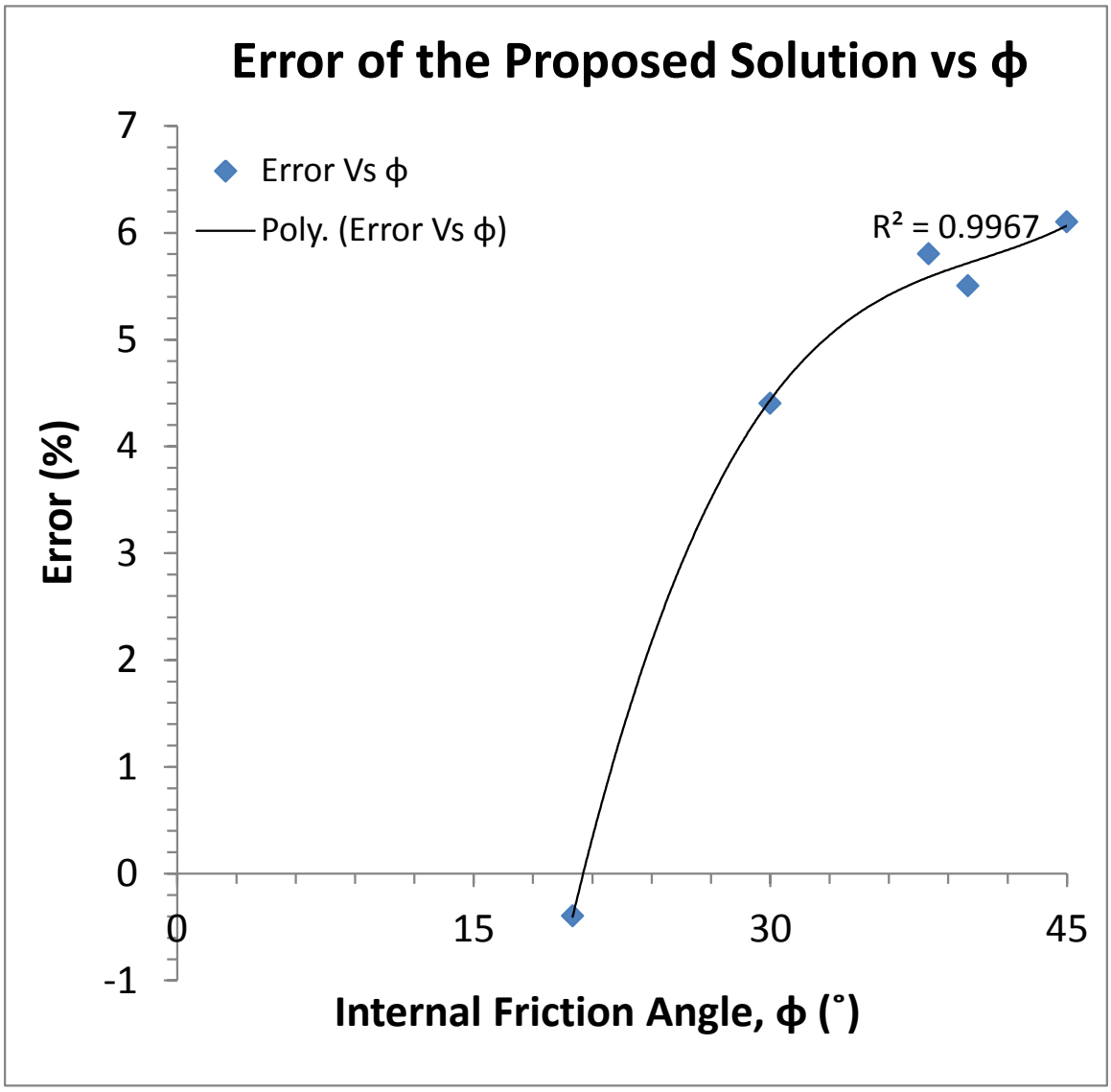

Figure 6-12 Estimated error of the proposed solution vs the internal friction angle, when $H \geq h_L$.

Convergence problems were found in some of the LEM analysis, especially for some models when the difference between ϕ and c/γ becomes large. For instance, the case when $\phi = 45^o$ and c/$\gamma = 0.27\ m$ showed FSs 3.6% higher than the steady value for slope heights over 28 m. Naturally, the critical slip surfaces found in these analyses differ from those at the steady condition, and therefore were excluded from the calculation of the mean h_L value. In LEM analyses, the shape of the failure surface is assumed and it does not run naturally as in the FEM analyses. In the case of the Simplified Bishop's method, a circular failure is assumed and consequently more than one surface can be the most critical. Hence, the necessity of averaging the h_L values obtained at each height stage of the critical slope shape, since they sometimes differ from one and other.

Since a specific value of ϕ and c/γ describes a unique curved slope contour and a unique average h_L associated with it, h_L has to be a function of the soil properties. Figure 6-13 shows that the relationship between the average h_L and c/γ is linear but varies slightly with internal friction angle. Neglecting any

computational errors, a linear regression of the complete h_L vs. c/γ data set was conducted. The control variable x was selected as c/γ, and the y variable to be averaged was selected as h_L since it has the higher variability on it. Over 99% of the variability can be explained by the model which numerically shows the appropriateness of a linear regression in this case. Eq. 6-60 shows the expression obtained from this linear regression model. This equation was introduced in the design procedure of concave slopes in Chapter 5 to investigate the most likely failure mechanism of a concave slope. It was also employed to have an estimation of the location of the most critical failure surface.

$$h_L = 15.8\,\frac{c}{\gamma} + 0.3 \qquad (6\text{-}60)$$

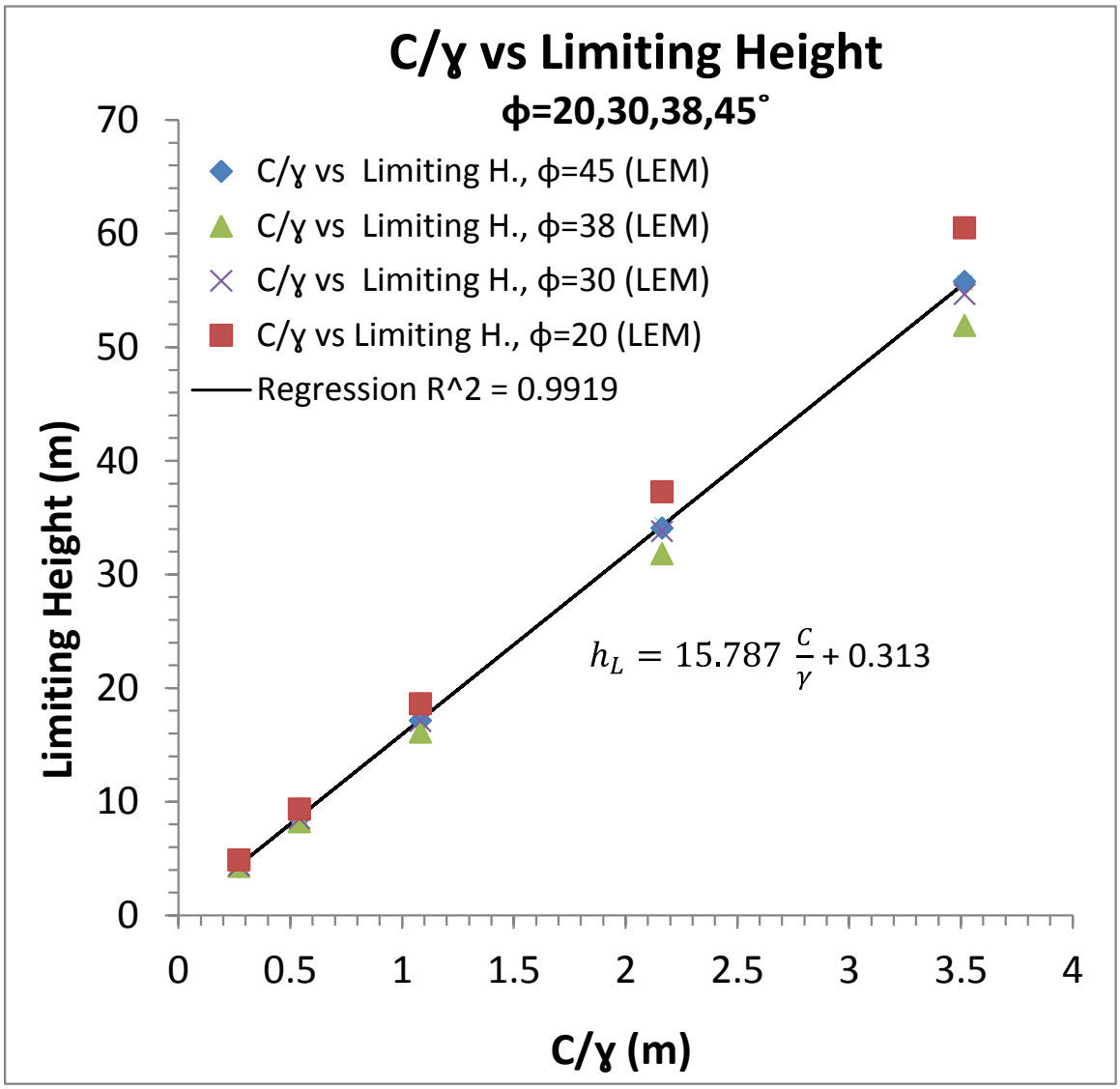

Figure 6-13 Relationship of the limiting height h_L vs c/γ

Conclusions

Sokolovski (1960), observed that the slope profile at limiting equilibrium or imminent failure (FS = 1) is concave and its profile can be mathematically described as a function of ϕ, c and γ. Unfortunately, the results of his numerical solution for the slope contour are restricted to specific values of ϕ. Also, the geometrical extension of the problem is limited by c/γ, making its implementation difficult in practice.

In searching for a simplified solution of this problem, the theory of critical equilibrium of a soil medium developed by Sokolovski (1960) was explored and an approximate solution in the form of an analytical expression for the problem of the slope at the critical state was proposed. Although the proposed solution is approximate, it shows good agreement with the available results reported by Sokolovski (1960), in terms of geometry, fundamental failure mechanisms, and obtained factors of safety.

The proposed solution revealed the existence of limiting slope height (h_L), for which the failure mechanism usually changes from a face to a toe failure. It was observed that when $Hs < h_L$, the proposed expression yields values of FS that are slightly higher than 1 and $1 \pm error$ for $Hs > h_L$. The limiting height was found to be an approximated function of c/γ. The error was observed to be a consequence of the approximate solution and a function of ϕ. However, the magnitude of errors associated with internal friction angles usually found in practice is small.

References:

Hill, R. (1950). *The mathematical theory of plasticity*, Clarendon Press, Oxford,.

Holtz, R. D., and Kovacs, W. D. (1981). *An introduction to geotechnical engineering*, Prentice-Hall, Englewood Cliffs, N.J.

Lambe, T. W., and Whitman, R. V. (1969). *Soil mechanics*, Wiley, New York.

Malvern, L. E. (1969). *Introduction to the mechanics of a continuous medium*, Prentice-Hall, Englewood Cliffs, N.J.,.

Perloff, W. H., and Baron, W. (1976). *Soil mechanics : principles and applications*, Ronald Press Co., New York.

Rocscience Inc. (2011). "Phase2." *Finite Elements software*, Rocscience Inc., Toronto, Canada.

Rocscience Inc. (2011). "Slide." *Slope Stability Software*, Rocscience Inc., Toronto, Canada.

Scott, R. F. (1963). *Principles of soil mechanics*, Addison-Wesley Pub. Co., Reading, Mass.,.

Sokolovski, V. V. (1960). *Statics of Soil Media*, Butterworths Scientific Publications.

Sokolovskii, V. V. (1965). *Statics of granular media*, Pergamon Press, Oxford; New York.

Yang, C. T., and Song, C. C. (1979). "Theory of Minimum Rate of Energy Dissipation." *Journal of the Hydraulics Division*, 105(HY7), 769-784.

Chapter 7 Curve Number Hydrology for Low Compacted Steep-Sloped Reclaimed Surface Mine Lands in the Southern Appalachian Region

Note: This chapter is under preparation as a manuscript to be submitted to the *ASCE Journal of Hydrologic Engineering* "Curve Number Hydrology for Low Compacted Steep-Sloped Reclaimed Surface Mine Lands in the Southern Appalachian Region"

Abstract

Establishment of native forest cover on reclaimed surfaces has recently become a priority directive of the US Department of Interior, Office of Surface Mining. Traditional construction methods have utilized compaction of the surface materials to assure more stable slopes and reduce erosion. However, these highly compacted surface soils are an obstacle with respect to root penetration. Consequently, the lower level of compaction as part of the Forestry Reclamation Approach (FRA) has become more prevalent in reclamation. Investigating the hydrology of these new reclaimed surfaces is vital for design of runoff and sediment control structures and understanding future hydrologic consequences. Engineers traditionally use the runoff curve number method to predict rainfall-runoff relationships for un-gauged disturbed watersheds, but the CN values typically assumed for these reclaimed mine surfaces have not been verified. Three different mining sites in the Appalachian region of east Tennessee were monitored during a year period for hydrograph parameters (discharge volume, peak discharge), and different methods were used to identify CN value for low compacted reclaimed surfaces. A new relationship was developed between the CN and the maximum 30 minute rainfall intensities. Results using this relationship found CN values ranging between 58.5 ~ 60.0, observing standard asymptotic behavior. Further, it is shown that there are no significant differences between CN values among three sites. This suggests that these CN values may have wide application for other sites in the southern Appalachian coal fields.

Introduction

The Surface Mining Control and Reclamation Act of 1977 (SMCRA), regulated by the US Department of Interior, Office of Surface Mining (OSM), requires that after active surface mining has been completed, all disturbed areas resulted from the mining operation must be reclaimed (U.S. Dept. of Interior, 1977). Mine reclamation activities have traditionally relied on the establishment of grass cover. However recently, the establishment of native forests on reclaimed sites has become an OSM priority under the Appalachian Reforestation Reclamation Initiative (ARRI) utilizing the Forestry Reclamation Approach (FRA). Prior to the FRA, establishment of forests in reclaimed mine lands had been difficult primarily due to construction techniques that focus on landform stability and erosion control, resulting in high levels of soil compaction with aggressive grass covers. This traditional reclamation approach results in a soil with poor growth properties and moisture competition with grasses limiting tree survival. To improve survival and growth of native forests on these reclaimed mine lands, the FRA recommends a lower level of compaction. Increasing slope gradient enables mine operators to store the same amount of spoil in place as before, but with lower level of compaction. While the FRA approach has been reported to be

effective on test plots utilizing low gradient slopes (3-10%), in which others observed 100% infiltration into the spoil material (Graves et al. 2000, Taylor et al. 2008), hydrological performance on slopes in the range of 25% to 35% has not been tested (Hoomehr et al., 2010). Understanding the hydrologic characteristic and impact of the FRA is vital for design of runoff and sediment control structures on reclaimed mine lands and it is also useful in predicting probable hydrologic consequences.

A common modeling tool for estimating runoff hydrology is the curve number (CN) method developed by the Soil Conservation Service (SCS). While the CN method usage was primarily for agricultural and urbanization practices, it also has been used on mine lands as well (Haan and Barfield,1981; Ritter et al., 1991; Schroeder, 1994; Camorani et al., 2005; Taylor et al., 2008). CN selection for watersheds is typically based on: 1) agricultural CN values using pre-mine soil classifications and post-mine land treatments; 2) calibrated CN values based on rainfall-runoff data from watersheds disturbed by surface mining and reclamation; or 3) simulated CN values from rainfall infilterometer tests on reclaimed-mine spoils. A major problem associated with the using CN method for surface-mine permitting and reclamation design is the limited data available for adequate calibration of CNs from watersheds disturbed by surface mining (Ritter et al., 1991).

CN values for reclaimed mine sites has been estimated by others, but do not represent values for FRA reclaimed mine lands. A median CN was estimated for reclaimed surfaces at a coal mining site in central Pennsylvania by Ritter et al. (1991). They monitored precipitation and resulting runoff to directly estimate CN value from natural data. Schroeder et al. (1994) applied simulated rainfall to 40 plots of reclaimed mine lands with different characteristics. Bonta et al. (1997) investigated effect of mining and reclamation on three small watersheds in Ohio. All of the mentioned studies were performed on reclaimed mine sites with high level of compaction. On the other hand, Taylor et al. (2008) reported CN values for loose-dumped spoil in the Cumberland Plateau of eastern Kentucky. Their study showed a wide range of CNs associated to study sites but no further investigation was made to estimate a unique, precipitation independent CN value for those sites. Estimating a precipitation independent CN value (P-independent CN) is important since it can be more usable in practice to estimate runoff leaving low compacted reclaimed sites, and also in designing sediment control basins and other best management practices (BMPs) for managing runoff and sediment leaving mine lands.

The overall project goal was to evaluate the potential impact of low compaction reclamation approach on hydrology, erosion, and sediment yield. The objective of this study, as presented in this chapter is to estimate a unique CN value for low compacted reclaimed surfaces, which can be practically usable to model runoff and help engineers design sediment control basins and stormwater BMPs. Also, this study evaluated new relationship between the CN and the maximum 30 minutes rainfall intensities based on the asymptotic method in order to estimate the best unique CN from field data collected from three sites in the southern Appalachian range in East Tennessee.

Methods

Study site locations

The study site locations are described in Chapter 2, and include the Premium mine site located in Anderson County 34 miles north of Knoxville; National site located in Campbell County 54 miles north of Knoxville; and Mountainside site located in Claiborne County 74 miles north of Knoxville at Jellico Mountains, near the Kentucky boarder.

The National Climatic Data Center divides each state into climate divisions and based on that these sites are located in the 1st climate division of TN. Average annual precipitation recorded over 30 years at these areas is around 122.5 cm (1225 mm) and typically the temperature range is between 0.0 and 33°C (NOAA 2010).

Weather, runoff volumes and sediment data collection

Each of the three sites was equipped with a full weather station. Per study site, four plots were equipped with an H-flume and Pinson et al. (2004) runoff collection devices (Figure 2-10). A detailed description of the field equipment to measure weather, runoff volumes, and sediment erosion is in Chapter 2.

SCS-CN method

The Curve Number method was developed by the U.S.D.A. Soil Conservation Service, or "SCS" (now the National Resources Conservation Service, or "NRCS"). It is an empirical method used to estimate storm runoff volume from rainfall events, and is fully described in Section 4 of the National Engineering Handbook, NEH-4 (Soil Conservation Service, 1972). Briefly, the fundamental relationships of method are,

$$Q = \frac{(P - I_a)^2}{(P - I_a) + S} \quad \text{for } P \geq I_a \tag{7-1}$$

$$Q = 0 \quad \text{for } P \leq I_a \tag{7-2}$$

$$I_a = \lambda S \tag{7-3}$$

The variable Q is the direct storm runoff volume, P is the storm rainfall, I_a is the initial abstraction, λ is the initial abstraction coefficient, and S is the storage or potential maximum retention variable. Units are in millimeters. While, λ can be variable in range of 0.01 to 0.18 (Schneider et al. 2005), the value of 0.2 is commonly used for initial abstraction coefficient based on agricultural land experiments. The λ values vary from event to event and location to location, but most of λ values have been found to be less than the traditional value of 0.20 used by practitioners. Under recent review of this value, a λ=0.05 has been reported as more accurate for general applications for disturbed land cover (Hawkins et al. 2002; Hawkins et al. 2009). The variable S can be empirically determined in terms of CN as,

$$S = \frac{25400}{CN} - 254 \tag{7-4}$$

By having P and Q data, the variable S can be determined by (Hawkins 1973),

$$S = [P + 2Q - (4Q^2 + 5PQ)^{0.5}] \tag{7-5}$$

The CN can vary from 0 to 100 while S varies from 0 to ∞. CN mainly depends on the soil, cover and hydrologic condition of the land surface. CN of 100 shows maximum possible runoff potential. CN values are typically given for three Antecedent Moisture Conditions, AMCs: dry condition, AMC I, average condition, AMC II and wet condition, AMC III. In this study AMC II was assumed.

In this study, P was measured from the weather station data, and Q was measured from the Pinson et al. (2004) runoff-sediment collection device. Knowing P and Q, and assuming a λ, a CN can be computed. CN were computed per storm event averaged per four plots for each study site. Computations of CN utilized λ, values of both 0.05 and 0.2 for comparison. An estimate for λ was attempted, but required the time of concentration (the time from the start of the rainfall event to the time runoff reaches the flume). The time of concentration was always less than 5 minutes, the interval the data logger was set for the H-flume TFLI and precipitation, and therefore an exact time was not obtained. The use of a λ of 0.05 and 0.2 is acceptable standard practice.

Results and Discussion

Hydrologic Data

Totally, 60 sampling measurements were collected from June 2009 to July 2010, in which 6 measurements were deemed outliers (3 Standard deviations or more distance from mean). Descriptions of 54 rainfall event measurements from three study sites, and used to estimate CN on low compacted reclaimed surfaces are summarized in Table 7-3.

Table 7-3 Summary of rainfall events including date, cumulative volume (mm), duration (hr), and maximum 5-min intensity for the Premium, National, and Mountainside study sites.

No.	Site	Sampling Date	Cum. Rainfall Depth, (mm)	Cum. Rainfall Duration,(hr)	Max 5 min. Intensity, (mm/hr)
1		June 24, 2009	38.1	17.5	31.5
2		July 17, 2009	127.3	44.9	75.0
3		August 3, 2009	106.1	48.0	39.0
4		August 13, 2009	20.8	5.6	37.5
5		August 24, 2009	75.9	28.0	82.5
6		September 22,	162.9	99.0	67.5
7		October 1, 2009	96.0	25.0	79.5
8		October 13, 2009	60.3	51.8	40.5
9	Premium	October 20, 2009	73.4	48.2	19.5
10		October 27, 2009	37.3	21.5	18.0
11		November 3,	14.6	17.8	9.0
12		November 24,	49.8	43.8	10.5
13		December 3,	39.3	30.8	27.0
14		December 17,	139.8	31.3	42.0
15		March 24, 2010	50.625	32.3	22.5
16		May 7, 2010	131.5	64.4	105.0
17		May 18, 2010	27.375	4.4	43.5
18		June 8, 2010	60.625	14.2	54.0
19		June 25, 2010	29.125	5.4	31.5
20		July 20, 2010	79.125	17.8	52.5

Table 7-3. (continued) Characteristic of rainfall events {needs formatting –JSS}

No.	Site	Sampling Date	Cum. Rainfall Depth, (mm)	Cum. Rainfall Duration,(hr)	Max 5 min. Intensity,
21	National	June 25. 2009	96.1	12.8	114.0
22		July 15, 2009	72.6	11.0	100.4
23		August 14, 2009	47.6	11.0	111.0
24		September 25,	138.8	104.4	43.5
25		September 29,	49.5	14.9	36.0
26		October 8, 2009	41.3	33.5	45.0
27		October 22, 2009	106.3	94.6	81.0
28		October 29, 2009	22.1	15.3	9.0
29		November 5,	31.3	16.8	21.0
30		November 12,	16.9	13.6	7.5
31		December 1,	44.9	35.6	16.5
32		December 14,	130.6	52.7	33.0
33		March 19, 2010	42.75	21.1	19.5
34		April 13, 2010	72.25	26.1	52.5
35		May 7, 2010	193	59.7	49.5
36		May 19, 2010	41	5.8	111.0
37		June 23, 2010	79.5	14.5	87.0
38		June 29, 2010	28.5	4.3	72.0
39		July 16, 2010	93.245	10.4	109.4
40	Mountain Side	July 2, 2009	132.8	3.6	54.4
41		July 14, 2009	62.6	21.9	75.6
42		July 27, 2009	214.0	28.8	101.3
43		September 22,	120.7	75.8	86.2
44		October 13, 2009	59.6	33.8	65.0
45		October 20, 2009	51.7	70.6	33.3
46		November 3,	36.0	21.3	13.6
47		December 1,	18.1	14.6	10.6
48		December 10,	99.3	35.3	24.2
49		December 14,	35.0	8.8	10.6
50		March 26, 2010	77.1	37.1	54.4
51		May 13, 2010	242.6	57.3	66.5
52		May 18, 2010	47.5	7.3	98.3
53		June 8, 2010	52.7	7.8	83.2
54		June 25, 2010	50.5	6.8	133.1

These data in Table 7.3 were also used to investigate effect of rainfall depth and rainfall intensity on the CN values. The cumulative rainfall duration for a sampling event varied from 3.6 to 104.4 hr, the cumulative rainfall depth varied from 14.6 mm (0.57 in) to 242.6 mm (9.55 in) with the average 75.34 mm (2.966 in), and rainfall intensity (during five minutes) varied from 7.5 mm/hr (0.3 in/hr) to 133.1 mm/hr (5.24 in/hr) with the average 54.0 mm/hr (2.126 in/hr). Study sites experienced different storm characteristics varing in rainfall depth, duration and intensity during the one year monitoring period, providing enough data diversity for this study. Because high intensity and short duration storms occurred during spring and summer 2009, rainfall intensities during five minute intervals were calculated to better characterize event intensity. Monitoring of sites was not possible during winter (January, February) due to high altitude and below freezing temperatures, which prevented road access to the study sites and froze water in sampling buckets.

Initial Abstraction Factor (λ) and CN

The initial abstraction factor (λ) can vary from 0.01 to 0.18 according to Schneider and McCuen (2005), while a value of 0.2 is commonly used in practice. However, recent studies suggest that the initial abstraction factor of 0.05 results in more accurate estimates of modeled runoff (Hawkins et al., 2002). In our study, curve numbers were calculated based on both λ = 0.05 and 0.2. Curve number values calculated for three different sites and two λ values using rainfall-runoff data are shown in Table 7-4. The computed values show that λ = 0.05 generates lower CN values than when a λ = 0.2 was used, however using λ = 0.05 caused higher variation in CN values. Differences between runoff values, predicted using λ = 0.2 and 0.05 decreases at higher curve numbers, which was also observed by Hawkins et al. (2002).

Using λ = 0.2, the CN values for the Premium site ranged from 30.71 to 98.84 with a mean of 76.28 and standard deviation (STD) of 19.54 (Table 7-4). CN values for the National site ranged from 40.48 to 97.8 with a mean of 76.02 and STD of 19.02. CN values for the Mountainside site ranged from 34 to 89.5 with a mean of 70.55 and STD of 13.54. CN values were also calculated for the λ = 0.05, and presented in Table 7-4.

Table 7-4 Rainfall depth and 30-min intensity, runoff depth, soil antecedent moisture conditions, and curve numbers per event date and study sites at Premium, National, and Mountainside.

Date	D (mm)	$I_{30,\ max}$ (mm/hr)	Q (mm)	AMC	CN λ = 0.2	CN λ = 0.05
			Premium			
June 24, 2009	38.1	13.5	34.8	III	98.8	98.6
July 17, 2009	127.3	51.5	28.8	II	57.4	44.3
August 3, 2009	106.1	21.5	46.7	II	75.5	68.8
August 13, 2009	20.8	10.0	11.1	III	95.5	94.1
August 24, 2009	75.9	34.2	16.5	II	68.7	56.2
September 22, 2009	162.9	31.0	3.8	I	30.7	13.4
October 1, 2009	96.0	44.5	53.3	II	83.0	78.8
October 13, 2009	60.3	23.2	24.6	II	83.1	77.5
October 20, 2009	73.4	11.2	12.9	I	66.4	52.0
October 27, 2009	37.3	8.7	0.6	II	64.9	38.1
November 3, 2009	14.6	5.7	3.6	III	92.6	88.4
November 24, 2009	49.8	5.5	1.8	III	96.3	37.6
December 3, 2009	39.3	8.2	2.7	II	70.7	50.9
December 17, 2009	139.8	19.7	14.1	I	44.0	27.1
March 24, 2010	50.625	16.0	42.5	III	97.1	96.5
May 7, 2010	131.5	22.7	24.6	I	53.4	39.1
May 18, 2010	27.375	20.0	14.0	III	93.7	91.8
June 8, 2010	60.625	32.5	53.4	III	97.5	97.0
June 25, 2010	29.125	13.2	6.6	II	85.5	77.7
July 20, 2010	79.125	23.0	21.0	II	71.0	60.3
				Mean ± SD	*76.28 ± 19.5*	*67.3 ± 26.2*

			National			
June 25, 2009	96.1	40.5	19.7	II	62.5	48.9
July 15, 2009	72.6	51.5	16.0	II	69.8	57.6
August 14, 2009	47.6	37.0	34.0	III	94.7	93.5
September 25, 2009	138.8	30.2	21.0	I	48.9	33.6
September 29, 2009	49.5	17.5	32.7	III	93.3	91.7
October 8, 2009	41.3	20.2	14.3	II	85.7	80.1
October 22, 2009	106.3	37.5	15.1	II	54.8	38.6
October 29, 2009	22.1	4.2	1.2	II	79.8	61.6

Table 7-4. (continue) Rainfall events and curve numbers

Date	D (mm)	$I_{30,\ max}$ (mm/hr)	Q (mm)	AMC	CN λ = 0.2	CN λ = 0.05
			National			
November 5, 2009	31.3	10.5	4.2	II	80.1	67.3
November 12, 2009	16.9	6.5	1.84	II	87.0	76.4
December 1, 2009	44.9	11.7	1.81	II	64.4	41.0
December 14, 2009	130.6	12.0	7.3	I	40.5	21.8
March 19, 2010	42.75	12.2	33.5	III	96.5	95.8
April 13, 2010	72.25	21.7	46.4	III	89.8	87.4
May 7, 2010	193	24.0	36.9	I	44.2	30.9
May 19, 2010	41	41.2	34.8	III	97.8	97.4
June 23, 2010	79.5	20.2	16.7	II	67.1	54.2
June 29, 2010	28.5	17.2	11.8	III	91.4	88.2
July 16, 2010	93.245	33.5	82.0	III	96.1	95.5
				Mean ± SD	*76.0 ± 19.0*	*66.4 ± 25.3*
			Mountain Side			
July 2, 2009	132.8	16.4	64.8	II	74.0	67.7
July 14, 2009	62.6	48.1	13.5	II	72.5	60.7
July 27, 2009	214.0	62.0	21.8	I	34.0	19.6
September 22, 2009	120.7	35.3	39.3	II	65.8	55.8
October 13, 2009	59.6	33.0	4.3	II	61.8	41.3
October 20, 2009	51.7	13.4	1.9	II	60.7	36.8
November 3, 2009	36.0	9.3	11.8	III	86.6	81.0
December 1, 2009	18.1	7.3	0.8	II	82.3	64.8
December 10, 2009	99.3	11.6	48.5	II	79.2	73.7
December 14, 2009	35.0	9.3	6.2	II	80.7	69.8
March 26, 2010	77.1	15.9	22.3	II	72.9	63.1
May 13, 2010	242.6	36.8	125.3	II	63.1	56.0
May 18, 2010	47.5	40.6	4.6	II	69.5	51.7
June 8, 2010	52.7	39.3	28.5	III	89.5	86.6
June 25, 2010	50.5	40.8	3.7	II	65.7	69.8
				Mean ± SD	*70.5 ± 15.0*	*59.9 ± 17.4*

The rainfall-runoff data and curves for CN values of 99, 72, and 30 are shown in Figure 7-4, and each data point relates to soil antecedent moisture conditions (AMC) I, II, and III. CN selections for AMC I, II, and III were based on the method that the CN for AMC I is the lower enveloping CN; for AMC II, the

median CN; and for AMC III, the upper enveloping CN (Rallison and Cronshey 1979, Ritter and Gardner 1991). Figures 7-5 and 7-6 show CN distributions in relation to precipitation depth for each study site. It is apparent that CN is not independent of rainfall depth and events with greater depths tend to have lower CN values, while there was a vivid bias to high CN values at smaller rainfall events (this phenomenon is discussed more in next section below). Both Figures 7-5 and 7-6 show that all three sites had almost the same response to rainfall events. Using t-test, the hypothesis that the CN means for three study sites are statistically equal was confirmed with the 95% confidence level. In Figure 7-7 all CN values of three sites were combined and plotted against their corresponding rainfall depths. Generally, Using $\lambda = 0.2$ in the CN calculations, results showed less scatter when a $\lambda = 0.05$ was used. This observation can be attributed to magnifying effect of maximum potential retention or storage (S) in Eq. (5) on the CN values.

CN and Rainfall Depth

A strong negative correlation exists between CN and rainfall depth ($r = 0.77$, $p = 0.05$). There is vivid bias for high CNs at small rainfall depths. Also, results show that rainfall events with higher volumes tend to result in lower CN values. This phenomenon was first observed and demonstrated by Sneller (1985) and then noted by Hawkins (1993) and Hjelmfelt (1996). It may be attributed to a combination of data censoring, hydrologic partial area effects, and model or data errors. Data censoring results from the common practice of excluding from the data sets all rainfall events without direct runoff, thus assuring $P \geq 0.2S$, and $100/(1+P/2) < CN < 100$. On the other hand, to the extent that any CNs are manifested at low rainfalls (for which there are many storms), they would –by definition- define high CNs (Hawkins et al., 2009). Figure 7-8 shows the frequency of CNs ($\lambda = 0.2$, $\lambda = 0.05$) combining results from all three study sites, within 14 sub-groups. A CN frequency distribution for $\lambda = 0.2$ showed almost a uniform distribution except for low CN values, while $\lambda = 0.05$ showed a higher tendency toward middle and high CN values. CN values for $\lambda = 0.2$ are higher than 51 for 78% of the total data, while for $\lambda = 0.05$, CN values are higher than 61 for 81% of the total data, with the maximum number between CNs 61 and 65. Knowing that $\lambda = 0.05$ has more consistency, the CN value for the low compacted reclaimed coal mining sites was found to be above 50 with a greater tendency toward a CN of 60. In order to find a unique CN value for low compacted reclaimed surfaces, a asymptotic method was used and results described below in the next section.

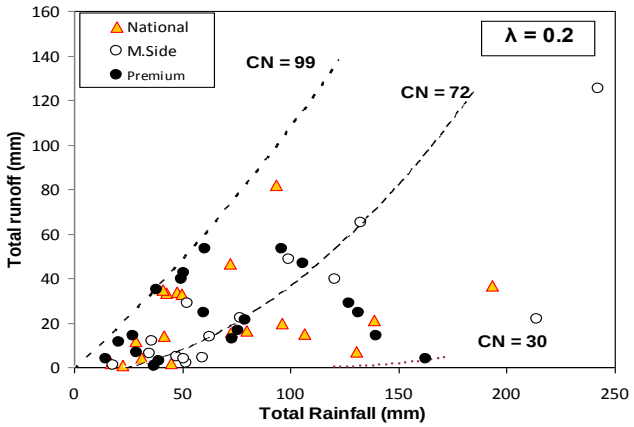

Figure 7-4 Observed rainfall – runoff events from plots and median AMC II CN (CN=70) and enveloping CNs for AMC I and III.

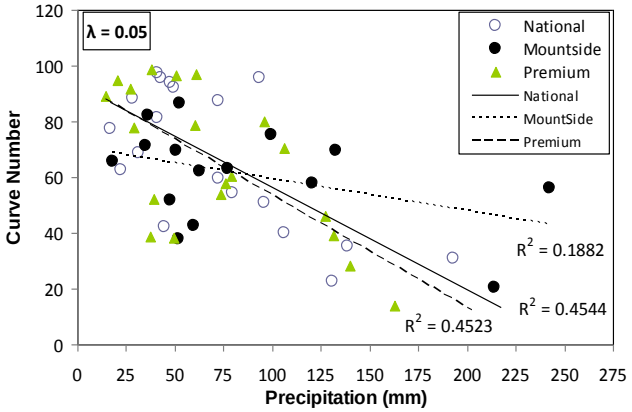

Figure 7-6 Curve numbers for each three sites in relation to precipitation amounts for λ = 0.05.

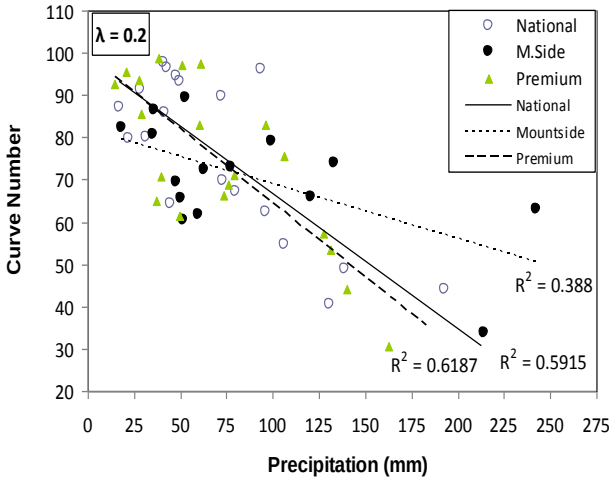

Figure 7-5 Curve numbers for each three sites in relation to precipitation amounts for λ = 0.2.

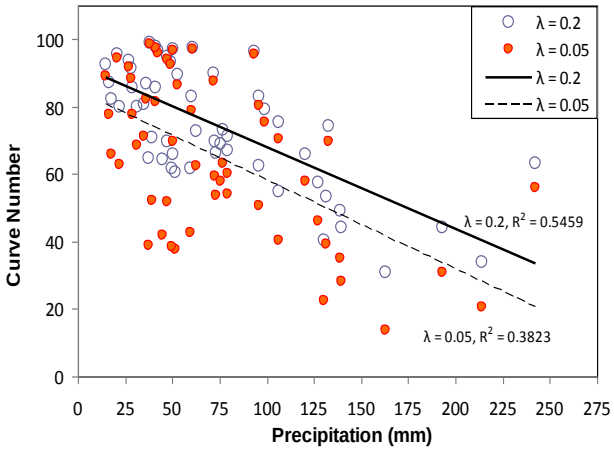

Figure 7-7 CN from all three sites in relation to precipitation amounts for λ = 0.2 and 0.05

Asymptotic Method for CN Estimates

The asymptotic method, a frequency matching method is based on equating rainfall and runoff events' return period. If the constant CN is not apparent but there is a recognizable partial trend toward a steady state condition, then asymptotic least square fitting may be completed to extend the trend to an equilibrium value (Hawkins et al., 2009). The rainfall depths and the runoff depths were sorted separately and then realigned on a ranked-order basis to form P-Q pairs of equal return periods. The individual runoffs may not necessarily be associated with the original causative rainfalls (Hawkins et al., 1993). After calculating CNs based on asymptotic method a secondary relationship between CN and rainfall depth emerges. Watersheds can be categorized into three groups based on these secondary relationships. These categories are (i) watersheds with complacent behavior, (ii) watersheds with standard response and (iii) watersheds with violent responses. Detail descriptions for each of these categories can be found in Hawkins et al. (1993).

In Figure 7-9, CNs obtained from original (unmatched) rainfall-runoff data were compared with CNs calculated using frequency matched rainfall-runoff data. The size of each data point bubble is scaled based on its correspondent rainfall intensity. A larger bubble size shows higher intensities of storm rainfall events. and vice versa. This figure also shows that after frequencies matched, a standard asymptotic response emerged. In addition, Figure 7-9 illustrated that this frequency match method considerably reduced CN estimate variation. CNs calculated using frequency matched rainfall-runoff data was more correlated (R^2 = 0.88) than when CNs were obtained from unmatched frequencies(R^2 = 0.52). A standard asymptotic relationship occurs when there is a tendency for CNs to decline, and then CNs converge onto a constant value with increasing P. A constant value defines a P-independent CN, and expressed by the following equation:

$$CN(P) = CN_{\infty} + (100 - CN_{\infty})\exp(-K_1 P) \qquad (7\text{-}6)$$

A CN can be found to fit *P-CN* data sets, where CN_{∞}= constant value approach as *P*→∞*;* and *K* = fitting constant. Although this is entirely a curve-fitting approach, it has been found to be appropriate for a wide array of watershed datasets. The variable CN_{∞} is the CN that characterizes runoff from the dataset for large rainfall events (Hawkins et al, 1993).

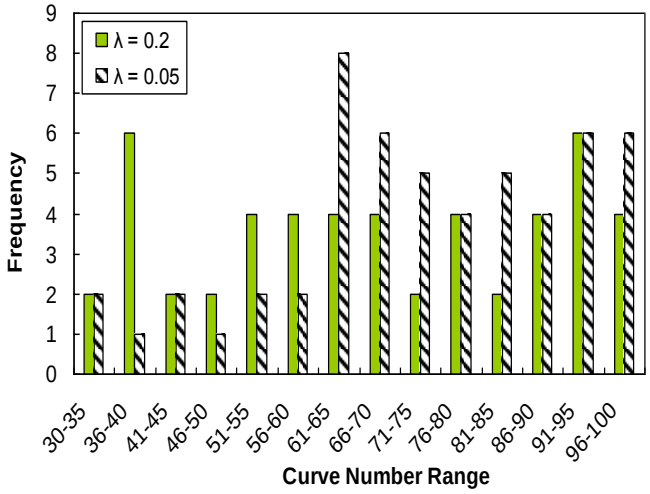

Figure 7-8 Distribution of curve numbers for all sites.

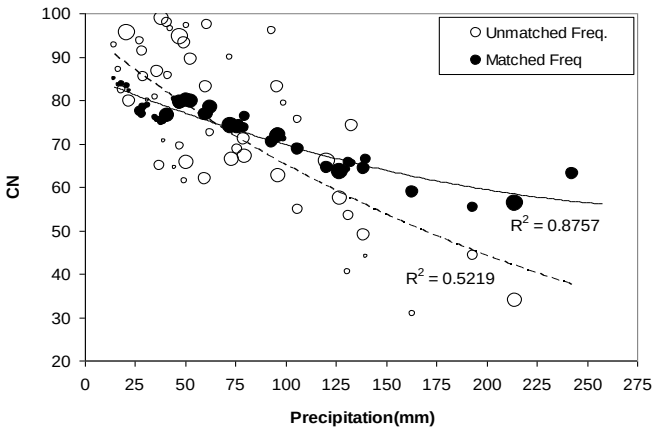

Figure 7-9 Original CN compared with ones obtained from matched frequency methods.

$$CN(P) = CN_{\infty} + (100 - CN_{\infty})\exp(-K_1 P)CN_{\infty}CN_{\infty}$$

CN and P-Q Freq. Match

Obtained from frequency matched rainfall-runoff data for CN data points (for λ = 0.2), the best fitted exponential curve is shown in Figure 7-10.. The equation for the fitted curve is as follows:

$$CN(P) = 58.5 + (100 - 58.5)\exp(-0.02253\,P) \qquad (7\text{-}7)$$

Using this equation the CN_{∞} was equal to 58.5, which is the P-independent CN value for the low compacted reclaimed surfaces at study sites (R^2=0.80). This result is consistent to previously presented results generated from CN frequency distribution plot in Figure 7-8. In general, these results suggest that the CN is above 50, and tends more towards a CN of 60.

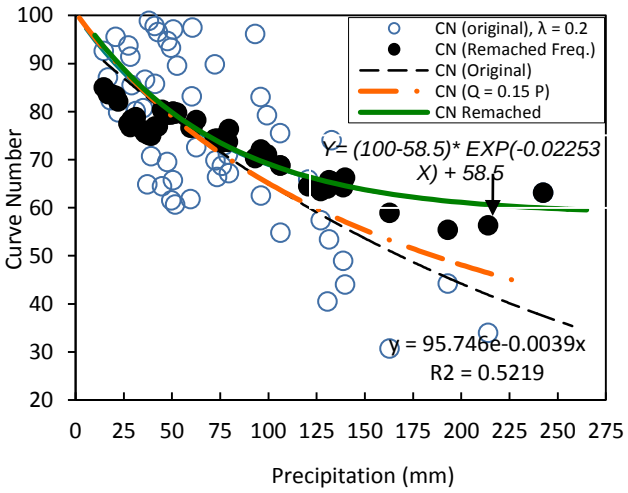

Figure 7-10 Best fitted exponential curve for P-Q re-matched frequency pairs and λ = 0.2.

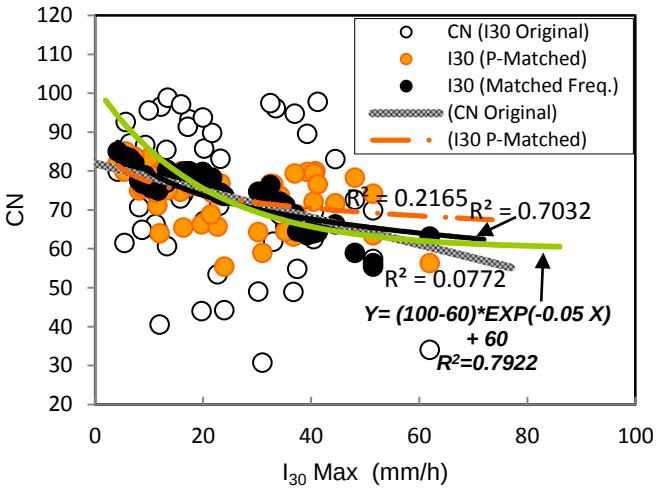

Figure 7-11 Best fitted exponential curve for I_{30} –Q re-matched frequency pairs and λ = 0.2.

CN and I30 -Q Freq. Match

Although the CN P-Q frequency match methodology provides a good estimate for a CN value with a standard asymptotic response, it does not consider rainfall distribution effects on estimating the CN value. In other words, the p-Q frequency match method assumes that rainfall amount is evenly distributed over the event duration. To incorporate the effects of varying rainfall distributions over time in estimating an independent CN, the same frequency match method was used but this time using the maximum 30 minute rainfall intensity (I_{30}) instead of rainfall depth. This analysis was done in two ways: 1) replacing sorted rainfall depths (P), which were used in original method, with their correspondent I_{30} ; and 2) sorting separately the rainfall I_{30}s and the runoff depths, then realigning them on a ranked-order basis to form I_{30}-Q pairs of equal return periods. The individual runoff measurements were not necessarily associated with the original causative rainfall I_{30} values.

Results of the I_{30}-Q Freq. Match method for estimating CNs are shown in Figure 7-11. The second approach using this method, as described above, resulted in less variation in calculated CN values compared with results from the first approach, therefore the curve fitting was accomplished using the second approach. Recall, this second approach is sorting separately the rainfall I_{30}s and the runoff depths. The curve fitting was done by following the same format as in Equation 6, and is shown as follows:

$$CN(P) = 60 + (100 - 60)\exp(-0.05\,P) \quad (7\text{-}8)$$

The CN_∞ was estimated as 60 using this approach (R^2=0.79). The P-independent CN value obtained from I_{30}-Q pairs frequency match data) was similar to what estimated by the curve fitting of CNs calculated based on P-Q frequency match data. Figure 7-11 also shows the reduction in CN variation by both approaches used in frequency match methods.

Conclusions

This study showed that the original CN values estimated for three different study sites were statistically similar, and the effects of spatial variation in rainfall distributions and different reclaimed spoil material on CN values were not significant. Results estimate CN values between 58.5 and 60 for the low compacted reclaimed surfaces in the east Tennessee Appalachian region as generated by the P-Q and I_{30}-Q Frequency Match approaches. Both approaches suggest a standard asymptotic behavior for the study sites generating common CN values. In comparison, CN estimates using a means approach found an average CN of 62.2 for a λ of 0.05, and an average CN of 72.2 for a λ of 0.20. These results can be used in practice to estimate runoff leaving low compacted reclaimed coal mining sites, and also in designing sediment control basins and stormwater BMPs.

References

Barfield, B. J., R. C. Warner, and C. T. Haan. 1981. Hydrology and Sedimentology for distributed areas. Oklahoma Technical Press, Stillwater, Oklahoma.

Camorani G., Attilio Castellarin, Armando Brath. 2005. Effects of land-use changes on the hydrologic response of reclamation systems Physics and Chemistry of the Earth. Vol. 30, pp 561–574

Graves, D.H., J.M. Ringe, M.H. Pelkki, R.J. Sweigard, and R.C. Warner. 2000. High value tree reclamation research Environmental Issues and Management of Waste in Energy and Mineral Production, Singhal, and Mehrotra, eds., Balkema, Rotterdam, pp. 413–421.

Hawkins, R. H. 1973. “Improved prediction of storm runoff in mountain watersheds.” J. Irrig. and Drain. Div., 99(4), 519–523.

Hawkins R.H., D.E. Woodward, and R. Jiang. 2002. Investigation of the runoff curve number abstraction ratio, USDA-NRCS Hydraulic Engineering Workshop, Las Vegas, NV.

Hawkins R.H., T.J. Ward, D.E. Woodward, J. A. Van Mullem. 2009. Curve Number Hydrology- State of the Practice. Publication of ASCE.

Hoomehr, S., J.S. Schwartz, W.C. Wright, and E.C. Drumm. 2010. Surface erosion and sediment yields on steep-sloped coal mining reclamation sites in the Appalachian region. in ASCE/EWRI, ed., World Water & Environmental Resources Congress: Providence, RI.

Pinson, W.T., Yoder, D.C., Buchanan, J.R., Wright, W.C., Wilkerson, J.B. 2003. Design and evaluation of an improved flow divider for sampling runoff plots. Journal of Applied Engineering in Agriculture. Vol. 20, No. 4, p433-437.

Ritter, J.B. and T.W. Gardner. 1991. Runoff curve numbers for reclaimed surface mines in Pennsylvania, J. Irrigation and Drainage Engineering. Vol. 117, pp. 656–666.

Schneider L.E. and R.H. McCuen, Statistical guidelines for curve number generation. 2005. J. Irrig. Drain Eng. Vol. 131, pp. 282–290.

Schroeder, S.A. 1994. Runoff curve number estimations for reshaped fine-textured spoils, Reclamation and Revegetation Research. Vol. 6, pp. 129–136.

Taylor T.J., Carmen T. Agouridis, Richard C. Warner and Christopher D. Barton. 2008. Runoff curve numbers for loose-dumped spoil in the Cumberland Plateau of eastern Kentucky. International Journal of Mining, Reclamation and Environment. pp. 1–17.

U.S. Department of Interior. 1977. Surface mining reclamation and enforcement provisions. Federal Register 42:62685-62688, December 13.

U.S. Soil Conservation Service. 1972. National Engineering Handbook, Section 4, Hydrology. U.S. Government Print. Office, Washington, DC.

Yoder, D.C., J.R. Buchanan, G.S. Honea, B.F. Staley, J.B. Wilkerson and R.E. Yoder. 1999. The Tennessee fluid level indicator. Appl. Engrg. in Agric. 15(1):49-52.

Chapter 8 Erodibility of Low-Compacted Steep-Sloped Reclaimed Surface Mine Lands in the Southern Appalachian Region

Note: this chapter is taken in part from a manuscript in preparation to be submitted to the *Journal of Hydrological Processes* as: Siavash Hoomehr, John S. Schwartz, Daniel C. Yoder, Wesley Wright, and Eric C. Drumm "Erodibility of Low-Compacted Steep-Sloped Reclaimed Surface Mine Lands in the Southern Appalachian Region"

Abstract

Reclamation of disturbed surfaces due to mining activities has been traditionally successful in reducing erosion by using grass cover and high level of compaction. Recent priority of the US Department of Interior, Office of Surface Mining in pursuing establishment of native forest covers on reclaimed surfaces has directed mine operators to employ lower levels of compaction to produce a better medium for tree survival by increasing root penetration. Although the FRA has been demonstrated to be effective with respect to enhancing the growth and survivability of the trees, there has been limited investigation on the effect of this technique on erosion and sediment delivery. Three coal mining sites in the Appalachian region of east Tennessee were monitored for a year to determine an appropriate value of the soil erodibility factor, K for reduced compaction reclaimed surface mine lands. This is an important parameter used in the widely accepted Revised Universal Soil Loss Equation (RUSLE) to predict erosion. Results of this study showed that the erodibility was a function of rill development, and that it changed with the time. Average K factors were estimated as 1) K = 0.30 during rill development, 2) K = 0.07 during the transition period to an equilibrium state, and 3) K =0.05 once the rills have stabilized. The particle size distribution of the delivered sediment was monitored over the study period to provide designers actual data on the particle size distribution of sediment for use in the design of sediment basins and selection of best management practices. Measurements of the temporal variation of the particle size distribution over the study period provides insight into how the sediment size distribution may change over time, leading to a better understanding of the erosion process and the development of best management practices.

Introduction

Mine land reclamation has traditionally been successful by using grass cover and high levels of compaction on steep slopes. A recently developed approach by the U.S. Department of Interior, Office of Surface Mining (OSM), focuses on growing forests with native species on reclaimed lands, called the Forest Reclamation Approach (FRA). Although high levels of compaction provides stability of slopes and reduces the amount of erosion and sediment yield from disturbed surfaces, it decreases the chance of root penetration and hinders tree survival (Graves et al., 2000; Shukla et al., 2004). To overcome this issue, the FRA is based on lower level of compaction in order to produce a better medium for tree survival (Ashby et al. 1978; Torbert and Burger 1994; Thomas et al. 1999; Graves et al. 2000), but it has only been tested on low to moderate slopes. This technique in steep slopes allows the placement of more mine waste materials and at the same time replicates the stable landforms observed in nature. While reclamation with low level of compaction is reported to be effective, there is a lack of scientific

information about its performance with respect to erosion and sediment yield under sites with steep slopes.

Research has shown creating steep slopes increases rates of soil erosion. Zhang et al. (2009) showed that sediment transport capacity increases as a power function with slope gradient. Meyer and Harmon (1989) showed that slope steepness affects erosion for more erodible soils while rills are under formation. Rills are considered as the first signs of major soil erosion. Rills begin to form when the runoff shear stress (the ability of surface runoff to detach soil particles) overcomes the soil's shear strength (the ability of soil to resist forces working parallel to the soil's surface). This begins the erosion process as water breaks soil particles free and carries them down the slope (Torri et al., 1987). The steepness of slope controls depth of the rills, while the length of slope controls their number. After rills begin forming, they are subjected to variety of other erosional forces which may increase their size and output volume. Up to 37% of erosion in a rill-filled area may derive from mass movement, or collapse, of rill sidewalls. As water flows through a rill, it will undercut into the walls, triggering collapse. Also, as water seeps into the soil of the walls, they weaken, amplifying the chance of wall collapse. The erosion created by these forces increases rill size while it also generates greater sediment yields (Govers, 1987).

One of the main factors estimating the amount of soil loss from a land is soil erodibility factor (K) as expressed in the Revised Universal Soil Loss Equation (RUSLE). The susceptibility of soil to erosion is termed erodibility. RUSLE is a revised version of Universal Soil Loss Equation (USLE) (Wischmeier and Smith, 1965, 1978), which has served as the most commonly used soil loss model for over 30 years (Toy et al., 1999). Erodibility of agricultural soils has been studied extensively over the past years (Mcintosh et al., 1993). There is limited information about erodibility of reclaimed surface mined lands, especially on low compacted and steep slope reclaimed mine lands. Most of research on erodibility has been conducted using rainfall simulation methods rather than in-situ field approaches (Gilley et al., 1977; Mitchell et al., 1983; Barfield et al., 1983; Mostaghimi and Mitchell, 1983; Stein et al., 1983). Also, those researchers who used natural rainfall events generally studied erosion on low slope gradients (3-10%) and high levels of compaction, or the studies were done on non-reclaimed spoils (Mcintosh et al., 1993; McKenzie and Studlick, 1979). Gilley et al. (1977) used rainfall simulation to study erosion characteristics of surface mined sites in western North Dakota. Their objective was to evaluate contribution of erosion on reclaimed surface mined to pollution of surface waters caused by sediment. Mcintosh et al. (1993) studied the erodibility of reconstructed mine spoils using natural rainfall events on low gradient slopes at 9 percent. In southeastern Ohio, McKenzie and Studlick (1979) used natural rainfall events to find erodibility of non-vegetated and non-reclaimed spoils, but did not use FRA (Hoomehr et al., 2010). The objective of this study was to estimate soil erodibility factor (K) for low compacted surface mine lands with steep slopes, in order to provide estimates of erosion rates. Also, particle size distributions of eroded sediment was estimated for the design of sediment control basins and choosing best management practices (BMPs) for controlling erosion on reclaimed surface mine lands.

Methods

Study site locations

The study site locations are described in Chapter 2, and include the Premium mine site located in Anderson County 34 miles north of Knoxville; National site located in Campbell County 54 miles north of Knoxville; and Mountainside site located in Claiborne County 74 miles north of Knoxville at Jellico Mountain, near the Kentucky border.

The National Climatic Data Center divides each state into climate divisions and based on that these sites are located in the 1st climate division of TN. Average annual precipitation recorded over 30 years at these areas is around 122.5 cm (1225 mm) and typically the temperature range is between 0.0 and 33°C (NOAA 2010).

Study site characterization

Site geometries, soil unit weights, shear strength parameters, and uplands soil particle size distributions were presented in Chapter 3. A hydrological analysis for estimating runoff curve number values was presented in Chapter7. These data support the erodibility analysis presented in this chapter. As described in Chapter 2, Section on Experimental Design, ground cover was not established on the four field plots per study site, therefore findings from this study represent erodibility factors for bare soil, and a geomorphic condition favorable for rill development.

Weather, runoff volumes and sediment data collection

Each of the three sites was equipped with a full weather station. Per study site, four plots were equipped with an H-flume and Pinson et al (2004) runoff collection devices (Figure 2-10). A detailed description of the field equipment to measure weather, runoff volumes, and sediment erosion is in Chapter 2.

RUSLE Soil Loss Equation

The Revised Universal Soil Loss Equation (RUSLE) was used to estimate the erodibility of reclaimed materials (SCS, 1993). RUSLE is the revised version of Universal Soil Loss Equation (USLE) equation (Wischmeier and Smith 1978), which is based on years of research on soil loss from numerous experimental field plots. Both USLE and RUSLE estimate the average annual erosion on land surfaces by the following equation:

$$A = 0.224 \cdot R \cdot K \cdot LS \cdot C \cdot P \qquad (8\text{-}1)$$

where,

A = amount of soil loss (kg/m2)
R = rainfall and runoff erosivity factor
K = soil erodibility factor, soil loss rate per erosion index unit for a specified soil as measured on a standard plot (72.6 ft and 9% slope)
LS= combined length-slope factor, for un-standard size plots
C = cover management factor
P = erosion control practice factor

Because there was no vegetative cover on study plots, the cover management factor (C) was equal to 1 (See Chapter 2, Experimental Design Section). Also no erosion control practice was utilized so P was equal to 1. The LS factor was computed based on the tabulated values in the USDA agricultural handbook number 703 (1997) for each plot length and slope. In this study, the amount of eroded sediment was measured, which is A in the RUSLE equation. The erosivity factor (R) is obtained from the onsite precipitation data, and the computational method is described in the following section. The

erodibility factor (K) was then estimated by knowing A, R, LS, C, and P variables in the RUSLE equation. The amount of erosion was averaged among the four plots within each site for each sampling event.

R- Factor

Based on USLE, soil loss is directly proportional to a rainstorm parameter, the total storm energy (E) times the maximum 30-min intensity (I_{30}). The relationship between soil loss (A) and the EI_{30} parameter is assumed to be linear, and individual parameters per storm events are directly additive. Summation of EI_{30} values for a period of storm events shows the rainfall erosive potential during that period. The Brown and Foster (1987) equation for calculating rainfall energy was used in this study:

$$e_m = 0.29\,[1 - 0.72\exp(-0.05 i_m)] \tag{8-2}$$

$$E = \sum \; e_m \times d_j \tag{8-3}$$

$$R = \frac{\sum_{i=1}^{n} EI_{30}}{N} \tag{8-4}$$

where, e_m has units of MJ.ha^{-1}.mm^{-1}of rain and i_m is rainfall intensity which has units mm . h^{-1}.

Brown and Foster (1987) stated that this equation has a finite positive value at zero intensity and approaches an asymptotic state at high intensities as a continuous function. For more information on above R factor terms, refer to Wischmeier and Smith (1978). Rainfall amount and intensity from each event were used to calculate R factor in this study as outlined in the USDA Agricultural Handbook Number 703 (1997). Storms having less than 13mm (0.5 in.) of rainfall were not used in the analysis with the only exception of rainfall events that had equal to or greater than 6 mm depth within 15 minutes (Wischmeier and Smith, 1978). Rainfall events were separated by 6 hour window lacking rainfall. The R factor data and the measured soil loss (A) were incorporated into Eq. (1) to estimate the soil erodibility (K) factor for low-compacted, mine land spoil material.

Particle Size Distributions

Eroded sediment size collected and brought back to the UT Geotechnical Engineering Laboratory was characterized by generating particle size distributions utilizing ASTM- D6913 procedures.

Results and Discussion

Table 8-1 shows measured erosion rates for each sampling day with its correspondent calculated erosivity (R) and erodibility (K) values. A total of 59 samplings were collected in 14 months, of which 7 were considered as outliers. Erosion rate values presented in the Table 3 were averaged for all four plots per study site and each sampling date. The average erosivity (R) for the entire study period was 124.8 (ft × tonf × in (100 ×ha ×h)$^{-1}$), which is equivalent to 260.21 (ft × tonf × in (100 ×acre× h)$^{-1}$) or 4428.77 (MJ× mm / (ha × h)). The reported annual R factor for this region of the eastern United States is 200 (ft × tonf × in (100 ×acre× h)$^{-1}$) (Renard et al., 1993).

Table 8-1 Measured erosion (A), calculated erosivity(R), and erodibility (K) values per date and site.

	Sampling Date	R ft. tonf . in (100 *ha h)$^{-1}$	Erosion ton / ha	K factor values* Mg. ha. hr (ha MJ mm)$^{-1}$
National	June 25, 2009	13.96	261.79	0.496
	July 7, 2009	6.34	112.54	0.469
	August 3, 2009	21.35	201.21	0.249
	July 15, 2009	18.21	78.80	0.283
	August 14, 2009	6.70	25.91	0.253
	September 25, 2009	11.42	11.21	0.064
	September 29, 2009	3.02	3.46	0.075
	October 8, 2009	2.75	3.17	0.075
	October 22, 2009	10.08	9.36	0.061
	October 29, 2009	0.24	0.21	0.058
	November 5, 2009	1.14	0.59	0.033
	November 12, 2009	0.30	0.17	0.038
	December 1, 2009	1.51	0.79	0.034
	December 14, 2009	4.38	2.69	0.040
	April 13, 2010	4.88	7.97	0.107
	May 7, 2010	14.78	21.26	0.094
	May 19, 2010	7.00	9.96	0.093
	June 23, 2010	4.01	5.89	0.096
	June 29, 2010	2.26	3.69	0.107
	July 16, 2010	13.19	16.48	0.082
Premium	June 24, 2009	17.29	48.98	0.102
	July 17, 2009	23.45	66.26	0.101
	August 24, 2009	10.90	34.94	0.115
	August 3, 2009	6.39	4.38	0.06
	August 13, 2009	2.64	1.72	0.06
	September 22, 2009	13.90	12.22	0.08
	October 1, 2009	18.63	20.23	0.10
	October 20, 2009	2.43	1.61	0.06
	October 27, 2009	0.85	0.43	0.04
	November 3, 2009	0.24	0.18	0.07
	November 24, 2009	0.70	0.41	0.05
	December 3, 2009	0.97	0.49	0.04
	December 17, 2009	10.71	7.93	0.07
	May 7, 2010	11.81	7.33	0.05
	May 18, 2010	2.23	1.11	0.04
	June 8, 2010	6.11	2.51	0.04
	July 20, 2010	5.34	3.77	0.06
Mountain Side	July 14, 2009	10.80	118.20	0.347
	July 2, 2009	0.80	3.19	0.313
	September 22, 2009	12.54	9.46	0.059
	October 1, 2009	16.24	18.97	0.091
	October 13, 2009	5.01	4.48	0.070
	October 20, 2009	1.88	1.82	0.076
	November 3, 2009	1.05	0.67	0.050
	December 1, 2009	0.39	0.21	0.043
	December 10, 2009	3.46	1.60	0.036
	December 14, 2009	1.09	0.67	0.048
	March 26, 2010	3.48	2.28	0.051
	May 13, 2010	14.56	8.66	0.047
	May 18, 2010	7.50	4.46	0.047
	June 8, 2010	7.22	3.81	0.041
	June 25, 2010	6.28	3.56	0.044

*USLE K factor as defined by Mitchell and Bubenzer (1980) where A= 0.224 RKLSCP, for each sampling date.

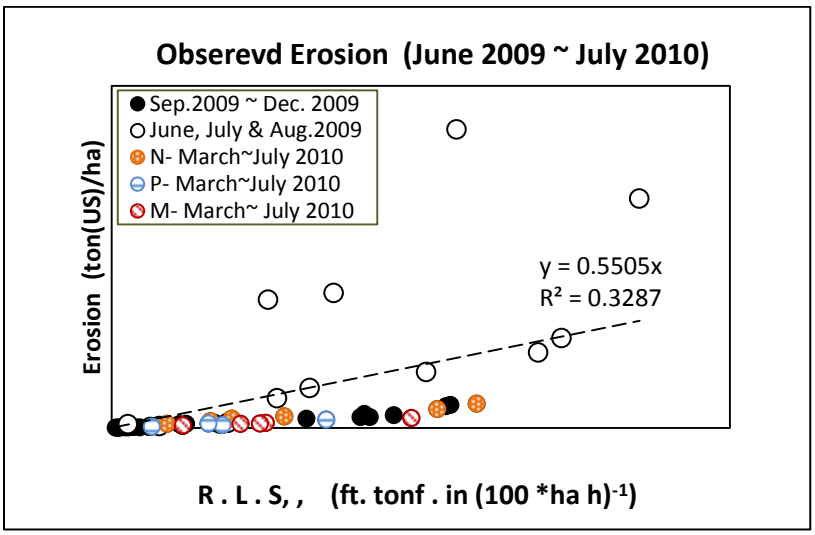

Figure 8-1 Observed erosion rate for each site, June 2009 till July 2010.

Figure 8-1 shows the observed erosion rate vs. erosivity of rainfall plus the LS (slope-length) factor for all three sites during 14 months of monitoring, June 2009 through July 2010. The graph shows two data clusters, one for rainfall events that occurred during June, July and August 2009 (cluster 1) representing early monitoring immediately after site construction, and one for the monitoring period after this initial period (cluster 2). The data gathered during June, July and August 2009 showed a much higher erosion rate compared to later periods. The rationale for this difference appears to be from rill development beginning in June, July and August 2009, shortly after site construction. Because the reclaimed slopes were steep with loose spoil material, and rainfall intensities during this summer period were high, rill formation was a dominant geomorphic process on the land surface. After 3 months near the end of August 2010 rills appeared to have come to a geomorphic equilibrium state showing little further growth. Further investigation of the K factor and rill development is presented in Figure 8-2.

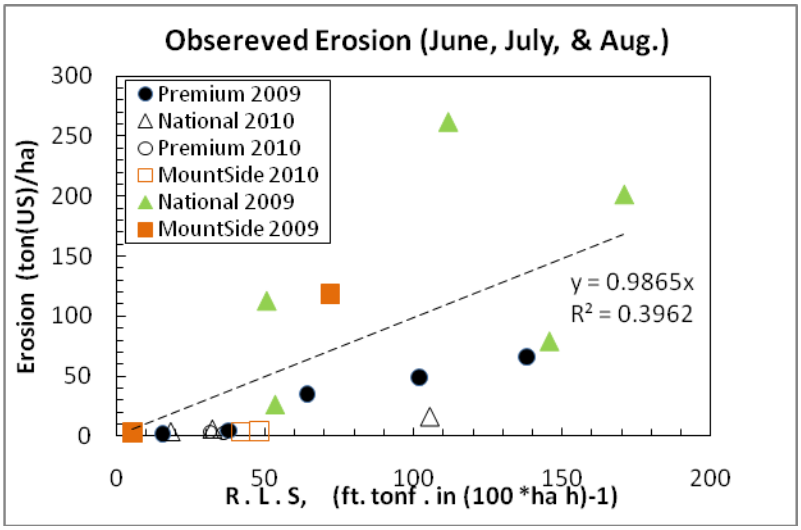

Figure 8-2 Observed erosion rates for each site during June, July and August of 2009 and March – July 2010

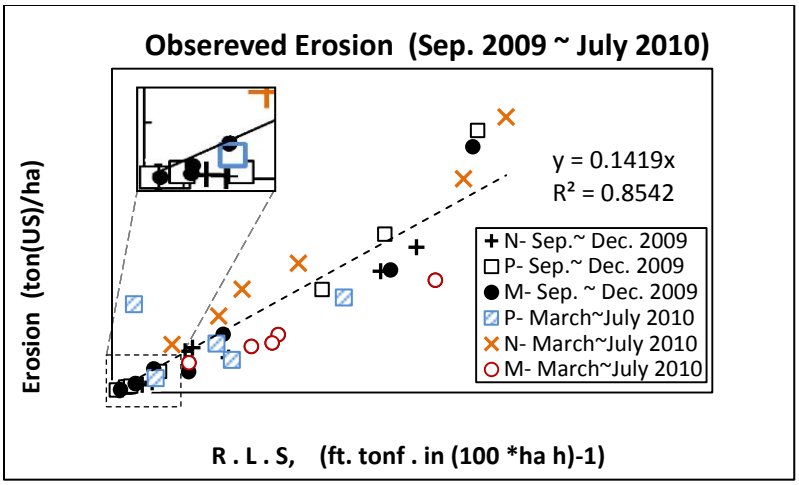

Figure 8-3 Observed erosion rates for each site, Sep. 2009 till July 2010

Figure 8-2 shows the observed erosion rate vs. erosivity of rainfall (LS, slope-length factor was also considered) for all three sites during first three months of monitoring, June, July and August 2009 (cluster 1), and the same time period for the next year (June, July and August 2010). Although the rainfall erosivity was generally lower for the period during 2010, the graph showed larger erosion reduction for those rainfalls which had similar erosivity in 2010 compared with 2009. This is likely the effect of both armoring and fully developed rills after first year period. Figure 8-3 shows the observed erosion rate vs. erosivity of rainfall (LS, slope-length factor was also considered) for all three sites during September 2009 till July 2010 (cluster 2). The variation in data points about fitted line was much less than in cluster 1 (R^2 = 0.85).

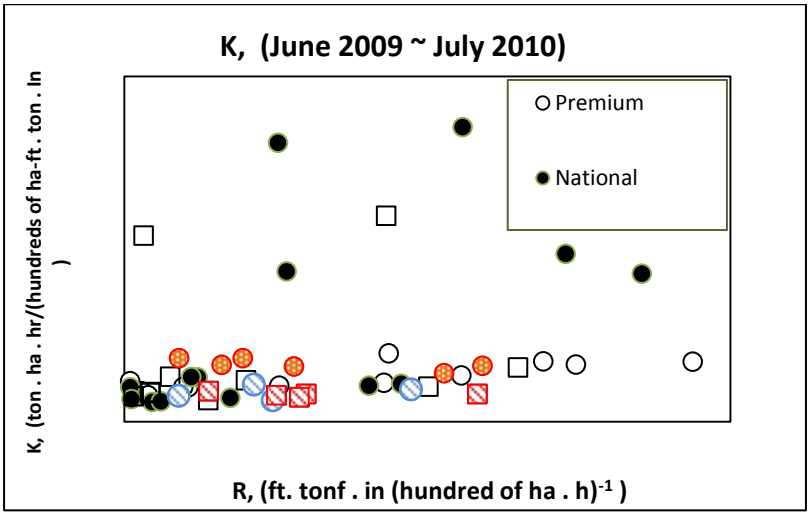

Figure 8-4 Computed erodibility, K, for the study monitoring period June 2009 through July 2010.

Generally, the National site had a slightly more erosion over time than the other two study sites with similar ranges of rainfall erosivity (R). Considering all mentioned above about the rate of erosion, a better insight on the erodibility of low compacted materials can be achieved by plotting erodibility against rainfall erosivity. Figure 8-4 shows the computed values of erodibility for the entire monitoring period. The same effect of rill development is vivid in this graph. While, most of the K values (cluster 2)

were ranging from 0.025 to 0.09 [ton . ha . hr/(hundreds of ha-ft . ton . in)], most of which were related to June, July and August 2009 having considerably higher values than the rest. As reported on the runoff studies in Chapter 7, the summer 2009 rainfall events produced significant runoff events on the steep slopes of the study sites. As a result, runoff developed shear stresses on the inter-surface of soil, and caused soil detachment and rill development, which resulted in high rates of erosion and sediment yields. The rill development continued through the summer until they reached an equilibrium state large enough to transport runoff produced on those plots. Due to occurrence of relatively high intensity storms just after site construction, this geomorphic process appeared to slow after the first three months following site construction (Figure 8-5).

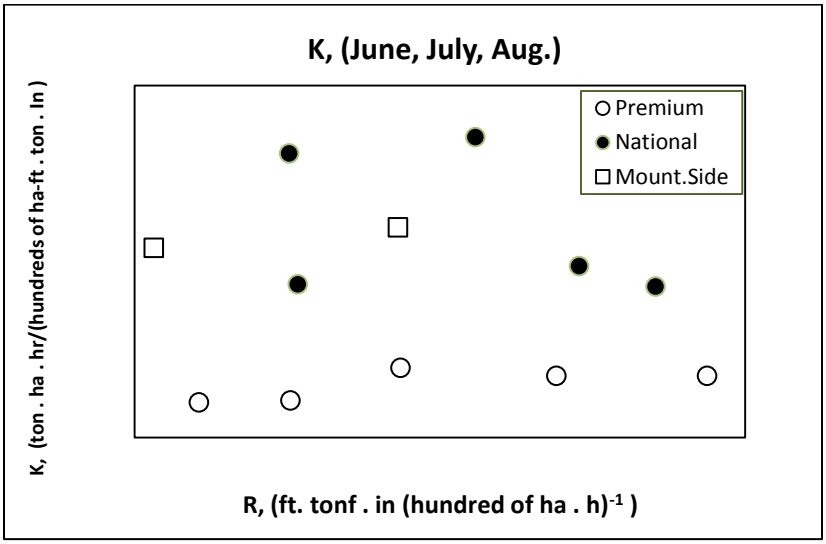

Figure 8-5 Computed erodibility, k, for June, July and August 2009.

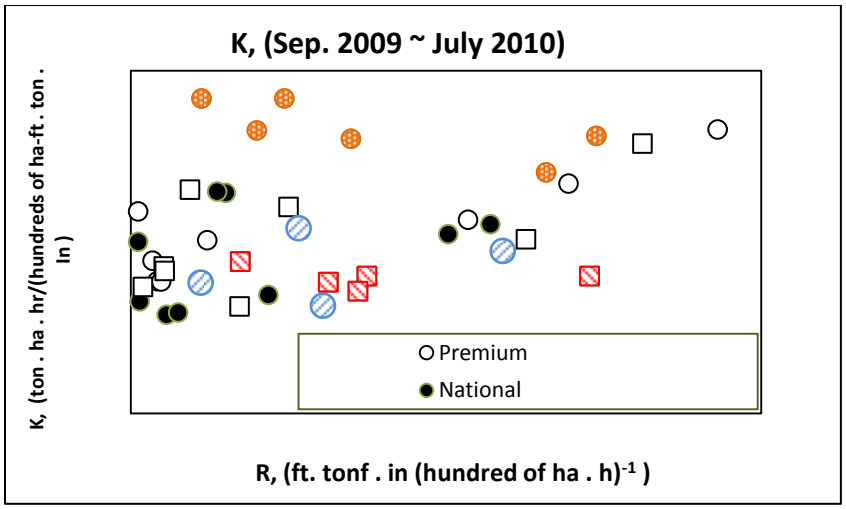

Figure 8-6 Computed erodibility, k, for Sep 2009 till July 2010

As observed in Figure 8-6, after rill development, K values appear to drop significantly as it reaches steady geomorphic equilibrium state some were around 0.05 $(ton\,.ha\,.hr)/(hundreds\ of\ ha-ft.ton.in)$. The dependence of K on the initiation of rill development is related to sheet erosion, which

primarly occurres from raindrop energy impact and land surface slope length. Sheet erosion increases slightly with slope, whereas rill erosion is strongly dependent on both slope length and gradient. Rill erosion results from the shear stress forces when flows are concentrated into a channel. Increases in runoff depth and velocity also increase rill erosion rates. Although the K value is generally assumed to be constant over time when applied in practice, this assumption is valid only on lands without rills or after rills have stabilzied. After rills become stabilized, the only source of erosion is sheet erosion and the only factor affecting erodibility is soil suceptibility to the rainfall energy impact, or erosivity (R).

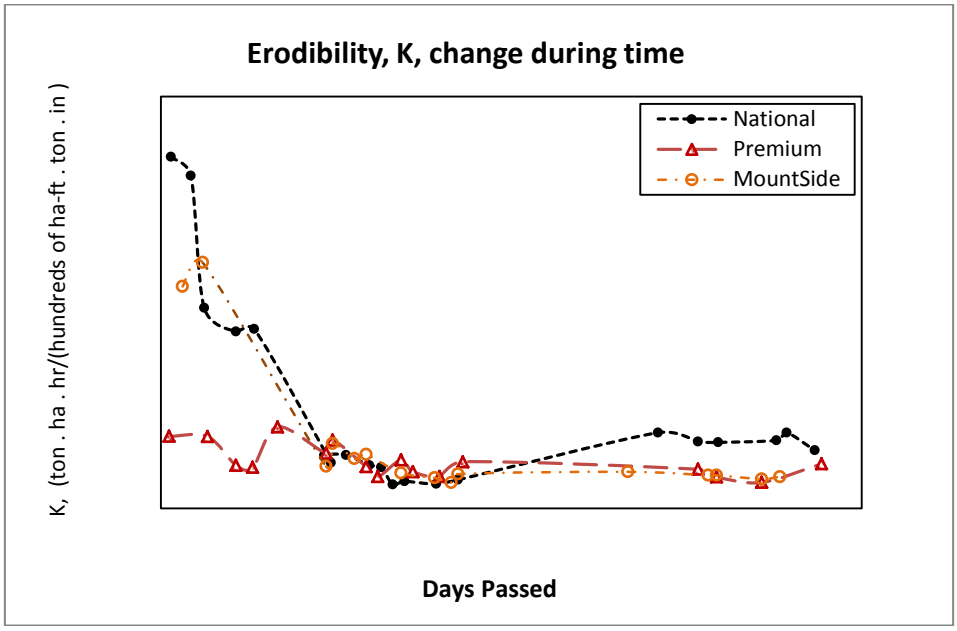

Figure 8-7 Erodibility, K, change during time (days passed form beginning of project).

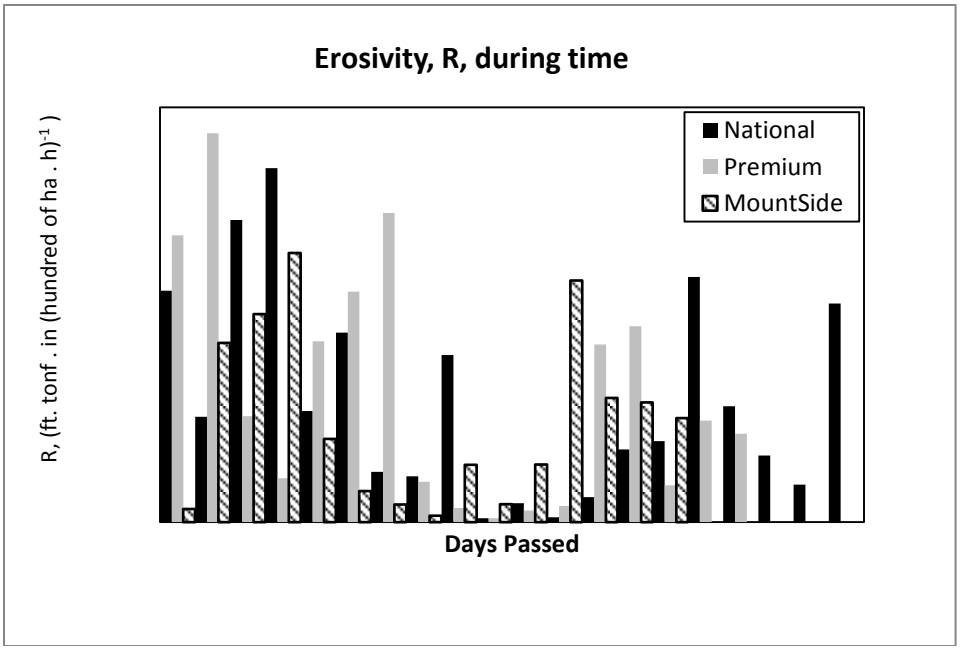

Figure 8-8 Erosivity, R, at each period of sampling.

Figure 8-7 illustrates how erodibility (K) changed over time (days passed after beginning site monitoring). Both the National and Mountainside sites showed a large reduction in erodibility (K) during first 90 days, and appear to have come to an equilibrium state after this period. The Premium site did not show that K value change due to rill development. Perhaps this can be attributed to the difference in the construction technique at Premium, which consisted of only a single or double pass with the dozer after spoil were dumped from above. Multiple passes were used at the National and Mountainside sites, while still attempting to limit compaction, presumably leading to the higher measured mean dry and wet unit weights. The lower unit weight at Premium corresponds to a higher porosity, leading to greater infiltration, lower runoff production, and appears to have resulted in slower rill development. Also at the Premium site the existence of large rocks in the reclaimed soil may have caused less erodible material as a percentage of the plot areas. Figure 8-8 shows the erosivity of rainfall events that each site experienced during the monitoring for each period of sampling.

Particle Size Distribution

The particle size distributions of eroded material during the monitoring period (June 2009 till end of July 2010) for all three sites are shown in Figures 8-8 through 8-12. While all three sites have almost the same shape, generally the National and Mountainside sites had more course eroded materials. The results showed that during the period Sept. -l Dec. 2009, between 50% and 60% of eroded material was silt and clay. This period is when rainfall events had low rainfall intensities among the study sites. During the other periods between 15% till 40% of the eroded material was silt and clay. OSM and mining consultants use a default particle size distribution in their SEDCAD software for detention pond design, but results from this study provide users better model input data. These results are important in design of sediment control basins and BMP selection for erosion control.

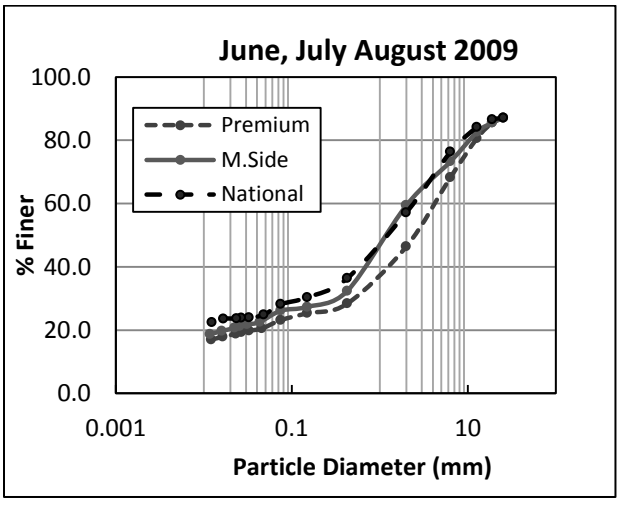

Figure 8-9 Typical particle size distributions for June, July and August 2009

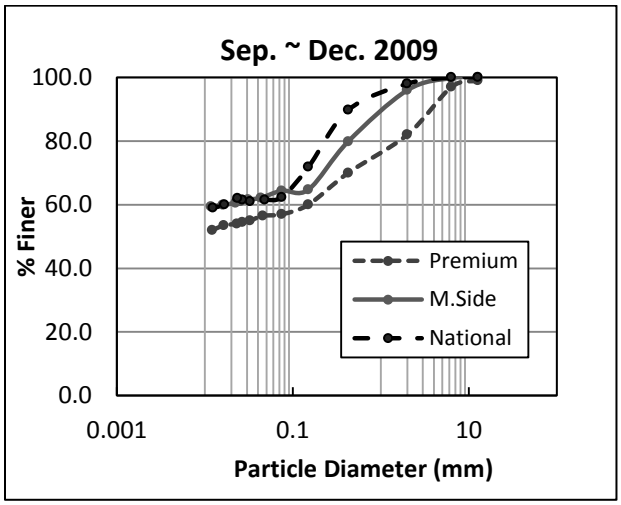

Figure 8-10 Typical particle size distributions for Sep. till Dec. 2009

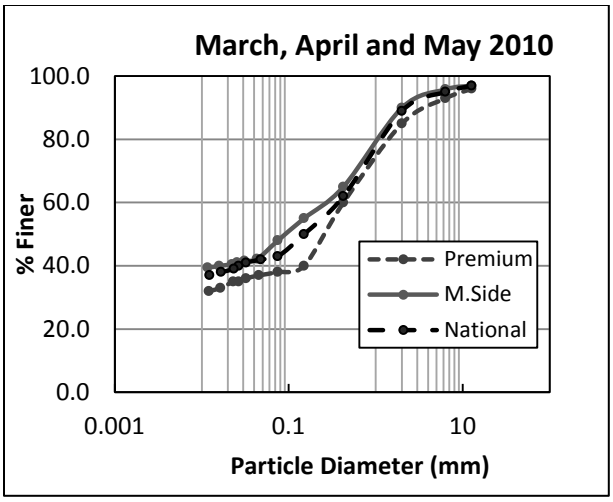

Figure 8-11 Typical particle size distributions for March, April and May 2010

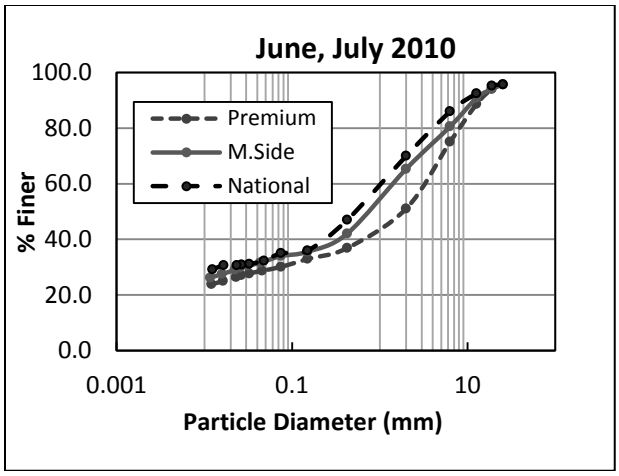

Figure 8-12 Typical particle size distributions for June, July 2010.

Conclusions

The erodibility of low compacted reclaimed material on steep-sloped coal mining lands was estimated in this study. Results of this study showed that the erodibility was a function of rill development, and changed with the time. Average K factors were estimated as 1) K = 0.30 during rill development, 2) K = 0.07 during the transition period to an equilibrium state, and 3) K =0.05 once the rills have stabilized. The particle size distributions of delivered sediment from the study plots were also calculated, ranged in the silt and clay size classes, with the median particle size lower over time as the rills developed and became stabilized. The results are important for the design of sediment control basins and BMP selection for controlling erosion on reclaimed mine lands.

References

Angel, P. C. Barton, R. Warner, C. Agouridis, T. Taylor, and S. Hall (2007) “Hydrologic Characteristics, tree growth, and natural regeneration on three loose-graded surface mine spoil types in Kentucky” presentation at the Mid-Atlantic Stream Restoration Conference, Rocky Gap Lodge, Cumberland, Maryland, November 2007.
http://www.canaanvi.org/canaanvi_web/events_ed.aspx?collection=cvi_workshops&id=140; Accessed December 15, 2007

Barfield, B. J., R. I. Barnhisel, J. L. Powell, M. C. Hirschi, and I. D. Moore. 1983. Eerodibilities and eroded size distribution of western Kentucky mine spoil and reconstructed topsoil. IMMR Final Report No. G1115211 and CRIS Project NO.907-15-2.

Gilley, J. E., G. W. Gee, A. Bauer, W. O. Willis, and R. A. Young. 1977. Runoff and erosion characteristics of surfaced-mined sites in western North Dakota. Am. Soc. Agr. Engr. 20:697-700.

Govers, G. 1987. Spatial and temporal variability in rill development processes at the Huldenberg experimental site. ELSEVIER SCIENCE, IDS No. J4089, ISSN: 0341-8162.

Graves DH, Ringe JM, Pelkki MH, Sweigard RJ, Warner RC. 2000. High value tree reclamation research. In Environmental Issues and Management of Waste in Energy and Mineral Production, Singhal RK, Mehrotra AK (eds). Balkema: Rotterdam.

Hoomehr, S., J.S. Schwartz, W.C. Wright, and E.C. Drumm. 2010. Surface erosion and sediment yields on steep-sloped coal mining reclamation sites in the Appalachian region. in ASCE/EWRI, ed., World Water & Environmental Resources Congress: Providence, RI.

Jeldes, Isaac A., Siavash Hoomehr, Wesley C. Wright, P.E., John S. Schwartz, P.E. David E. Lane, P.E., Eric C. Drumm, P.E. 2010. National Meeting of the American Society of Mining and Reclamation, Pittsburgh, PA Bridging Reclamation, Science and the Community June 5 - 11, 2010. R.I. Barnhisel (Ed.) Published by ASMR, 3134 Montavesta Rd., Lexington, KY 40502.

Mcintosh J. E. and R. I. Barnhisel. 1993. Erodibility and sediment yield by natural rainfall from reconstructed mine spoils. Journal of soil science, Volume 156, Issue 2, pp. 118-126.

McKenzie, G. D., and J. R. J. Studlick. 1979. Erodibility of surface-mine spoil banks in southeastern Ohio: An approximation. J. Soil Water Conserv. 34: 187-190.

Meyer L. D., and W. C. Harmon 1989. How side slope length and steepness affect side slope erosion. Trans. ASAE 32:639-644.

Mitchell, J. K., W. C. Moldenhauer, and D. D. Gustavson. 1983. Erodibility of selected reclaimed surface mined soils. Am. Soc. Agr. Engr. 26:1413-1417.

Mostaghimi, S., and J. K. Mitchell. 1983. Erosion characteristics of surface mined soils. Proc. 1983 Symposium Surf. Mining Hydrol., Sediment., and Reclam. University of Kentucky, Lexington, pp. 537-541.

Pinson, W.T., Yoder, D.C., Buchanan, J.R., Wright, W.C., Wilkerson, J.B. 2003. Design and evaluation of an improved flow divider for sampling runoff plots. J. Applied Engineering in Agriculture Vol. 20, No. 4, p433-437.

Renard, K. G., McCool, D. K., Cooley, K. R. Mutchler, C. K., and Foster, G. R. 1993. Rainfall-runoff erosivity factor (R). Chapter 2 in Renard, Foster and Weesies (eds) " Predicting Soil Erosion by Water-A Guide to Conservation Planning with the Revised Universal Soil Loss Equation RUSLE", Publication ARS. U.S. Department of Agriculture, Washington, DC, in press.

Shukla M.K., Lal R, Underwood J, Ebinger M. 2004. Physical and hydrological characteristics of reclaimed minesoils in southeastern Ohio. Soil Science Society of America Journal 68(4): 1352–1359.

Torbert, J.L. and J.A. Burger, Influence of grading intensity on ground cover establishment, erosion, and tree establishment on steep slopes. International Land Reclamation and Mine. Drainage Conference and the Third International Conference on the Abatement of Acidic Drainage, Pittsburgh, 1994.

Torri, D., M. Sfalanga and G. Chisci. 1987. Threshold Conditions for Incipient Rilling. Bryan, R.B. (ed). Rill Erosion: Processes and Significance. Catena Supplement 8. W. Germany:Catena Verlag. 97-105.

Toy T. J., G. R. Foster, and K. G. Renard. 1999. RUSLE for mining, construction and reclamation lands. Journal of Soil and Water Conservation, Volume 54, Issue 2, pp. 462-467.

U.S. Dept. of the Interior. 1977. Surface mining reclamation and enforcement provisions. Federal Register 42:62685-62688, December 13.

W.C. Ashby, C.A. Kolar, and M.L. Guerke, Our Reclamation Future with Trees, Coal Extraction and Utilization, Research Center, Southern Illinois at Carbondale, 1978.

William R. Thomas; Matthew H. Peikki; James M. Ringe 1999. Proceedings, 12th central hardwood forest conference; 1999 February 28-March 1-2; Lexington, KY.Gen. Tech. Rep. SRS-24. Asheville, NC: U.S. Department of Agriculture, Forest Service, Southern Research Station.293 p. [Peer-reviewed paper]. 79

Wischmeier, W. H, and D. D. Smith. 1965. Predicting rainfall-erosion losses from cropland east of the Mountains-Guide for selection of practices for soil and water conservation. Agr. Handbook. No. 282. U.S. Dept. of Agriculture, Washington, DC.

Wischmeier, W. H. and D. D. smith. 1978. Predicting rainfall erosion losses. Agriculture Handbook No. 537, USDA, Washington, D.C.

Zhang G. H., Yu-mei Liu, Yan-feng Han, X. C. Zhang 2009. Sediment Transport and Soil Detachment on Steep Slopes: I. Transport Capacity Estimation. Soil Science Society of America Journal Vol. 73 No. 4, pp. 1291-1297.

Renard, K. G., McCool, D. K., Cooley, K. R. Mutchler, C. K., and Foster, G. R. 1993. Rainfall-runoff erosivity factor (R). Chapter 2 in Renard, Foster and Weesies (eds) " Predicting Soil Erosion by Water-A Guide to Conservation Planning with the Revised Universal Soil Loss Equation RUSLE", Publication ARS. U.S. Department of Agriculture, Washington, DC, in press.

Chapter 9 Evaluating Performance of SEDCAD Model on Low Compacted Steep Sloped Reclaimed Surfaces in the Southern Appalachian Region

(In preparation for submittal to ASCE, *Journal of Irrigation and Drainage Engineering*)

Abstract

SEDCAD is a comprehensive hydrology and sedimentology package which has been widely used in designing runoff and sediment control structures primarily in the mining industry. This study investigated the performance of SEDCAD in estimating erosion and sediment delivery from low-compacted, steep-sloped mine lands reclaimed using the Forest Reclamation Approach. In addition, SEDCAD model input parameters were assessed with respect their sensitivity to SEDCAD outputs. The input parameters included curve number value (CN) and erodibility (K) factor of reclaimed spoil material. Model output were compared to measured sediment yields from three mine sites in East Tennessee for a one-year monitoring period. In general, SEDCAD appeared to overestimate sediment yield compared to that what was measured from these sites. In addition, CN selection was found to be sensitive in affecting modeled sediment yields. The results of this study can give a better understanding of the interpretation of SEDCAD outputs and will be useful in designing runoff and sediment control structures and selection of best management practices (BMPs) in the mining industry.

Introduction

In the Appalachia region, more than 600,000 ha have been mined for coal, and more than 10,000 additional ha are being mined each year (Zipper et al. 2011). The Surface Mining Control and Reclamation Act (SMCRA) requires reclamation of all areas disturbed by mining operations (US Dept. of Interior, 1977). Mine reclamation has traditionally been successful by using grass cover on highly compacted, steep-sloped soils. A recent approach to reclamation, termed the Forest Reclamation Approach (FRA), promotes growing native forests on reclaimed areas using a lower level of compaction to improve the soil conditions for tree survival (Hoomehr et al. 2011a). In general, whether the traditional approach or FRA is used, erosion prevention and sediment control is required by SMCRA.

Design of the sediment control basins and stormwater best management practices (BMPs) is typically performed with the support of computer software, such as the Sediment, Erosion, Discharge by Computer Aided Design (SEDCAD) program. SEDCAD is a suite of curve number-based watershed rainfall-runoff models, RUSLE-based sediment yield analysis, and channel and hydraulic structure design utilities (Warner, Schwab & Marshall 1998). SEDCAD is primarily used by the Office of Surface Mining (OSM), state mining programs, industry and engineering consultant firms for hydrologic, erosion and sediment control designs (US Dept. of Interior, Office of Surface Mining, 2010). OSM provides SEDCAD to the 24 states with primacy under the SMCRA for use in permit review and in design of Abandoned Mine Lands (AML) reclamation projects and remediation plans for bond forfeiture sites. OSM uses SEDCAD to review permit applications from industry. OSM also utilizes SEDCAD in preparation of Cumulative Hydrologic Impact Assessments (CHIA's) to determine the cumulative hydrologic effects of multiple mining operations on adjacent lands and watersheds during and after mining (SEDCAD Design manual

and User's Guide). SEDCAD includes hydrology and hydraulics design and evaluation of the effectiveness of both individual and integrated systems of surface water, erosion and sediment control measures with respect to sediment trap efficiency and prediction of effluent sediment concentration (Warner, Schwab & Marshall 1998).

Specifically, SEDCAD has been used by engineers, geologists, hydrologists, and soil scientists to: 1) model hydrologic mine systems including channels, ponds, and sediment control structures; 2) evaluate the effectiveness of sediment ponds and other sediment control structures such as check dams, grass filters, and silt fences for a mining reclamation plan; 3) evaluate diversion channel designs, including riprap, grass-lined, and bar soil conditions; 4) evaluate culvert and plunge pool designs, and recommend changes for permits under review; and 5) analyze the impact of the addition or removal of a hydrologic structure - sediment pond, permanent impoundment, plunge pool, etc. under permit review (US Dept. of Interior, 2008).

SEDCAD's input parameters are basin size, stream and land slope, time of concentration, curve number, soil erodibility (RUSLE K factor), hydrologic soil groups, hydrograph response, storm frequency and particle size distribution of eroded material. SEDCAD allows division of the watershed into relatively homogenous sub-basins with respect to expected hydrologic and sedimentologic responses. Hydrologic and sediment data will be tabulated at a position in a model that SEDCAD refers to as a "structure."A "structure" can be a physical or non-physical entity and is simply a position in the model where hydrographs and sediment-graphs are generated. While SEDCAD has been used extensively as a tool in hydrologic, erosion and sediment control designs, there is limited information on its performance estimating erosion and sediment yield from disturbed mine lands. Also, sensitivity of the software's results to its hydrologic and sedimentologic input parameters has never been investigated.

The overall objective of this study was to evaluate performance of SEDCAD in predicting runoff, erosion and sediment yield from three coal mining study sites in the southern Appalachian region for one year period. In addition, the sensitivity of SEDCAD main hydrologic and sedimentologic input parameters, curve number value (CN) and erodibility of reclaimed material (K) were investigated with respect to the model's output and compares with measured data. Results of this study allows for a better interpretation of SEDCAD output, which will be useful to practitioners in the mining industry designing runoff and sediment control structures and selecting stormwater BMPs.

Methods

Study site locations

The study site locations are described in Chapter 2, and include the Premium mine site located in Anderson County 34 miles north of Knoxville; National site located in Campbell County 54 miles north of Knoxville; and Mountainside site located in Claiborne County 74 miles north of Knoxville at Jellico Mountain, near the Kentucky boarder.

The National Climatic Data Center divides each state into climate divisions and based on that these sites are located in the 1st climate division of TN. Average annual precipitation recorded over 30 years at these areas is around 122.5 cm (1225 mm) and typically the temperature range is between 0.0 and 33^{o}C (NOAA 2010).

Study site characterization

Site geometries, soil unit weights, shear strength parameters, and uplands soil particle size distributions were presented in Chapter 3. A hydrological analysis for estimating runoff curve number values was presented in Chapter 7. These data support the erodibility analysis presented in this chapter. As described in Chapter 2, Section on Experimental Design, ground cover was not established on the four field plots per study site, therefore findings from this study represent erodibility factors for bare soil, and a geomorphic condition favorable for rill development.

Weather, runoff volumes and sediment data collection

Each of the three sites was equipped with a full weather station. Per study site, four plots were equipped with an H-flume and Pinson et al. (2004) runoff collection devices (Figure 2-10). A detailed description of the field equipment to measure weather, runoff volumes, and sediment erosion is in Chapter 2.

Erodibility of Spoil Material

SEDCAD uses the Revised Universal Soil Loss Equation's (RUSLE) as the basis for all of the sedimentology routines in the software (SCS, 1993). Recall from Chapter 8, RUSLE estimates the average annual erosion from field sites by the following equation:

$$A = 0.224 \cdot R \cdot K \cdot LS \cdot C \cdot P \qquad (9\text{-}1)$$

where,

A = amount of soil loss occurred (kg/m2)
R = rainfall and runoff erosivity factor
K = soil erodibility factor, soil loss rate per erosion index unit for a specified soil as measured on a standard plot (72.6 ft and 9% slope)
LS= combined length-slope factor, for un-standard size plots
C = cover management factor
P = erosion control practice factor

The soil erodibility or K factor is a numerical representation of the soil's susceptibility to erosion. Rainfall erosivity (R) was estimated also from this study's on-site precipitation data, and reported in Chapter 8. Because there was no vegetative cover on the study plots and no erosion control practices, C and P were equal to 1. The LS factors were computed based on the tabulated values in the USDA agricultural handbook number 703 (1997). The amount of erosion (A) was both measured and computed using SEDCAD (Hoomehr et al., 2011).

The estimated erodibility for the study sites changed over time due to rill development. The National and Mountainside sites were observed to have high values for K-factor just after site construction and 100 days following. After which once the rills developed the K factor remained constant, at a lower value. The Premium site was observed with a constant value for erodibility, and appears not to be affected by rill development. The average K-factor for National and Mountainside sites during rill development is about 0.312 (ton .ha .hr)/(hundreds of ha-ft.ton.in). Values for K were determined by a field study on the three coal mining sites and study details can be found in Chapter 8. Summarizing the results of that study, average K factors were estimated as 1) K = 0.30 during rill development, 2) K = 0.07 during the transition period to an equilibrium state, and 3) K =0.05).once the rills have stabilized.

SCS-CN method

The Curve Number method was developed by the USDA Soil Conservation Service (SCS), or now the National Resources Conservation Service (NRCS). It is a popular means that provide an index to estimate storm runoff from rainfall events. SEDCAD uses CN in TR-55 Emulator. Section 4 of the National Engineering Handbook, NEH-4, is the primary source of Curve Number method (SCS, 1972). Chapter 7 describes the fundamental of this method, and the field study to estimate a CN for reclaimed mine lands using the FRA (Hoomehr et al., 2011b).

Results estimate CN values between 58.5 and 60 for the low compacted reclaimed surfaces in east of Tennessee, Appalachian region as generated by the P-Q and I_{30}-Q Frequency Match approaches. Both approaches suggest a standard asymptotic behavior for the study sites generating common CN values. In comparison, CN estimates using a means approach found an average CN of 62.2 for a λ of 0.05, and an average CN of 72.2 for a λ of 0.20.

SEDCAD

Storm Event Information: The NRCS Storm Type II with 241 point distribution was used for this study. The Design Storm frequency (years) and duration (hours) was chosen in a way that by setting rainfall depth equal to observed values (from the monitoring period), the calculated erosivity (R-storm) by SEDCAD equal to the erosivity computed from measured rainfall data at the study sites. The R-storm in SEDCAD is based on the rainfall quantity and storm distribution specified in the storm type, Design Storm and Rainfall Depth input values, and was calculated using the updated equation by Brown and Foster (1987) which includes more data for its development and has a better functional form at low rainfall intensities (Renard, et. al., 1997)

Sub-watershed Hydrology:

SEDCAD requires for each sub-watershed area the following parameters: CN, time of concentration, erodibility (K), and selection of a dimensionless unit hydrograph shape. The area of the sub-watershed, (the study plots), was calculated and entered as an average for each study site. The time of concentration represents how long it takes for runoff from the entire sub-watershed to reach the watershed outlet. Time of concentration was estimated for each site using Manning's equation and averaging over all plots. Time of concentration affects peak flow and hydrograph shape, but not runoff volume. The estimated CN for all sites was used as input for SEDCAD.

Sub-watershed Sedimentology:

SEDCAD uses peak flow, runoff volume, soil erodibility, slope length and gradient, soil cover type, and type of control practices to estimate amount of erosion and sediment delivery at the watershed outlet. As mentioned before, the runoff volume and peak flow are calculated in the software's hydrology routine. Slope length and gradient were entered as inputs to SEDCAD based on Table 2-2.

Particle Size Distribution

SEDCAD requires particle size distributions (PSDs) of the eroded material, or spoil material. SEDCAD is a rather unique model in that it tracks the change in particle size distribution as sediment-laden flow proceeds from the slope where it originates to the sub-watershed outlet, routed to a structure, passes through a sediment control structure, and finally down-gradient (SEDCAD Design manual and User's Guide). The PSD was determined from the eroded samples gathered from 5 gallon buckets that were used in the runoff- sediment collection systems at the sites (Hoomehr et al., 2010, 2011).

RESULTS

SEDCAD Model

Using the values obtained for K-factor and CN as inputs for SEDCAD, the amount of erosion and sediment delivery was estimated for each site. The estimated values were compared with the actual measured amounts obtained during the monitoring period. The results are shown in Figure 9-1 which shows the amount of sediment yield from the study sites for low to high rainfall erosivity that were typically experienced during the 12-month monitoring period. In most cases, SEDCAD overestimates sediment yield from study plots.

To investigate the sensitivity of SEDCAD outputs to K-factor and CN input parameters, the "true or measured" values for K-factor and CN (Hoomehr et al., 2011) were used as baseline. An analysis of the sensitivity of those parameters was performed on each independent of each other. Because SEDCAD uses RUSLE, and the amount of erosion is linearly dependent on the K factor, the amount of error in estimated erosion due to error in K-factor selection is equal to amount of error for the erodibility selection (Figure 9-2).

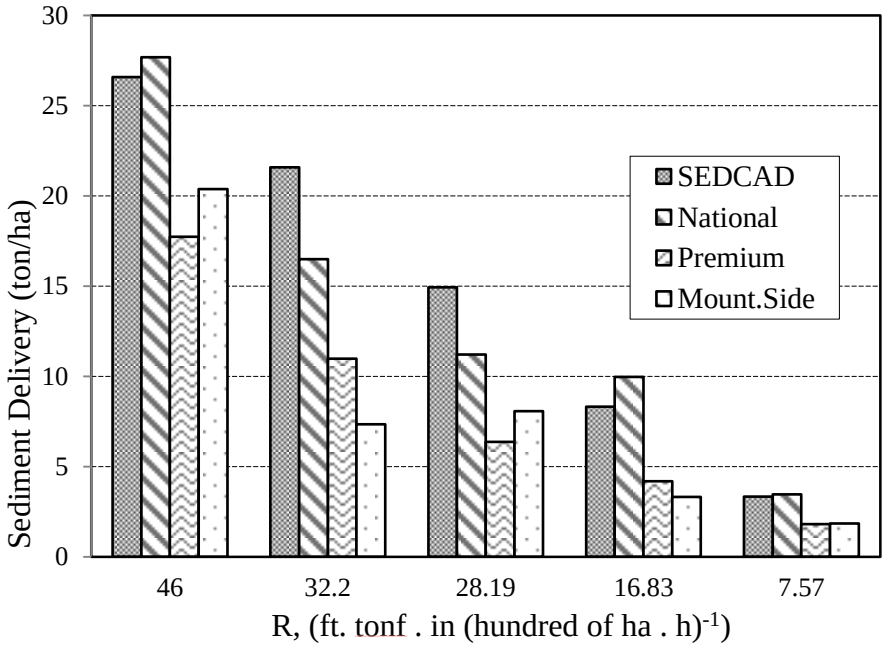

Figure 9-1 SEDCAD calculated and measured sediment yield from the three study sites.

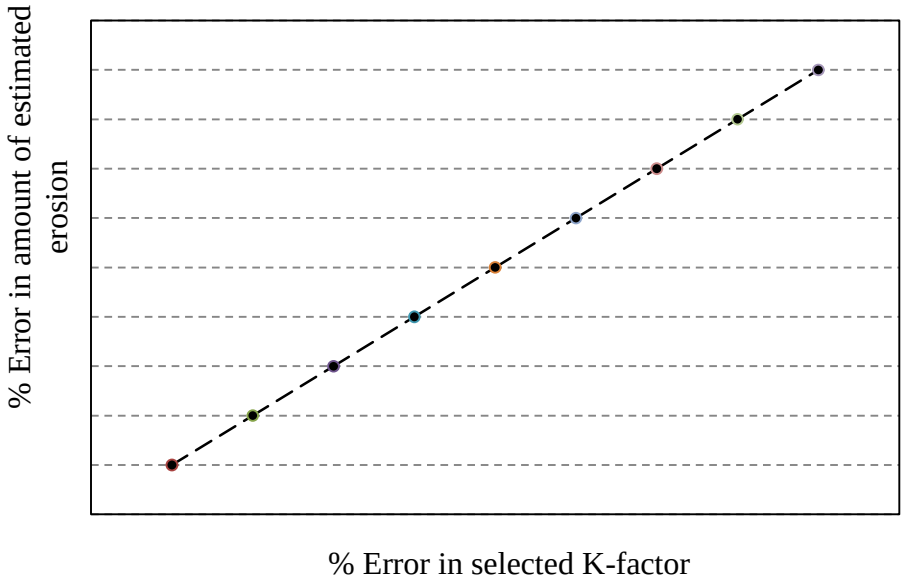

Figure 9-2 % Error in amount of estimated erosion relative to % Error in K-factor selection

Table 9-1 Error in amount of estimated erosion relative to Error in CN selection

CN	Erosion ton/ha	Error in CN			Error in estimated erosion		
		CN = 60 *	+ 5% **	- 5% ***	CN=60 *	+ 5% **	- 5% ***
40	1.1	-0.33	-0.38	-0.27	-0.92	-0.94	-0.88
45	3.5	-0.25	-0.31	-0.18	-0.74	-0.81	-0.63
50	6.2	-0.17	-0.23	-0.09	-0.54	-0.66	-0.34
55	9.4	-0.08	-0.15	0.00	-0.31	-0.48	0.00
60	13.6	0.00	-0.08	0.09	0.00	-0.25	0.45
65	18.2	0.08	0.00	0.18	0.34	0.00	0.94
70	23.2	0.17	0.08	0.27	0.71	0.27	1.47
75	28.6	0.25	0.15	0.36	1.10	0.57	2.04
80	34.2	0.33	0.23	0.45	1.51	0.88	2.64
85	40.1	0.42	0.31	0.55	1.95	1.20	3.27
90	46	0.50	0.38	0.64	2.38	1.53	3.89
95	51.6	0.58	0.46	0.73	2.79	1.84	4.49
100	56.2	0.67	0.54	0.82	3.13	2.09	4.98

* The “True” value of CN obtained using asymptotic method (Hoomehr et al. 2011b)
** + 5% increase in estimating “True” value of CN
*** - 5% increase in estimating “True” value of CN

To investigate sensitivity of SEDCAD output with respect to the CN selection, 60 was considered as the “true” value for CN (Chapter 7), and it was based on the estimated amount of erosion for that value (SEDCAD output) and the percent change in estimated erosion due to departure from that “true” value (Figure 9-3). SEDCAD appears to be sensitive to CN selection and small changes in CN selection

generates large changes in sediment yield. For example, having a 40% error in selecting CN will double the estimation of eroded material. One may argue that there is a level of uncertainty for the value of CN=60 (as a "true" value), which is correct; so to address that complimentary curves for +/- 5% confidence interval in "true" CN selection are also shown in Figure 9-3. The range of error in CN selection was determined by considering the range of CN values obtained from monitoring study sites, and the SEDCAD ability to reflect that change in its outputs. Table 9-1 summarizes the values used to construct Figure 9-3.

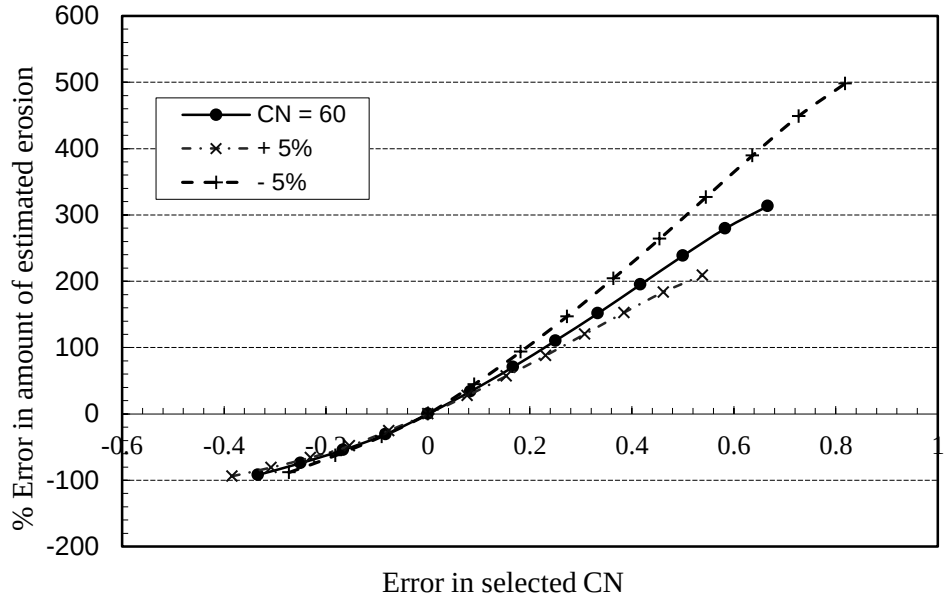

Figure 9-3 % Error in amount of estimated erosion relative to Error in CN selection

SEDCAD and AnnAGNPS Models

SEDCAD is a site specific model that computes runoff and sediment yield at local plots for the purpose of design of sediment control structures, i.e., detention ponds. AnnAGNPS is a watershed scale model that computes runoff and sediment yields also. Both models use CN hydrology and RUSLE erosion factors, and similar channel routing functions. It was proposed to compare these two models since they are based on the same basic hydrology and sediment erosion technology, however AnnAGNPS could not generate runoff and sediment yield at the field plot scale. AnnAGNPS requires a GIS-based digital elevation model (DEM) to generate flow paths, and public domain DEMs from the USGS are 30 m by 30 m grid. This DEM grid size was too large for AnnAGNPS to operate on a 25 m by 30 m field plots.

References

Angel, P. C. Barton, R. Warner, C. Agouridis, T. Taylor, and S. Hall (2007) "Hydrologic Characteristics, tree growth, and natural regeneration on three loose-graded surface mine spoil types in Kentucky" presentation at the Mid-Atlantic Stream Restoration Conference, Rocky Gap Lodge, Cumberland, Maryland, November 2007. http://www.canaanvi.org/canaanvi_web/events_ed.aspx?collection=cvi_workshops&id=140 accessed December 15, 2007

Barfield, B. J., R. I. Barnhisel, J. L. Powell, M. C. Hirschi, and I. D. Moore. 1983. Eerodibilities and eroded size distribution of western Kentucky mine spoil and reconstructed topsoil. IMMR Final Report No. G1115211 and CRIS Project NO.907-15-2.

Gilley, J. E., G. W. Gee, A. Bauer, W. O. Willis, and R. A. Young. 1977. Runoff and erosion characteristics of surfaced-mined sites in western North Dakota. Am. Soc. Agr. Engr. 20:697-700.

Govers, G. 1987. Spatial and temporal variability in rill development processes at the Huldenberg experimental site. ELSEVIER SCIENCE, IDS No. J4089, ISSN: 0341-8162.

Graves DH, Ringe JM, Pelkki MH, Sweigard RJ, Warner RC. 2000. High value tree reclamation research. In Environmental Issues and Management of Waste in Energy and Mineral Production, Singhal RK, Mehrotra AK (eds). Balkema: Rotterdam.

Hoomehr, S., J.S. Schwartz, and E. Drumm. 2011. *Evaluating the performance of SEDCAD model on steep sloped reclaimed surfaces in the southern Appalachian region*. ASCE/ EWRI World Water & Environmental Resources Congress; Palm Springs CA; May 22-26, 2011.

Hoomehr, S., J.S. Schwartz, W.C. Wright, and E.C. Drumm. 2010. Surface erosion and sediment yields on steep-sloped coal mining reclamation sites in the Appalachian region. in ASCE/EWRI, ed., World Water & Environmental Resources Congress: Providence, RI.

Jeldes, Isaac A., Siavash Hoomehr, Wesley C. Wright, P.E., John S. Schwartz, P.E. David E. Lane, P.E., Eric C. Drumm, P.E. 2010. National Meeting of the American Society of Mining and Reclamation, Pittsburgh, PA Bridging Reclamation, Science and the Community June 5 - 11, 2010. R.I. Barnhisel (Ed.) Published by ASMR, 3134 Montavesta Rd., Lexington, KY 40502.

Mcintosh J. E. and R. I. Barnhisel. 1993. Erodibility and sediment yield by natural rainfall from reconstructed mine spoils. Journal of soil science, Volume 156, Issue 2, pp. 118-126.

McKenzie, G. D., and J. R. J. Studlick. 1979. Erodibility of surface-mine spoil banks in southeastern Ohio: An approximation. J. Soil Water Conserv. 34: 187-190.

Meyer L. D., and W. C. Harmon 1989. How side slope length and steepness affect side slope erosion. Trans. ASAE 32:639-644.

Mitchell, J. K., W. C. Moldenhauer, and D. D. Gustavson. 1983. Erodibility of selected reclaimed surface mined soils. Am. Soc. Agr. Engr. 26:1413-1417.

Mostaghimi, S., and J. K. Mitchell. 1983. Erosion characteristics of surface mined soils. Proc. 1983 Symposium Surf. Mining Hydrol., Sediment., and Reclam. University of Kentucky, Lexington, pp. 537-541.

Pinson, W.T., Yoder, D.C., Buchanan, J.R., Wright, W.C., Wilkerson, J.B. 2003. Design and evaluation of an improved flow divider for sampling runoff plots. J. Applied Engineering in Agriculture Vol. 20, No. 4, p433-437.

Renard, K. G., McCool, D. K., Cooley, K. R. Mutchler, C. K., and Foster, G. R. 1993. Rainfall-runoff erosivity factor (R). Chapter 2 in Renard, Foster and Weesies (eds) " Predicting Soil Erosion by Water-A Guide to

Conservation Planning with the Revised Universal Soil Loss Equation RUSLE", Publication ARS. U.S. Department of Agriculture, Washington, DC, in press.

Shukla M.K., Lal R, Underwood J, Ebinger M. 2004. Physical and hydrological characteristics of reclaimed minesoils in southeastern Ohio. Soil Science Society of America Journal 68(4): 1352–1359.

Torbert, J.L. and J.A. Burger, Influence of grading intensity on ground cover establishment, erosion, and tree establishment on steep slopes. International Land Reclamation and Mine. Drainage Conference and the Third International Conference on the Abatement of Acidic Drainage, Pittsburgh, 1994.

Torri, D., M. Sfalanga and G. Chisci. 1987. Threshold Conditions for Incipient Rilling. Bryan, R.B. (ed). Rill Erosion: Processes and Significance. Catena Supplement 8. W. Germany:Catena Verlag. 97-105.

Toy T. J., G. R. Foster, and K. G. Renard. 1999. RUSLE for mining, construction and reclamation lands. Journal of Soil and Water Conservation, Volume 54, Issue 2, pp. 462-467.

U.S. Dept. of the Interior. 1977. Surface mining reclamation and enforcement provisions. Federal Register 42:62685-62688, December 13.

W.C. Ashby, C.A. Kolar, and M.L. Guerke, Our Reclamation Future with Trees, Coal Extraction and Utilization, Research Center, Southern Illinois at Carbondale, 1978.

William R. Thomas; Matthew H. Peikki; James M. Ringe 1999. Proceedings, 12th central hardwood forest conference; 1999 February 28-March 1-2; Lexington, KY.Gen. Tech. Rep. SRS-24. Asheville, NC: U.S. Department of Agriculture, Forest Service, Southern Research Station.293 p. [Peer-reviewed paper]. 79

Wischmeier, W. H, and D. D. Smith. 1965. Predicting rainfall-erosion losses from cropland east of the Mountains-Guide for selection of practices for soil and water conservation. Agr. Handbook. No. 282. U.S. Dept. of Agriculture, Washington, DC.

Wischmeier, W. H. and D. D. smith. 1978. Predicting rainfall erosion losses. Agriculture Handbook No. 537, USDA, Washington, D.C.

Zhang G. H., Yu-mei Liu, Yan-feng Han, X. C. Zhang 2009. Sediment Transport and Soil Detachment on Steep Slopes: I. Transport Capacity Estimation. Soil Science Society of America Journal Vol. 73 No. 4, pp. 1291-1297.

Renard, K. G., McCool, D. K., Cooley, K. R. Mutchler, C. K., and Foster, G. R. 1993. Rainfall-runoff erosivity factor (R). Chapter 2 in Renard, Foster and Weesies (eds) " Predicting Soil Erosion by Water-A Guide to Conservation Planning with the Revised Universal Soil Loss Equation RUSLE", Publication ARS. U.S. Department of Agriculture, Washington, DC, in press.

Chapter 10 Summary and Conclusions

Background

Mine reclamation activities have traditionally been very successful with regard to the establishment of grass covers, especially in areas where the slopes are moderate to low. Establishment of forest cover in reclaimed areas has been less successful, primarily due to construction techniques which focus on stability of the landforms and erosion control using high levels of compaction and aggressive grass covers. Research has established that over-compaction of the reclaimed surface soils impedes the establishment of healthy fast growing forests, which has led to the development and promotion of the Forestry Reclamation Approach (FRA). One of the most critical aspects of the FRA is the use of low compaction grading techniques to assure that a zone of "loose" material remains at the surface to encourage tree survival and growth. Unfortunately, the mass stability of steep slopes is dependent on these greater compaction levels, since the strength of the reclaimed materials is highly dependent upon the level of compaction. The increased strength associated with higher levels of compaction is also needed to reduce erosion and the limit the potential for sediment to enter nearby streams. Previous research studies on low compaction grading methods have concentrated on reclamation work in relatively flat terrain (1-3 degrees), yet the reforestation of reclaimed areas with steep slopes is perhaps even more important.

To investigate the effects of low compaction grading on slope stability, erosion, and sediment yield on steep slopes (> 20 degrees), three reclaimed mine sites in Tennessee were identified, and instruments installed to measure weather/precipitation, surface runoff, and suspended sediment load. Each of the three sites was subdivided into four plots with different ground cover treatments. Ground covers and trees were planted in March 2009 as part of a separate research project conducted by others. However, it should be noted that ground covers were never effectively established due to the number and intensity of spring/summer storms events in 2009. The runoff and sediment erosion data were used to develop hydrologic and soil erosion parameters for CHIA modeling efforts and sediment pond design using the SEDCAD model. The overall objectives of the research were:

1. Develop/document appropriate construction procedures for reclamation of steep slopes to satisfy the conflicting concerns of providing a loosely compacted rooting medium for tree growth yet assuring there are zones of sufficient compaction to provide structural stability;
2. Investigate the influence of low compaction surface growth zones on the stability of steep slopes, and the extent to which complex slope geometries may serve as a strategy for increasing slope stability while avoiding long planar slopes which may lead to excessive erosion; and
3. Demonstrate that these methods provide satisfactory erosion and sediment control in order surface water quality from mine lands can be maintained. Based on field measurements, estimate appropriate input parameters for commonly used hydrologic and sediment models, primarily developing a CN runoff value and sediment erodibility parameter (RUSLE K factor) for low-compacted steep slopes reclaimed mine lands.

Instrumented Study Sites

Three mine sites in eastern Tennessee reclaimed using low compaction techniques were identified with the assistance of local mine operators. The construction process was described, and a summary of the ground cover application rates and cover implemented by others was described. Details of the site instrumentation were provided, which included flumes with pressure (stage) sensors to measure runoff duration, a runoff-sediment collection system, and weather stations which recorded precipitation, solar radiation, wind speed, wind direction, and temperature. All data were recorded at intervals of 5 minutes, and could be downloaded from the acquisition-storage hardware off-site by telemetry.

Site characterization and slope stability

Survey data and the slope inclination were obtained for each of the three study sites, and the reclaimed materials were characterized with respect to the particle size distribution and unit weight. To explore the spatial variability of the unit weight, measurements were obtained across each site on a 3m by 3m grid. It was suggested that field observations of the angle of repose of the surface materials during reclamation could be taken as an estimate the shear strength of the loose soil layer of material, and that the infinite slope method was a simple yet appropriate method of evaluating the mass stability of the slopes. The stability determined from the infinite slope method was verified by both the traditional limit equilibrium method and by the Finite Element method. The long term stability of the slopes at all three sites was found to be satisfactory, producing Factors of Safety well above the value of 1.3 specified in the general requirements for surface mining in 30 CFR 816/817.102(a)(3). The infinite slope method was extended to evaluate the seismic stability of reclaimed mine slopes, and demonstrated through an example.

Stability of non planar slopes

Constructed slopes and reclaimed land are often designed to follow planar geometries because engineering analysis techniques and typical surveying and construction practices tend to favor this shape slope profile. However, in nature, slopes are seldom planar in cross section, and more complex slope geometries are common with the cross section often tending to be concave. Laboratory and computational studies have shown that a concave slope contours may reduce erosion and sediment yield, suggesting that the concave slope profiles observed in nature may be very efficient with respect to limiting erosion and sediment. The geomorphological evolution of slopes toward an equilibrium shape from the generalized principle of minimum rate of energy dissipation was discussed, suggesting that for certain boundary conditions, slopes may evolve into concave shapes in the long term. Based on the critical equilibrium theory developed by Sokolovski in 1960, a relatively simple approximate solution was developed for determining the shape of the concave slope contour for a given factor of safety (FS). This new method was demonstrated through an example reclaimed slope, and solutions using the traditional Limit Equilibrium method (LEM) and Finite element (FEM) analyses showed that the proposed design methodology is accurate. For general readability and to facilitate the practical application of the design method for non planar slopes, the details, mathematical derivation, and error analysis for the concave slope approach are separated from the general description of the method and example problem.

Hydrology of the sites and Curve Numbers for the rainfall-runoff relationships

Investigating the runoff hydrology of reclaimed surfaces is vital for design of storm water sediment control structures on FRA-constructed sites. Engineers traditionally use the runoff curve number (CN) method to predict rainfall-runoff relationships for ungauged watersheds, which method was developed by the USDA Soil Conservation Service (SCS), now the Natural Resource Conservation Service (NRCS). CN values typically assumed for reclaimed mine surfaces have not been verified, particularly when the low compaction construction methods recommended by the FRA are used on steep slopes. The three instrumented sites were monitored over time to determine the discharge volume for a range of precipitation events, and no ground cover. The NRCS rainfall-runoff relationship is dependent on hydrologic initial abstraction (Ia) and it is a function of the maximum potential retention or storage (S) on the land surface. Historically Ia was assumed to be equal to 0.2·S, however more recent references suggest it should be closer to 0.05·S. An attempt was made to compute the factor (λ) between Ia and S, but due to the rapid response time for runoff to begin at these sites (< 5 minutes) an accurate estimate for λ could not be obtained. In our analysis, we assumed a λ of both 0.05 and 02. Results determined that for a λ of 0.05, the average CN to be 62.2 (range 20.5 to 98.8). Results determined that for a λ of 0.2, the average CN to be 71.8 (range 30.7 to 98.8). Further, it is shown that there are no significant differences between CN values among three sites - that they are statistically the same. CN values were estimated between 58.5 and 60 using an asymptotic method applying both P-Q and I_{30}-Q Frequency Match analysis techniques; these estimates represent the best values to use for predicting runoff. Overall, these CN values can be used in hydrologic modeling efforts and represent the maximum potential runoff from a site because of the lack of ground cover. They have wide application in practice in southern Appalachia region in order to estimate runoff from reclaimed mine sites employing the FRA methods, and to size sediment control ponds.

Observed erosion and predicted soil loss relationships

Although the FRA has been demonstrated to be effective with respect to enhancing the growth and survivability of the trees, there has been limited investigation on the effect of this technique on erosion and sediment yield. Data collected from the instrumented sites was used to determine an appropriate value of the soil erodibility factor, K, for mine sites reclaimed using low compaction methods. This is an important parameter used in the widely accepted Revised Universal Soil Loss Equation (RUSLE), to predict erosion. It is also used along the CN in SEDCAD, which is used by OSM engineers to design sediment control basins. Because each site had a full weather station, rainfall erosivity or the R factor in RUSLE was computed and could be compared with the K factor relative to that factor. The R factor is based on total storm rainfall energy and the maximum 30-minute intensity. Because the sites were steep and lacked ground cover rills developed over the period of study. To date, a changing K factor for a soil-land character has not been reported, however our data illustrates the K factor that changed with time until rills reached geomorphic equilibrium. In summary, results found the average K factor to be 0.30 during rapid rill growth, 0.07 during the transition period towards geomorphic equilibrium, and 0.05 when the rills were assumed to be geomorphically stable.

In addition to the RUSLE factor computations, measurements of the particle size distribution (PSD) of the eroded and transported sediment were obtained over the study period. PSD is another key input parameter used in SEDCAD and the design of sediment control ponds and selection of other best

management practices (BMPs) used to control sediment. During rill development, the median particle size was approximately 2 mm, and after the rills stabilized the median was less than 0.01 mm. Measurements of the temporal variation of the particle size distribution over the study period provides insight into how the sediment size distribution may change over time with rill development, leading to a better understanding of the erosional process on loose-compacted steep-sloped sites.

Sediment modeling of reclaimed slopes

To support the design of runoff and sediment control structures, computer-based hydrology and sediment erosion models are frequently used. SEDCAD is a comprehensive package which has been widely used in the mining industry, primarily used in the design of sediment control basins. However, most experience with SEDCAD has been on low to moderate sloped surfaces, and it has not been verified on steep slopes constructed with low compaction/FRA methods. To address this issue, SEDCAD was investigated for the estimation of erosion and sediment delivery from the instrumented sites, and the sensitivity of SEDCAD outputs was evaluated with respect to curve number value (CN) and erodibility of reclaimed material (K). The results of this study found that generally SEDCAD overestimated the sediment yield from the three study sites when erosivity (R factor) was greater than about 25 ft·tonf. The CN and K factor estimates derived in this study can also be used in watershed-scale sediment yield models such as AnnAGNPS or SWAT. Because AnnAGNPS was developed for watershed scale applications and SEDCAD was developed for local site specific applications, performance of the two could not be compared. In general these results provide a better understanding in interpretation of SEDCAD outputs, and the suggested parameters will be highly useful in designing runoff and sediment control structures and selection of best management practices (BMPs) in the mining industry.

Appendix A

Details on Site Characterization

Slope profiles of Mountainside, National and Premium sites

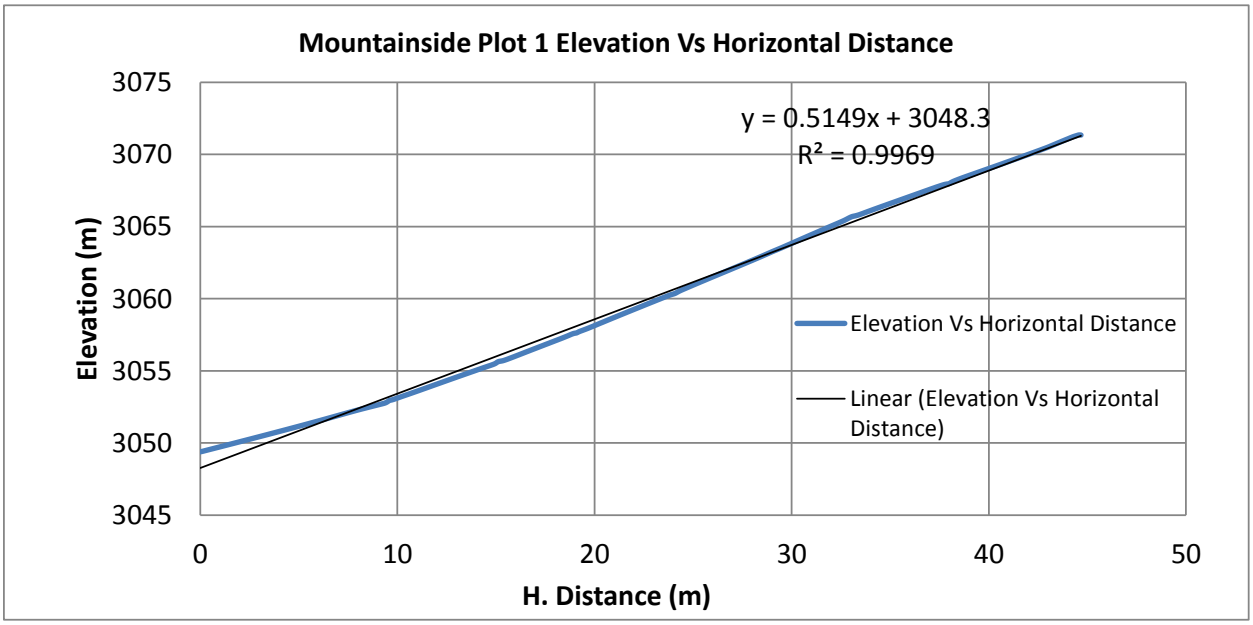

Figure B-1 Slope profile. Plot 1 at Mountainside site (slope angle = arctan (0.5149) = 27.2˚)

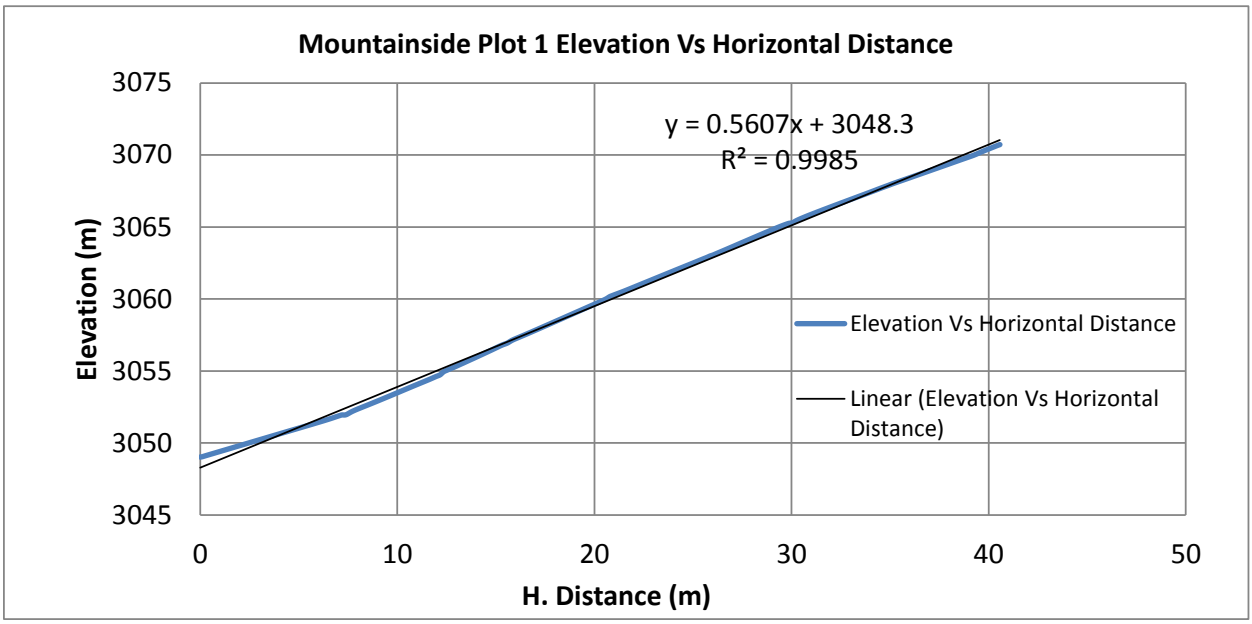

Figure B-2 Slope profile. Plot 2 at Mountainside site (slope angle = arctan (0.5607) = 29.3˚)

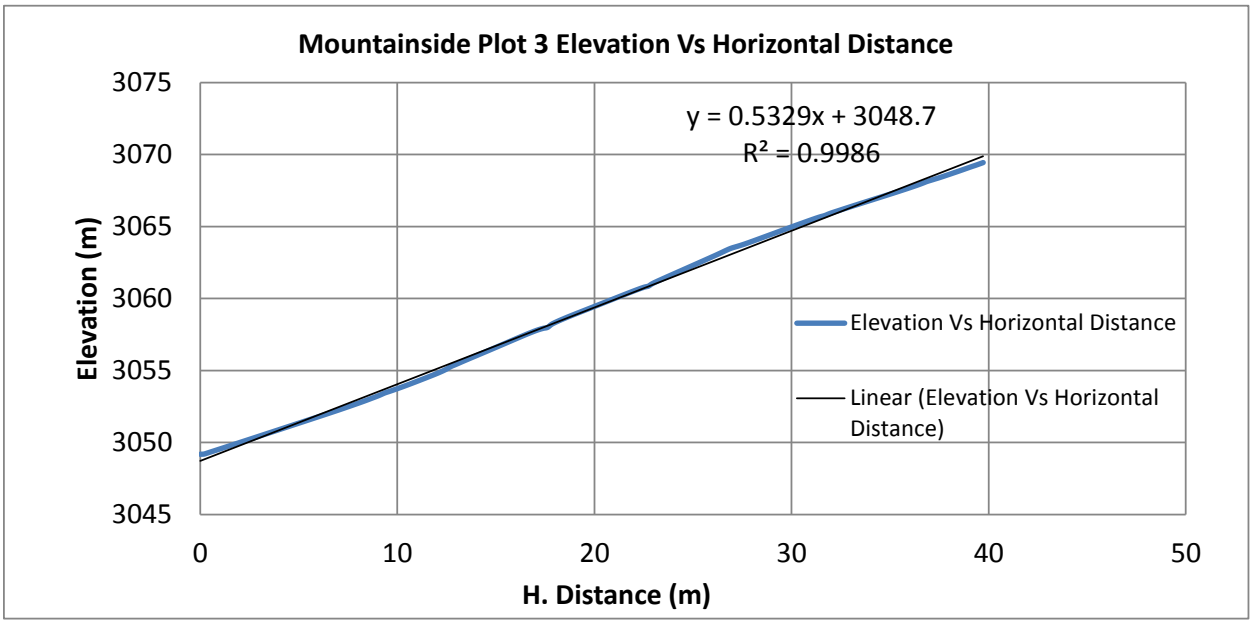

Figure B-3 Slope profile. Plot 3 at Mountainside site (slope angle = arctan (0.5329) = 28.05˚)

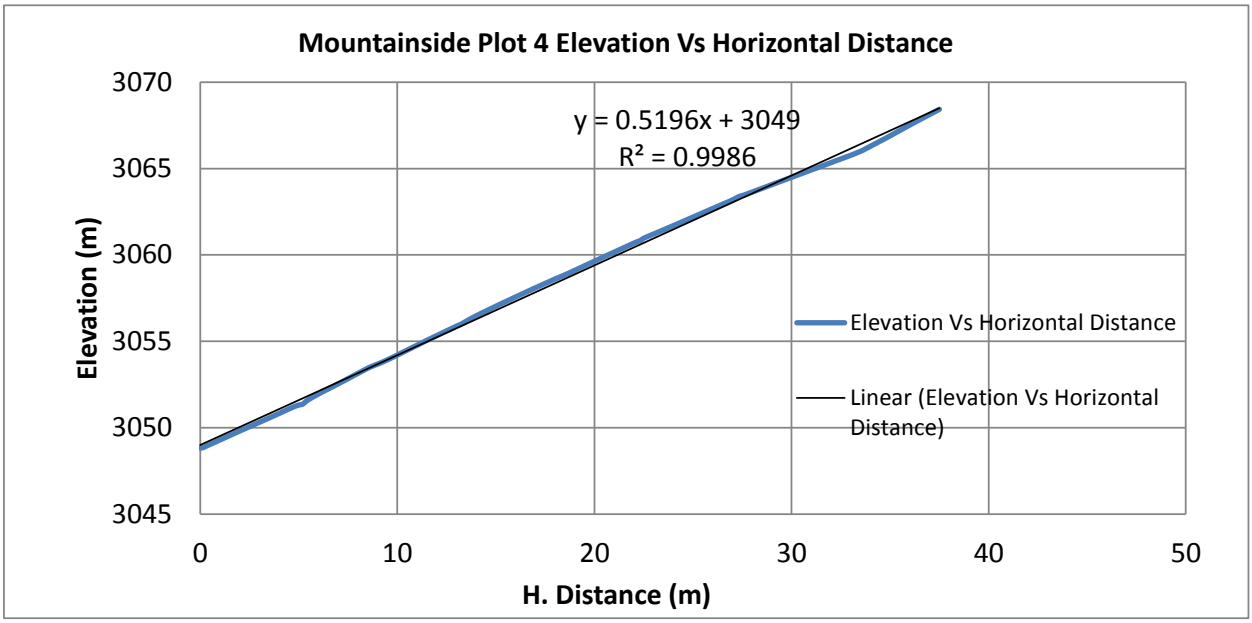

Figure B-4 Slope profile. Plot 4 at Mountainside site (slope angle = arctan (0.5196) = 27.5˚)

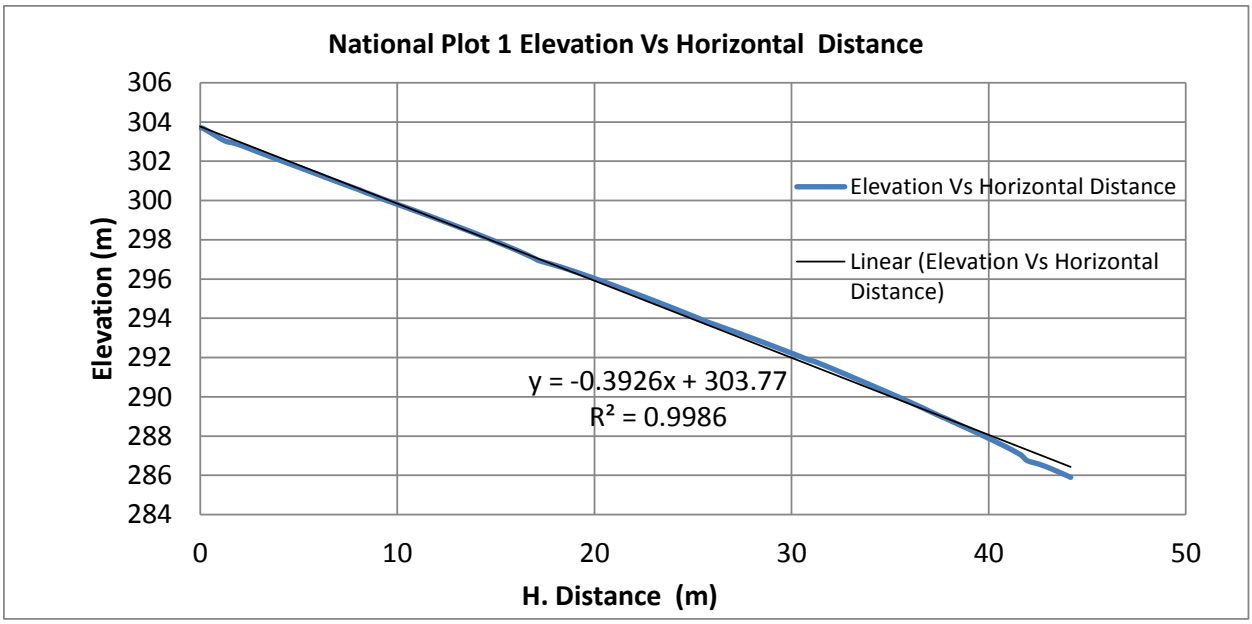

Figure B-5 Slope profile. Plot 1 at National site (slope angle = arctan (0.3926) = 21.4˚)

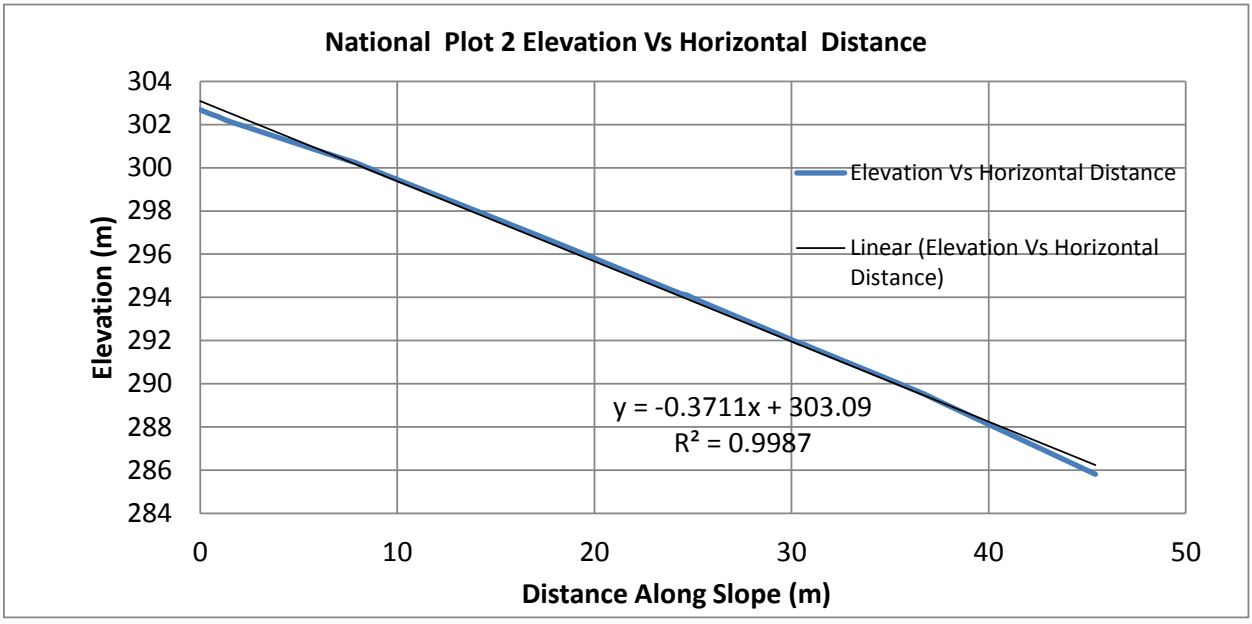

Figure B-6 Slope profile. Plot 2 at National site (slope angle = arctan (0.3711) = 20.4˚)

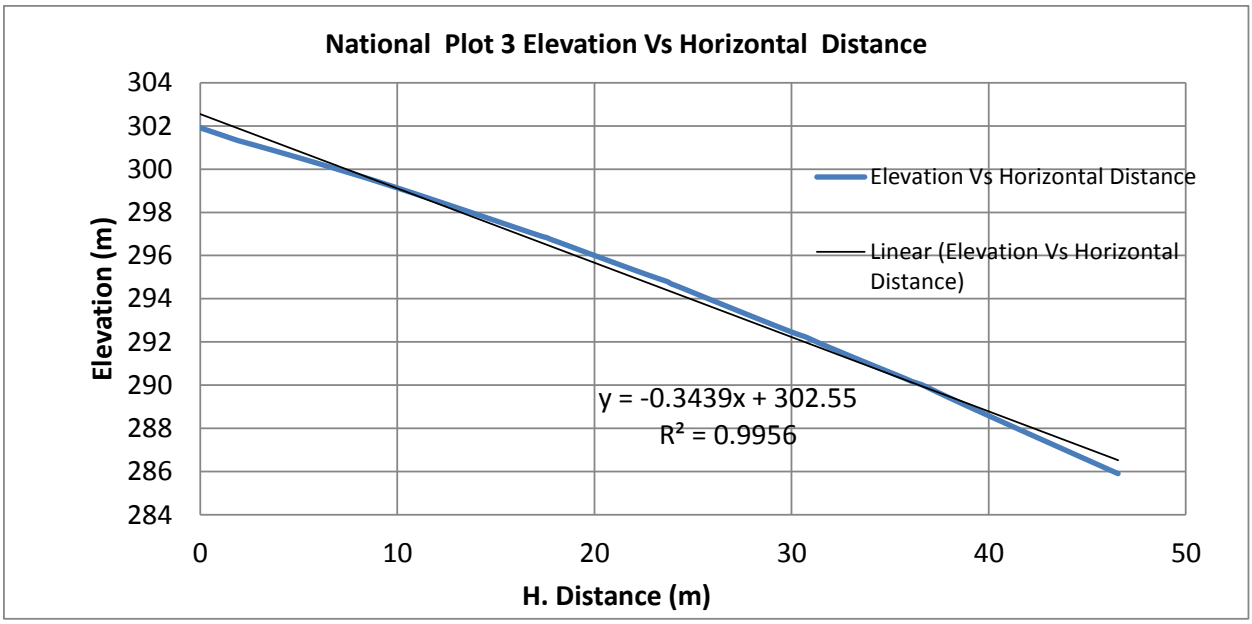

Figure B-7 Slope profile. Plot 3 at National site (slope angle = arctan (0.3439) = 19˚)

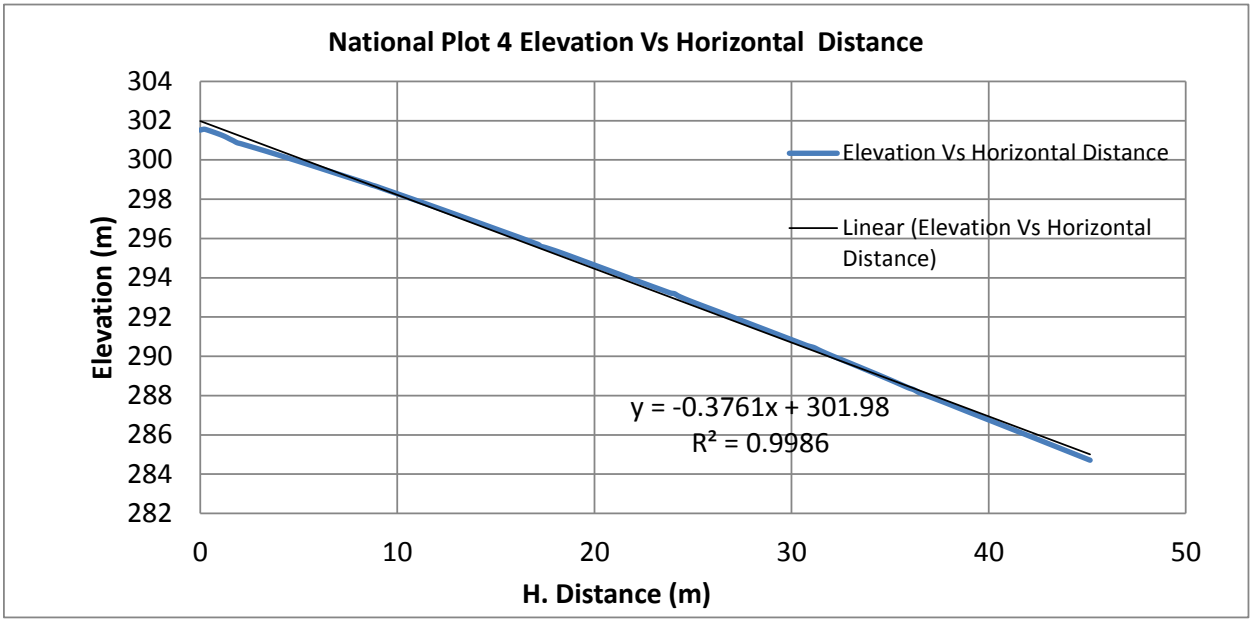

Figure B-8 Slope profile. Plot 4 at National site (slope angle = arctan (0.3761) = 20.6˚)

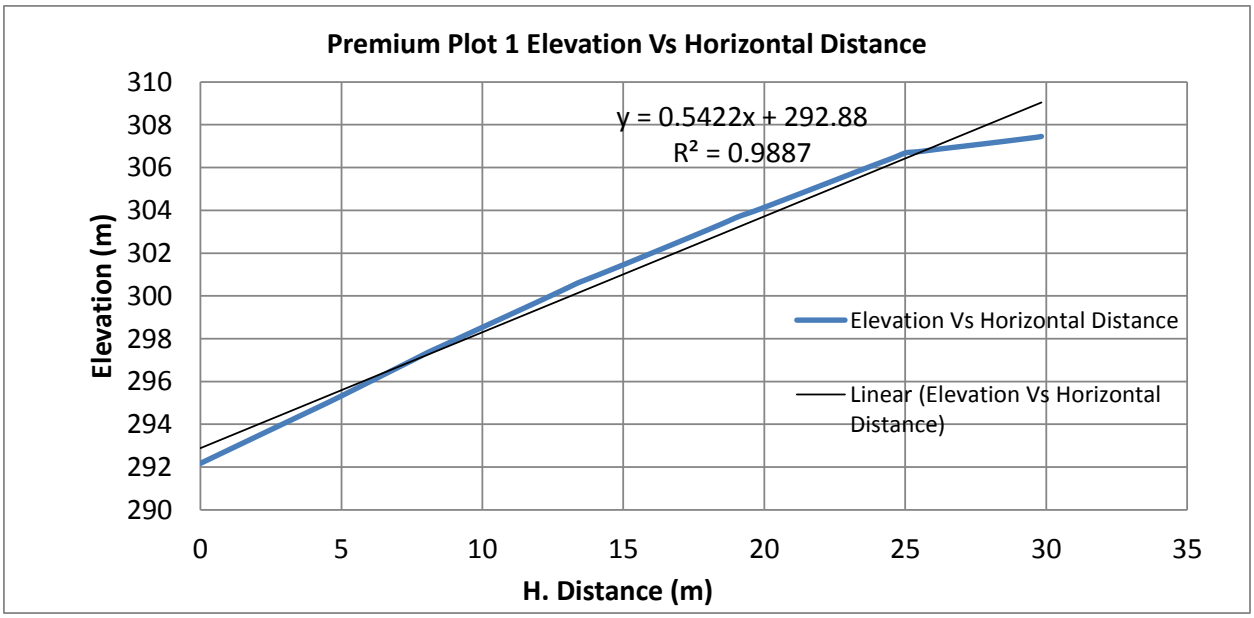

Figure B-9 Slope profile. Plot 1 at Premium site (slope angle = arctan (0.5422) = 28.5˚)

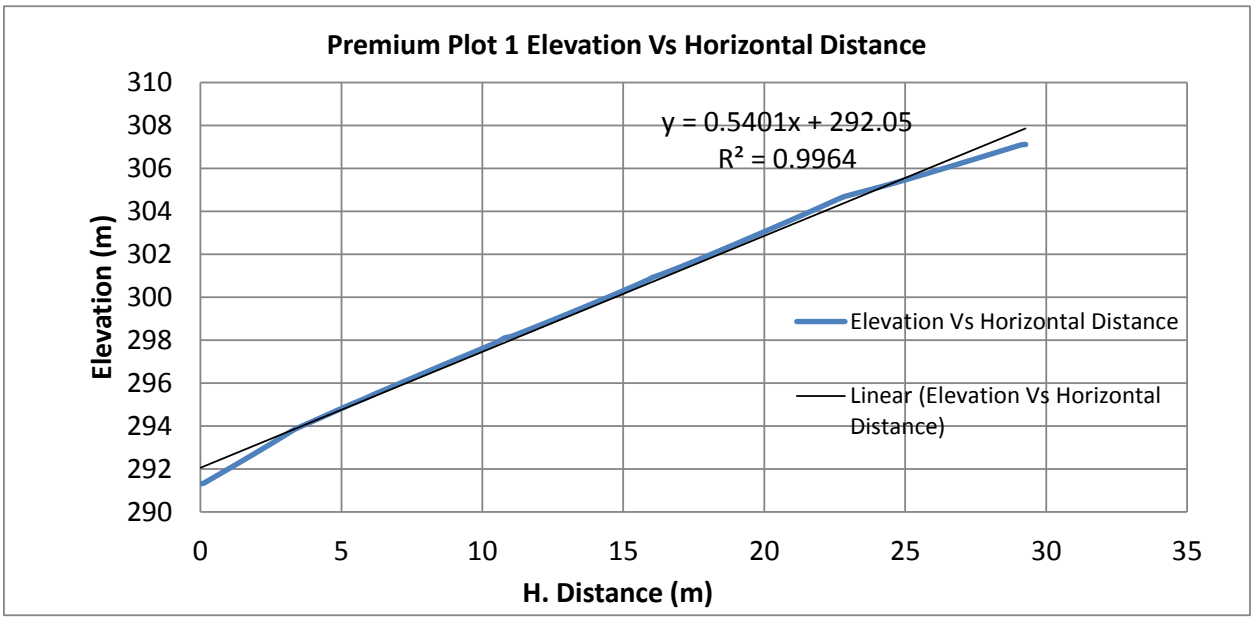

Figure B-10. Slope profile. Plot 2 at Premium site (slope angle = arctan (0.5401) = 28.4˚)

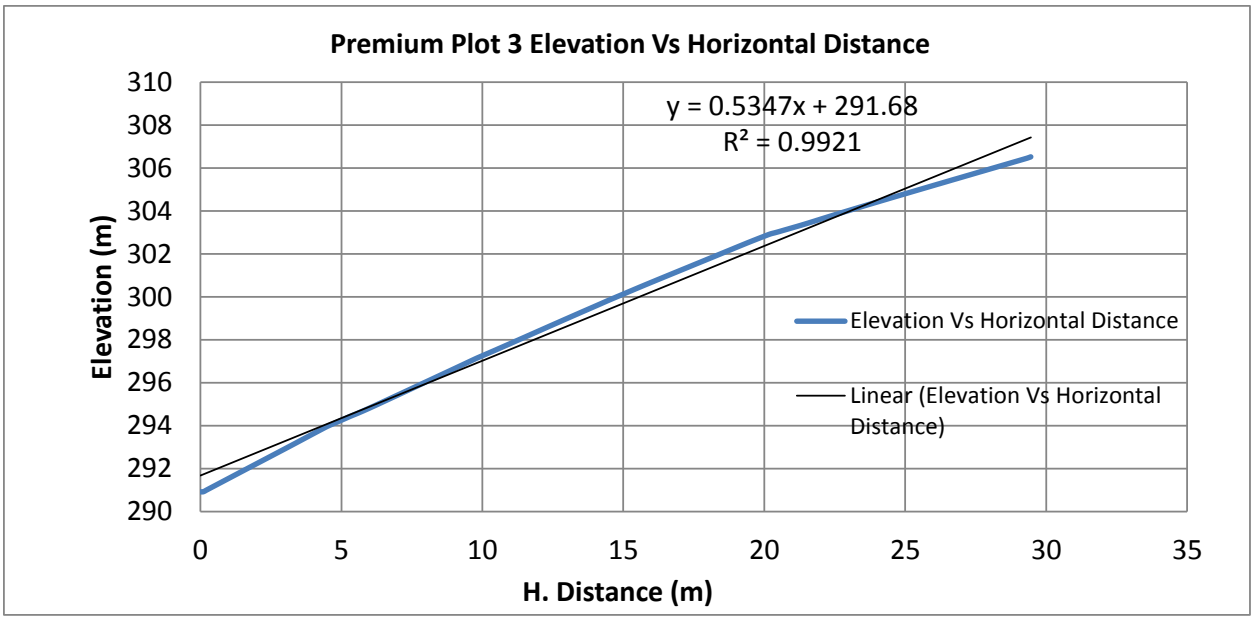

Figure B-11. Slope profile. Plot 3 at Premium site (slope angle = arctan (0.5347) = 28.1˚)

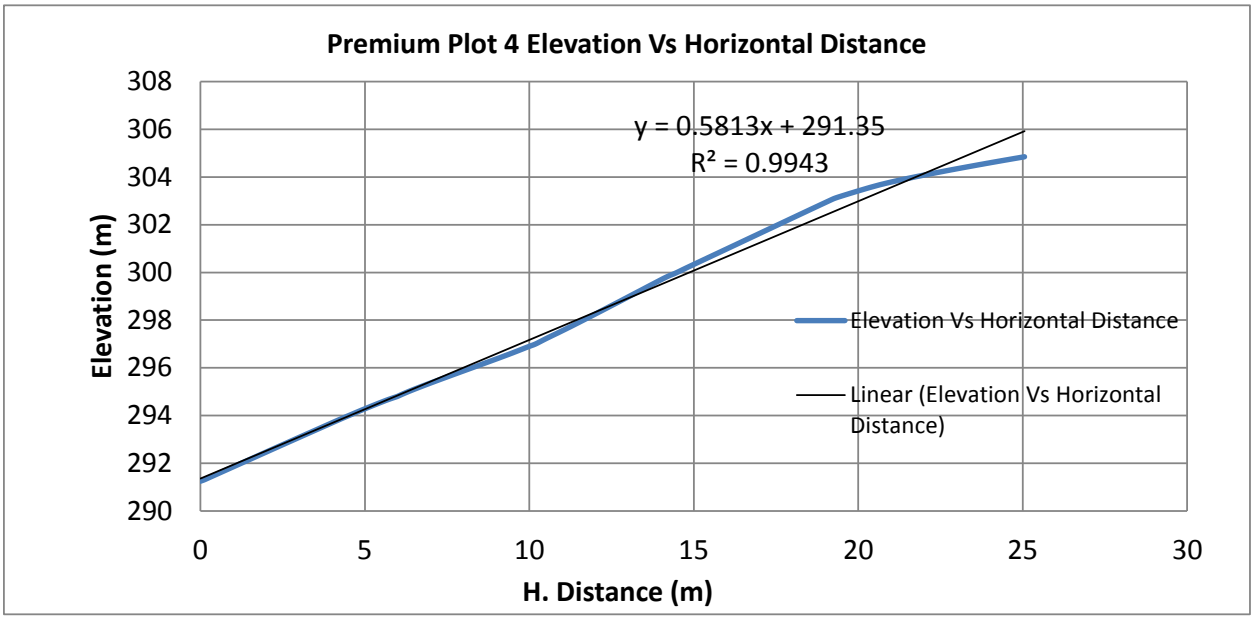

Figure B-12. Slope profile. Plot 4 at Premium site (slope angle = arctan (0.5813) = 30.2˚)

Bulk dry unit weight, bulk wet unit weight and moisture content at Mountainside, National and Premium sites

Table B-1. Values of bulk dry and bulk wet unit weights and moisture content measured within each 3 m by 3 m sampling area at Mountainside site

		Top of the Plot						
	Sample Location	Column A	Column B	Column C	Column D	Column E	Column F	Column G
Depth (m)	Row 1	0.3048	0.3048	0.3048	0.3048	0.3048	0.3048	0.3048
WD (kN/m3)		18.94	19.73	19.43	19.53	18.46	17.99	19.84
DD (kN/m3)		16.96	17.78	17.42	17.42	16.68	16.40	18.19
M%		11.7	11.0	11.6	12.1	10.7	9.7	9.1
Depth (m)	Row 2	0.3048	0.3048	0.3048	0.3048	0.3048	0.3048	0.3048
WD (kN/m3)		19.42	18.71	18.76	18.06	18.82	19.62	19.84
DD (kN/m3)		17.67	17.06	17.18	16.29	16.98	17.78	17.72
M%		9.9	9.7	9.1	10.9	10.8	10.3	12.0
Depth (m)	Row 3	0.3048	0.3048	0.3048	0.3048	0.3048	0.3048	0.3048
WD (kN/m3)		18.33	19.24	20.19	19.04	20.34	19.04	19.23
DD (kN/m3)		16.48	17.28	18.55	17.15	18.50	17.20	17.51
M%		11.3	11.4	8.8	11.0	9.9	10.7	9.8
Depth (m)	Row 4	0.3048	0.3048	0.3048	0.3048	0.3048	0.3048	0.3048
WD (kN/m3)		17.89	19.05	18.76	18.35	18.00	18.74	18.98
DD (kN/m3)		16.48	17.47	17.15	16.71	16.62	17.04	17.03
M%		8.6	9.1	9.3	9.8	8.3	10.0	11.4
Depth (m)	Row 5	0.3048	0.3048	0.3048	0.3048	0.3048	0.3048	0.3048
WD (kN/m3)		18.60	16.99	17.99	18.60	17.70	18.65	18.63
DD (kN/m3)		16.90	15.58	16.33	17.04	15.83	17.07	17.14
M%		10.0	9.1	10.1	9.1	11.8	9.2	8.7
Depth (m)	Row 6	0.3048	0.3048	0.3048	0.3048	0.3048	0.3048	0.3048
WD (kN/m3)		18.58	17.99	18.72	17.78	18.87	18.79	18.35
DD (kN/m3)		16.82	16.22	17.07	16.16	17.07	17.04	16.46
M%		10.5	10.9	9.7	10.0	10.5	10.2	11.5
Depth (m)	Row 7	0.3048	0.3048	0.3048	0.3048	0.3048	0.3048	0.3048
WD (kN/m3)		16.81	18.61	18.83	18.93	19.29	19.46	19.43
DD (kN/m3)		14.94	16.87	16.98	17.28	17.70	17.70	17.72
M%		12.5	10.3	10.9	9.6	9.0	9.9	9.7
Depth (m)	Row 8	0.3048	0.3048	0.3048	0.3048	0.3048	0.3048	0.3048
WD (kN/m3)		23.38	22.48	21.99	23.82	22.51	21.92	23.57
DD (kN/m3)		20.50	19.64	19.20	21.03	20.30	20.31	21.90
M%		14.0	14.5	14.6	13.2	10.9	7.9	7.6
Depth (m)	Row 9	0.3048	0.3048	0.3048	0.3048	0.3048	0.3048	0.3048
WD (kN/m3)		22.65	22.81	23.46	23.17	22.31	22.97	24.62
DD (kN/m3)		20.94	20.83	21.60	21.43	20.36	21.49	22.75
M%		8.2	9.5	8.6	8.1	9.6	6.9	8.2
Depth (m)	Row 10	0.3048	0.3048	0.3048	0.3048	0.3048	0.3048	0.3048
WD (kN/m3)		23.80	23.14	23.49	23.77	22.92	23.02	23.02
DD (kN/m3)		22.06	21.55	21.71	22.47	21.44	21.40	21.54
M%		7.9	7.4	8.2	5.8	6.9	7.6	6.9
Depth (m)	Row 11	0.3048	0.3048	0.3048	0.3048	0.3048	0.3048	0.3048
WD (kN/m3)		23.16	22.64	23.13	23.64	23.20	22.81	23.57
DD (kN/m3)		20.94	20.75	21.40	21.68	21.26	21.03	21.77
M%		10.6	9.1	8.1	9.1	9.2	8.4	8.2
Depth (m)	Row 12			0.3048				
WD (kN/m3)				23.44				
DD (kN/m3)				21.95				
M%				6.8				
		Bottom of the Plot						

Table B-2. Values of bulk dry and bulk wet unit weights and moisture content measured within each 3 m by 3 m sampling area at National site

		Top of the Plot							
	Sample Location	Column A	Column B	Column C	Column D	Column E	Column F	Column G	Column H
Depth (m)	Row 1			0.3048	0.2032	0.3048	0.3048	0.3048	0.3048
WD (kN/m3)				20.31	22.51	22.83	21.33	20.91	19.71
DD (kN/m3)				18.65	20.59	21.44	20.26	19.84	18.69
M%				8.9	9.3	6.5	5.3	5.4	5.5
Depth (m)	Row 2		0.3048	0.3048	0.3048	0.3048	0.3048		0.3048
WD (kN/m3)			20.59	20.31	19.87	22.09	20.63		20.78
DD (kN/m3)			18.98	17.87	17.47	19.09	18.10		18.55
M%			8.5	13.6	13.8	15.7	14.0		12.0
Depth (m)	Row 3		0.3048	0.3048	0.3048	0.3048	0.3048	0.3048	0.3048
WD (kN/m3)			21.41	20.99	20.94	22.43	20.75	20.63	19.87
DD (kN/m3)			19.57	18.50	19.09	20.58	18.32	18.36	18.14
M%			9.4	13.4	9.7	9.0	13.3	12.3	9.5
Depth (m)	Row 4		0.3048	0.3048	0.3048	0.3048	0.2794	0.3048	0.3048
WD (kN/m3)			20.88	20.96	21.22	21.14	18.28	21.66	22.39
DD (kN/m3)			18.43	19.24	18.83	19.54	16.92	19.26	20.26
M%			13.3	8.9	12.7	8.2	8.1	12.5	10.5
Depth (m)	Row 5		0.3048	0.3048	0.3048	0.3048	0.3048	0.3048	0.3048
WD (kN/m3)			20.66	19.79	20.63	21.79	19.70	20.56	21.02
DD (kN/m3)			18.93	17.94	19.20	19.75	18.22	18.88	18.50
M%			9.1	10.3	7.5	10.4	8.1	8.9	13.6
Depth (m)	Row 6		0.3048	0.3048	0.3048	0.3048	0.3048	0.3048	0.3048
WD (kN/m3)			20.64	20.36	20.53	20.56	19.93	22.09	21.38
DD (kN/m3)			18.33	18.77	18.87	18.90	18.19	20.56	19.04
M%			12.6	8.5	8.8	8.8	9.6	7.4	12.3
Depth (m)	Row 7		0.3048	0.3048	0.3048	0.3048	0.3048	0.3048	0.3048
WD (kN/m3)			20.89	21.29	22.59	21.24	20.34	20.74	21.84
DD (kN/m3)			19.65	19.45	20.64	19.84	18.44	18.47	19.82
M%			6.3	9.5	9.4	7.1	10.3	12.3	10.2
Depth (m)	Row 8		0.3048	0.3048	0.3048	0.3048	0.3048	0.3048	0.3048
WD (kN/m3)			19.51	20.11	20.11	19.60	18.69	20.34	21.00
DD (kN/m3)			18.17	18.24	18.08	18.00	17.62	18.68	19.42
M%			7.4	10.3	11.2	8.9	6.1	8.9	8.2
Depth (m)	Row 9	0.3048	0.3048	0.3048	0.3048	0.3048	0.3048	0.3048	0.3048
WD (kN/m3)		21.77	19.82	19.26	20.64	21.16	20.14	20.39	19.23
DD (kN/m3)		19.79	17.95	17.91	18.94	19.62	18.72	18.43	17.51
M%		10.0	10.4	7.6	9.0	7.9	7.6	10.7	9.8
Depth (m)	Row 10	0.3048	0.3048	0.3048	0.3048	0.3048	0.3048	0.3048	0.3048
WD (kN/m3)		20.14	19.90	19.29	19.38	20.08	19.56	20.01	19.45
DD (kN/m3)		18.43	18.80	18.27	17.99	18.74	18.16	18.27	18.21
M%		9.3	5.9	5.6	7.8	7.1	7.7	9.6	6.8
Depth (m)	Row 11	0.3048	0.3048	0.3048	0.3048	0.3048	0.3048	0.3048	0.3048
WD (kN/m3)		19.82	19.12	18.80	19.57	19.73	20.15	20.03	20.85
DD (kN/m3)		18.44	17.73	17.14	18.36	18.32	18.71	18.33	18.55
M%		7.5	7.8	9.7	6.6	7.7	7.7	9.3	12.4
Depth (m)	Row 12	0.3048	0.3048	0.3048	0.3048	0.3048	0.3048	0.3048	0.3048
WD (kN/m3)		19.68	19.40	20.22	19.38	19.53	19.20	20.58	20.45
DD (kN/m3)		18.16	17.94	18.69	17.86	17.86	17.17	18.88	18.33
M%		8.4	8.2	8.2	8.5	9.3	11.8	9.0	11.6
Depth (m)	Row 13	0.3048	0.3048	0.3048	0.3048	0.3048	0.3048	0.3048	0.3048
WD (kN/m3)		19.45	19.81	19.05	19.76	16.96	19.67	19.97	20.04
DD (kN/m3)		18.25	17.94	17.48	17.51	14.56	17.54	18.63	17.84
M%		6.5	10.4	9.0	12.8	16.5	12.1	7.2	12.3
Depth (m)	Row 14		0.3048	0.3048	0.3048	0.3048	0.3048	0.3048	
WD (kN/m3)			19.48	19.86	19.53	18.14	18.82	19.23	
DD (kN/m3)			18.14	17.42	17.03	15.97	17.42	17.65	
M%			7.4	14.0	14.7	13.6	8.0	8.9	
		Bottom of the Plot							

Table B-3. Values of bulk dry and wet unit weights and moisture content measured within each 3 m by 3 m sampling area at the Premium site

		Top of the Plot						
	Sample Location	Column A	Column B	Column C	Column D	Column E	Column F	Column G
Depth (m)	Row 1	0.3048	0.3048	0.2286	0.3048	0.3048	0.3048	0.3048
WD (kN/m3)		20.14	19.84	19.16	16.92	17.29	17.06	17.67
DD (kN/m3)		17.10	17.28	16.71	14.42	15.03	14.24	15.33
M%		17.7	14.8	14.7	17.3	15.1	19.8	15.3
Depth (m)	Row 2	0.3048	0.3048	0.3048	0.3048	0.3048	0.3048	0.3048
WD (kN/m3)		18.16	17.69	18.10	18.14	18.99	17.87	19.23
DD (kN/m3)		15.80	15.58	16.48	15.96	16.95	15.58	15.50
M%		14.9	13.5	9.8	13.7	12.1	14.7	24.0
Depth (m)	Row 3	0.3048	0.3048	0.3048	0.3048	0.3048	0.3048	0.254
WD (kN/m3)		18.21	16.68	18.96	19.53	19.46	20.63	20.15
DD (kN/m3)		16.16	14.04	16.77	17.83	17.07	18.83	18.38
M%		12.6	18.8	13.0	9.5	14.0	9.5	9.7
Depth (m)	Row 4	0.3048	0.254	0.3048	0.3048	0.254	0.3048	0.3048
WD (kN/m3)		18.93	20.88	19.26	17.29	18.25	19.75	19.89
DD (kN/m3)		16.77	18.61	17.54	15.50	16.22	17.47	17.73
M%		12.8	12.2	9.8	11.6	12.5	13.1	12.1
Depth (m)	Row 5	0.3048	0.3048	0.3048	0.3048	0.3048	0.3048	0.3048
WD (kN/m3)		19.68	19.24	17.37	18.58	19.23	19.29	18.35
DD (kN/m3)		17.81	16.57	14.49	15.83	17.18	17.12	16.27
M%		10.5	16.1	19.8	17.4	11.9	12.7	12.8
Depth (m)	Row 6	0.3048	0.2794	0.2794	0.3048	0.2921	0.3048	0.3048
WD (kN/m3)		19.76	17.80	17.06	18.58	19.05	19.81	18.63
DD (kN/m3)		16.85	14.81	15.06	14.98	16.33	17.64	16.29
M%		17.3	20.2	13.3	24.0	16.7	12.3	14.4
Depth (m)	Row 7	0.3048	0.3048	0.3048	0.3048	0.2794	0.3048	0.2794
WD (kN/m3)		20.47	19.54	17.70	17.48	19.12	17.78	14.95
DD (kN/m3)		17.94	17.17	14.54	14.32	15.78	15.63	13.32
M%		14.1	13.8	21.7	22.1	21.1	13.8	12.3
Depth (m)	Row 8	0.3048	0.3048	0.3048	0.3048	0.2794	0.2286	0.2667
WD (kN/m3)		18.32	19.13	18.47	18.25	16.27	14.75	18.83
DD (kN/m3)		15.82	16.49	15.75	15.80	14.81	12.95	17.25
M%		15.8	16.0	17.3	15.5	9.9	13.8	9.2
Depth (m)	Row 9	0.3048	0.3048	0.3048		0.3048	0.3048	0.3048
WD (kN/m3)		19.21	20.23	16.63		17.84	16.57	17.81
DD (kN/m3)		16.71	18.06	13.79		16.66	14.68	16.13
M%		15.0	12.0	20.6		7.1	12.8	10.4
		Bottom of the Plot						

Spatial distribution of the dry unit weight at Mountainside, National and Premium sites

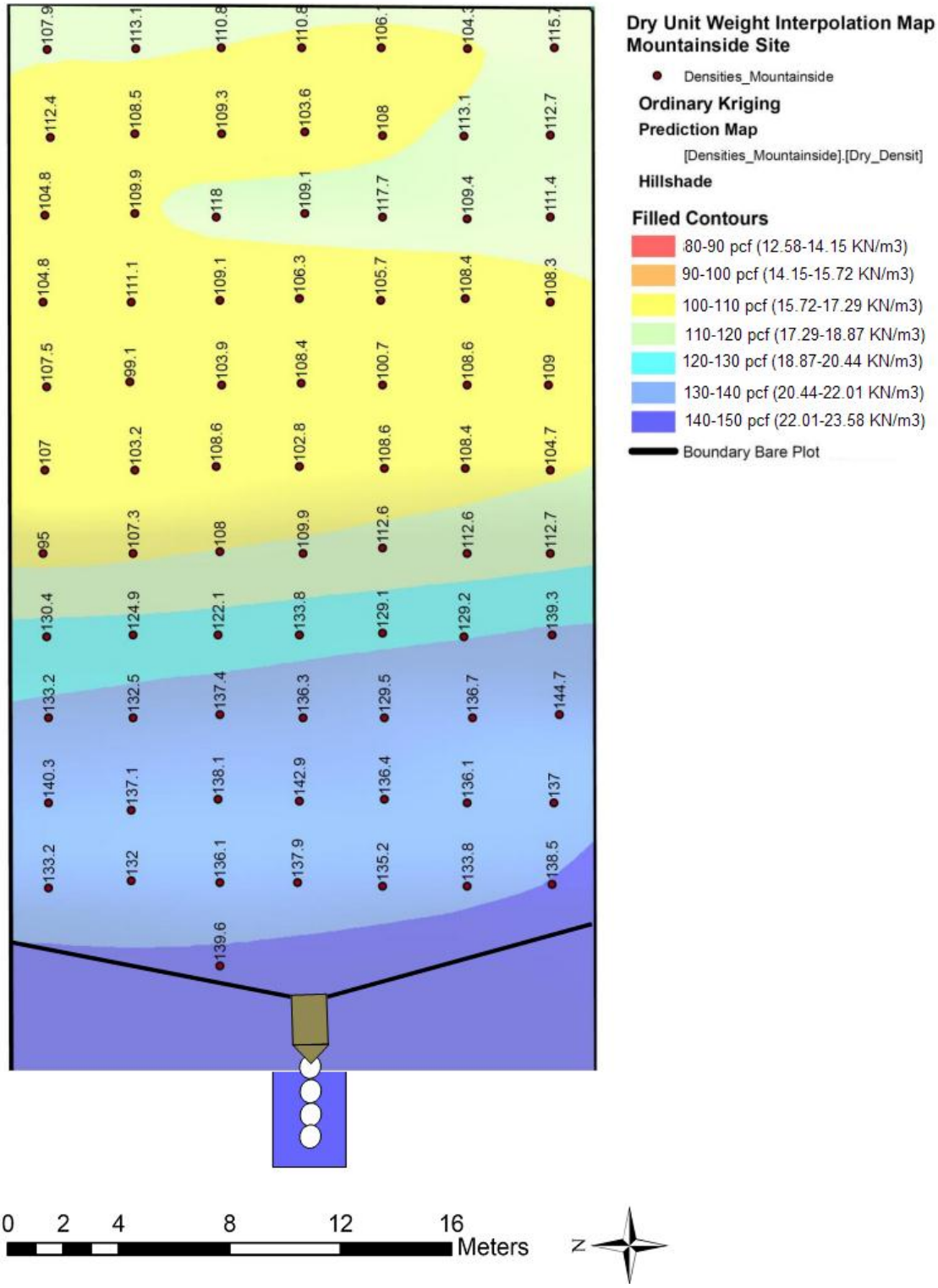

Figure B-13 Spatial distribution of the dry unit weight of the looser layer along the bare plot in Mountainside site (numerical results on figure are shown in pcf)

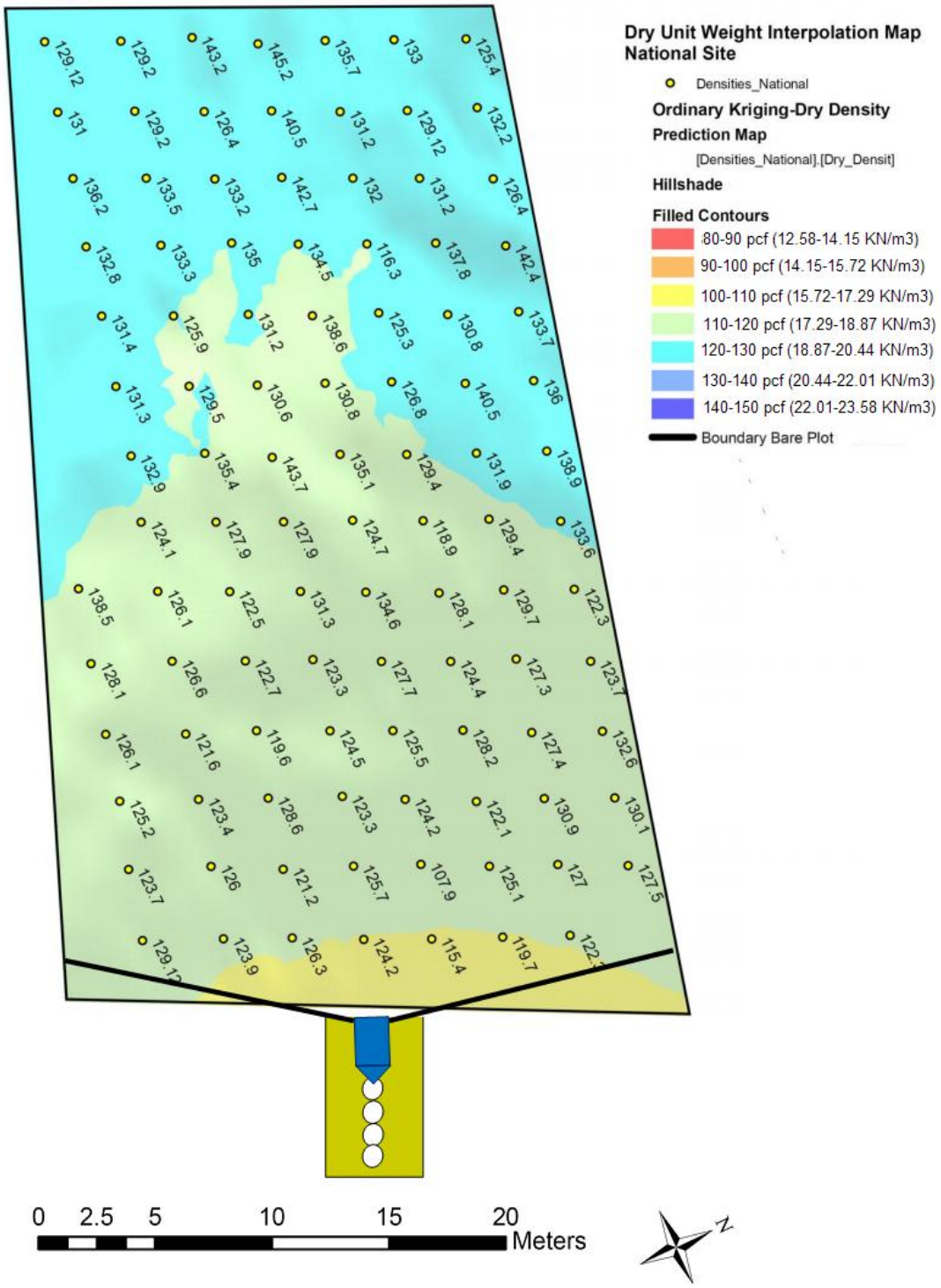

Figure B-14 Spatial distribution of the dry unit weight of the looser layer along the bare plot in National site (numerical results on figure are shown in pcf)

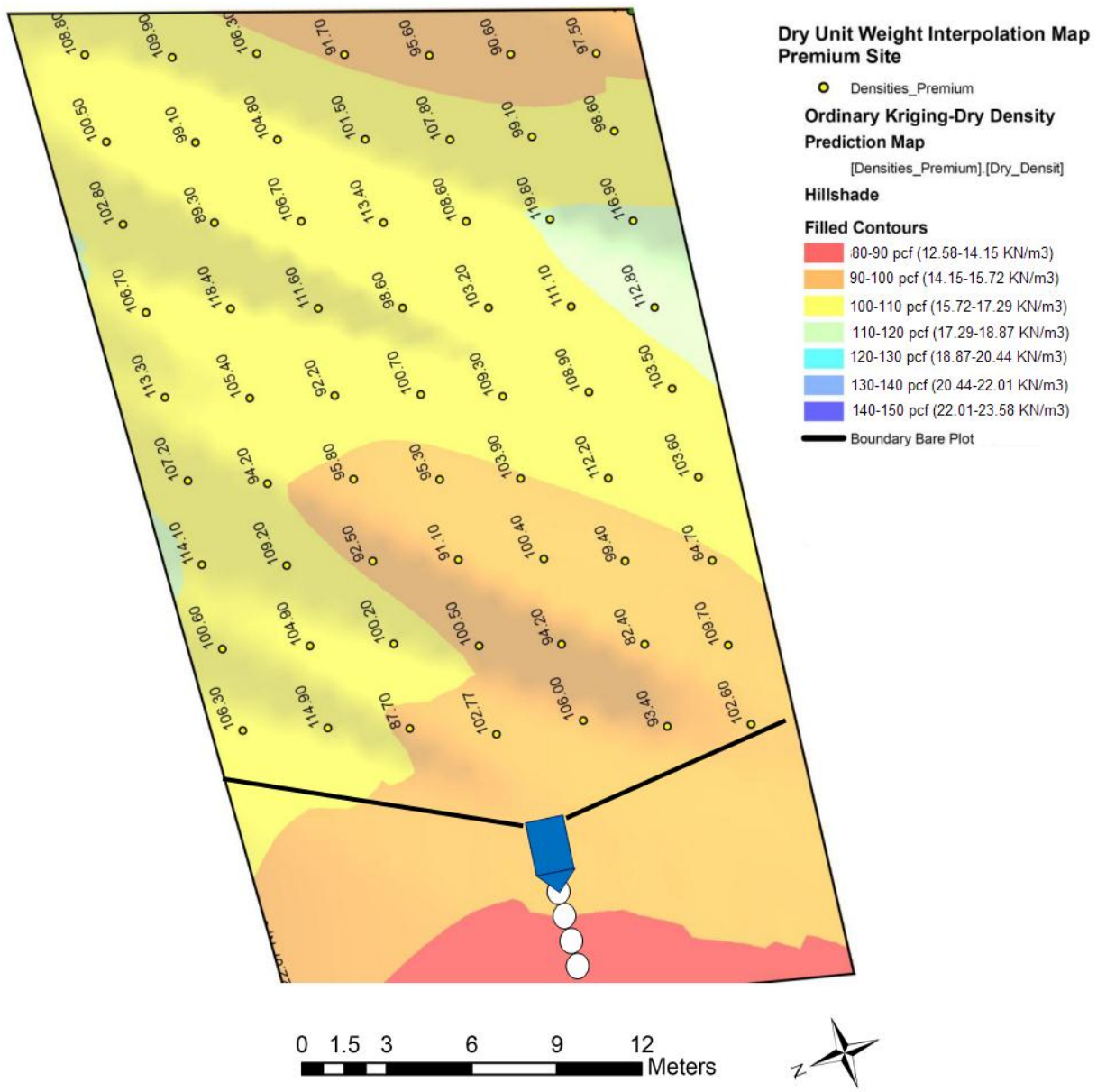

Figure B-15 Spatial distribution of the dry unit weight of the looser layer along the bare plot in Premium site (numerical results on figure are shown in pcf)

Unit weight statistical analysis output

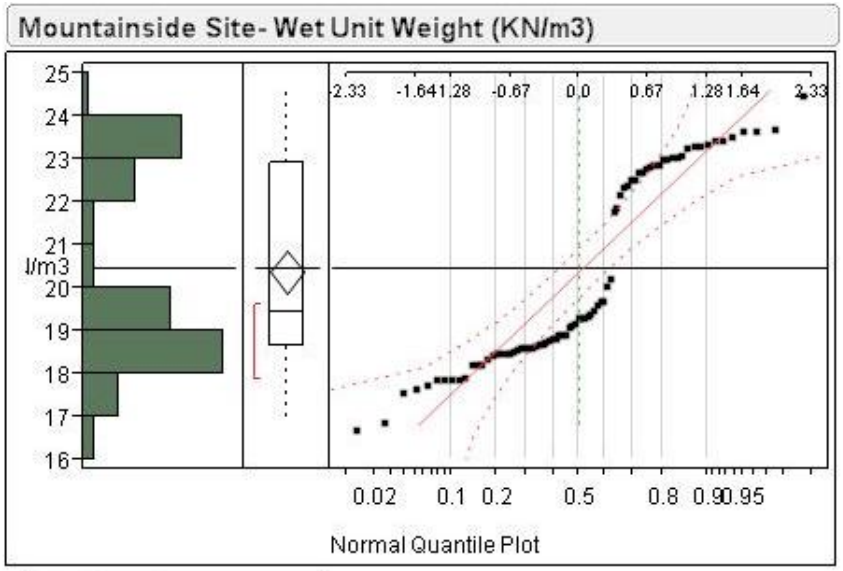

Quantiles

100.0%	maximum	24.619
99.5%		24.619
97.5%		23.838
90.0%		23.495
75.0%	quartile	22.933
50.0%	median	19.423
25.0%	quartile	18.641
10.0%		17.985
2.5%		16.990
0.5%		16.806
0.0%	minimum	16.806

Moments

Mean	20.388321
Std Dev	2.2180056
Std Err Mean	0.2511397
Upper 95% Mean	20.888404
Lower 95% Mean	19.888238
N	78
Sum Wgt	78
Sum	1590.289
Variance	4.9195488
Skewness	0.4060523
Kurtosis	-1.45693
CV	10.878805
N Missing	0

Tolerance Intervals

Proportion	Lower TI	Upper TI	1-Alpha
0.800	17.18771	23.58893	0.900

Figure B-16 Wet unit weight statistical analysis output for Mountainside site

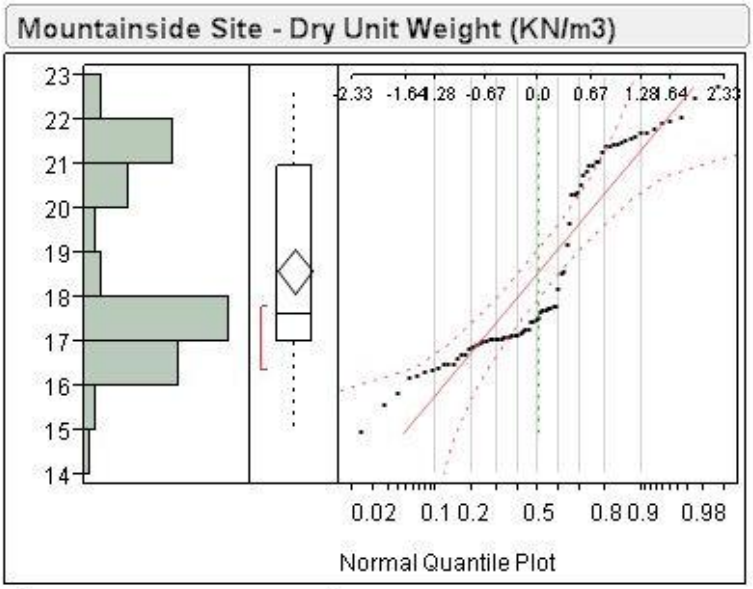

Quantiles

100.0%	maximum	22.749
99.5%		22.749
97.5%		22.473
90.0%		21.683
75.0%	quartile	20.964
50.0%	median	17.592
25.0%	quartile	16.979
10.0%		16.391
2.5%		15.564
0.5%		14.935
0.0%	minimum	14.935

Moments

Mean	18.587644
Std Dev	2.1560356
Std Err Mean	0.244123
Upper 95% Mean	19.073755
Lower 95% Mean	18.101533
N	78
Sum Wgt	78
Sum	1449.8363
Variance	4.6484895
Skewness	0.476396
Kurtosis	-1.344782
CV	11.599294
N Missing	0

Tolerance Intervals

Proportion	Lower TI	Upper TI	1-Alpha
0.800	15.47646	21.69883	0.900

Figure B-17 Dry unit weight statistical analysis output for Mountainside site

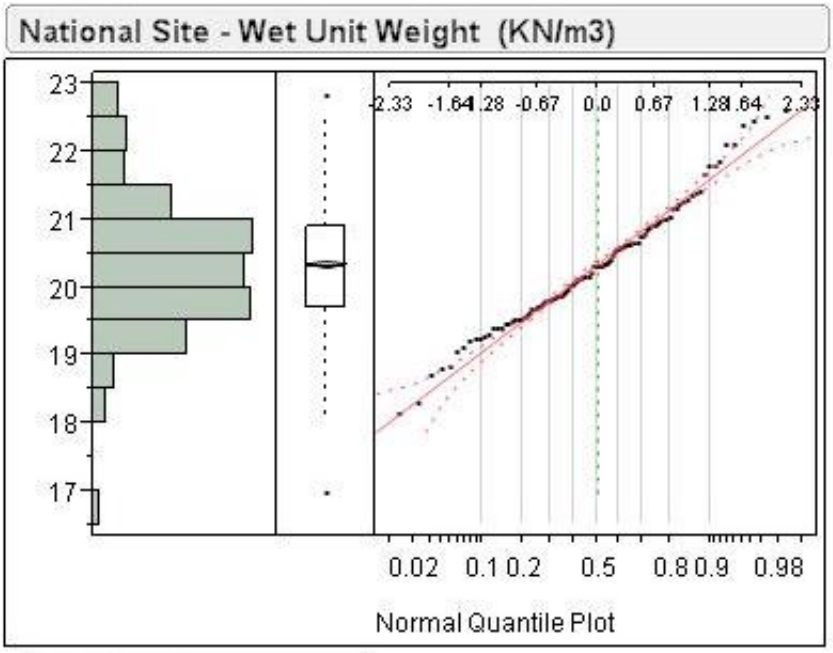

Quantiles

100.0%	maximum	22.827
99.5%		22.827
97.5%		22.513
90.0%		21.774
75.0%	quartile	20.909
50.0%	median	20.299
25.0%	quartile	19.699
10.0%		19.258
2.5%		18.284
0.5%		16.963
0.0%	minimum	16.963

Moments

Mean	20.348362
Std Dev	0.9924046
Std Err Mean	0.0219776
Upper 95% Mean	20.391463
Lower 95% Mean	20.305261
N	2039
Sum Wgt	2039
Sum	41490.31
Variance	0.9848669
Skewness	0.1263595
Kurtosis	0.630337
CV	4.8770737
N Missing	0

Figure B-18 Wet unit weight statistical analysis output for National Site

National Site - Dry Unit Weight (KN/m3)

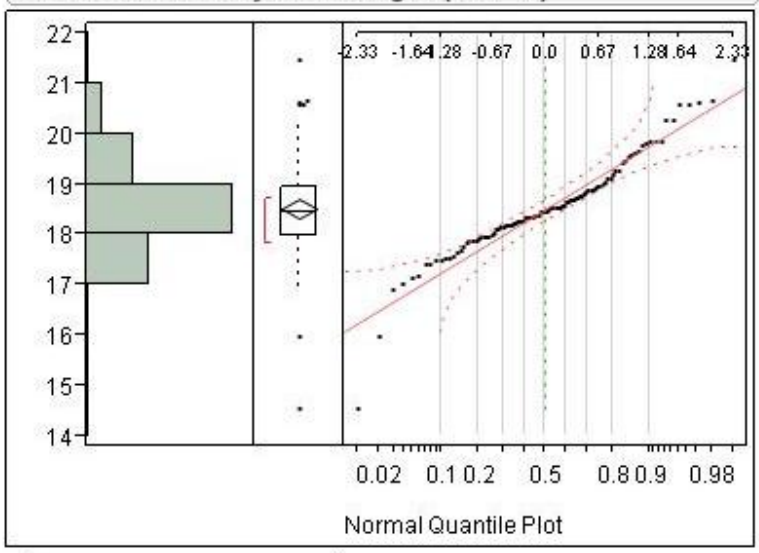

Quantiles

100.0%	maximum	21.444
99.5%		21.444
97.5%		20.614
90.0%		19.812
75.0%	quartile	18.944
50.0%	median	18.441
25.0%	quartile	17.985
10.0%		17.495
2.5%		16.539
0.5%		14.558
0.0%	minimum	14.558

Moments

Mean	18.527532
Std Dev	0.9745263
Std Err Mean	0.0960229
Upper 95% Mean	18.717993
Lower 95% Mean	18.337071
N	103
Sum Wgt	103
Sum	1908.3358
Variance	0.9497015
Skewness	-0.168847
Kurtosis	2.7538437
CV	5.2598818
N Missing	0

Tolerance Intervals

Proportion	Lower TI	Upper TI	1-Alpha
0.800	17.14554	19.90953	0.900

Figure B-19 Dry unit weight statistical analysis output for National Site

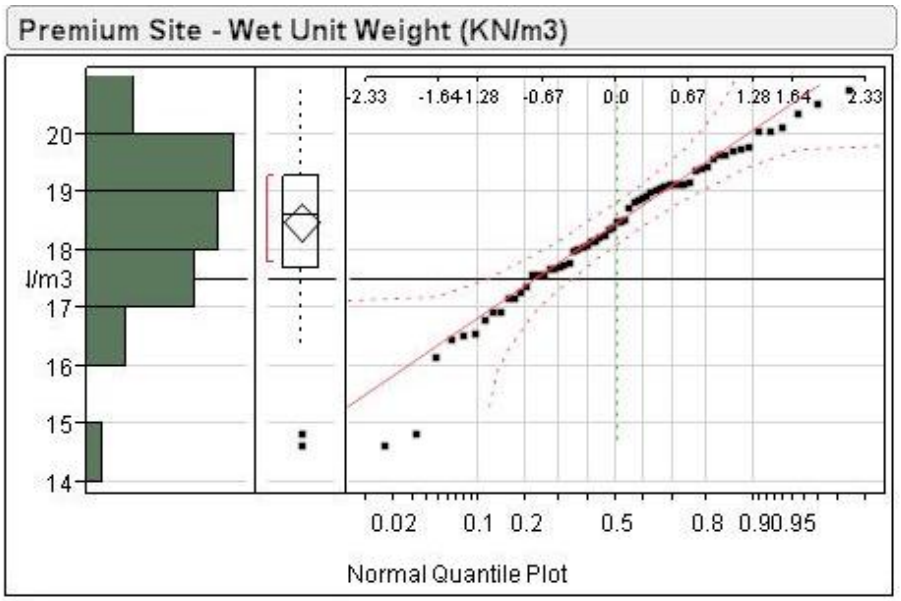

Quantiles

100.0%	maximum	20.878
99.5%		20.878
97.5%		20.727
90.0%		20.038
75.0%	quartile	19.290
50.0%	median	18.582
25.0%	quartile	17.702
10.0%		16.774
2.5%		14.869
0.5%		14.746
0.0%	minimum	14.746

Moments

Mean	18.482487
Std Dev	1.2709948
Std Err Mean	0.1601303
Upper 95% Mean	18.802583
Lower 95% Mean	18.162391
N	63
Sum Wgt	63
Sum	1164.3967
Variance	1.6154277
Skewness	-0.632217
Kurtosis	0.6021727
CV	6.8767517
N Missing	0

Tolerance Intervals

Proportion	Lower TI	Upper TI	1-Alpha
0.800	16.61949	20.34548	0.900

Figure B-20 Wet unit weight statistical analysis output for Premium Site

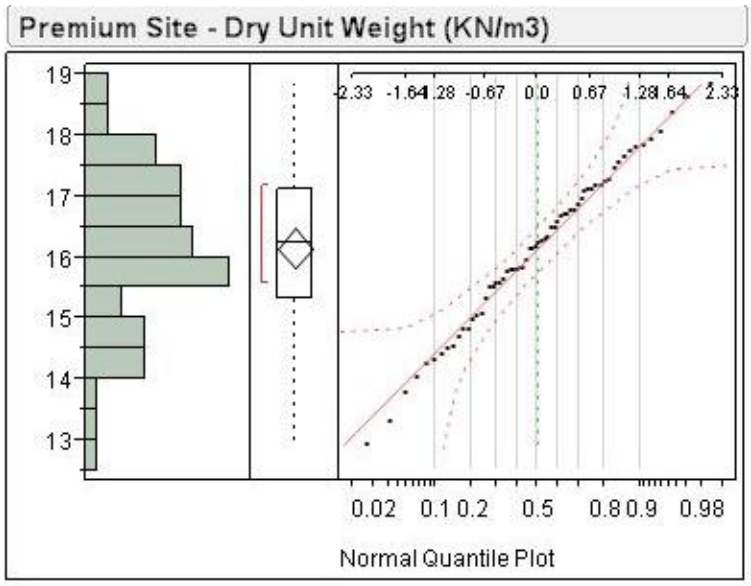

Quantiles

100.0%	maximum	18.834
99.5%		18.834
97.5%		18.702
90.0%		17.822
75.0%	quartile	17.120
50.0%	median	16.224
25.0%	quartile	15.328
10.0%		14.360
2.5%		13.171
0.5%		12.954
0.0%	minimum	12.954

Moments

Mean	16.157279
Std Dev	1.3075717
Std Err Mean	0.1647386
Upper 95% Mean	16.486586
Lower 95% Mean	15.827971
N	63
Sum Wgt	63
Sum	1017.9086
Variance	1.7097438
Skewness	-0.240581
Kurtosis	-0.324227
CV	8.092772
N Missing	0

Tolerance Intervals

Proportion	Lower TI	Upper TI	1-Alpha
0.800	14.24067	18.07388	0.900

Figure B-21 Dry unit weight statistical analysis output for Premium Site

Mean grain size distribution charts for Mountainside, National and Premium sites

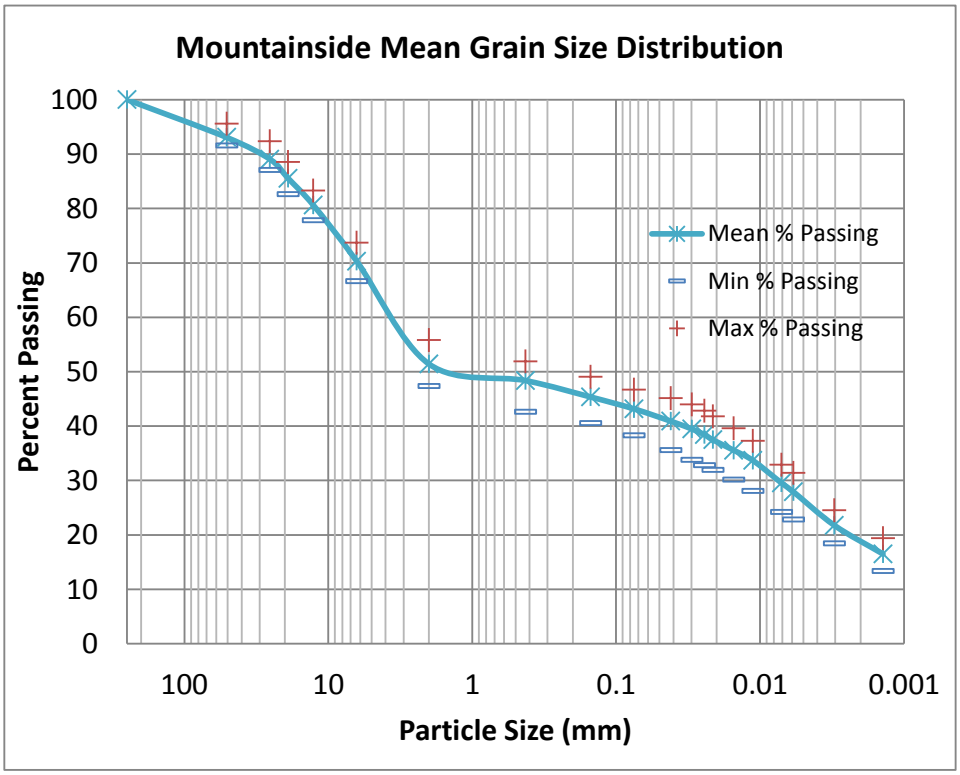

Figure B-22 Mean grain size distribution at Mountainside site.

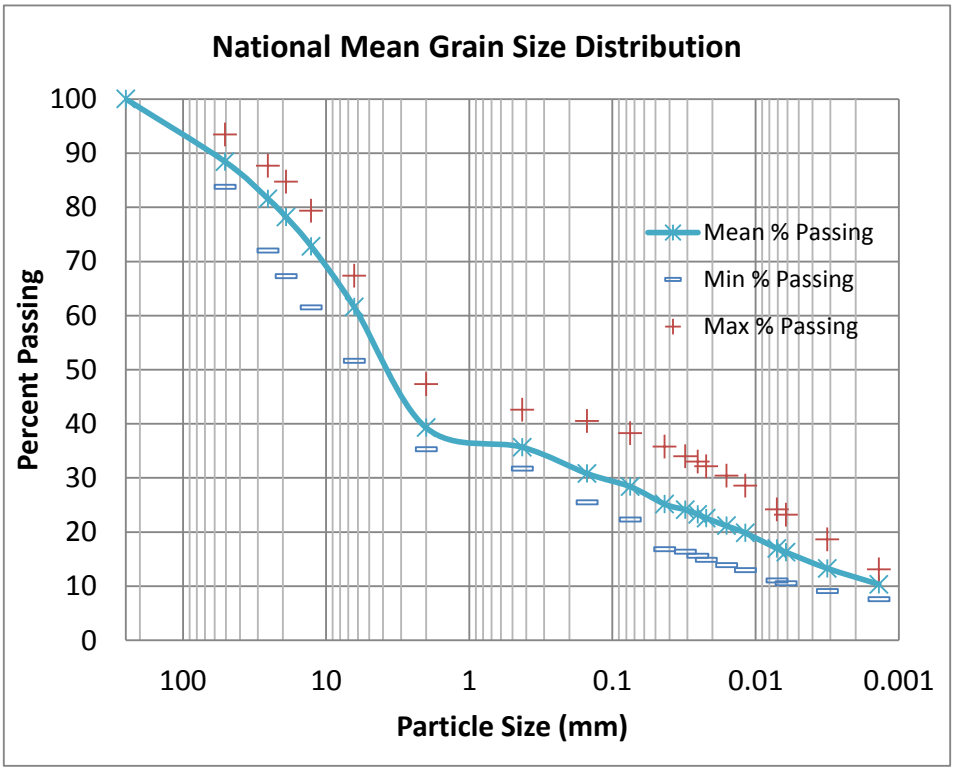

Figure B-23 Mean grain size distribution at National site.

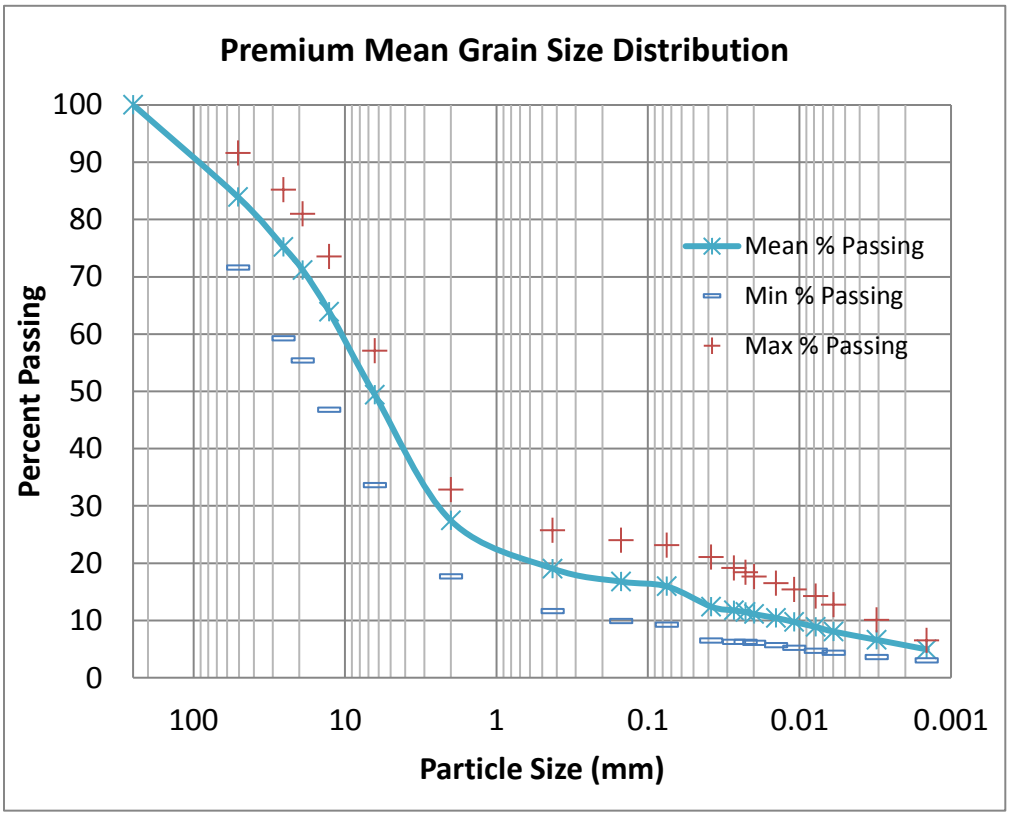

Figure B-24 Mean grain size distribution from the Premium site.

Details on Slope Stability of Instrumented Sites

Spectral acceleration plots for Mountainside, National and Premium sites

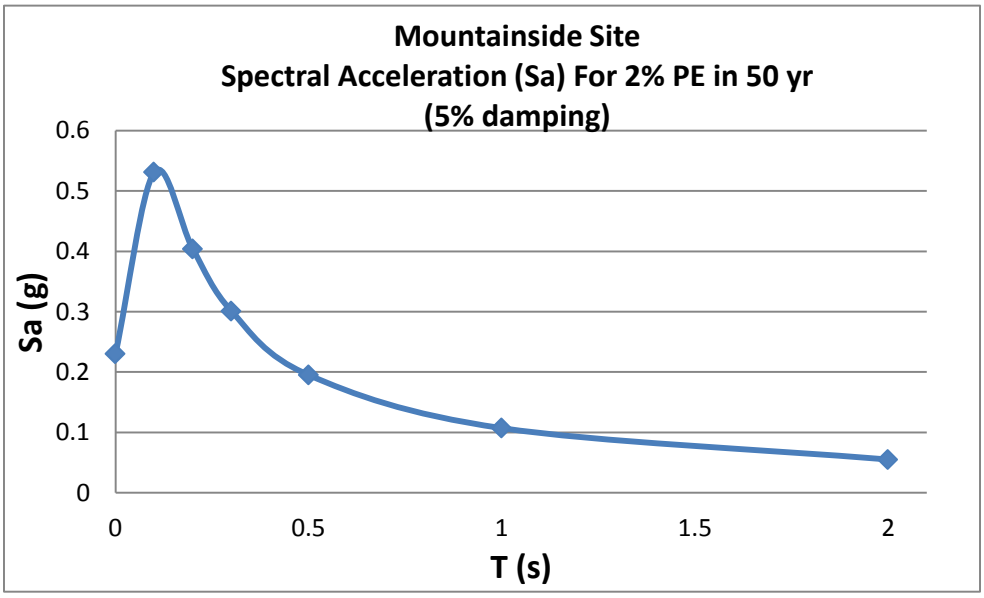

Figure B-25 2% P.E. Spectral Acceleration Plot for Mountainside site (USGS)

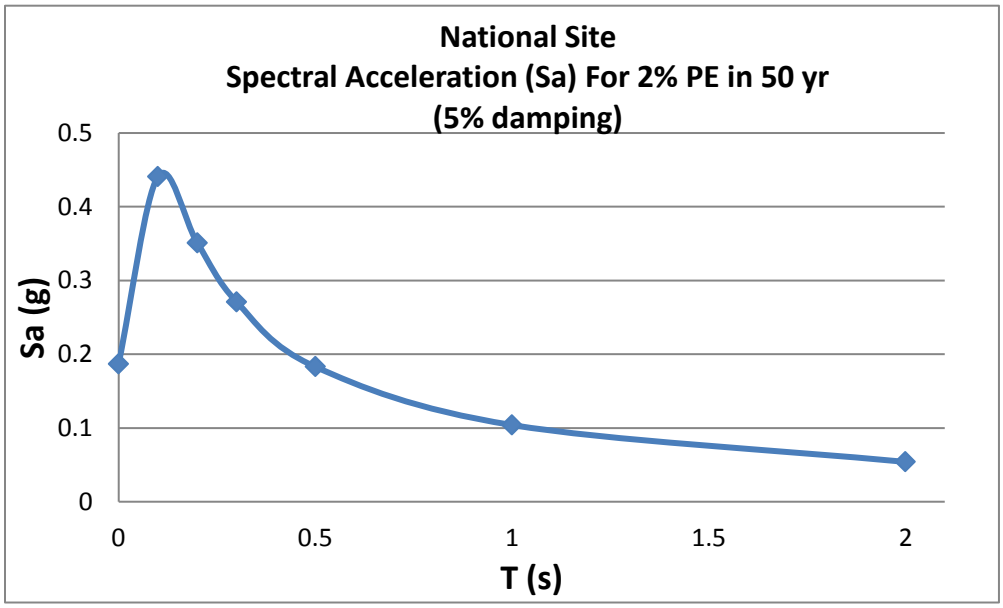

Figure B-26 2% P.E. Spectral Acceleration Plot for National site (USGS)

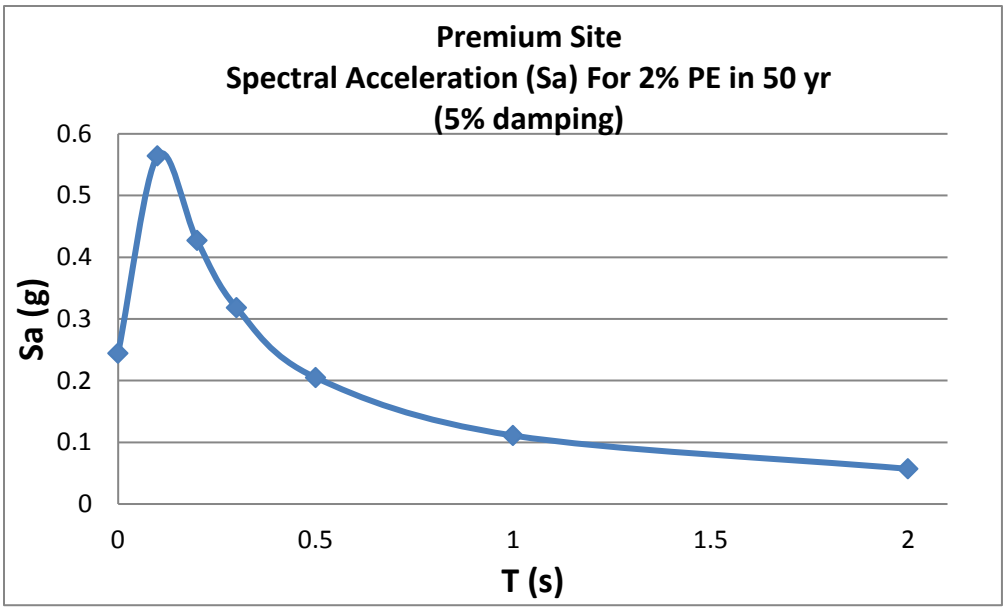

Figure B-27 2% P.E. Spectral Acceleration Plot for Premium site (USGS)

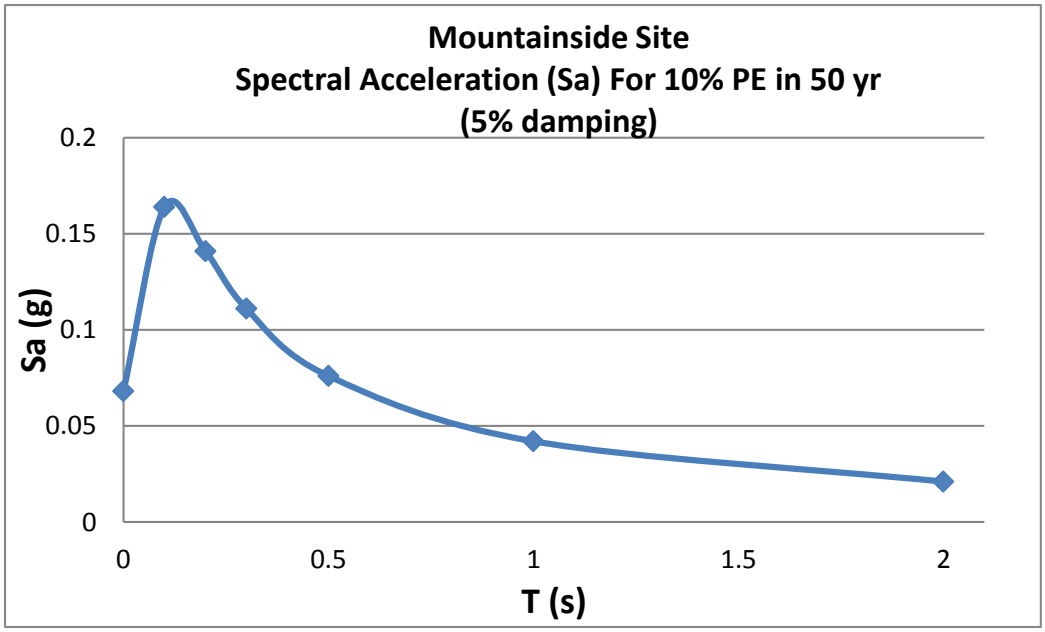

Figure B-28 10% P.E. Spectral Acceleration Plot for Mountainside site (USGS)

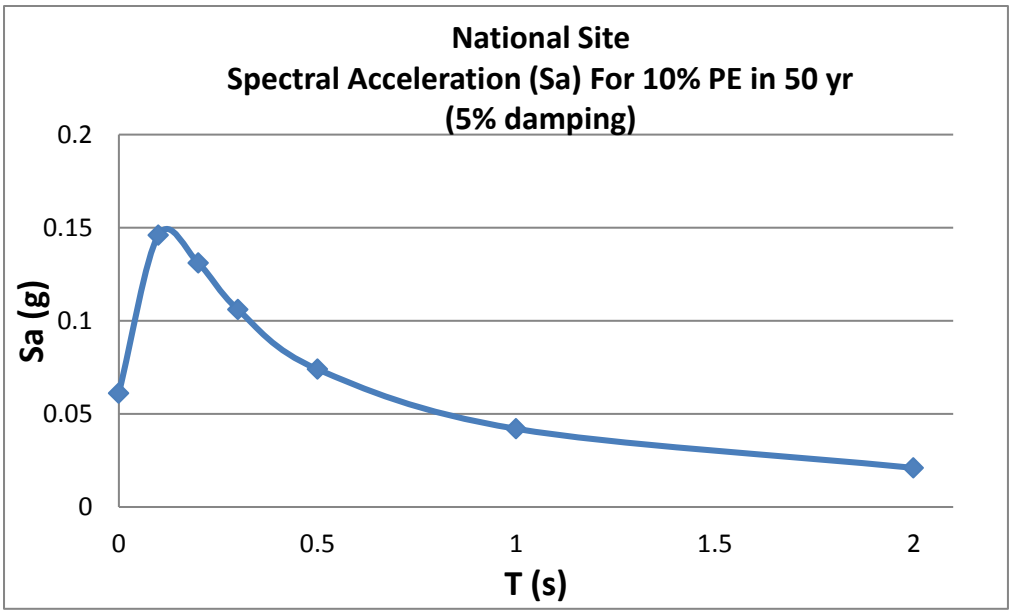

Figure B-29 10% P.E. Spectral Acceleration Plot for National site (USGS)

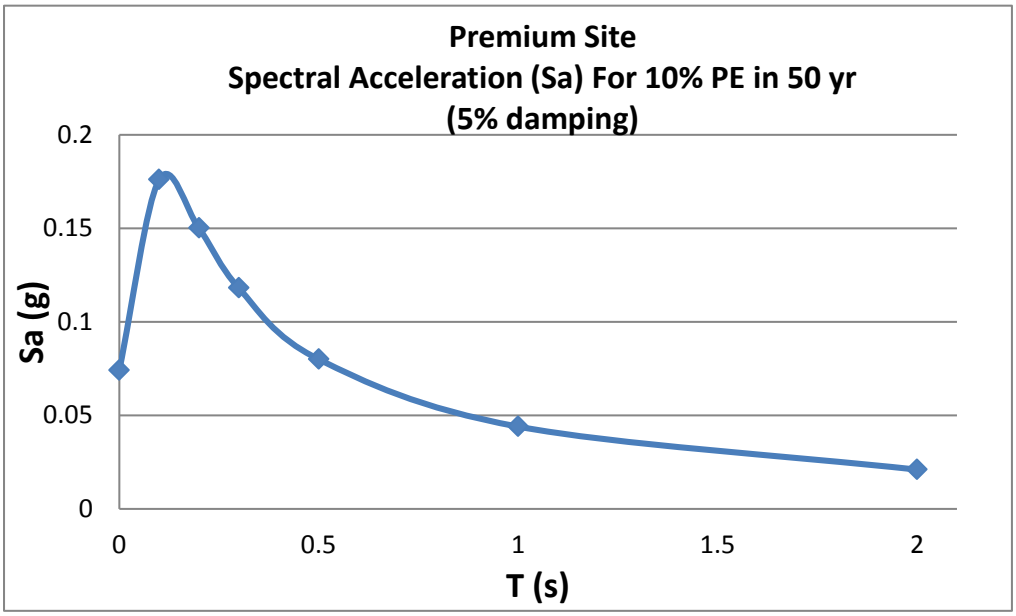

Figure B-30 10% P.E. Spectral Acceleration Plot for Premium site (USGS)

Slope stability charts based on spectral accelerations for Mountainside, National and Premium sites

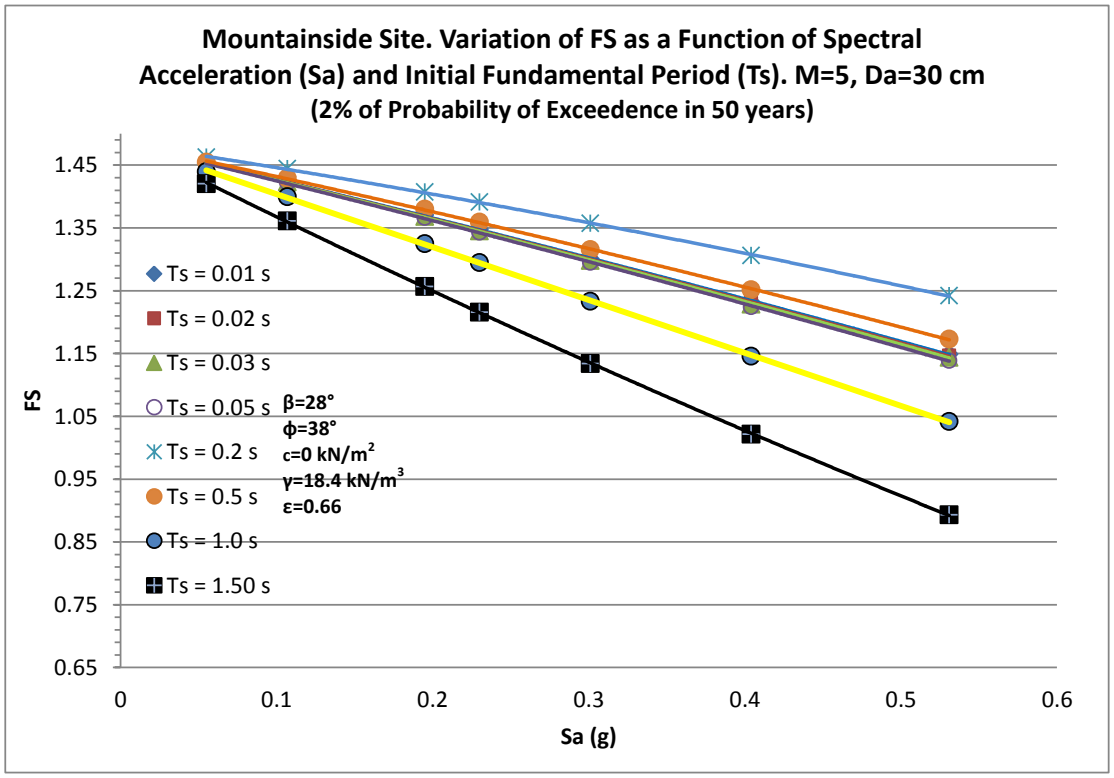

Figure B-31 2% P.E. FS Solution chart for Mountainside site. Da=30cm

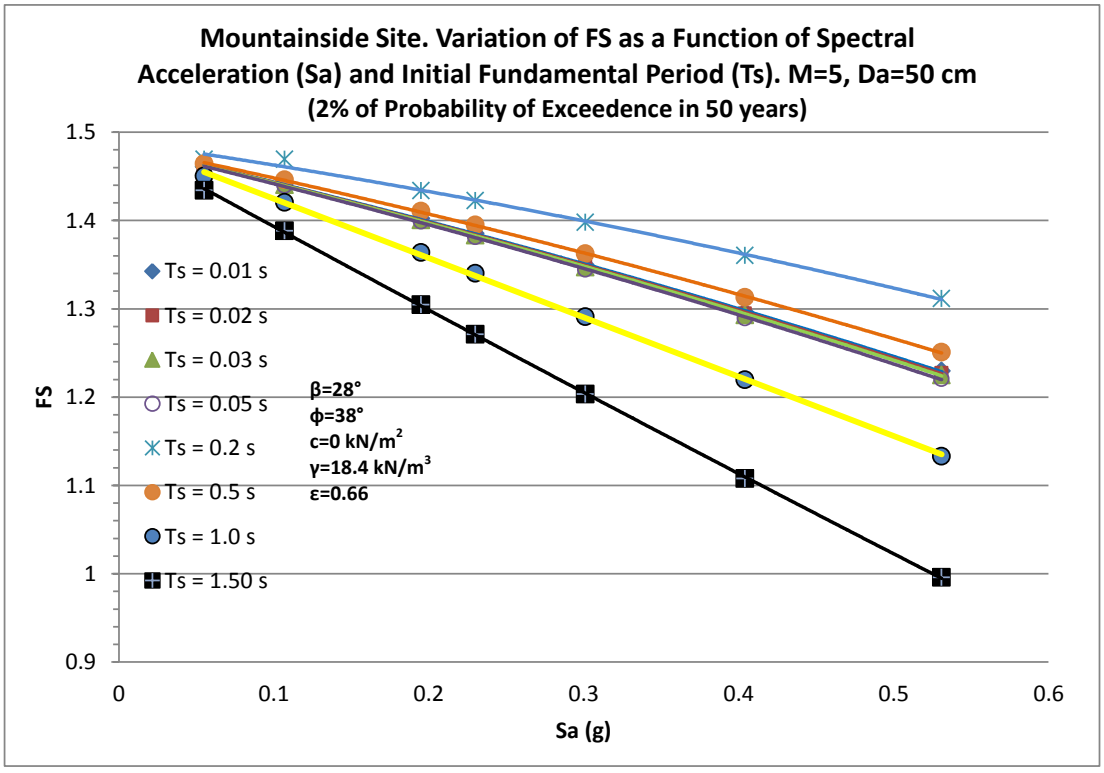

Figure B-32 2% P.E. Solution chart for Mountainside site. Da=50cm

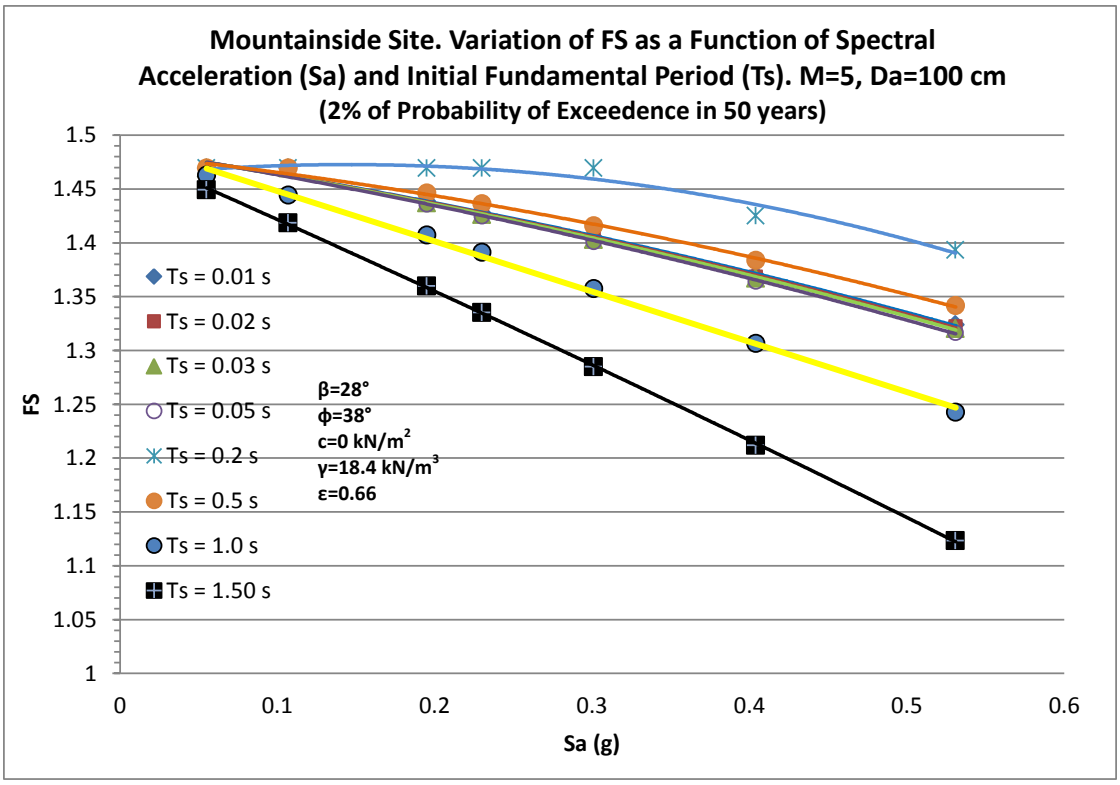

Figure B-33 2% P.E. Solution chart for Mountainside site. Da=100cm

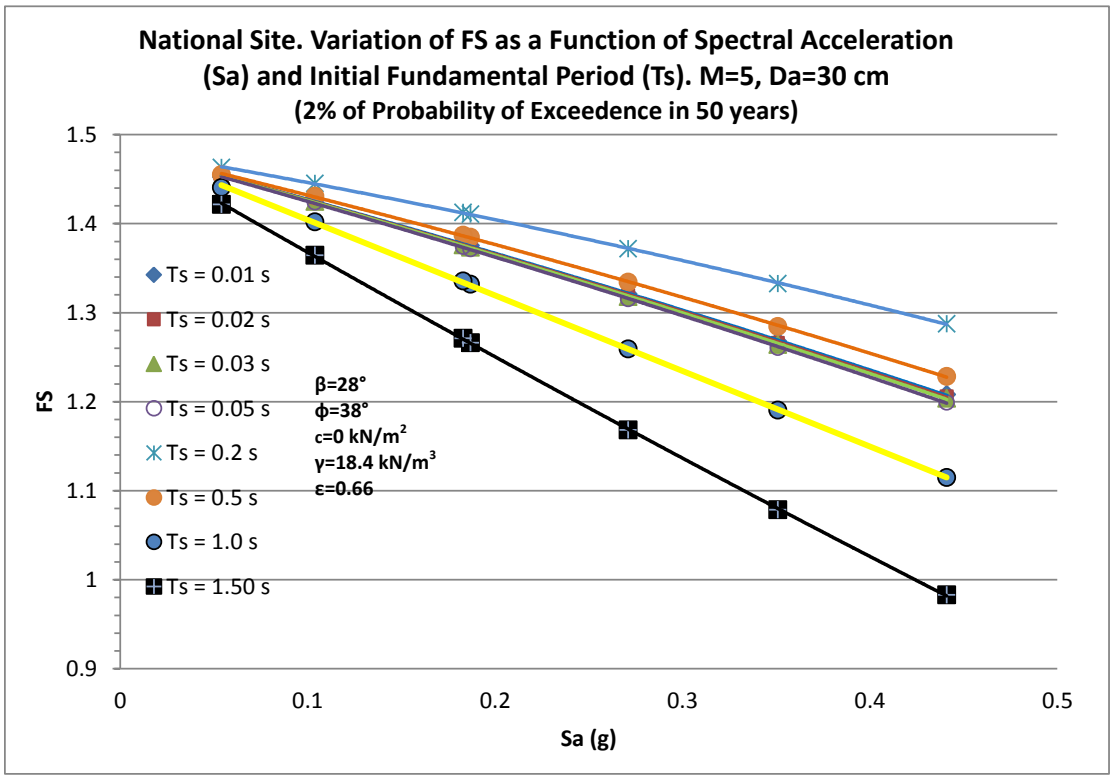

Figure B-34 2% P.E. Solution chart for National site. Da=30cm

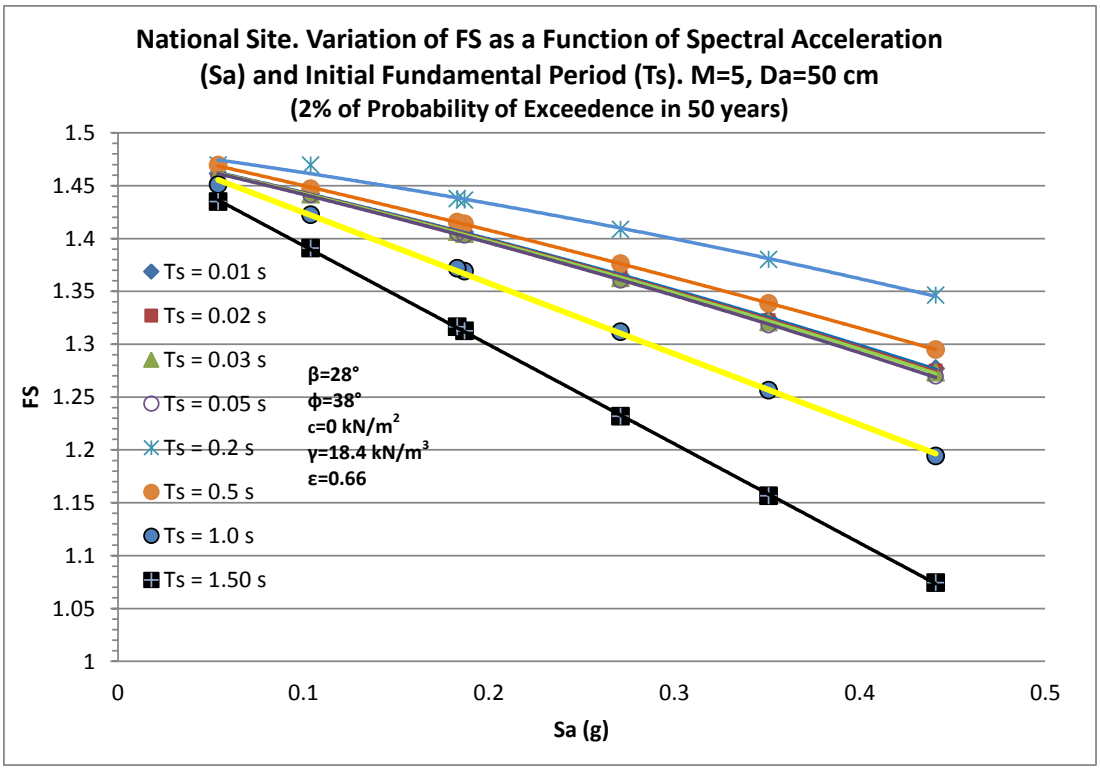

Figure B-35 2% P.E. Solution chart for National site. Da=50cm

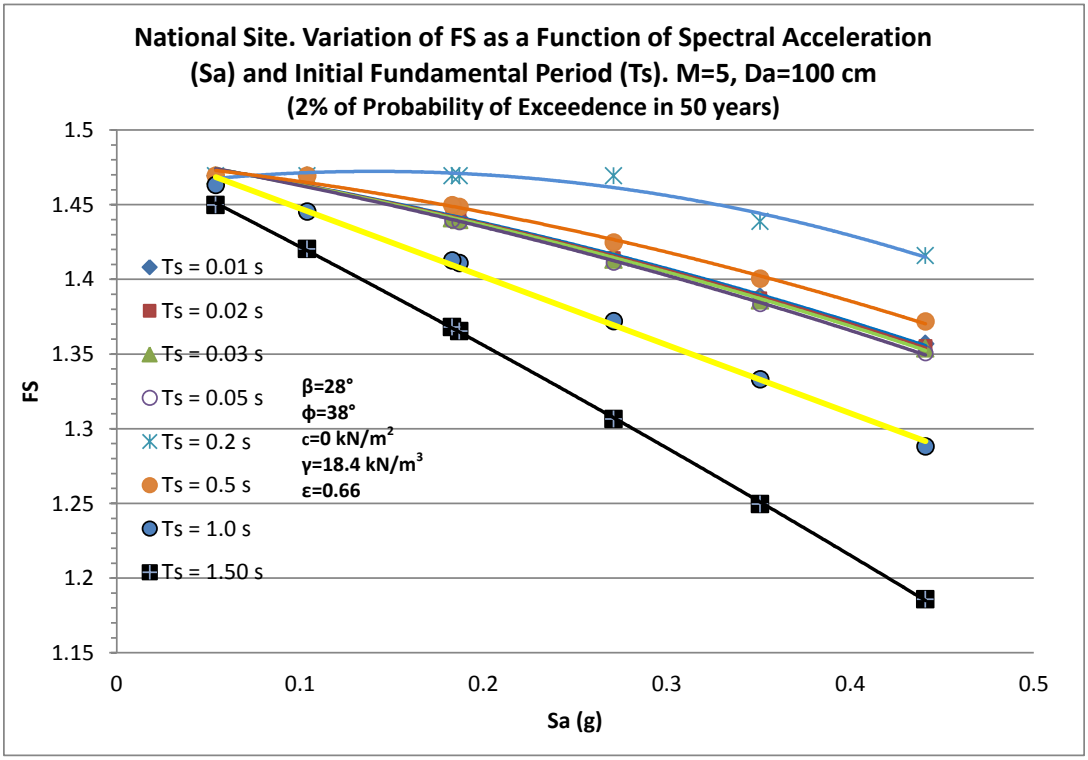

Figure B-36 2% P.E. Solution chart for National site. Da=100cm

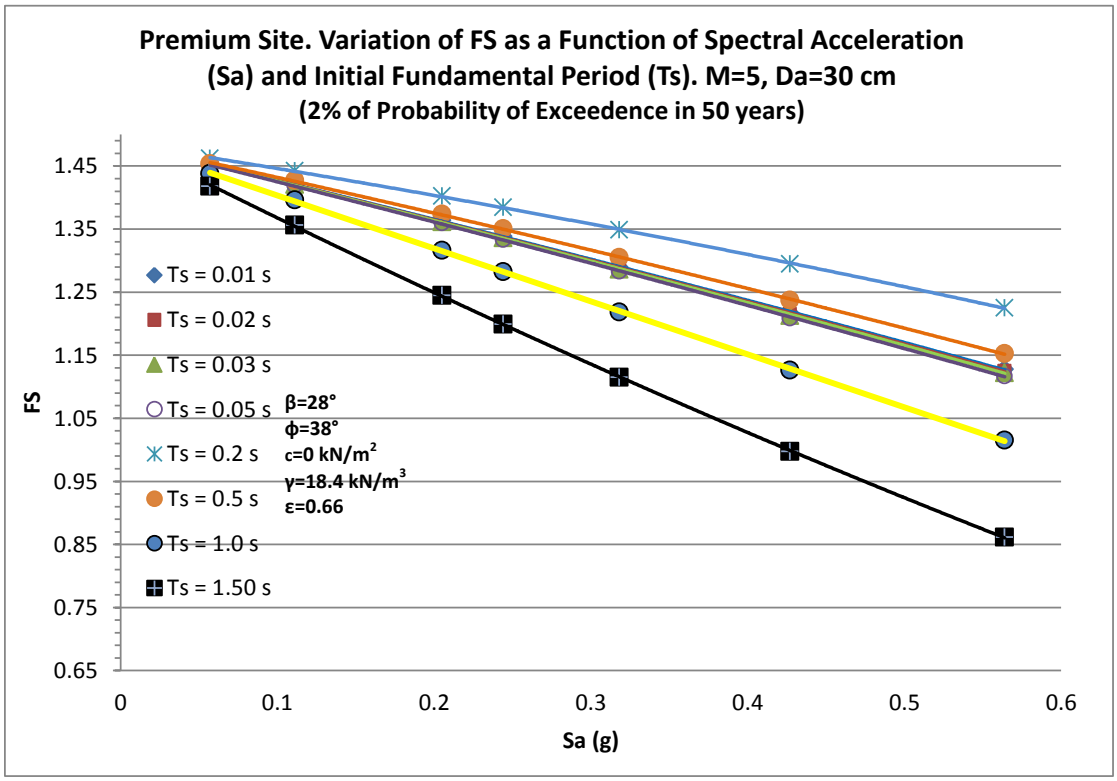

Figure B-37 2% P.E. Solution chart for Premium site. Da=30cm

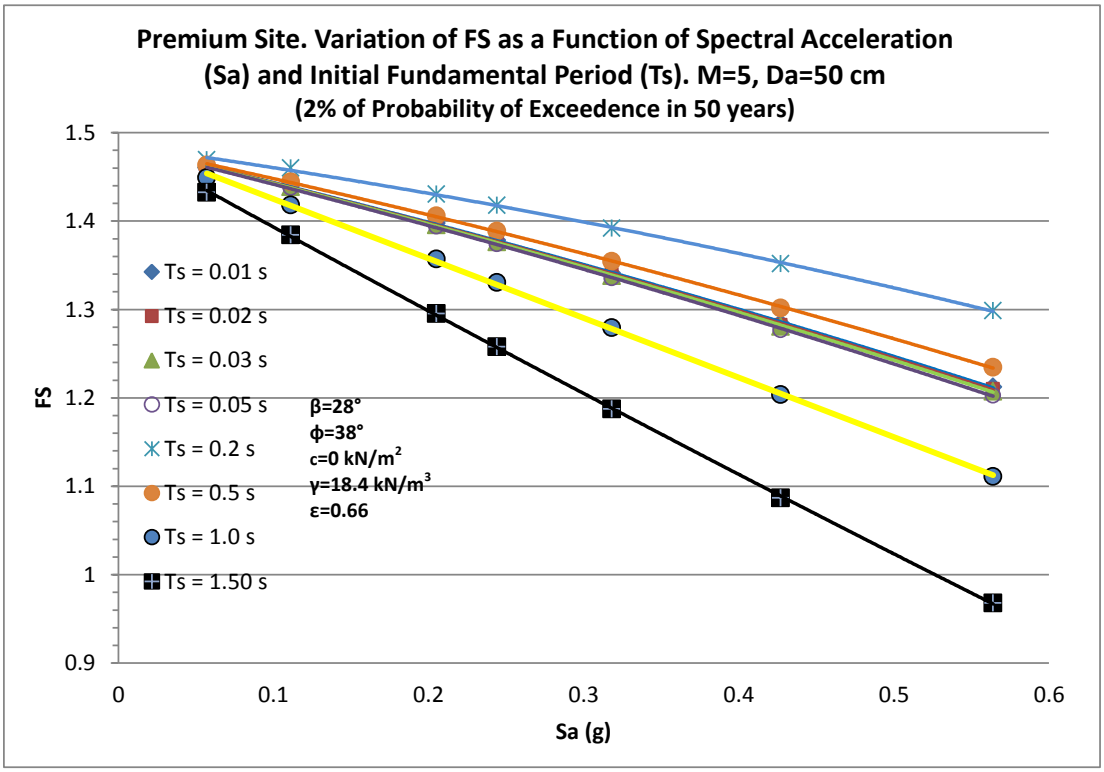

Figure B-38 2% P.E. Solution chart for Premium site. Da=50cm

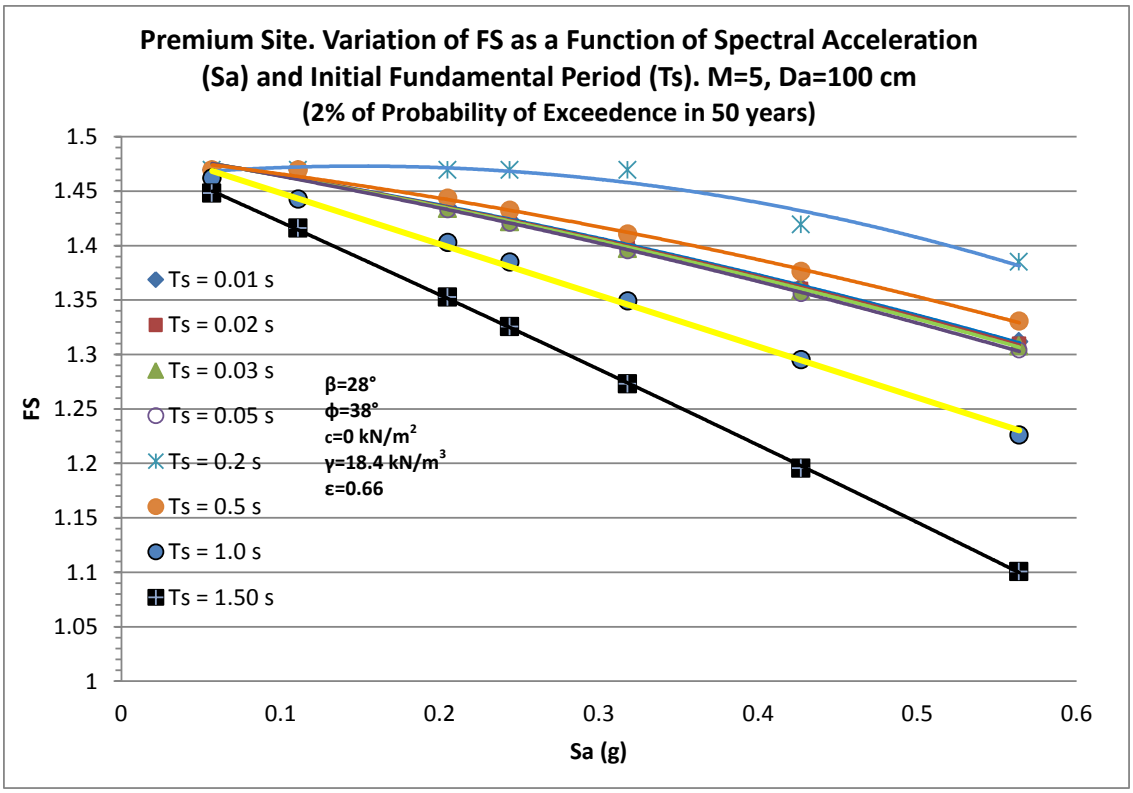

Figure B-39 2% P.E. Solution chart for Premium site. Da=100cm

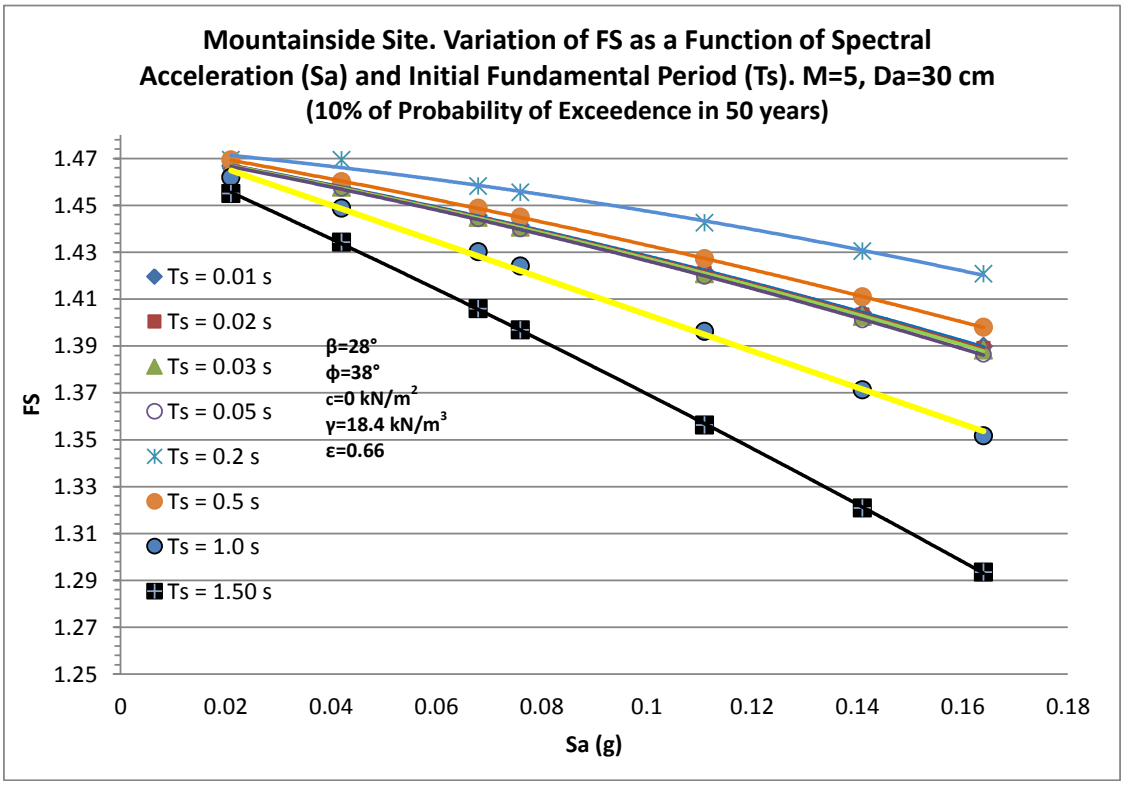

Figure B-40 10% P.E. Solution chart for Mountainside site. Da=30cm

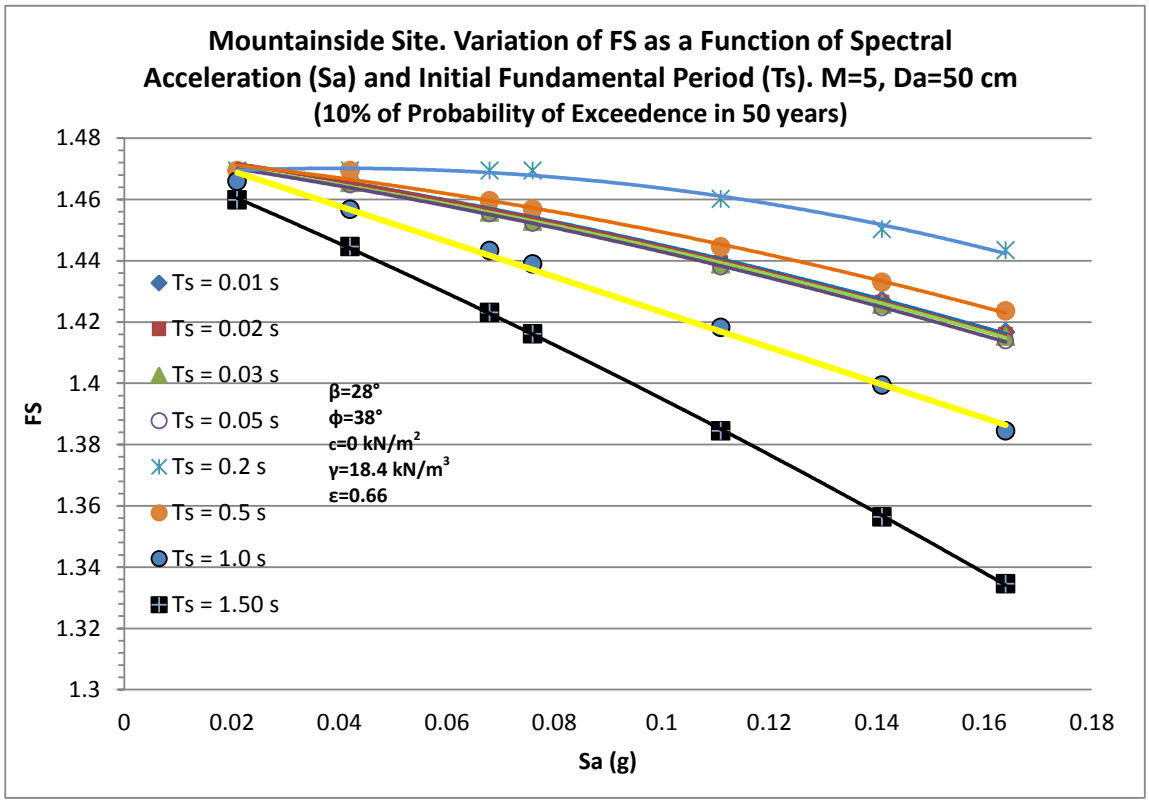

Figure B-41 10% P.E. Solution chart for Mountainside site. Da=50cm

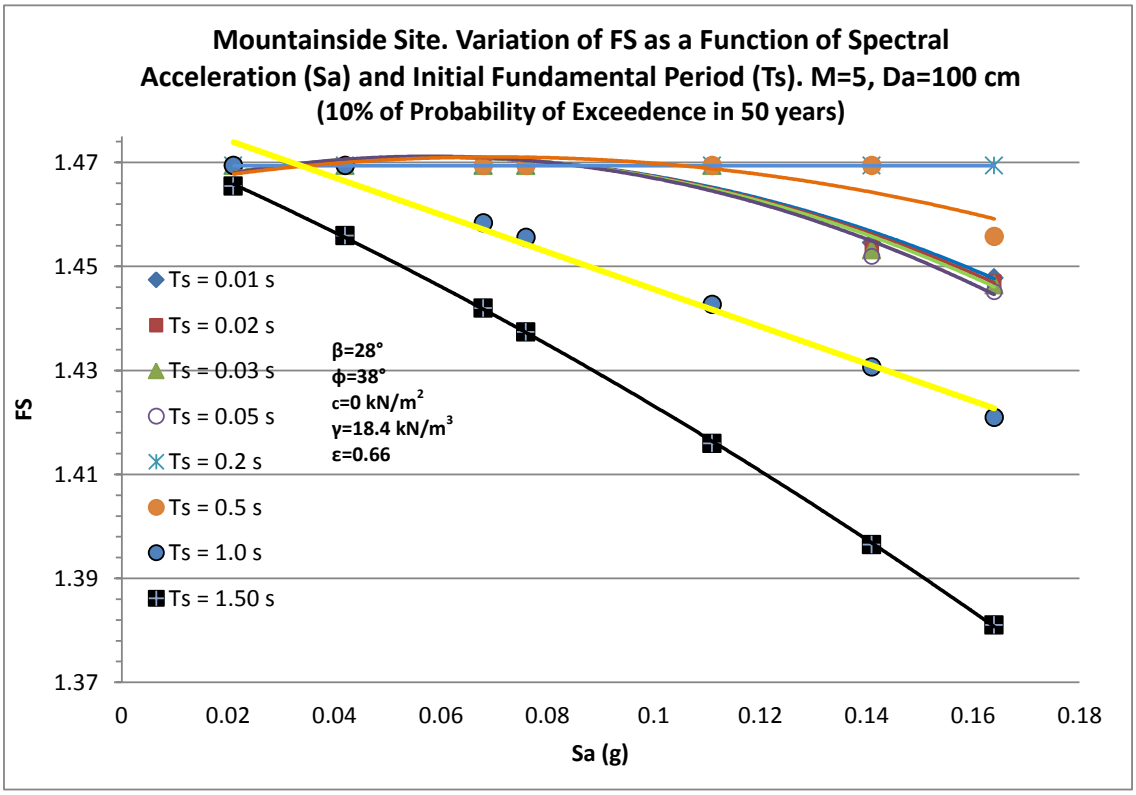

Figure B-42 10% P.E. Solution chart for Mountainside site. Da=100cm

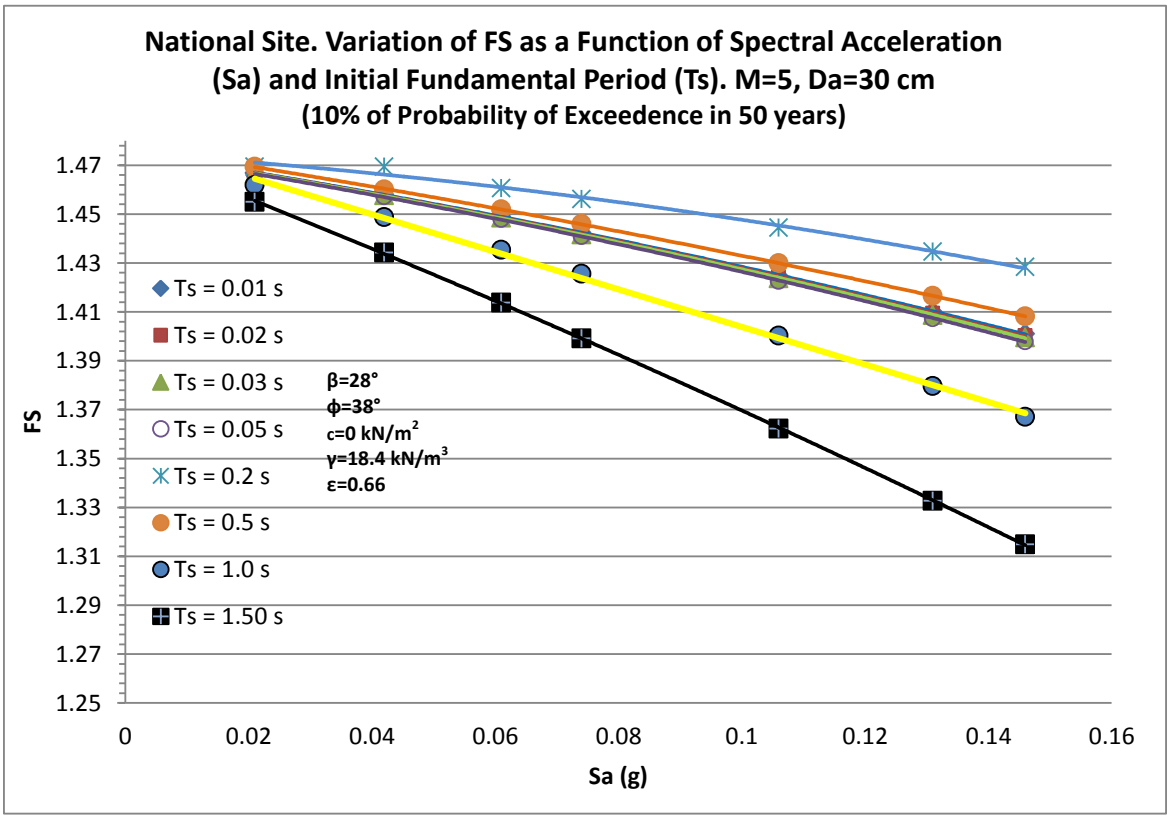

Figure B-43 10% P.E. Solution chart for National site. Da=30cm

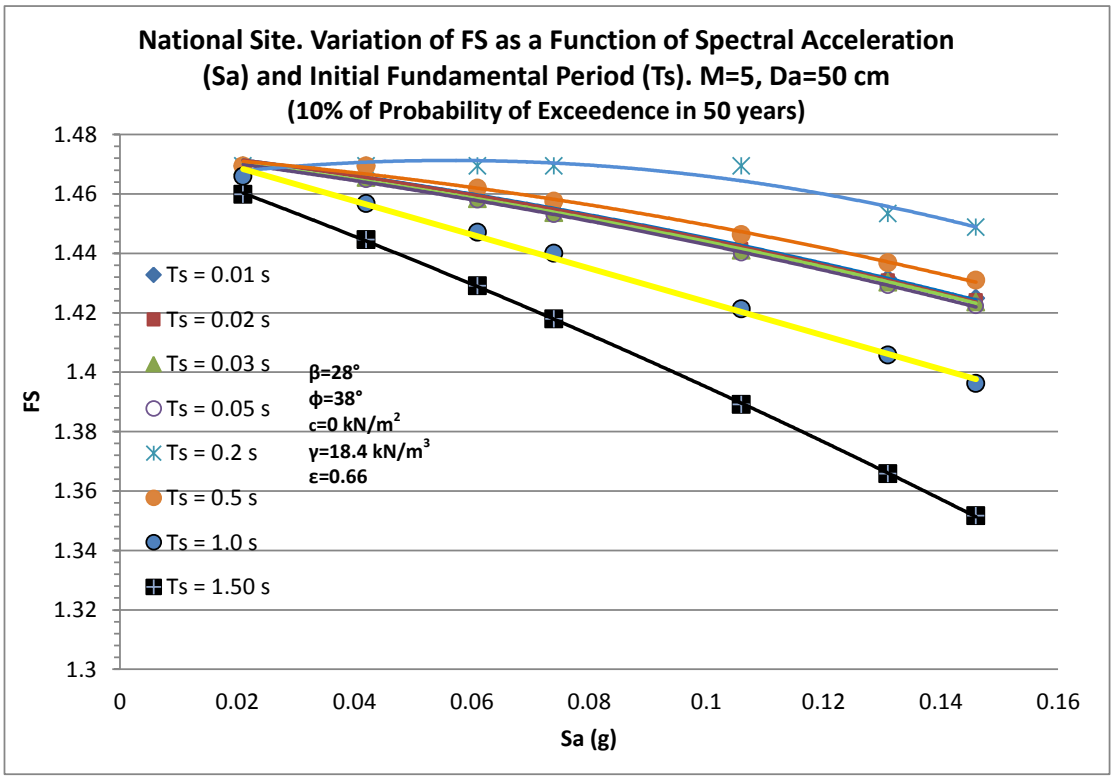

Figure B-44 10% P.E. Solution chart for National site. Da=50cm

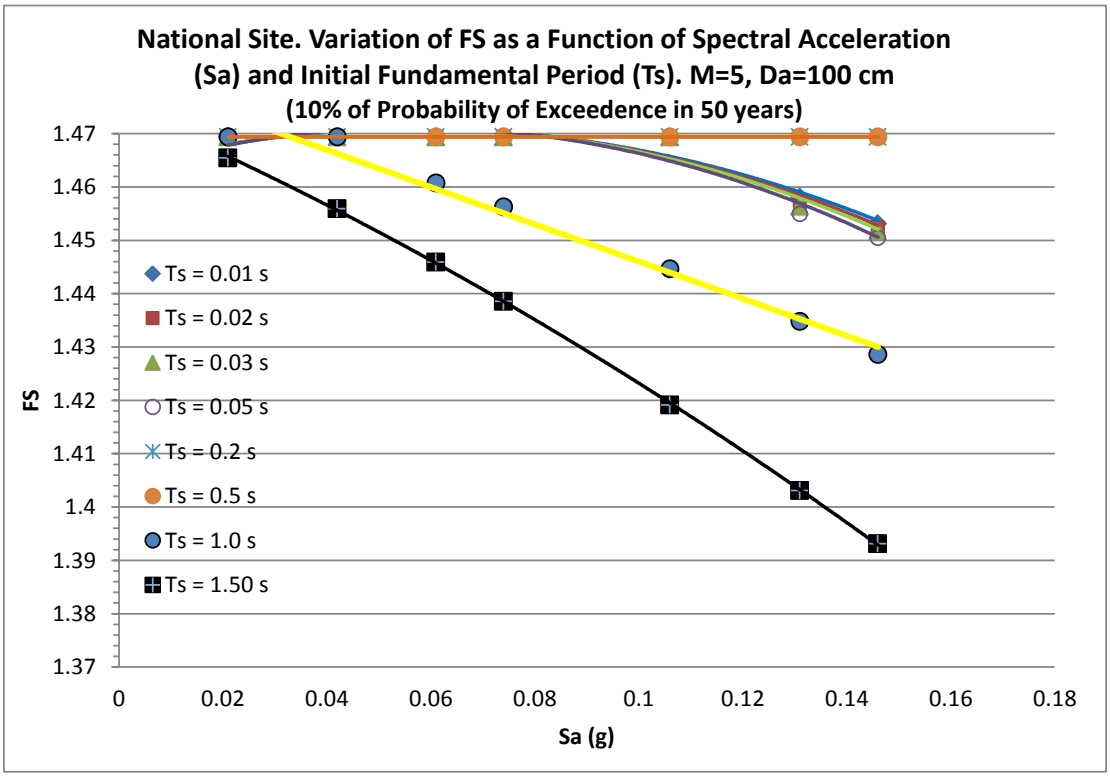

Figure B-45 10% P.E. Solution chart for National site. Da=100cm

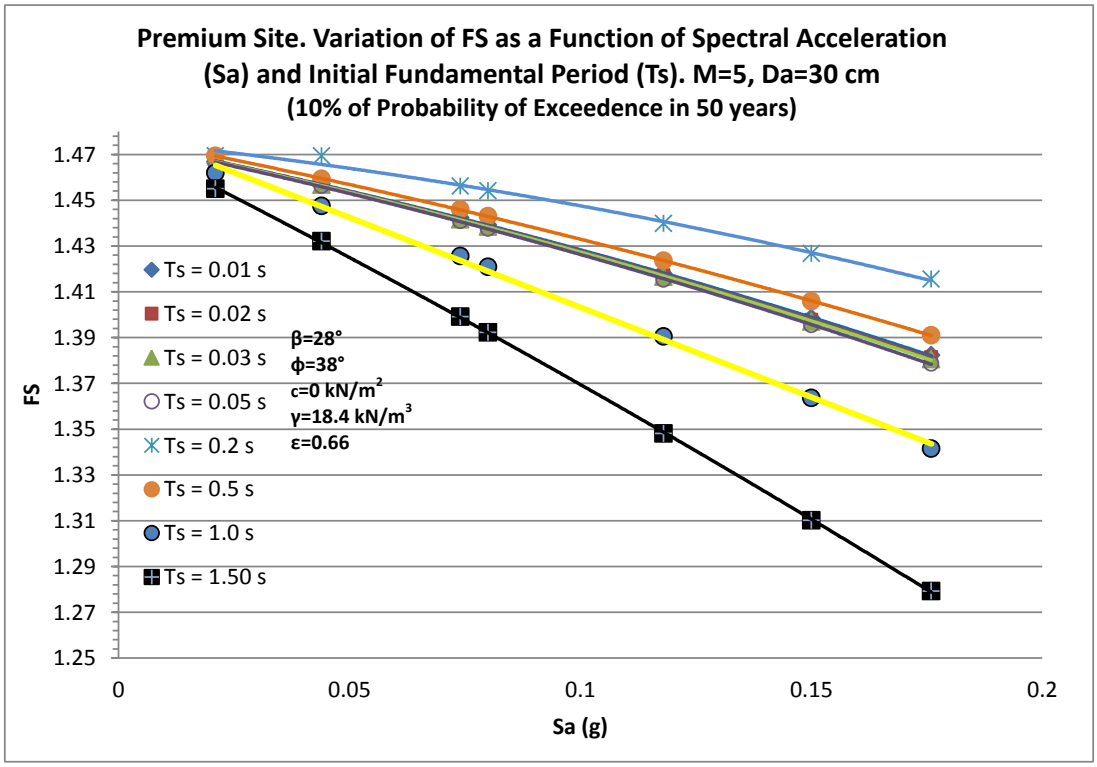

Figure B-46 10% P.E. Solution chart for Premium site. Da=30cm

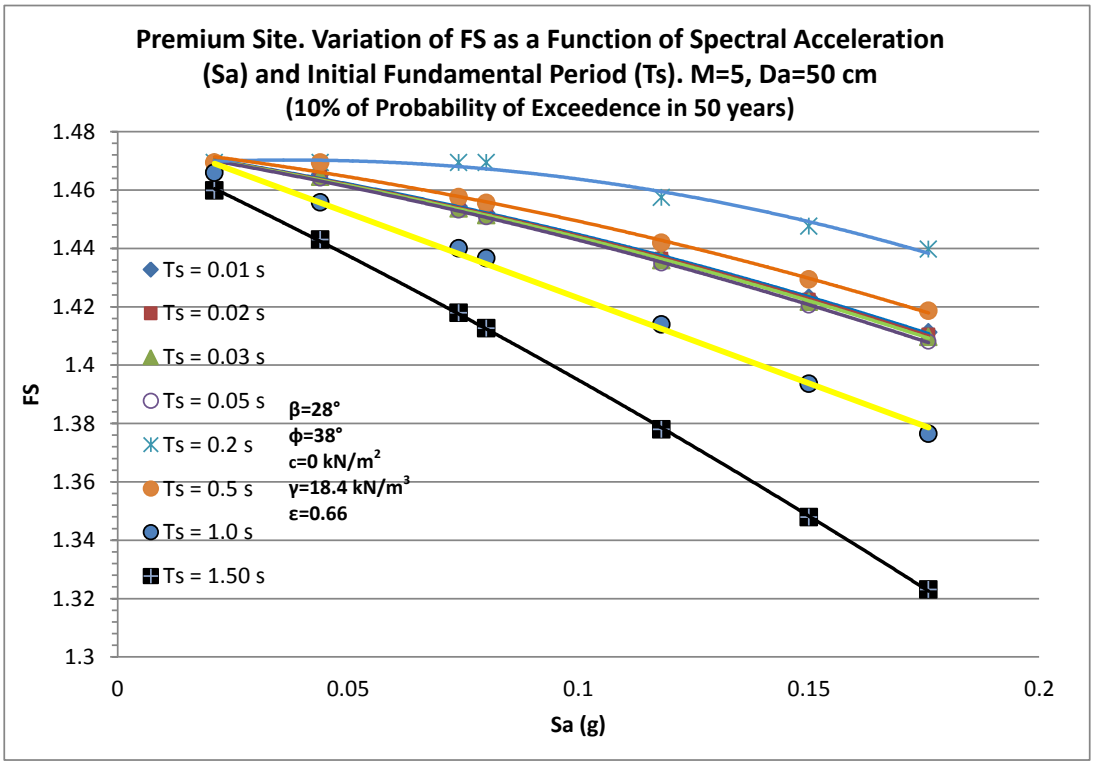

Figure B-47 10% P.E. Solution chart for Premium site. Da=50cm

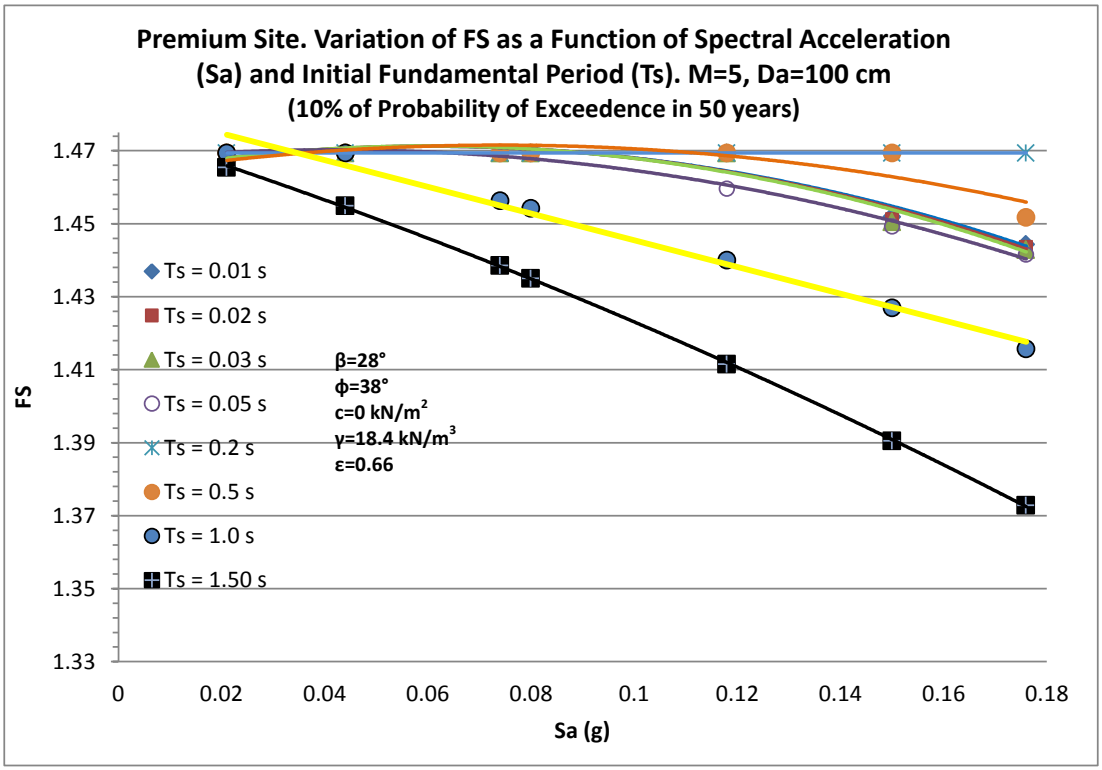

Figure B-48 10% P.E. Solution chart for Premium site. Da=100cm

Details on Non-Planar Slopes

Comparison of the obtained contours in critical state from the proposed solution and Sokolovski's (1960) solution

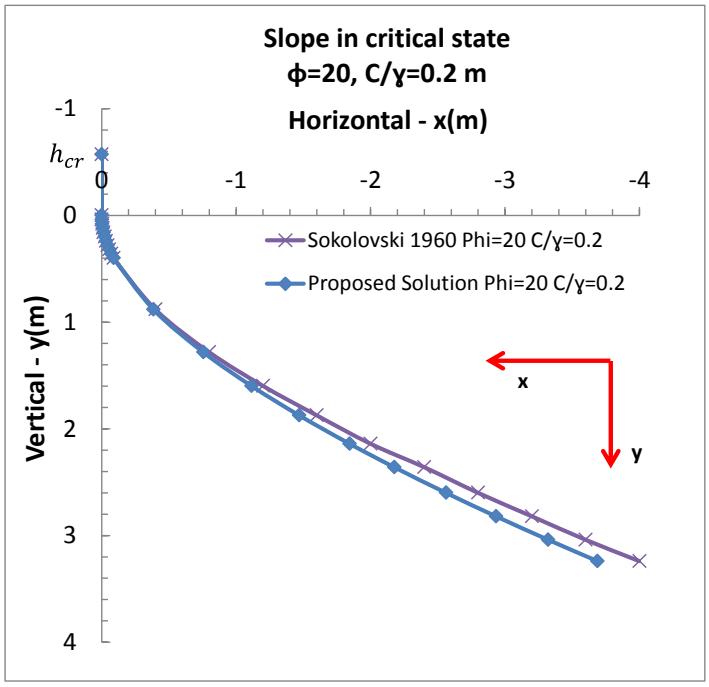

Figure B-49 Concave slope profiles obtained from Sokolovski (1960) and the proposed solution (Eq. 6-54) for $\phi = 20^o$ and $c/\gamma = 0.2\ m$

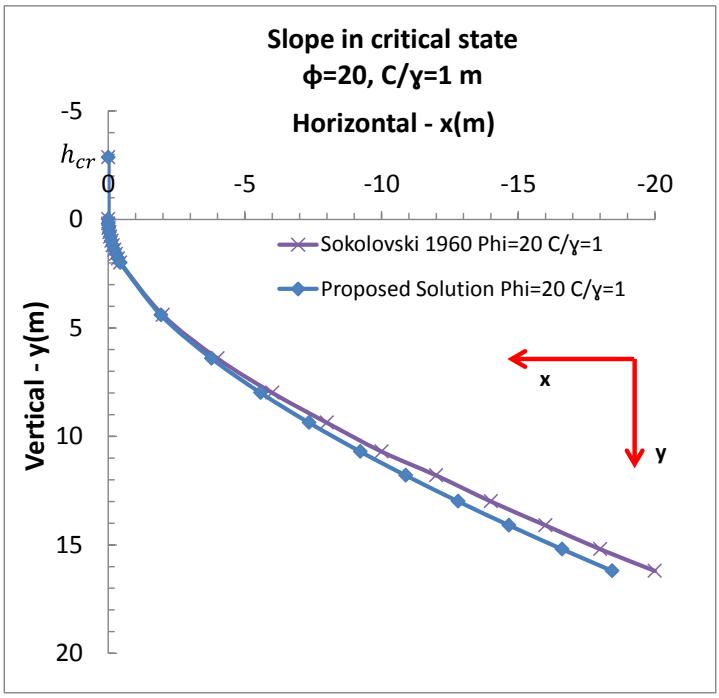

Figure B-50 Concave slope profiles obtained from Sokolovski (1960) and the proposed solution (Eq. 6-54) for $\phi = 20^o$ and $c/\gamma = 1\ m$

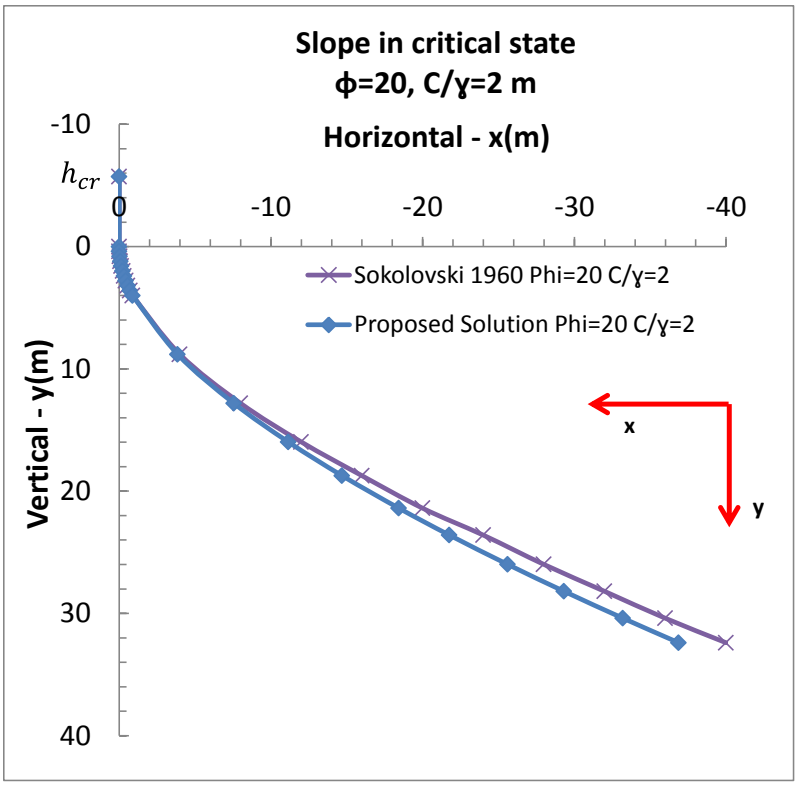

Figure B-51 Concave slope profiles obtained from Sokolovski (1960) and the proposed solution (Eq. 6-54) for $\phi = 20^o$ and $c/\gamma = 2\ m$

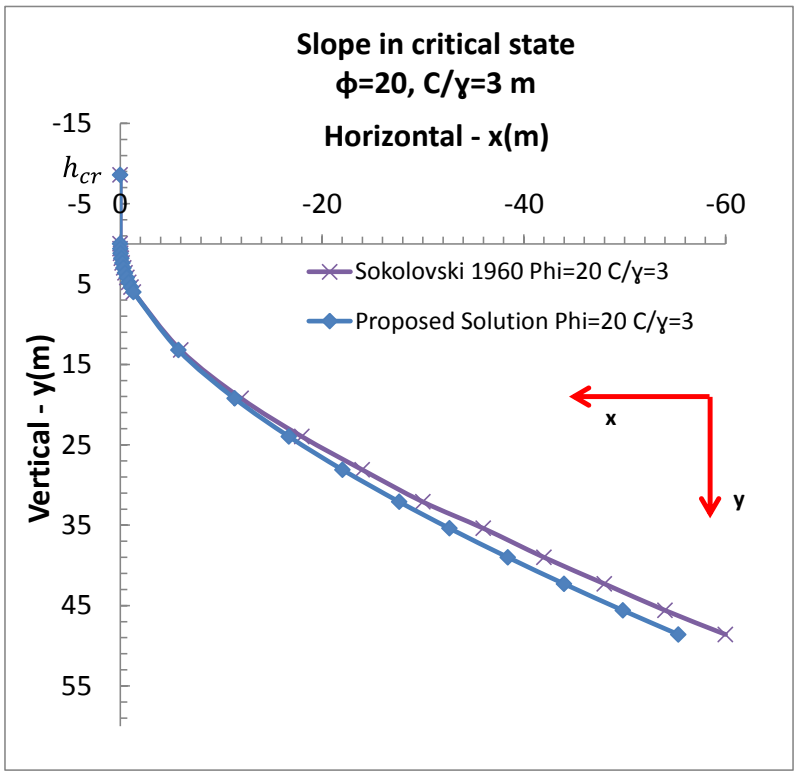

Figure B-52 Concave slope profiles obtained from Sokolovski (1960) and the proposed solution (Eq. 6-54) for $\phi = 20^o$ and $c/\gamma = 3\ m$

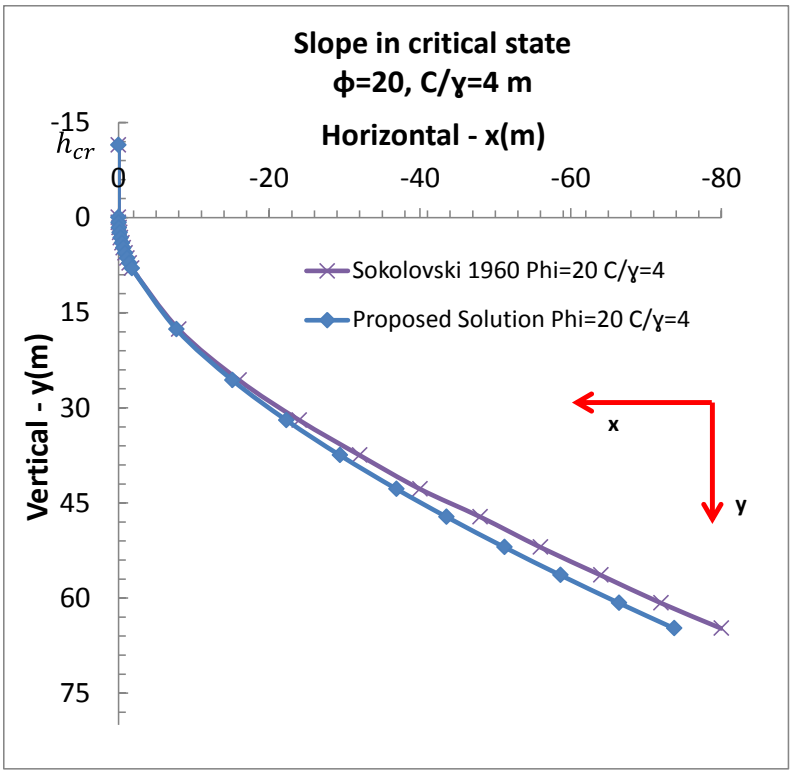

Figure B-53 Concave slope profiles obtained from Sokolovski (1960) and the proposed solution (Eq. 6-54) for $\phi = 20^o$ and $c/\gamma = 4\ m$

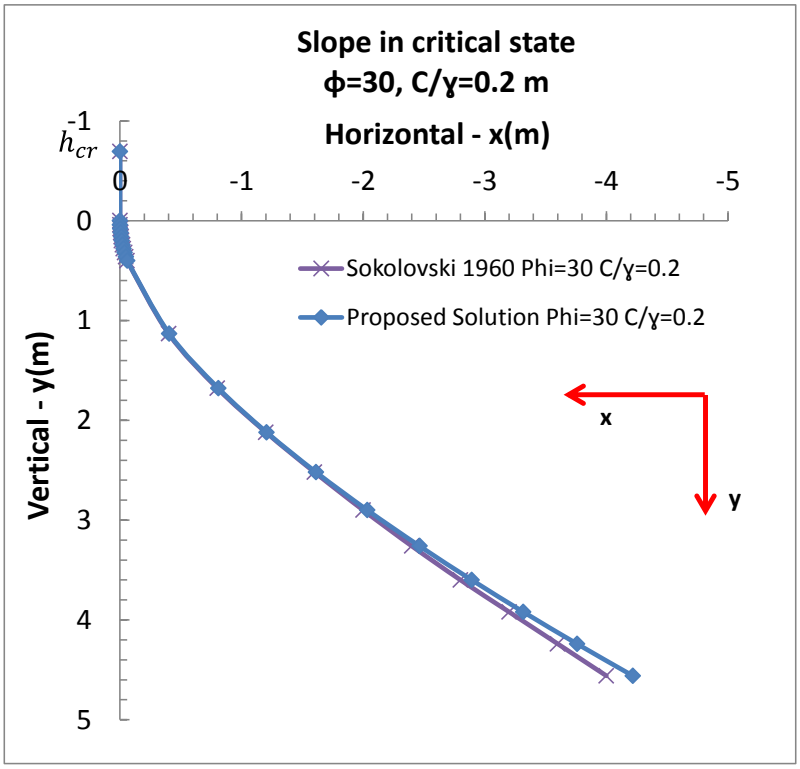

Figure B-54 Concave slope profiles obtained from Sokolovski (1960) and the proposed solution (Eq. 6-54) for $\phi = 30^o$ and $c/\gamma = 0.2\ m$

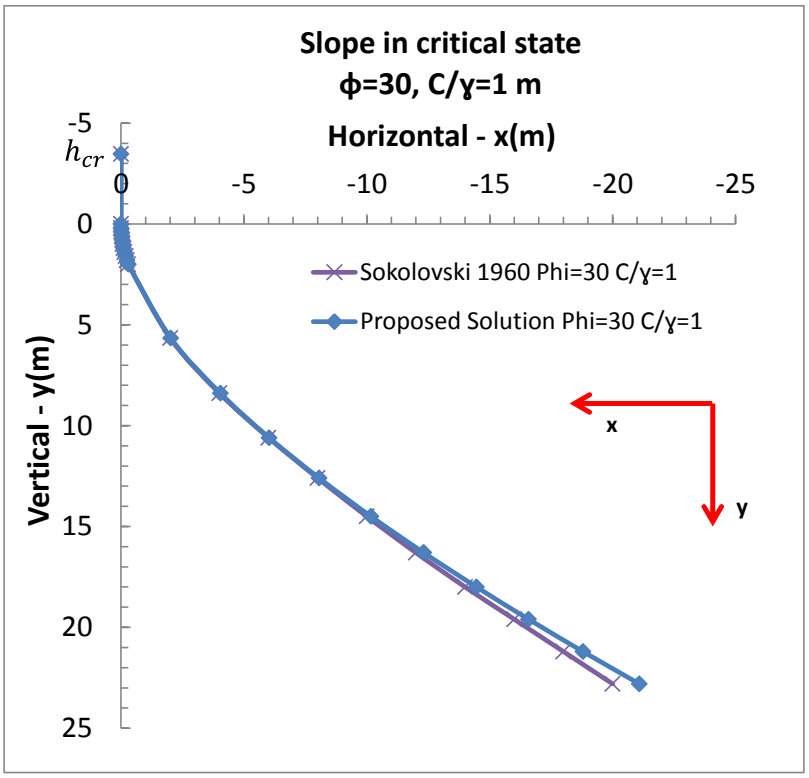

Figure B-55 Concave slope profiles obtained from Sokolovski (1960) and the proposed solution (Eq. 6-54) for $\phi = 30^o$ and $c/\gamma = 1\ m$

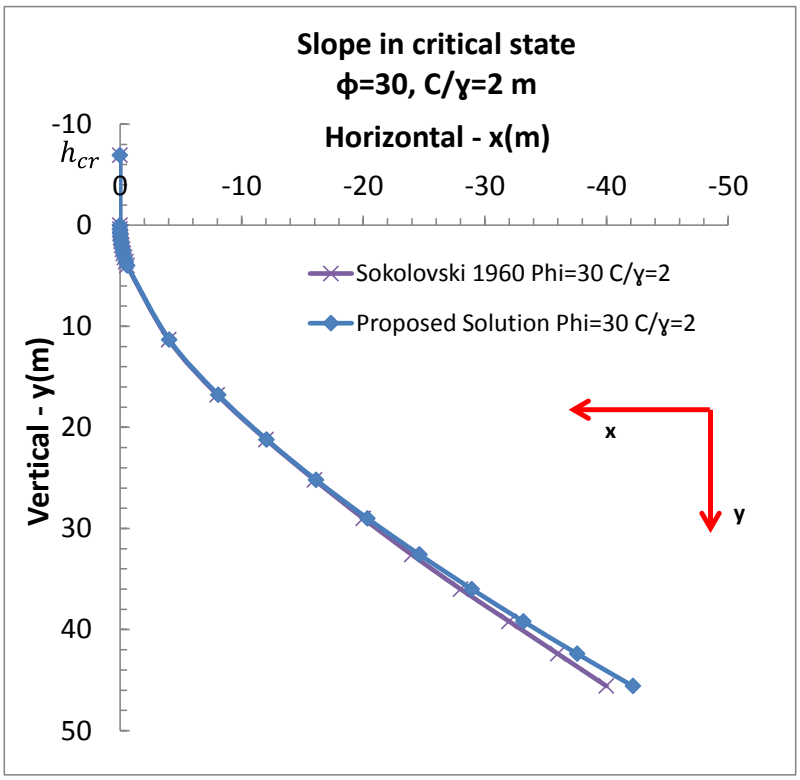

Figure B-56 Concave slope profiles obtained from Sokolovski (1960) and the proposed solution (Eq. 6-54) for $\phi = 30^o$ and $c/\gamma = 2\ m$

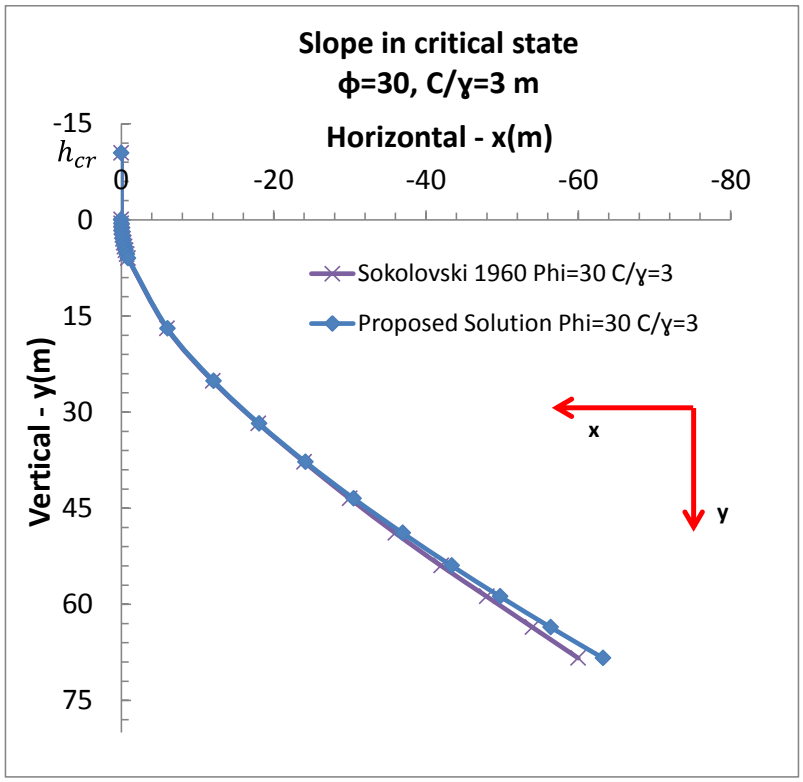

Figure B-57 Concave slope profiles obtained from Sokolovski (1960) and the proposed solution (Eq. 6-54) for $\phi = 30^o$ and $c/\gamma = 3\ m$

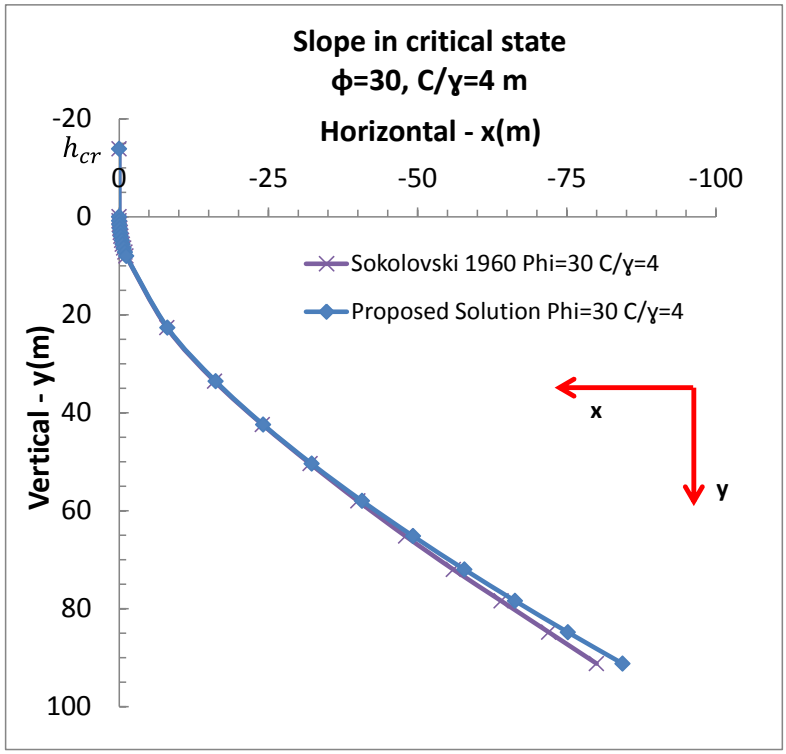

Figure B-58 Concave slope profiles obtained from Sokolovski (1960) and the proposed solution (Eq. 6-54) for $\phi = 30^o$ and $c/\gamma = 4\ m$

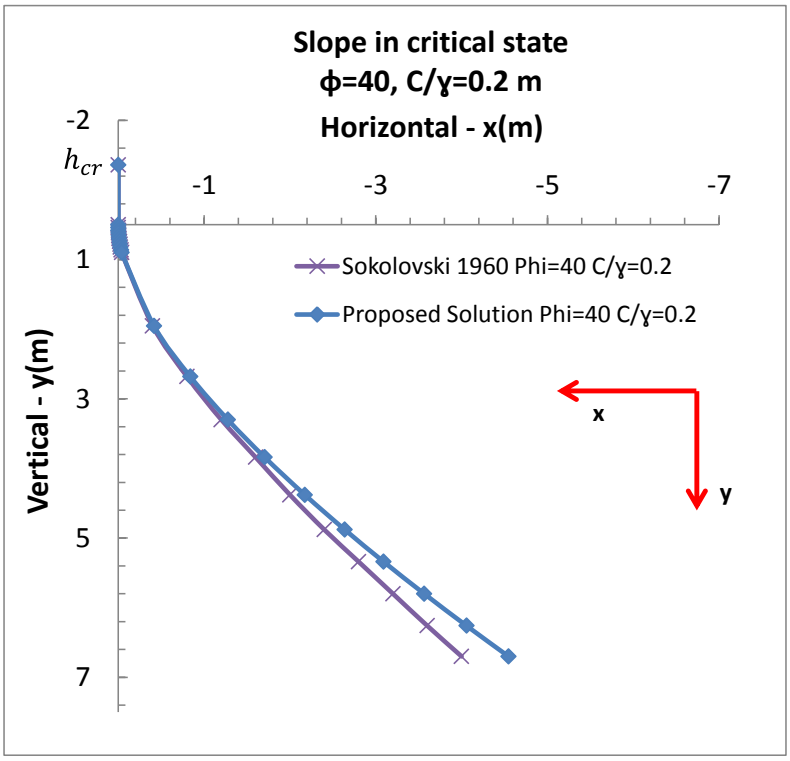

Figure B-59 Concave slope profiles obtained from Sokolovski (1960) and the proposed solution (Eq. 6-54) for $\phi = 40^o$ and $c/\gamma = 0.2\ m$

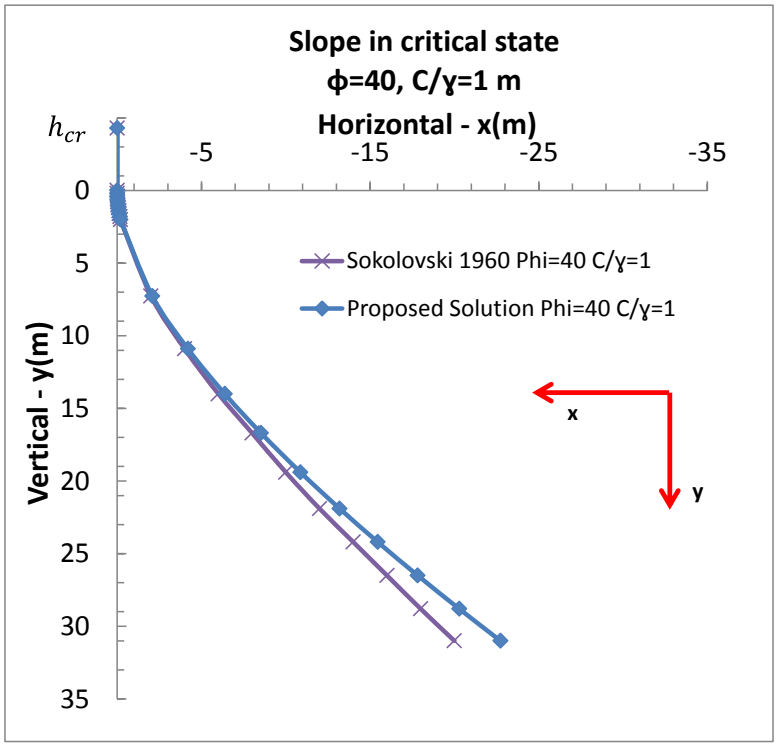

Figure B-60 Concave slope profiles obtained from Sokolovski (1960) and the proposed solution (Eq. 6-54) for $\phi = 40^o$ and $c/\gamma = 1\ m$

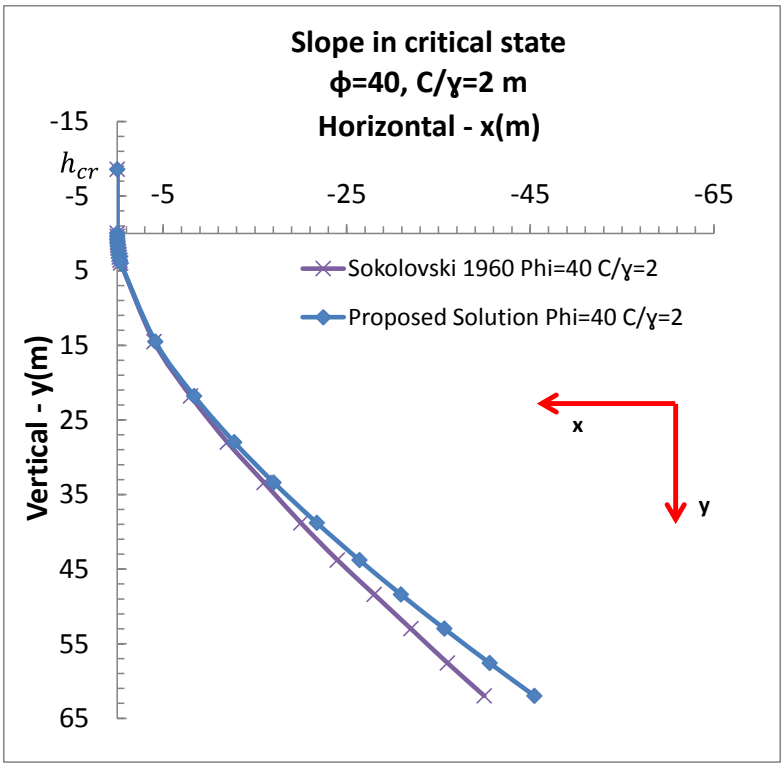

Figure B-61 Concave slope profiles obtained from Sokolovski (1960) and the proposed solution (Eq. 6-54) for $\phi = 40^o$ and $c/\gamma = 2\ m$

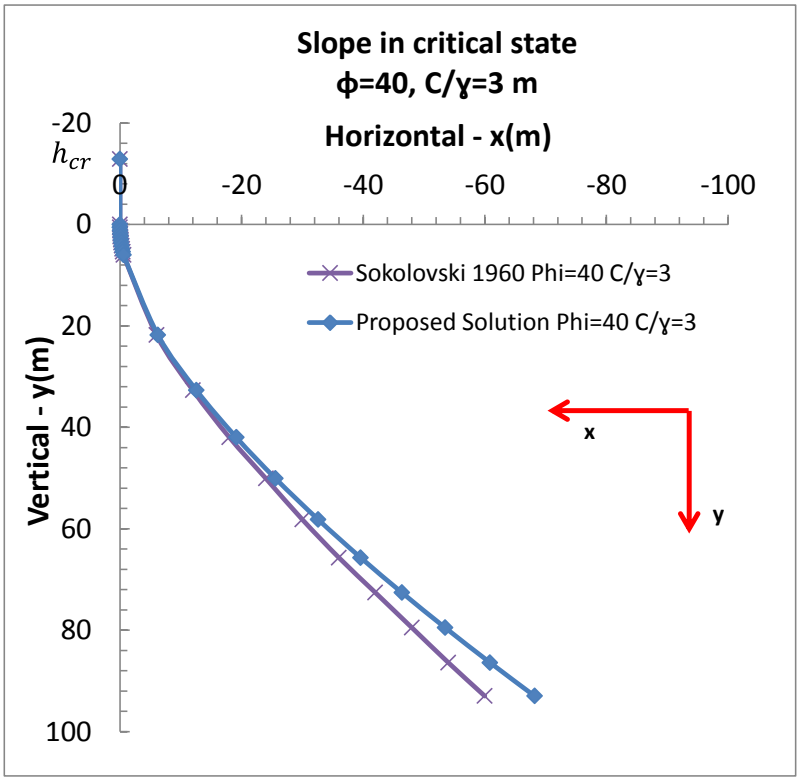

Figure B-62 Concave slope profiles obtained from Sokolovski (1960) and the proposed solution (Eq. 6-54) for $\phi = 40^o$ and $c/\gamma = 3\ m$

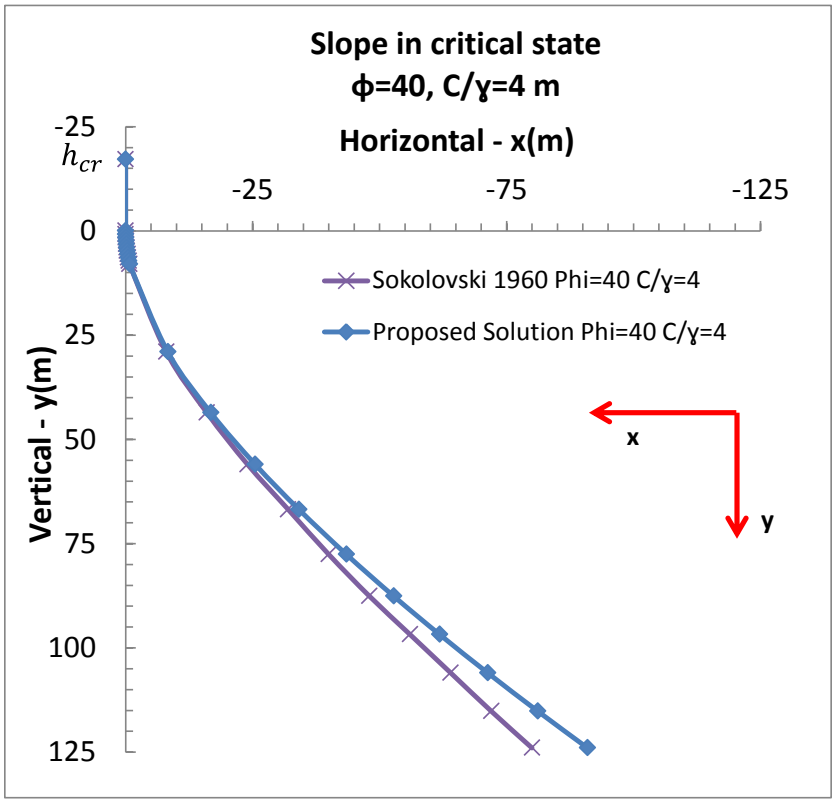

Figure B-63 Concave slope profiles obtained from Sokolovski (1960) and the proposed solution (Eq. 6-54) for $\phi = 40^o$ and $c/\gamma = 4\ m$

Comparison of factors of safety between the proposed solution and Sokolovski's (1960) solution for concave slopes in critical state

Table B-4. Adopted material properties for the FEM analyses

Material Properties	Value
Poisson's ratio υ	0.3
Young's modulus E (kN/m2)	20000
Tensile strength (kN/m2)	0
Dilatancy angle ψ (˚)	0
Earth pressure coefficient at rest Ko	1

Table B-5. Summary of FS obtained from FEM analysis for both sets of curved slopes (1500 T6 elements after 500 iterations. SRF tolerance = 0.01)

	FEM (1500 T6 elements after 500 Iterations. SRF tolerance = 0.01)					
	ϕ = 20		ϕ = 30		ϕ = 40	
	Sokolovski Solution	Proposed Solution	Sokolovski Solution	Proposed Solution	Sokolovski Solution	Proposed Solution
C/γ = 0.2 m	Hcr = 0.57 m	H = 3.81 m	Hcr = 0.69 m	H = 5.25 m	Hcr = 0.86 m	H = 7.06 m
	1.01	**0.99**	**1.04**	**1.05**	**1.04**	**1.05**
C/γ = 1 m	Hcr = 2.86 m	H = 19.06 m	Hcr = 3.46 m	H = 26.26 m	Hcr = 4.29 m	H = 35.29 m
	1.01	**0.98**	**1.02**	**1.03**	**1.01**	**1.05**
C/γ = 2 m	Hcr = 5.71 m	H = 38.11 m	Hcr = 6.93 m	H = 52.53 m	Hcr = 8.58 m	H = 70.58 m
	1.02	**0.98**	**1.02**	**1.03**	**1.00**	**1.07**
C/γ = 3 m	Hcr = 8.57 m	H = 57.17 m	Hcr = 10.39 m	H = 78.79 m	Hcr = 12.87 m	H = 105.87 m
	1.01	**0.98**	**1.01**	**1.03**	**1.03**	**1.06**
C/γ = 4 m	Hcr = 11.43 m	H = 76.23 m	Hcr = 13.86 m	H = 105.06 m	Hcr = 17.16 m	H = 141.16 m
	1.01	**0.98**	**1.02**	**1.02**	**1.02**	**1.05**

Table B-6 Summary of FS obtained from LEM analysis for both sets of curved slopes (Simplified Bishop's method with 495000 surfaces computed)

	LEM Simplified Bishop's method (4950 interpreted surfaces)					
	ϕ = 20		ϕ = 30		ϕ = 40	
	Sokolovski Solution	**Proposed Solution**	**Sokolovski Solution**	**Proposed Solution**	**Sokolovski Solution**	**Proposed Solution**
c/γ = 0.2 m	Hcr = 0.57 m	H = 3.81 m	Hcr = 0.69 m	H = 5.25 m	Hcr = 0.86 m	H = 7.06 m
	1.04	**1.00**	**1.03**	**1.04**	**1.03**	**1.06**
c/γ = 1 m	Hcr = 2.86 m	H = 19.06 m	Hcr = 3.46 m	H = 26.26 m	Hcr = 4.29 m	H = 35.29 m
	1.04	**1.00**	**1.03**	**1.04**	**1.03**	**1.06**
c/γ = 2 m	Hcr = 5.71 m	H = 38.11 m	Hcr = 6.93 m	H = 52.53 m	Hcr = 8.58 m	H = 70.58 m
	1.04	**1.00**	**1.03**	**1.04**	**1.03**	**1.06**
c/γ = 3 m	Hcr = 8.57 m	H = 57.17 m	Hcr = 10.39 m	H = 78.79 m	Hcr = 12.87 m	H = 105.87 m
	1.04	**1.00**	**1.03**	**1.04**	**1.03**	**1.05**
c/γ = 4 m	Hcr = 11.43 m	H = 76.23 m	Hcr = 13.86 m	H = 105.06 m	Hcr = 17.16 m	H = 141.16 m
	1.04	**1.00**	**1.03**	**1.04**	**1.03**	**1.06**

Behavior of the failure mechanisms and factors of safety (FS) with respect the height of the concave slope obtained from the proposed solution (Eq. 6-54)

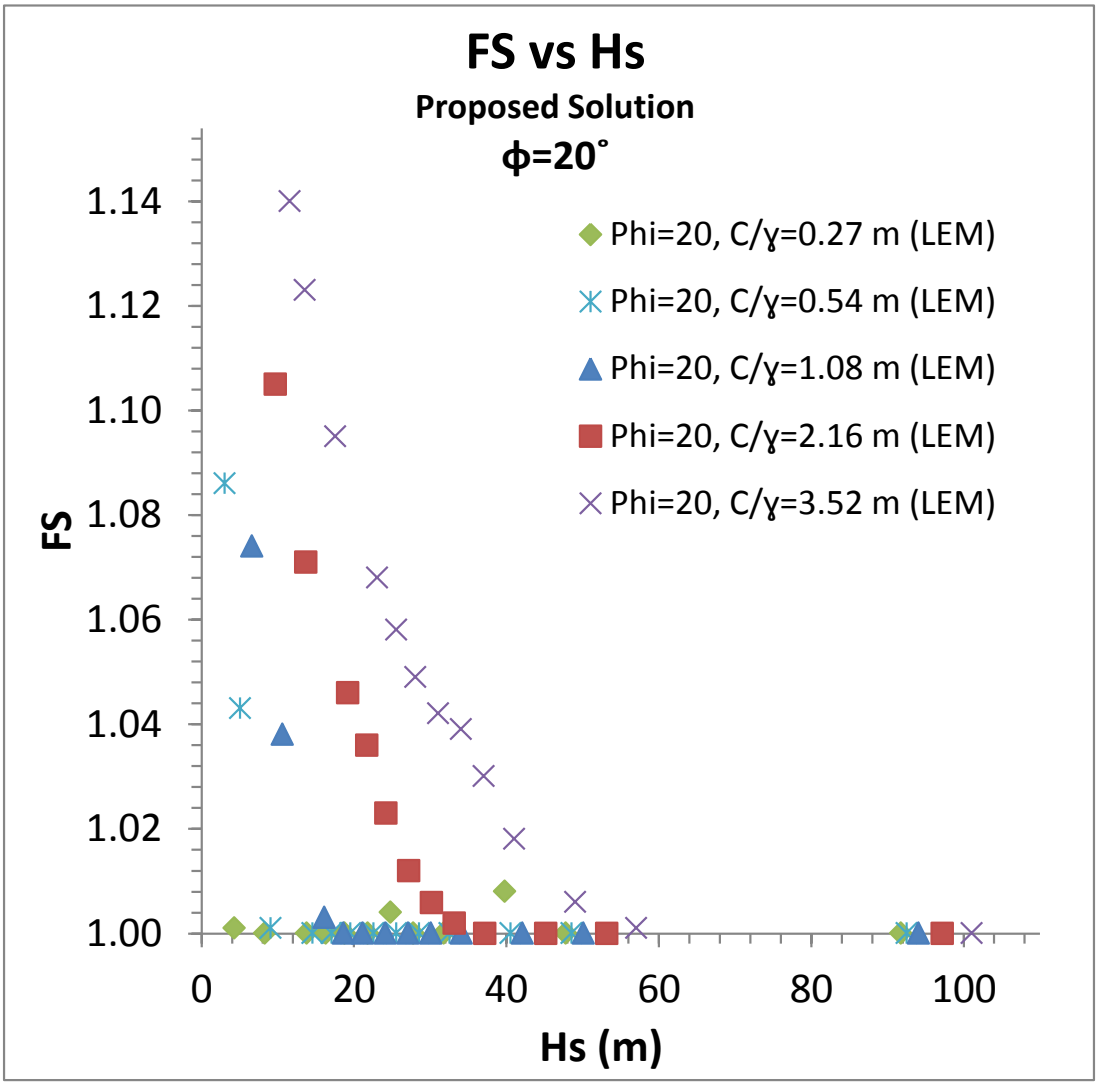

Figure B-64 Factor of safety (FS) vs Slope Height (Hs) for $\phi = 20^o$, $C/\gamma = 0.27, 0.54,\ 1.08, 2.16, 3.52\ m$. LEM analysis.

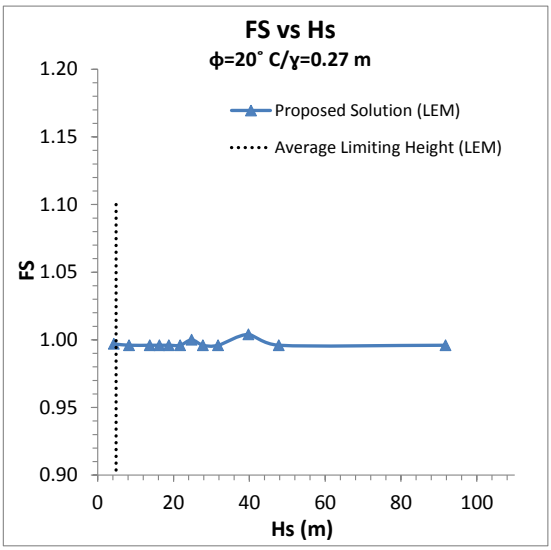

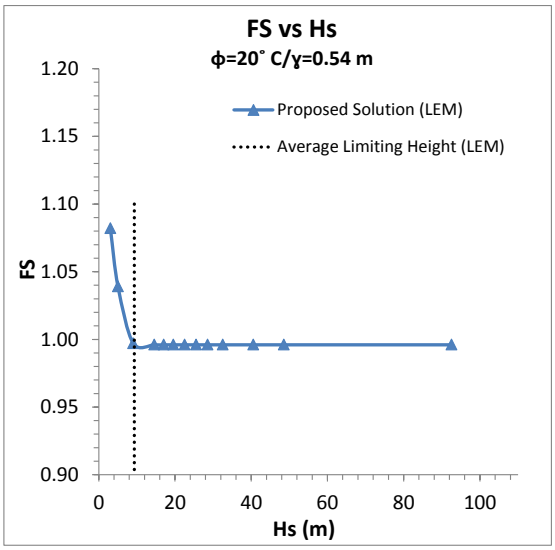

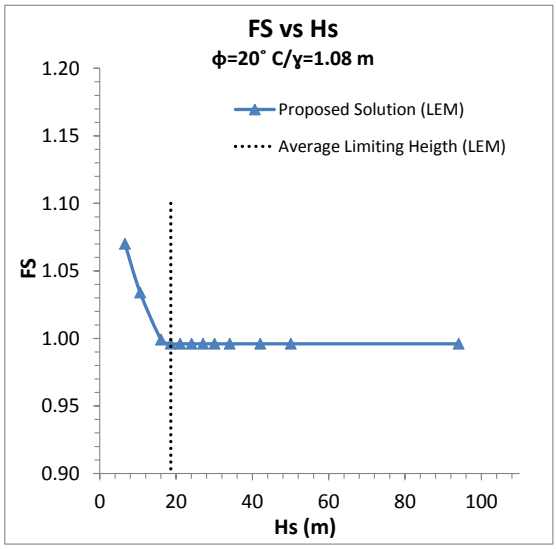

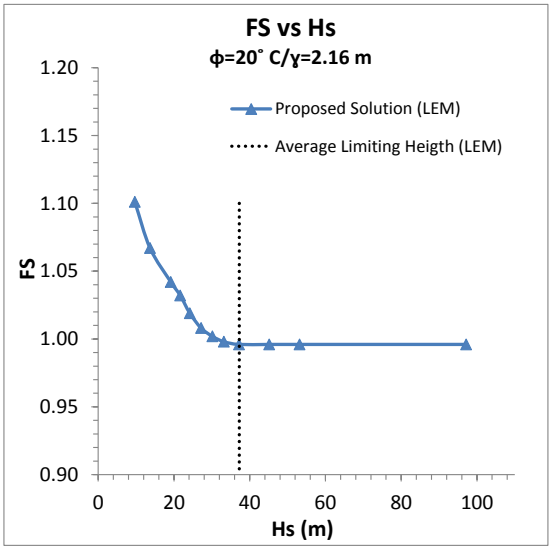

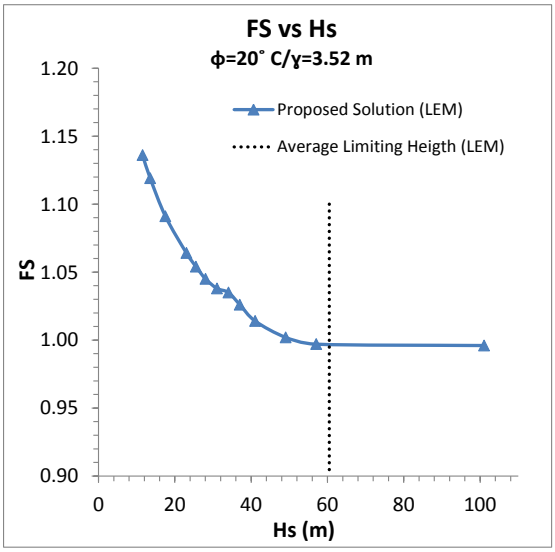

Figure B-65 Factor of safety (FS) vs Slope Height (Hs) and Limiting Height (h_L) for $\phi = 20^o$, $C/\gamma = 0.27, 0.54,\ 1.08, 2.16, 3.52\ m$. LEM analysis.

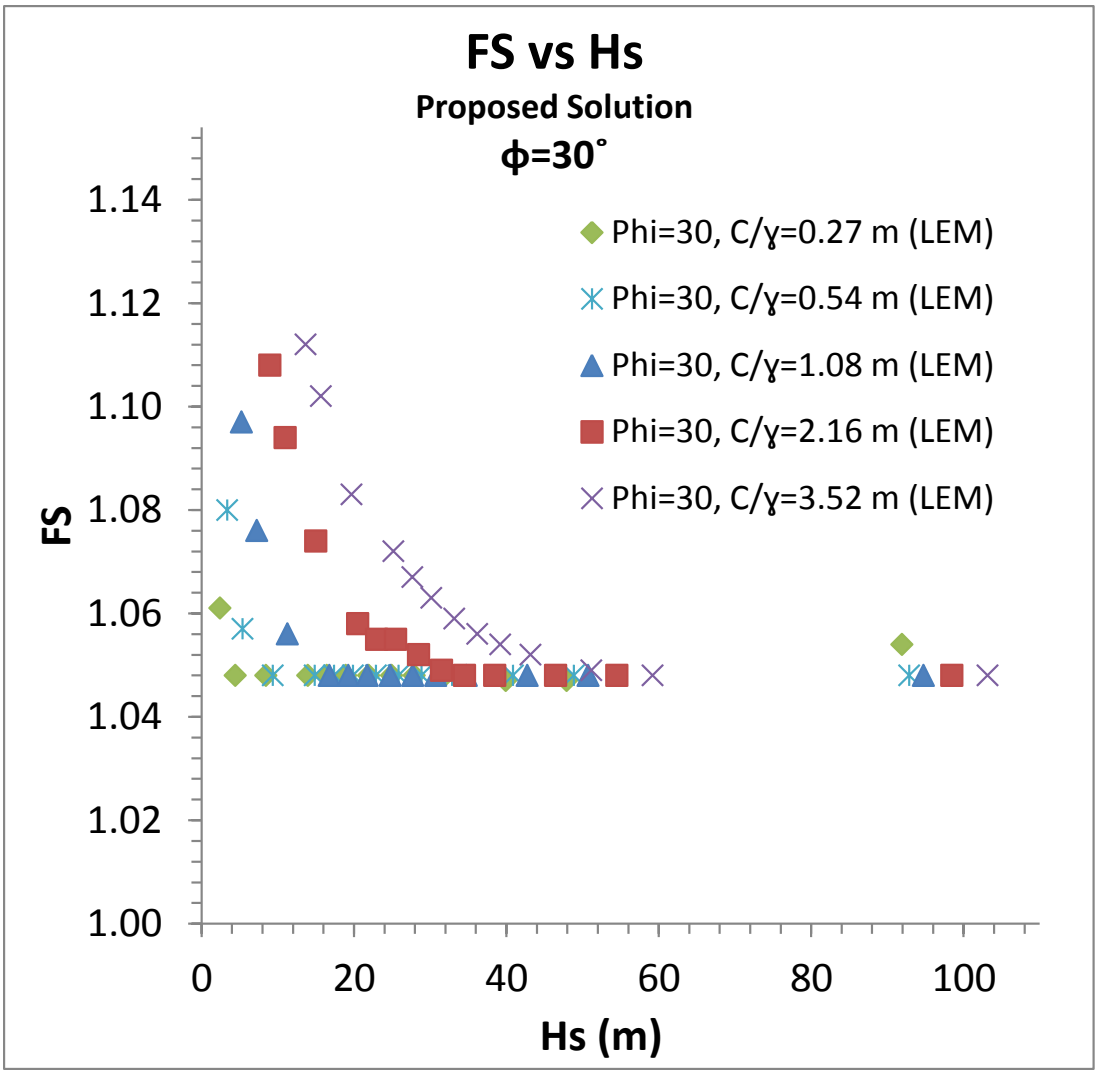

Figure B-66 Factor of safety (FS) vs Slope Height (Hs) for $\phi = 30^o$, $C/\gamma = 0.27, 0.54,\ 1.08, 2.16, 3.52\ m$. LEM analysis.

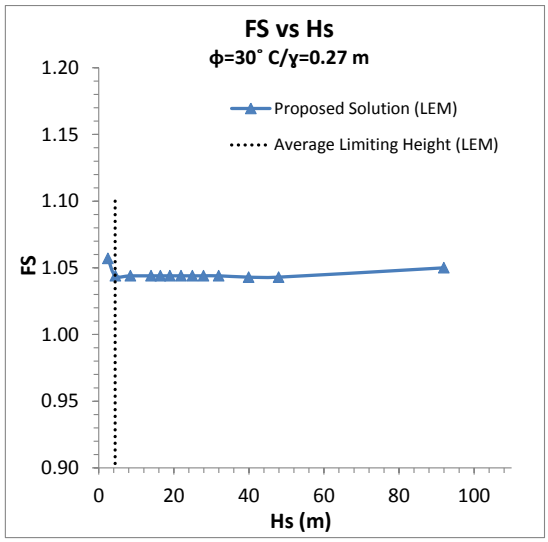

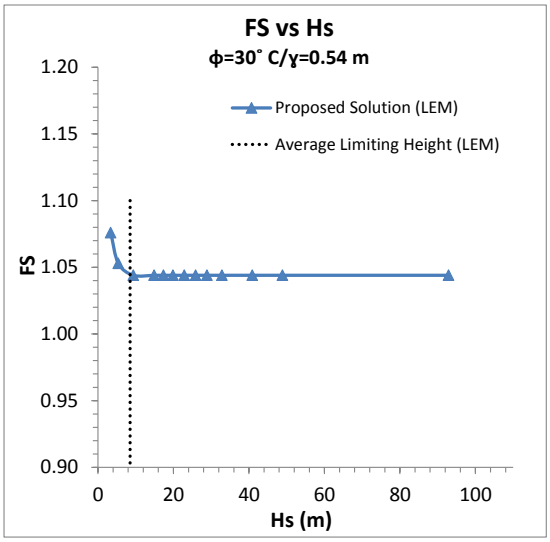

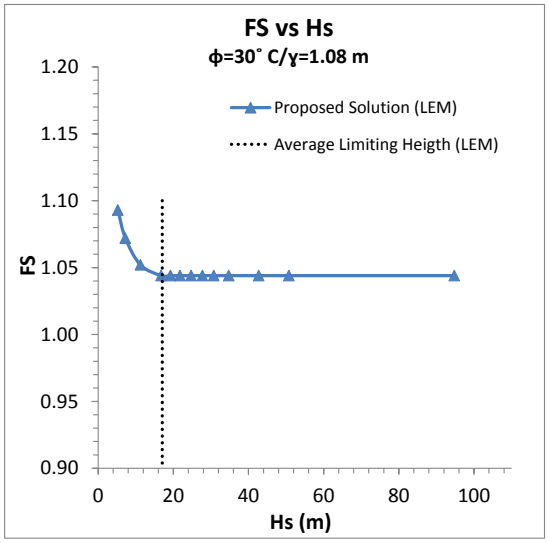

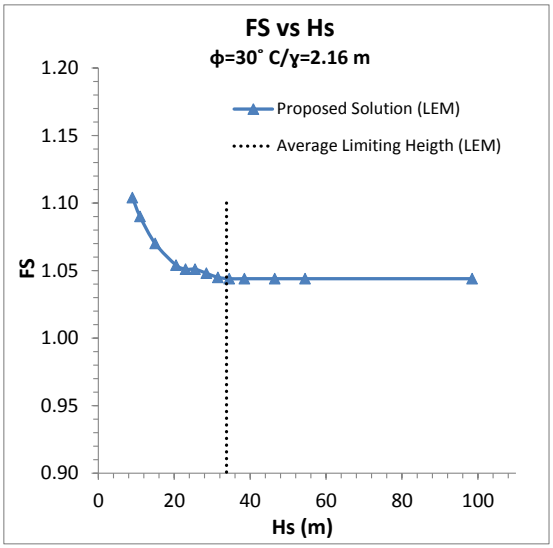

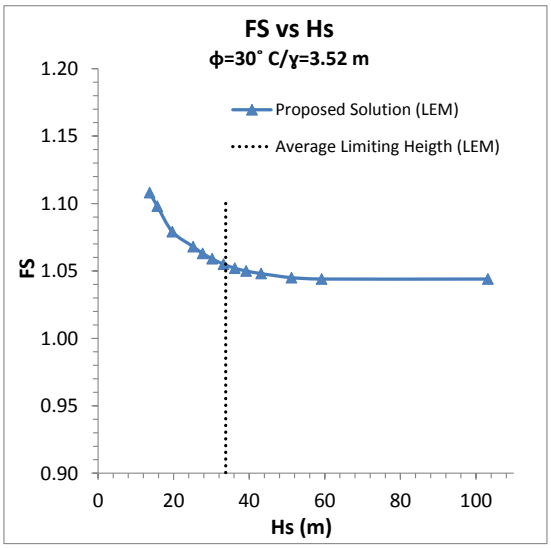

Figure B-67 Factor of safety (FS) vs Slope Height (Hs) and Limiting Height (h_L) for $\phi = 30^o$, $C/\gamma = 0.27, 0.54,\ 1.08, 2.16, 3.52\ m$. LEM analysis.

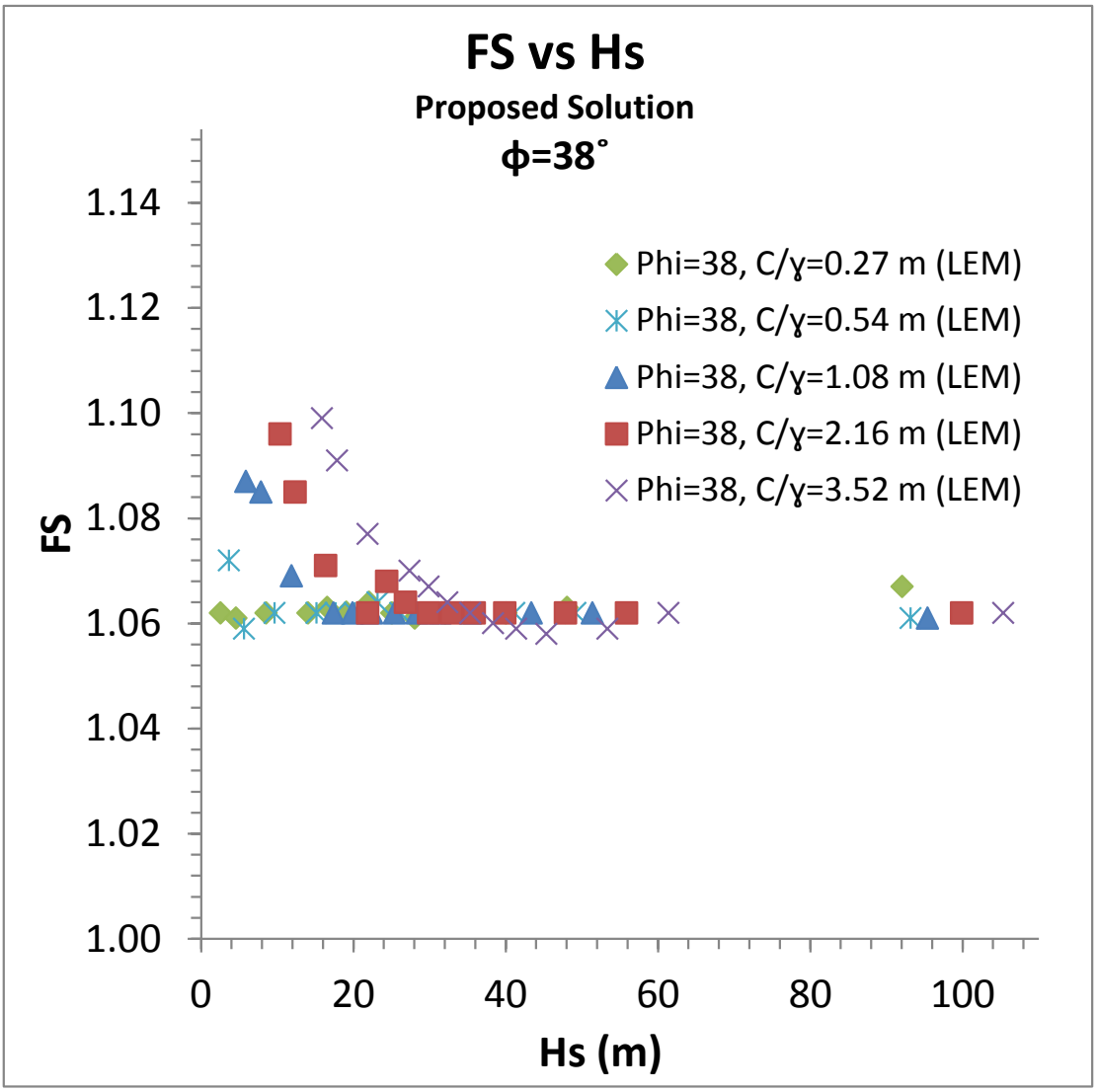

Figure B-68 Factor of safety (FS) vs Slope Height (Hs) for $\phi = 38^o$, $C/\gamma = 0.27, 0.54,\ 1.08, 2.16, 3.52\ m$. LEM analysis.

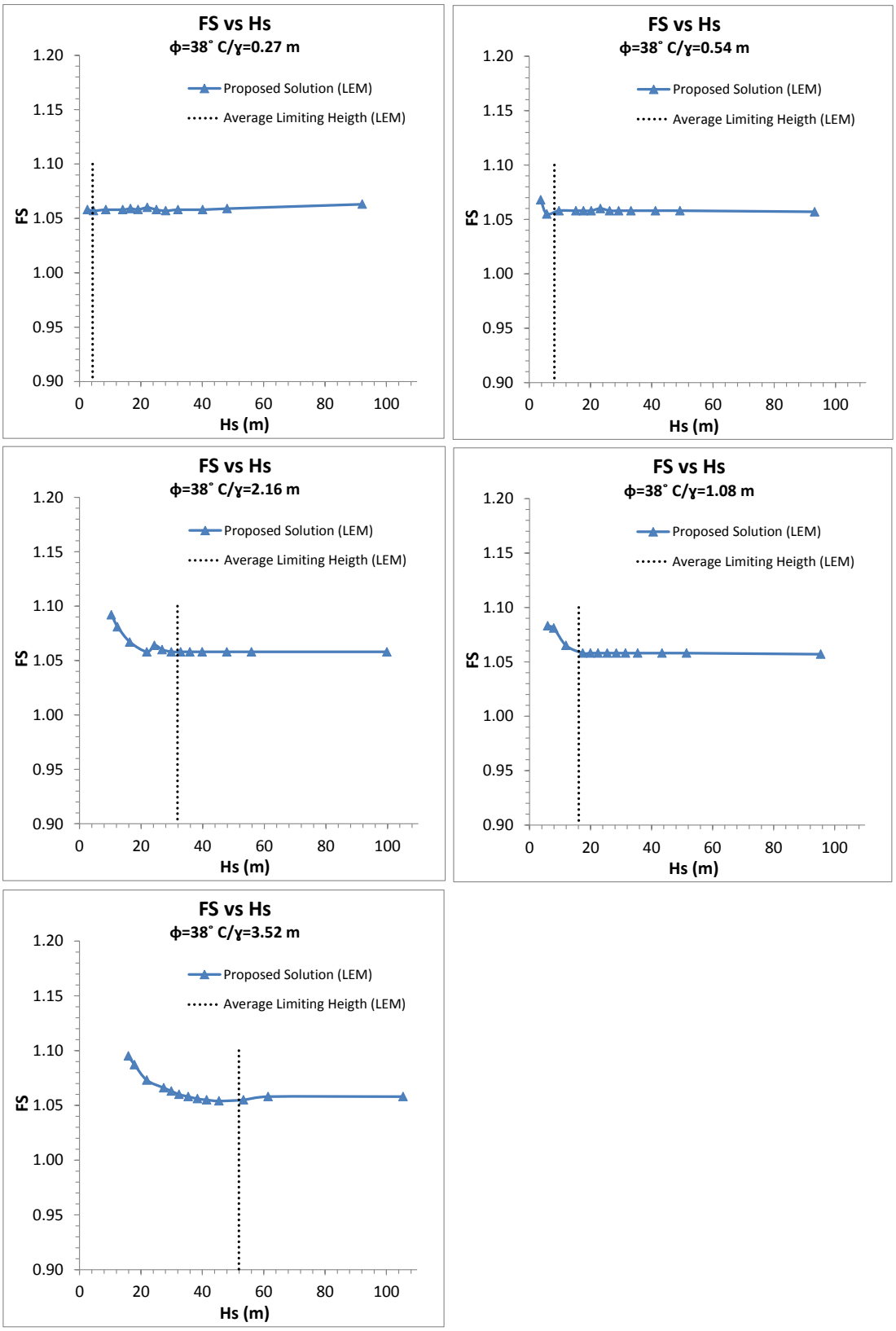

Figure B-69 Factor of safety (FS) vs Slope Height (Hs) and Limiting Height (h_L) for $\phi = 38^o$, $C/\gamma = 0.27, 0.54,\ 1.08, 2.16, 3.52\ m$. LEM analysis.

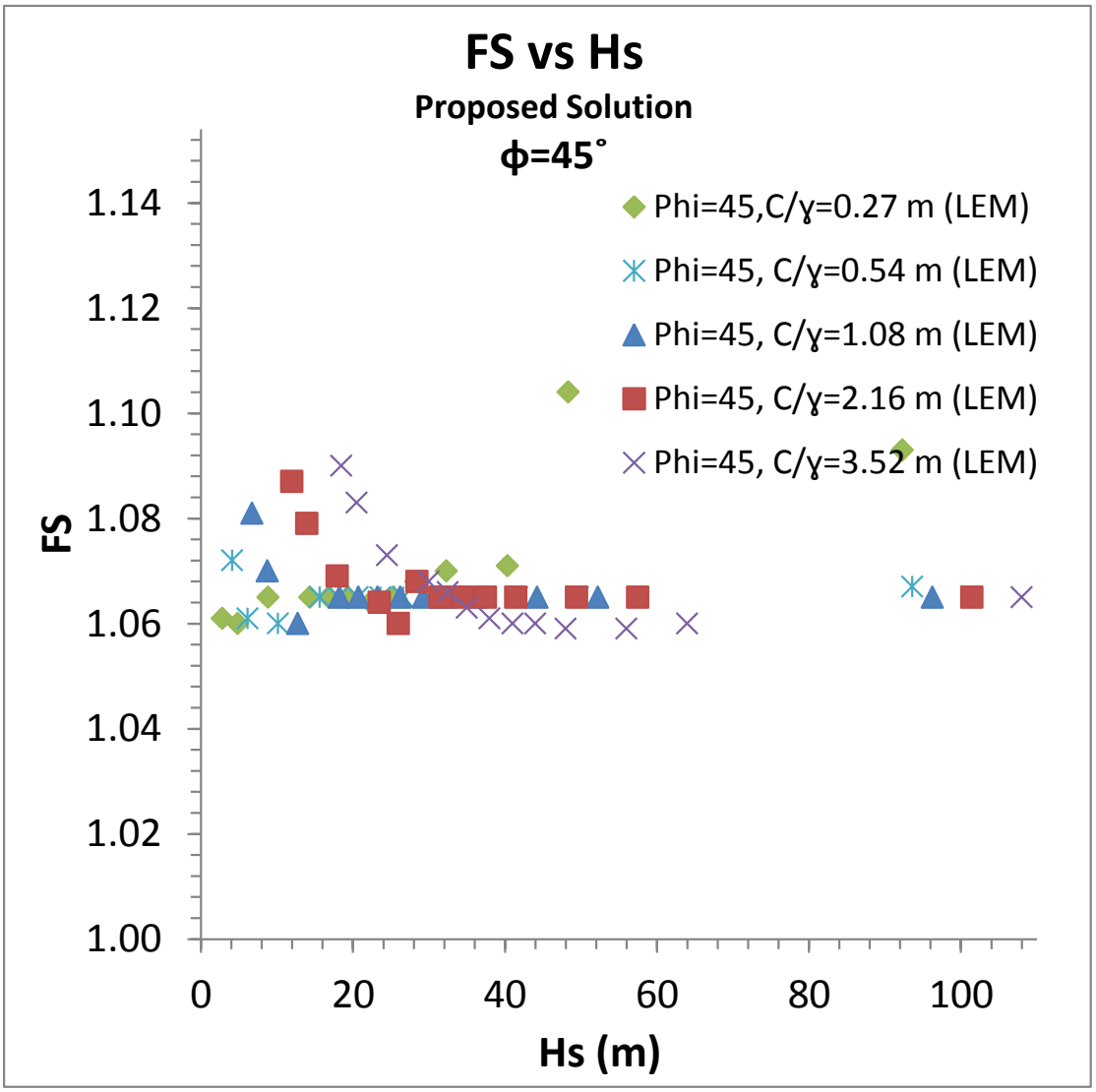

Figure B-70 Factor of safety (FS) vs Slope Height (Hs) for $\phi = 45^o$, $C/\gamma = 0.27, 0.54,\ 1.08, 2.16, 3.52\ m$. LEM analysis.

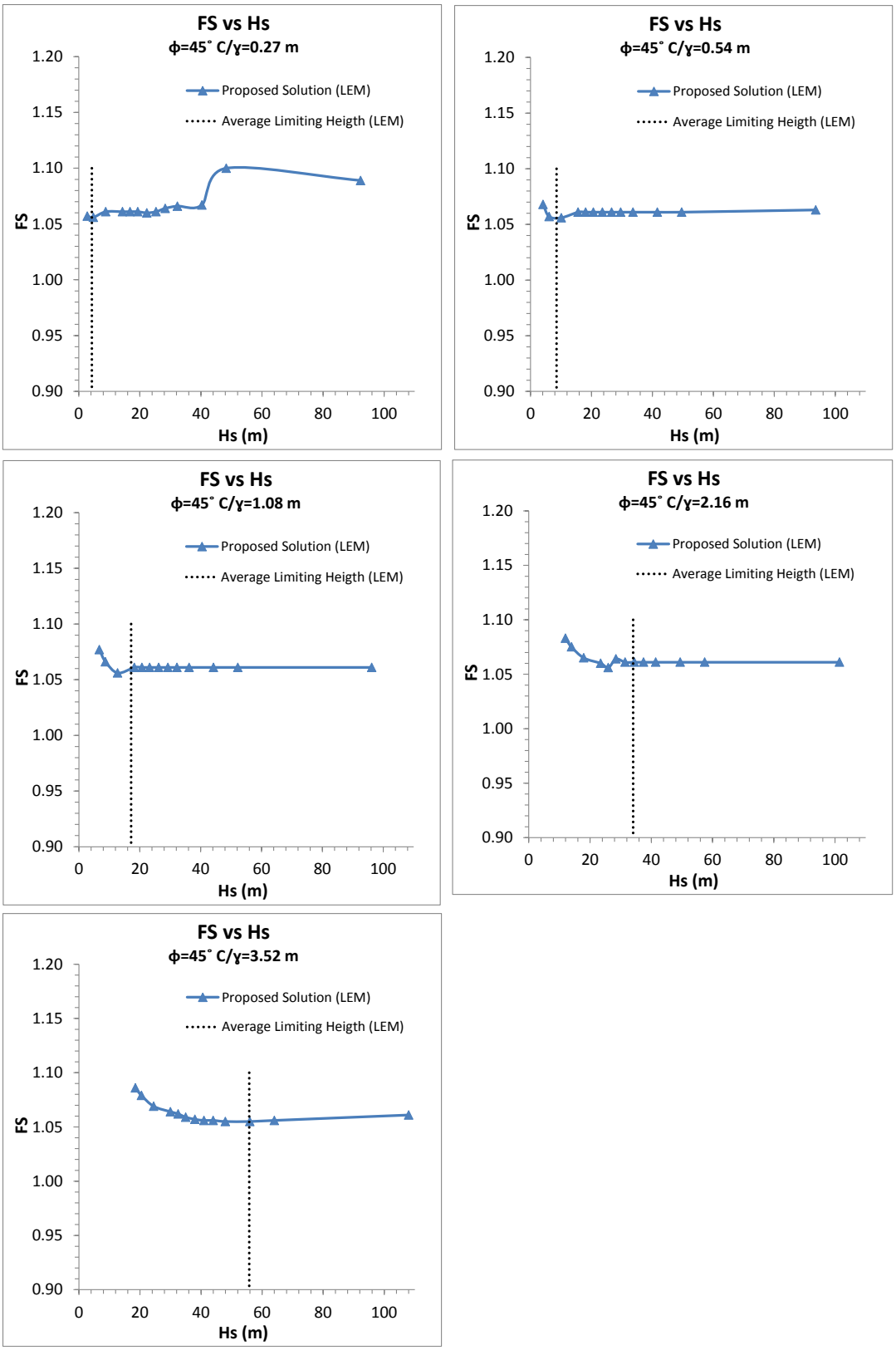

Figure B-71 Factor of safety (FS) vs Slope Height (Hs) and Limiting Height (h_L) for $\phi = 45^o$, $C/\gamma = 0.27, 0.54,\ 1.08, 2.16, 3.52\ m$. LEM analysis.

Factor of safety (FS) vs. the height of the critical curved slope (H) obtained from the proposed solution (Eq. 6-52) for different strength reduction factors (SRF)

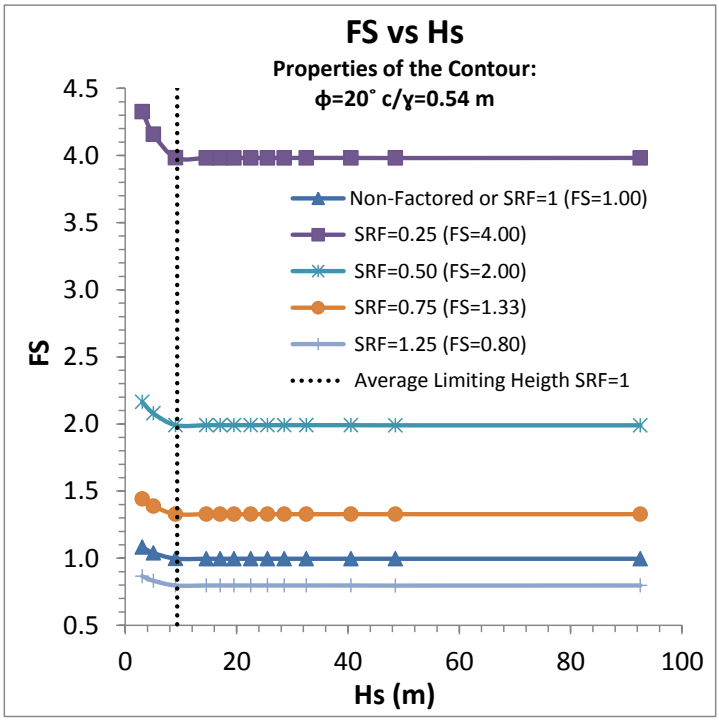

Figure B-72 Factor of safety (FS) from Limiting Equilibrium analysis vs Slope Height (Hs) for $\phi = 20^o$, $c/\gamma = 0.54\ m$ and $SRF = 0.25, 0.5, 0.75, 1.25$.

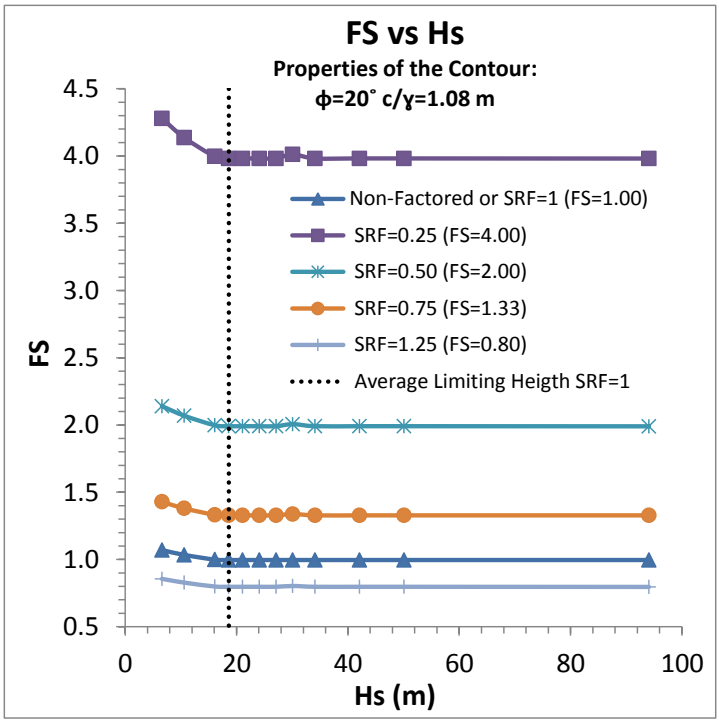

Figure B-73 Factor of safety (FS) from Limiting Equilibrium analysis vs Slope Height (Hs) for $\phi = 20^o$, $c/\gamma = 1.08\ m$ and $SRF = 0.25, 0.5, 0.75, 1.25$.

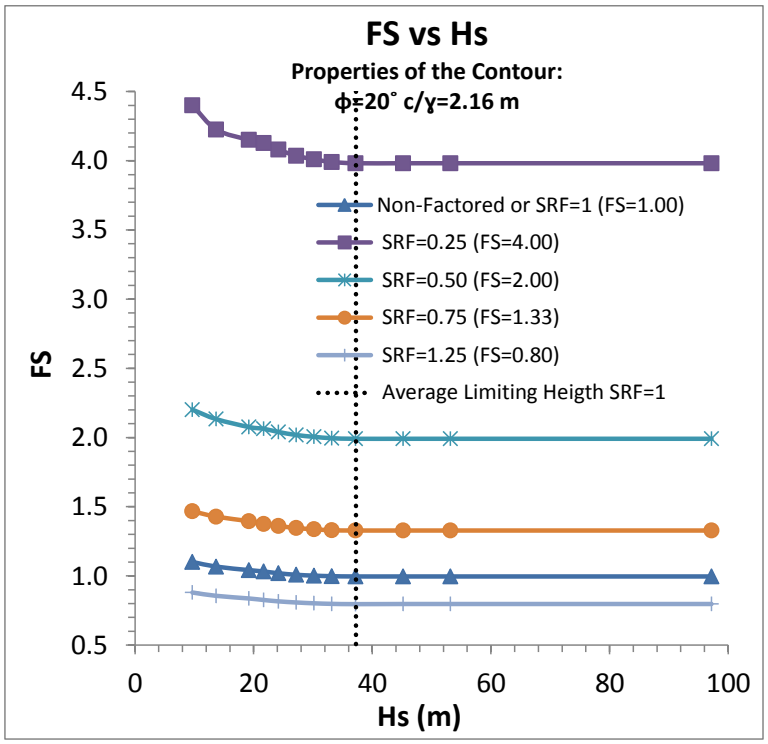

Figure B-74 Factor of safety (FS) from Limiting Equilibrium analysis vs Slope Height (Hs) for $\phi = 20^o$, $c/\gamma = 2.16\ m$ and $SRF = 0.25, 0.5, 0.75, 1.25$.

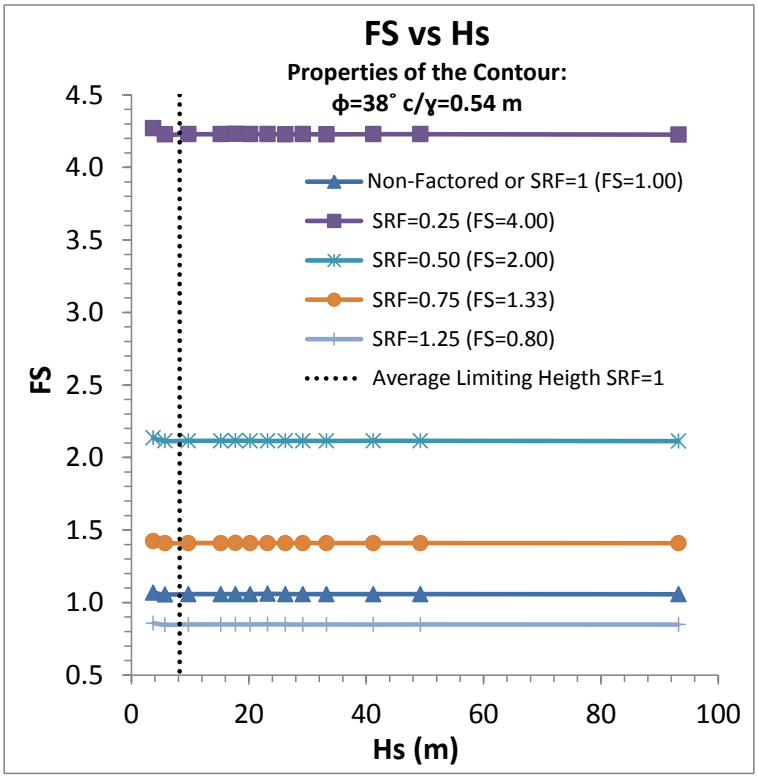

Figure B-75 Factor of safety (FS) from Limiting Equilibrium analysis vs Slope Height (Hs) for $\phi = 38^o$, $c/\gamma = 0.54\ m$ and $SRF = 0.25, 0.5, 0.75, 1.25$.

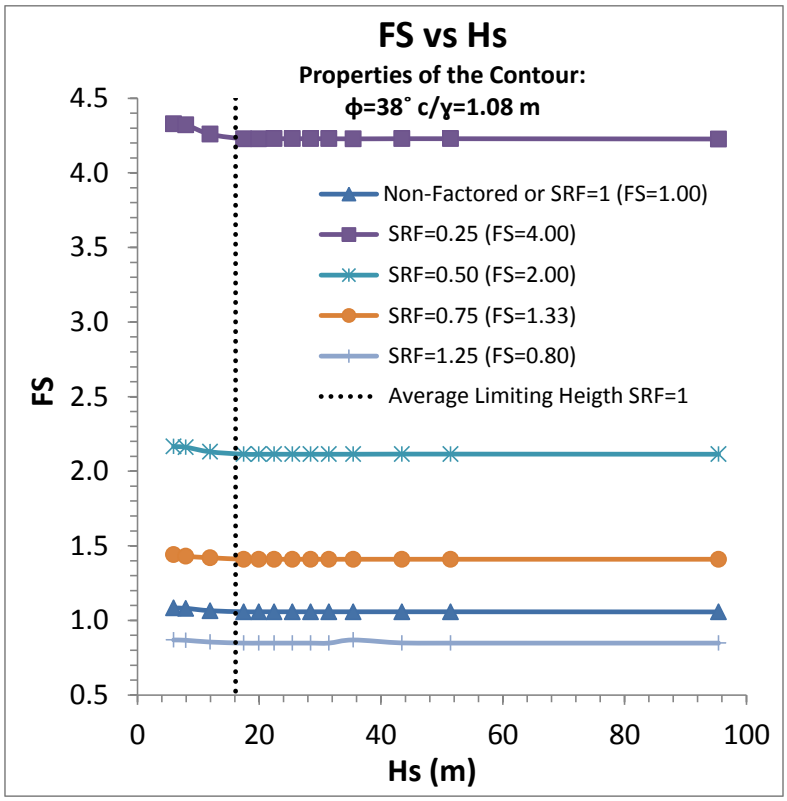

Figure B-76 Factor of safety (FS) from Limiting Equilibrium analysis vs Slope Height (Hs) for $\phi = 38^o$, $c/\gamma = 1.08\ m$ and $SRF = 0.25, 0.5, 0.75, 1.25$.

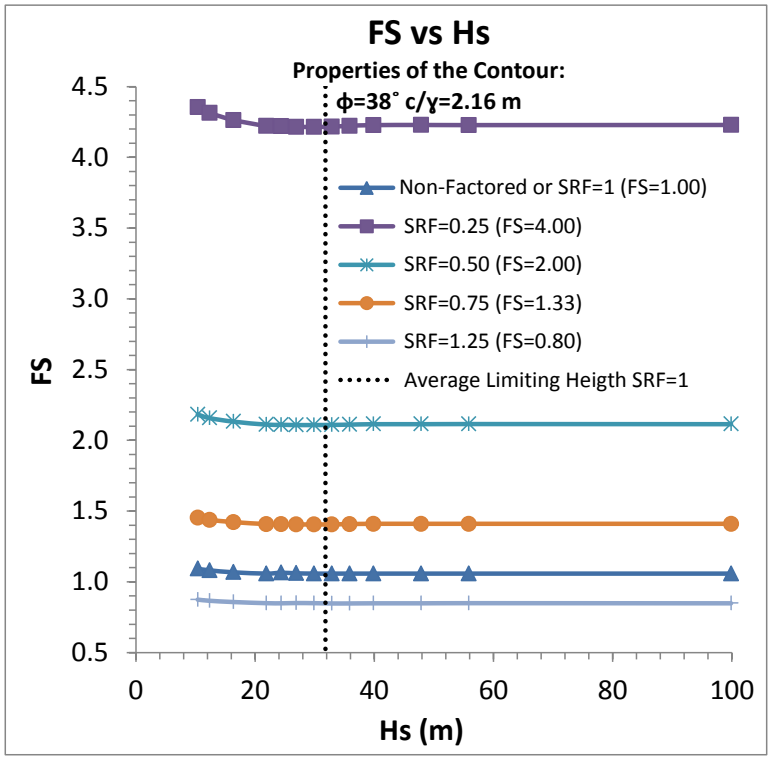

Figure B-77 Factor of safety (FS) from Limiting Equilibrium analysis vs Slope Height (Hs) for $\phi = 38^o$, $c/\gamma = 2.16\ m$ and $SRF = 0.25, 0.5, 0.75, 1.25$.

Taylor's slope stability chart

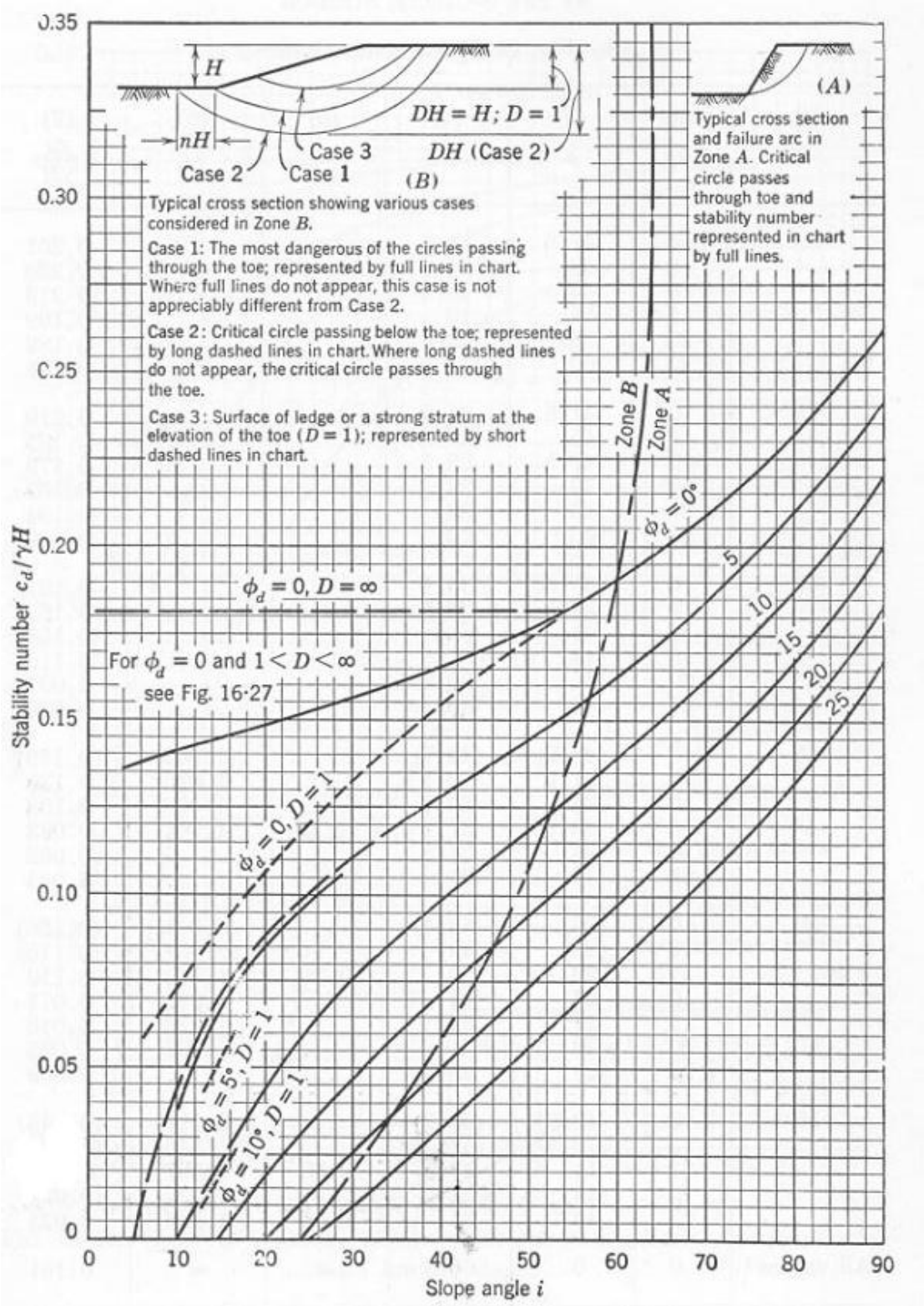

Figure B-78 Taylor's slope stability chart (Taylor, 1948)